The Effect of Loading, Plantar Ligament Disruption and Surgical Repair on Canine Tarsal Bone Kinematics

Presented by

Christopher John Tan

Sydney School of Veterinary Science

Faculty of Science, The University of Sydney

February 2018

A thesis submitted to fulfil requirements for the degree of Doctor of Philosophy

To my wonderful family

This is to certify that to the best of my knowledge, the content of this thesis is my own work. This thesis has not been submitted for any degree or other purposes.

I certify that the intellectual content of this thesis is the product of my own work and that all the assistance received in preparing this thesis and sources have been acknowledged.

Signature

Name: Christopher John Tan

Table of contents

Table of figures

Table of tables

Table of equations

Abbreviations

2D	two dimensional
3D	three dimensional
AA	alignment angle
CT	computed tomography
CTB	central tarsal bone
DICOM	Digital Imaging and Communications in Medicine
GRF	Ground Reaction Force
HU	Hounsfield units
ICP	Iterative Closest Point
MRI	Magnetic Resonance Imaging
MT	Metatarsal
N	Newtons
PIT	Proximal Intertarsal
RSA	Radiostereometric Analysis
SD	standard deviation
SDA	Sagittal Deviation Angle
STL	Stereolithograph
TB	Tarsal bone

Author attribution statement

Chapter 3 represents work that has been published as

"Influence of Scan Resolution, Thresholding, and Reconstruction Algorithm on Computed Tomography-Based Kinematic Measurements"

Christopher John Tan, William C. H. Parr, William R. Walsh, Mariano Makara and Kenneth A. Johnson

J Biomech Eng 139(10), 104503 (Aug 23, 2017) (5 pages)

Paper No: BIO-16-1436; doi: 10.1115/1.4037558

Christopher Tan was responsible for developing the concept, performing the experiment and the kinematic calculations and writing the manuscript

William Parr was responsible for writing the mathematic code to calculate the recorded motions from the 4 X 4 matrix

William Walsh contributed to the original concept and manuscript preparation

Mariano Makara contributed to optimisation of imaging parameters

Kenneth Johnson contributed to the original concept and manuscript preparation

Summary

Our desire to describe the complex kinematic patterns found in nature often exceeds our ability to record, quantify and characterise them. Constantly faced with technological limitations, investigators may attempt to develop new techniques or reduce the complex motions to more simplified models. Perhaps due to technical limitations, the canine pes is commonly considered as a rigid structure, when in reality, this limb segment is comprised of multiple bones and ligaments and motion can readily be demonstrated during palpation. Despite the potentially important role that tarsal bone kinematics may play in energy conservation mechanisms and pathogenesis of injury or disease, there are no descriptions of normal canine tarsal kinematics during locomotion.

A radiolucent cadaveric limb loading device was developed and used in conjunction with a computed tomography based kinematic measurement technique to produce the first description of canine tarsal bone kinematics in three dimensions. Tarsal bones were shown to undergo a complex, yet coordinated patterns of motion that facilitate dorsiflexion of the pes in the normal animal. The same technique was applied to specimens following sequential transection of the plantar ligament and revealed the roles of the various components of this ligament. Complete luxation of the proximal intertarsal joint occurred only after transection of the entire ligament, resulting in an inability to transmit force through this limb segment. The final chapter of this thesis, evaluated the ability of a laterally applied bone plate to re-establish force transmission through this limb segment, providing important information that may help to resolve the open question of what the most appropriate surgical repair technique is in these clinical cases.

,

Preface

Jig construction and modification was performed at the University Veterinary Teaching Hospital-Sydney, University of Sydney and the Surgical and Orthopaedic Research Laboratories, Prince of Wales Clinical School, University of New South Wales.

All computed tomography scans were performed at the University Veterinary Teaching Hospital, Sydney.

All post scanning processing including bone segmentation, 3D model generation and kinematic calculations were performed at the Surgical and Orthopaedic Research Laboratories, Prince of Wales Clinical School, University of New South Wales.

Surgical implants were donated by DuPuy Synthes.

Chapter 1 Introduction

It all started with a bet!

Or so the legend goes. In the late 1800s there was much controversy surrounding whether the trotting horse had an aerial suspension phase, with all 4 feet off the ground at one time. Leland Stanford, the ex-governor of California, commissioned a photographer by the name of Eadweard Muybridge to use photography to help resolve this intriguing question (Premeaux, 2003). Despite being met with initial scepticism (unknown, 1879), Muybridge continued to refine his photographic technique until shutter speeds of 1/1000th of a second were possible, allowing him to produce the iconic images that provided the first clear evidence of an aerial suspension phase in the horse, finally putting the long running debate to rest (Shimamura, 2002).

For the first time, the human race could effectively pause time, allowing the study of motion in ways previously thought impossible. This great advance in technology allowed the displacement of limb segments in space to be accurately recorded, welcoming in the modern age of kinematic investigations. Since this time, ongoing technological advances have continued to increase our understanding of the intricacy and diversity of movement patterns in humans and a variety of other species. From Muybridge's ground-breaking studies of two-dimensional (2D) movement, motion capture techniques now allow real time recording of motion in three dimensions. Skin mounted markers have been used extensively to help reveal the motion of the underlying bones, which is of greater clinical importance than the motion of the skin surface, however, soft tissue artefact continues to limit its accuracy. Direct implantation of marker sets into bone overcome the soft tissue artefact but requires invasive surgery, limiting its regular clinical use. Non-invasive imaging techniques, such as fluoroscopy, allow accurate recognition of the bones in two dimensions, whilst biplanar fluoroscopy or tomographic imaging techniques, such as magnetic resonance imaging and computed tomography allow accurate determination of three-dimensional (3D) bone kinematics.

Advancing, refining and validating new and existing techniques used for kinematic investigations is an essential component to ensuring our understanding of normal body motion continues to expand

in the future. Understanding the normal pattern of movement within and across various body segments allows identification of how disease or injury may affect function and provides the opportunity to objectively assessment the effect of treatments, such as surgery (McLaughlin, 2001). In addition to the horse, one of the first species Muybridge photographed was the dog, an example of a highly athletic terrestrial mammal, capable of amazing feats of speed and endurance (Poole and Erickson, 2011). Like other terrestrial mammals, the limbs of dogs have long been considered as biological springs, capable of storing kinetic and potential energy as elastic strain energy during the early stages of the stance phase, only to release this energy back into kinetic energy during take-off (Alexander, 1984).

Whilst the contribution of stifle and hock flexion have been investigated as components of the biological spring mechanism, little attention has been given to the pes, or foot. This limb segment acts as a lever arm, balancing the ground reaction force with the tensile pull of the common calcaneal tendon to prevent collapse of the talocrural joint (Pratt, 1935). This may be one reason why the canine pes is generally modelled as a rigid beam despite motion that can be consistently elicited on palpation.

Currently, the ability to capture and characterise motion within the pes is limited by available technology. As dogs may complete a full gait cycle within one third of a second and travel at speeds of up to 70kph, accurately capturing small displacements of irregular, overlapping bones in three dimensions produces significant challenges for investigators and significant risk for study subjects. Just as Muybridge developed new technologies to overcome the limitations of the day, this thesis comprises chapters which describe and detail the evolution and validation of novel techniques, which could then be applied to characterise motion within the pes during weight bearing.

In contrast to normal motion within the pes, abnormal motion secondary to disruption of the integrity of the pes is well reported and may occur secondary to fractures or ligamentous damage (Allen et al., 1993; Arwedsson, 1954; Barnes et al., 2013; Boudrieau et al., 1984a; Campbell et al.,

1976; Dyce et al., 1998; Lawson, 1960). These conditions will result in the failure of the pes to act as an effective lever arm and significant lameness will be observed. Whilst traumatic injury is the most common cause of loss of the integrity of the pes, degeneration of the plantar ligament may be responsible for subluxation at the level of the proximal intertarsal joint. The work in this thesis provides new insights into our understanding of the pathogenesis and principles of repair of subluxation of the proximal intertarsal joint.

1.1 Overview

Chapter 2 comprises a review of the published literature regarding various techniques that have been used to study kinematics in both humans and animals. The accuracy, convenience and limitations of these various methods are examined and discussed with respect to the aims of this thesis. The concept of limbs acting as biological springs is explored for dogs and related terrestrial mammals and the effect of disruption of the integrity of the pes is reviewed. The techniques, complications and outcomes associated with repair of the pes are evaluated, facilitating the development of the major research questions of this thesis.

Chapter 3 describes, in detail, the technique of computed tomography based kinematic measurement and investigates the effect of three different parameters on the calculated bone motion in and around the three cardinal axes. Based on the results of this chapter, a highly accurate protocol for measuring bone kinematics was developed and utilised in all subsequent chapters.

Chapter 4 describes the evolution and validation of a radiolucent limb loading jig that was capable of replicating both the major internal and external forces acting on the canine pes. A series of experiments were conducted to assess the ability of the jig to replicate the ground reaction force and joint angles previously measured in galloping dogs.

Chapter 5 utilises the limb loading jig and kinematic measurement techniques described in the previous chapters to characterise the motion that occurs within the pes during limb loading. The displacements of the individual tarsal and metatarsal bones are reported as six degrees of freedom as well as a summative total rotation around a single helical axis. The concept of interdependent, coupled motions between the individual bones was explored and a simplified model of the canine pes was proposed.

Chapter 6 examines the role the plantar ligament plays in maintaining the integrity of the canine pes. Following a description of the plantar ligament, the effects of sequential transection of this ligament on individual tarsal bone kinematics and force transmission through the pes are reported.

Chapter 7 investigates the effect of lateral plating of the pes following complete transection of the plantar ligament and subsequent proximal tarsal luxation. The effect on individual tarsal bone motion, kinematic coupling and force transmission through the pes was examined.

Chapter 8 summaries the most significant findings of this thesis and how they may relate to improving our understanding of the pathogenesis of various conditions and optimising strategies used to repair such conditions. Areas of future research are identified.

Chapter 2 Literature review

In human and veterinary medicine, improving clinical outcomes is the ultimate goal of many scientific investigations. However, in order to reach this point, considerable work must be directed towards understanding normal body function and the effect of injury or disease. Technological advances will often accompany improvements in our understanding of physiology and pathophysiology.

The following chapter is divided into five sections and follows the general pattern of this thesis:

- Section 2.1 will review the various techniques used to measure bone kinematics and evaluate the feasibility of using these techniques in the canine tarsus.
- Section 2.2 will appraise the literature regarding the role of the tarsal joints in locomotion in a variety of species, including the dog.
- Section 2.3 will describe the vital role of both bones and ligaments in the canine tarsus and the clinical effects of degeneration or trauma to bones and ligaments of the pes.
- Section 2.4 will evaluate the various surgical procedures and other treatments that have been described to treat ligament incompetence in the canine tarsus.
- Section 2.5 will describe the most significant elements of the review is identify the major purpose of this thesis.

Section 2.1: Kinematics

2.1.1 Introduction

Classical mechanics considers how various forces produce motion (Taylor, 2005) and when applied to living systems, this field in known as biomechanics. Biomechanical investigations have had great and widespread impacts, from improving athletic performance to increasing our understanding and ability to treat a variety of injuries and disease (Alexander, 2005). Kinematics is one branch of classical mechanics that refers to the study of the geometry of motion (Beggs, 1983), without regards to the forces that produced the motion.

Describing the complex and varied motion of living creatures has intrigued human kind for thousands of years. Since Aristotle wrote the first known scientific manuscript describing both human and animal motion (About the Movements of Animals) in approximately 350 B.C. (Nussbaum, 1978), subsequent investigators have utilised increasingly complex techniques to more accurately characterise both human and animal motion.

During the renaissance, Leonardo Da Vinci performed numerous dissections of cadavers to gain insight into the mechanism behind human motion. His work would be followed by the first anatomy text, "*De Humani Corporis Fabrica*" (1543) written by Andreas Vesalius, and the first publications applying mechanical theory to animal movement; Galileo Galilei's *De Animaliam Motibus* (The movement of Animals) and Giovani Alfonso Borelli's *De Motu Animalum* (On the Motion of Animals), published in 1680 and earning him the title "Father of Biomechanics"(Lu and Chang, 2012; Nigg and Herzog, 2007)

Later, technological advances would see the field of kinematics transition from observational reports to recorded measurements. In a major advance of the time, the brothers Wilhelm Eduard Weber and Eduard Friedrich Weber used a telescope, measuring tape and stopwatch to produce a more

objective assessment of gait, publishing their work as *Mechanik der Gehwerkzeuge* (Mechanics of the Human Walking Apparatus) in 1836 (Weber and Weber, 1992).

Jules Etienne Marey, in collaboration with his student, Gaston Carlet, used instrumented shoes to record the timing and force exerted during footfalls in the human and equine gait cycle (Carlet, 1872). The highly accurate mechanisms utilised in these studies allowed characterisation of higher speed gaits, that could not be previously evaluated based on observation alone (Baker, 2007). Despite accurately identifying the timing of ground contact, one limitation of these techniques was that they could not produce data relating to the displacement of various limb segments during the gait cycle.

The famous landscape photographer Eadweard Muybridge used his experience of photography to continue to develop techniques that would allow objective measurements to help characterise human and animal motion. In the late 19th century, he developed a technique that could capture sequential images using shutter speeds of 1/1000th second. (Shimamura, 2002). From these images, the position of the limbs and trunk in space at given points in time could clearly be seen.

Marey, a doctor by profession, continued to build on the work of Muybridge, after meeting with him in Paris in 1881. With a new student, Georges Demeny, Marey developed a new photographic technique, the chronophotograph, which produced multiple sequential images on the same photographic plate (Baker, 2007). However, one problem associated with these images was the ability to identify the same point in sequential exposures for measurement purposes. Their solution was to use markers which then made identification of landmarks and subsequent measurements easier and more accurate (Baker, 2007).

Although these advances marked a significant breakthrough in the ability to record motion in space, they were limited to measurements recorded in two dimensions. Otto Fischer and Willhelm Braune are credited with the first description of 3D gait analysis. (Baker, 2007). They utilised four cameras positioned around the subject to simultaneously record the position of the limbs, which were

modelled as rigid segments, in 3D space. (Medved, 2000). This highly accurate technique took 6-8 hours to collect the data, and several months of calculations (Medved, 2000), however, their published work, *Der Gang Des Menschen,* "the Human Gait", published in 1895 (Braune and Fischer, 2012) would lay the foundations for many future 3D studies of gait.

The challenges that plagued the early pioneers of kinematics, including recording at high speeds, identification of the same points in consecutive frames and recording motion in three dimensions, continue to confront today's researchers. Many of the innovative techniques these researchers developed to overcome these issues, such as ever faster shutter speeds, use of markers for landmark identification and stereophotography, are still used in modern techniques.

A full chronological review of all techniques developed and validated for kinematic measurement in various species is beyond the scope of this thesis, so the following section will review the most relevant techniques that have been described for use in human and animal gait analysis.

2.1.2 Modern techniques in kinematic investigations

The ideal technique used for kinematic investigations would be conducted in a live subject who is able to move unencumbered. It should allow accurate registration of the motion of the rigid components of the limbs, the skeleton, in real time in three dimensions without the need for invasive markers or instrumentation. In addition, the technique should be cost effective, convenient and able to be easily replicated in laboratories or clinical settings worldwide (DeCamp et al., 1993; Gillette and Angle, 2008; Tashman and Anderst, 2003). Although kinematic measurement techniques are constantly being improved and refined, all modern techniques still have some limitations which will be reviewed below:

2.1.2.1 Marker based kinematic techniques.

First pioneered by Marey in the late nineteenth century (Baker, 2007), the use of markers allows precise identification of the same point in sequential photographic or video images and has been used in both 2D and 3D kinematic measurements in animals (Agostinho et al., 2011; Feeney et al., 2007; Fu et al., 2010; Torres et al., 2010). There are several variables that must be considered when interpreting or comparing marker based kinematic studies including, the type of marker used, the mounting of the marker on the subject or specimen and the method of motion capture.

2.1.2.1.1 Types of markers

The role of markers in the earliest kinematic studies was to provide a convenient and reproducible means of identifying landmarks. For this reason, markers simply had to be a different colour to the background (Biewener and Blickhan, 1988). Although non-reflective markers are appropriate for manual identification, reflective markers and light emitting diode (LED) markers have become more popular as the landmarks can be accurately identified and registered by the motion capture devices (Gillette and Angle, 2008) allowing automated and real time kinematic results. However, these

studies must be conducted in a low light environment for optimal results. One potential limitation with LED markers compared to reflective markers is that the animal remains tethered to the computer system.

2.1.2.1.2 Mounting of markers

If the body is modelled as a series of rigid body segments (bones) that articulate at joints with a precise centre of rotation (linear-link model), then placement of a marker directly over the centre of rotation of the joint should produce highly accurate results (Fu et al., 2010). These are the assumptions made when single markers are placed over each articulation of the tri-segmented limb (Fischer and Blickhan, 2006), which divides the limb into the thigh, crus (or lower limb) and the pes (or foot). In many studies, the proximal segment (pelvis) is also included to allow measurements to be made about the coxofemoral (hip) joint (Agostinho et al., 2011; DeCamp et al., 1993; Holler et al., 2010; Hottinger et al., 1996).

There are a number of limitations with measuring kinematics using single skin markers positioned over the presumed centre of rotation. Firstly, the markers are firmly attached to the skin rather than the rigid skeleton, resulting in soft tissue artefact, which has been demonstrated in a number of species including dogs (Kim et al., 2011; Schwencke et al., 2012; Taylor et al., 2005). Soft tissue artefact may produce inaccuracy from the entire marker set shifting in unison or the inter-marker distance changing due to non-rigid movement and it can be challenging to differentiate between the two sources of error (Taylor et al., 2005). In a series of 4 Labradors, these inaccuracies were quantified by simultaneously performing fluoroscopy and motion capture using infrared cameras and reflective markers. The distance between markers varied from -18% to +6% and the displacement of markers from the bone landmarks ranged from 0.4-1.2cm (Schwencke et al., 2012). This change in inter-marker distance was also identified by (Kim et al., 2011), who went on to describe a repeatable pattern of inaccuracy. Some investigators of human kinematics have tried to

calculate an algorithm that can take this pattern into account and compensate for soft tissue artefacts therefore producing a more accurate reflection of the underlying bone motion (Leardini et al., 2005), however, unless patient specific patterns are determined and utilised, compensation methods are likely to be inaccurate.

Although increasing error is seen with increasing soft tissue coverage, kinematics of limb segments with minimal coverage, such as the ovine metatarsus, could still not be precisely reconstructed using skin markers alone (Taylor et al., 2005), suggesting that soft tissue artefact is extremely difficult to overcome with skin markers alone. Errors due to soft tissue artefacts have been shown to be far greater than error due to instrumentation (Leardini et al., 2005).

The second source of inaccuracy with skin mounted markers relates to the variation in application of the skin markers. Limb position during application was shown to significantly affect kinematic results (Kim et al., 2017), whilst in another study, kinematic results were different between different examiners using the same model (Torres et al., 2015), due primarily to variation in marker placement.

When evaluating 2D, sagittal plane kinematics, some joints, such as the talocrural joint, may have an axis of rotation that approximates a single point, over which a marker can be placed (Colborne et al., 2013). Other joints, such as the stifle joint, undergo a more complex motion comprising flexion and internal rotation (Evans et al., 2012), making the representation of the axis of rotation as a single point less appropriate. To overcome this issue, additional markers have been suggested to allow different models of the limb to be developed. The segmental model (Schwencke et al., 2012) uses at least two makers per limb segment which allows motion of each segment to recorded individually, whilst the joint co-ordinate system uses a cluster of markers which achieves a similar outcome (Torres et al., 2010). Although these models still suffer from soft tissue artefact, they also allow 3D recording of marker movement, allowing internal/external rotation and abduction/adduction to be recorded.

Invasive bone markers, which are directly implanted into bone, are an alternative to skin mounted markers and have been shown to more accurately represent the underlying bone motion (Benoit et al., 2006; Nester et al., 2007). There are limited reports of their use in dogs, where a reduction in ground force of up to 25% was observed (Korvick et al., 1994), prompting concerns regarding the effect of marker implantation on gait. Invasive markers have been utilised in several human cadaver studies (Hamel et al., 2004; Whittaker et al., 2011), where direct implantation of markers in not problematic and also in live subjects (Arndt et al., 2007; Lundgren et al., 2008; Wolf, 2006; Wolf et al., 2008), where they were used to measure the motion in the individual small, irregular bones of the tarsus, where surface mounted markers are not possible (Wolf et al., 2008).

2.1.2.1.3 Motion capture

Video cameras are used to track the motion of the reflective markers of pulsed LEDs which are attached to anatomical landmarks as described above. The motion capture system can directly measure the infrared light emitted from the LED marker or alternatively, infrared light can be emitted from around the camera, and the reflected light from the markers recorded (Gillette and Angle, 2008). The data are recorded as a binary code making direct and real time analysis possible, further reducing the incidence of errors in calculations, a far cry from the months of manual processing required by early investigators! (Baker, 2007). To avoid data loss through obscuring of markers during motion and to allow measurement of motion in three dimensions, most motion capture systems utilise multiple cameras positioned around the subject(Gillette and Angle, 2008). However, 2D motion capture systems have been shown to accurately describe sagittal plane motion in canine gait analysis despite being unable to record out of plane motion (Kim et al., 2008). When available, 3D motion capture provides investigators with the opportunity to more completely characterise kinematics, which commonly involves motions out of the sagittal plane (Agostinho et al., 2011; Fu et al., 2010; Torres et al., 2010).

2.1.2.2 Image based kinematic techniques

In order to overcome the problems of soft tissue artefact and other limitations of marker-based systems, some investigators have utilised image based kinematic techniques which allow direct visualisation of the skeleton. These techniques have utilised radiography, fluoroscopy, computed tomography (CT) and magnetic resonance imaging (MRI). Despite allowing direct identification of skeletal landmarks, these techniques still have limitations such as the time required to obtain a single image, dangers of irradiation and constraints of the imaging machinery. The following section will discuss the advantages and disadvantages of imaging based kinematic techniques.

2.1.2.2.1 Radiographic techniques

Radiography is readily available in veterinary practice and therefore represents a measurement technique that can be easily reproduced in large numbers of hospitals or research facilities around the world. Radiographs have been used to investigate normal kinematics, kinematics following disease conditions or injury and to quantify the effect of surgical repair on 2D kinematics in companion animal species (Kneifel et al., 2017; Reichert et al., 2013; Reif et al., 2002; Roe et al., 2008; Warzee et al., 2001).

Radiographs taken before and after the application of a load allows determination of displacement, which may be increased or decreased as a result of injury or disease. In joints that comprise multiple levels, such as the carpus and tarsus, radiographs allow determination of the level of injury, which may influence the selection of surgical procedure (Denny and Barr, 1991).

Radiographs have also been used to evaluate the kinematic effect of a number of surgical procedures, including tibial plateau levelling osteotomy (Reif et al., 2002; Warzee et al., 2001), tibial tuberosity advancement (Apelt et al., 2007; Hoffmann et al., 2011) and extracapsular repairs (Kneifel

et al., 2017). In these studies, radiographs were obtained following application of a simulated load to cadaveric limbs both before and after the procedure and have greatly improved our understanding of the effect of these interventions. More recently, weight bearing radiographs have been used to identify tibial subluxation as a measure of surgical success (Kim et al., 2012; Skinner et al., 2013).

Just as the addition of multiple cameras in motion capture has allowed measurements to be made in three dimensions, the addition of further x-ray sources can allow 3D measurements to be made using roentgen rays. First described in 1936, the practice of taking two simultaneous radiographic exposures with x-ray sources and films placed at 90 degrees to each other is known as radiostereometric analysis (RSA), and has been shown to be a highly accurate technique (Kärrholm et al., 2006; Kedgley et al., 2009).

Whether measurements are made in two or three dimensions, the ability to detect repeatable landmarks has a significant influence on accuracy. When phantoms consisting of three radio-opaque markers alone are used, RSA has been shown to be accurate within 0.032mm and 0.121 degrees (Kedgley et al., 2009). In clinical use, the implantation of radio-opaque tantalum markers has been shown to improve the accuracy of RSA as normal bony anatomy generally involves smoothed contours with a limited number of clearly defined points (Bottner et al., 2005). Fiduciary markers (Reichert et al., 2013; Warzee et al., 2001) or fitted geometric shaped (Kneifel et al., 2017) have been used to consistently identify radiographic landmarks and allow accurate measurement of bone kinematics in these veterinary radiographic based studies.

2.1.2.2.2 Fluoroscopic techniques

Like radiographic studies, fluoroscopic based kinematic measurements eliminate the problems associated with soft tissue artefact but can also record motion of the skeleton in continuous dynamic fashion. Traditional single plane fluoroscopy allows analysis in only two dimensions and is

prone to errors due to parallax error and motion blur (Prins et al., 2014; Tashman and Anderst, 2003; Wearing et al., 2005). This technique has been used to subjectively evaluate in vivo subluxation of the tibia during treadmill walking in dogs with cranial cruciate ligament disease (Rey et al., 2014).

As 2D kinematic techniques are rapidly becoming superseded, two fluoroscopic techniques have emerged that allow measurement of 3D kinematics using fluoroscopy (Miranda et al., 2011).

Firstly, biplanar fluoroscopy utilises the same principles as RSA, utilising two image intensifiers with an inter-beam angle of 60 degrees to accommodate the treadmill. With the use of implanted bone markers, this system has been shown to accurate to 0.064mm in translation and 0.31 degrees in rotation for dogs walking on a treadmill (Tashman and Anderst, 2003; Tashman et al., 2004) and 0.037mm for markers implanted in the porcine mandible (Brainerd et al., 2010) . When compared to static RSA and optical tracking, biplanar fluoroscopy showed comparable but slightly less accuracy than static RSA, however, both were superior to optical tracking (Kedgley et al., 2009).

More recently, marker-less biplanar fluoroscopy has been used in kinematic investigations, including studies of human tarsal bone motion (Ito et al., 2015; Ito et al., 2017; Kozanek et al., 2009; Wang et al., 2016). This technique has a distinct advantage over systems which require surgical implantation of bone markers, due to the fact it can easily be transitioned into the clinical setting. In this technique, the limb must undergo CT or MRI scanning to allow construction of 3D bone models which are then registered to the biplanar fluoroscopic images in a frame by frame manner, using an edge matching algorithm. The reported accuracy was a mean error of 0.27mm and 0.24 degrees in translation and rotation respectively for static testing. Dynamic testing produced slightly higher error (0.36mm and 0.42 degrees) and there was less accuracy with the more distal bones (navicular and cuboid bones) compared to the more proximal talus and calcaneus, which are less globoid in shape (Ito et al., 2015).

The second major fluoroscopic technique that can produce 3D kinematic data is 2D to 3D matching. This technique has now been reported in investigations of canine femorotibial kinematics (Jones et

al., 2014; Kim et al., 2015; Moore et al., 2016) and is very similar to the marker-less biplanar technique outlined above. A CT or MRI allows generation of 3D bone models, which are then fitted to the single fluoroscopic images in a frame to frame manner. (Moro-oka et al., 2008). When compared to marker based biplanar fluoroscopy, the results of 2D to 3D matching techniques using single plane fluoroscopy were comparable (Jones et al., 2014). This validation was performed using the femur and tibia which show little superimposition, however, further validation would be required for this technique when imaging anatomical regions where significant overlapping of bones occurs, such as the carpus and tarsus.

Like marker-based techniques, imaging based techniques can also suffer from instrument inaccuracy. Any fluoroscopic technique used must overcome the problem of distortion (Brainerd et al., 2010; Iaquinto et al., 2014) as it has been shown to be a major source of error if correct calibration is not performed prior to kinematic measurements (Baltzopoulos, 1995; Banks and Hodge, 1996).

2.1.2.2.3 CT based kinematics

The method of CT based measurement of bone kinematics is a non-invasive technique that has primarily been used to investigate the kinematics of the extremities in cadaveric (Leardini et al., 1999; Pfaeffle et al., 2005), and live patients (Beimers et al., 2008; Rainbow et al., 2013). More recently, this technique has been used to evaluate patients before and after surgical repair demonstrating its clinical application (Shores et al., 2013). Similar to other imaging-based techniques, it tracks the motion of the bones directly and therefore eliminates soft tissue artefact.

CT based measurement of kinematics is comprised of the following series of steps; Digital Imaging and Communications in Medicine (DICOM) image acquisition, threshold segmentation of the bones of interest, 3D reconstruction of a virtual bone model, alignment of bones within a global reference

coordinate system (for meaningful data presentation), and registration of bones between different scans (Moore et al., 2015). The accuracy of the measured kinematics could be potentially influenced by errors induced at any of these steps.

CT image acquisition requires exposing the subject to potentially damaging ionizing radiation (Pearce et al., 2012). In the absence of any data, the tendency is to acquire images at the highest possible resolution(Moore et al., 2015), which may increase radiation exposure by 30-50% (Nickoloff and Alderson, 2001), however, the effect of scan resolution on kinematic calculation is currently unknown.

Many segmentation protocols have been evaluated to assess their influence on the accuracy of the 3D reconstructions when compared to laser scanned bone specimens (DeVries et al., 2008; Gelaude et al., 2008; Rathnayaka et al., 2011; Van den Broeck et al., 2014), demonstrating that highly accurate reconstructions, with root mean square errors of less than one voxel size, are readily achievable. Reconstruction accuracy is of vital importance when the exact bone surface morphology is required, for example, in planning surgical procedures, designing custom implants or comparative anatomical studies. In these cases, segmentation technique, smoothing and scan resolution may all influence the accuracy of the 3D bone model (DeVries et al., 2008; Gelaude et al., 2008; Rathnayaka et al., 2011). However, the effect of changes to these parameters on calculated kinematics is yet to be determined.

Registration techniques used to detect bone motion must overcome the complex and variable geometry of bones. Placing radiopaque fiducial markers within bone (Ellis et al., 1996) reduces bone geometry to a series of points, whose location can be tracked in 3D space. Alternatively, radiopaque registration blocks can be rigidly attached to bone, allowing kinematic calculations to be performed on the geometrically simple block rather than the bone itself(Fischer et al., 2001). Registration techniques that rely solely upon the bone geometry are mathematically more expensive but have the advantage of being performed non-invasively. Inertia based techniques reduce bone geometry

to a point, the centre of mass, and the principle axes (Crisco and McGovern, 1997), which are then used to register bones(Crisco et al., 1999). Surface based registration (Besl and McKay, 1992; Pelizzari et al., 1989) matches the morphological features of the bone surface to register shapes to each other. Voxel based techniques (Marai et al., 2006; Snel et al., 2000) utilize the entire image data set for registration and, hence, are even more computationally expensive but do not require timely segmentation of every scan.

One limitation of the CT based techniques of kinematic measurement is the inability to record dynamic real time motion, due to the time required to acquire each image. Whilst concerns have been raised that results from static investigations may differ from dynamic studies (Wolfe et al., 2000), a number of investigators have demonstrated little difference when comparing results from static and dynamic measurements (Anderson and Pandy, 2001; Clément et al., 2014; Foumani et al., 2009; Mu et al., 2011; Saevarsson et al., 2013), suggesting that static measurements may be appropriate depending on the clinical question being asked.

Another limitation of CT based techniques is the size constraint imposed by the detector ring of the CT machine which is vital to image acquisition. This will continue to limit the use of this modality to anatomical regions that can be positioned within the machine.

2.1.2.2.4 MRI based techniques

Similar to CT scans, MRI scans produce tomographic images well suited regions of complex anatomy where significant overlapping exists (Udupa et al., 1998; Wolf et al., 2007) but can also be used to evaluate motion in soft tissue structures, such as the meniscus (Shefelbine et al., 2006). The technique for kinematic measurement is very similar to those outlined in the previous section with the major difference being that the MRI scan (rather than a CT scan) is used to create the 3D model (Patel et al., 2004).

2.1.2.3 Other techniques

Another approach to kinematic measurement is the application of wearable sensors that can produce real time, dynamic data that have been shown to be highly accurate (Cuesta-Vargas et al., 2010; Woodburn et al., 1999). One of the major advantages of these techniques is that they do not require imaging or video setups making clinical application far easier. Electromagnetic sensors are highly accurate (Duck et al., 2004; Hassan et al., 2007) but are prone to the same soft tissue artefacts as skin mounted markers if mounted non-invasively and may suffer from interference with other metals (Cuesta-Vargas et al., 2010). In the veterinary field, electromagnetic sensors have been used in cadaveric studies to accurately detect small changes in motion, however, direct application to bone is required (Aulakh et al., 2013; Bitton et al., 2013; Chailleux et al., 2007; Sidaway et al., 2004).

Unlike electromagnetic sensors, inertial sensors do not require tethering to a recording system and have been proposed as a convenient means of evaluating patient movement in a clinical setting for both human patients (Cuesta-Vargas et al., 2010; Mayagoitia et al., 2002) and canine patients (Duerr et al., 2016). These sensors show high levels of accuracy but are relatively large compared to reflective markers and may therefore not be practical to measure motion in all limb segments simultaneously, however, depending on the parameters being measured, inertial sensors show great promise in clinical setting in both the human and veterinary fields (Duerr et al., 2016). Due to their size and skin mounting, it is unlikely that these sensors are appropriate to measure canine tarsal bone kinematics.

2.1.3 Presentation and application of kinematic data

The previous section has reviewed the most common techniques used to acquire kinematic data, however, there are a number of ways that investigators may choose to present this data to provide meaningful information to their audience.

Initial investigations into canine kinematics, modelled the limbs as simple linear linkage models in two dimensions, producing intuitive results that described flexion and extension angles in the sagittal plane at various time points (Agostinho et al., 2011; DeCamp et al., 1993; Hottinger et al., 1996) . As 3D kinematics become commonplace, more complex patterns of motion emerge and a 3D description of motion must be provided (Fu et al., 2010).

Classically, 3D rigid body motion is described in relation to a series of three reference axes, all orientated perpendicular to each other. Any motion can therefore be resolved into a series of three translations along each axis and three rotations around each axis, known as 6 degrees of freedom motion (Fu et al., 2010). To produce more clinically relevant information, the axes are generally aligned to anatomical features of the specimen allowing translations and rotations to be described using conventional clinical terms such as flexion/extension and abduction/adduction (Wu et al., 2002). In the human literature recommendations have been provided that establish standard alignment of the reference axes to readily identifiable landmarks (Grood and Suntay, 1983; Wu et al., 2002; Wu et al., 2005). No such recommendations exist in the canine literature.

Although this approach accurately describes the various vector components of motion, it is subject to misinterpretation or inaccuracy if there is variability in the positioning of the reference axes or if motion is not well aligned to the reference axes (Sennwald et al., 1993). An alternative method to describe motion is to resolve all vectors into a single helical axis around which the rigid body rotates (Panjabi, 1979; Sennwald et al., 1993; Spoor and Veldpaus, 1980; Woltring et al., 1985). This single axis of rotation has been defined for some canine joints using kinematic measurements (Colborne et

al., 2013) and may contribute to refinement of surgical techniques such as hinged external skeletal fixators (Jaeger et al., 2005).

Furthermore, kinematic data may be combined with kinetic data to facilitate more complex modelling of limb function, such as inverse dynamics (Colborne et al., 2011; Colborne et al., 2005; Colborne et al., 2006; Headrick et al., 2014b), which derives values for work and power across each joint and may improve our understanding of locomotion and our ability to evaluate outcomes after surgical intervention (Headrick et al., 2014a; Ragetly et al., 2010).

The following sections further demonstrate how kinematic data can be applied to improve our understanding of normal locomotion, effect of injury or disease and refining and evaluating various repair techniques.

Section 2.2: Biological springs

2.2.1 Introduction

The legs of terrestrial animals are commonly described as biological springs, able to store elastic energy in the early stance phase only to return this elastic energy during take-off (Cavagna et al., 1977; Roberts and Azizi, 2011). In fact, the recorded energy consumption per unit distance travelled in the hopping kangaroo has been shown to decrease with increasing speed (Dawson and Taylor, 1973), whilst remaining constant in human running with increasing speeds (Cavagna et al., 1964), suggesting a significant amount of energy can be delivered at very low cost. It has been suggested that animals may conserve up to 50% of the energy that would otherwise be required did these mechanisms not exist (Alexander and Vernon, 1975; Cavagna et al., 1964). Numerous studies have been performed to detail the nature of these energy conservation mechanisms in a variety of species (Alexander, 1974; Alexander et al., 1982; Alexander and Vernon, 1975; Dimery and Alexander, 1985; Ker et al., 1987; Vereecke and Aerts, 2008) and in the following section, I will review the literature regarding what tissue characteristics and anatomical arrangements allow limbs to act in this fashion.

2.2.2 The components of biological springs

2.2.2.1 Energy storage in different musculoskeletal tissues.

The limbs of animals are comprised of several tissue types, all capable of storing elastic energy during the gait cycle. Energy can be stored through compression of tissue, as in articular cartilage, bending of tissues, as with bone, or it may be stored by stretching of tissue, as in tendons and ligaments (Alexander, 1984; Biewener and Blickhan, 1988). The amount of energy that can be stored in tissues relates to both the mechanical properties of the tissue itself and the anatomical arrangement of tissues.

Despite being a highly efficient means of energy storage (Silver et al., 2002), articular cartilage has limited capacity to store energy due to the fact that this layer is extremely thin (Alexander, 1984).

Bone is capable of storage of elastic energy, through both axial and bending loads (Biewener and Blickhan, 1988), however, the magnitude of deformation is small due to the tissue properties of bone and its contribution to energy storage is considered much less than that of other tissues (Alexander, 1984).

Although stated by some authors that ligaments may only store very small amounts of elastic energy (Alexander, 1984), biomechanical testing of various ligaments shows an repeatable and consistent ability to store elastic energy (Castile et al., 2016; Dommelen et al., 2006; Kwan et al., 1993; Smith, 1954) as the ligament deforms and then returns to its original shape. Smith (1954) highlights that it is this return to shape when a force is removed that characterises an elastic tissue and not the degree of extensibility when the force is being actively applied. The assumption that elastic energy cannot be stored in a structure that shows little extensibility may have led to the incorrect assumption that ligaments cannot store large amount of energy.

Indeed, less extensible structures (with fewer elastic fibres) have a higher capacity to store elastic energy compared to more extensible structures with a higher proportion of elastic fibres (Smith,

1954). Like many other musculoskeletal tissues, ligaments are viscoelastic, demonstrating different properties depending on the rate of loading (Provenzano et al., 2001). The degree of extensibility and ultimate strength of ligaments (i.e. their elastic limit) depends on numerous factors including anatomical location, dimensions, sex, age, body weight of the animal and post mortem storage technique (Matthews and Ellis, 1968; Provenzano et al., 2001; Smith, 1954; Viidik et al., 1965; Woo et al., 1981).

In general, ligaments are considered to display a non-linear viscoelasticity when a constant strain rate is applied. Initially, when a load is applied to a ligament, fibres straighten in a strain-stiffening fashion until they are no longer crimped creating the “toe” region of the stress strain curve. This is followed by a more linear segment of the curve as fibres elongate (Provenzano et al., 2001). If the load exceeds the elastic limit of the ligament, permanent damage to the structure is seen and results in a failure to return to the original shape (Smith, 1954).

Muscles and their tendons are capable of large amounts of elastic energy storage, with tendons shown to be highly efficient “springs”, able to return 93% of the work done stretching it and only dissipating 7% as heat (Alexander, 2002). However, within the body, there exists significant differences between the structural architecture of different muscles and their associated tendons that produce marked variation in their mechanical performance, a fact which has helped investigators determine the primary function of each of these muscles (Alexander, 1984; Goslow et al., 1981).

Muscles that have long fibre lengths and relatively short tendons are capable of significant shortening and hence produce the greatest movement of bones from which they arise and insert. The maintenance of tension in these muscles requires the continued application of energy. In contrast, other muscles display very short muscle fibres arranged within a pennate architecture and have markedly elongated tendons. (Alexander, 1984). This arrangement precludes significant shortening of these muscles, however, they are capable of maintaining tension with decreased

energy input when compared to muscles with longer fibres. The ratio of muscle fibre: tendon length has been suggested as a means of categorising the role that various muscles play in the body, with a ratio of > 0.4, considered to indicate the muscle acts as a "biological spring", capable of storage of large amounts of elastic strain energy (Williams et al., 2008).

2.2.2.2 Anatomic arrangement of tissues for energy conservation

The limbs of terrestrial mammals are generally modelled as a series of rigid segments which articulate at mobile joints (Fischer and Blickhan, 2006). These segments include the thigh (proximal limb between the coxofemoral joint and stifle joint), crus (distal limb between the stifle and hock) and the pes (foot), located between the hock and digits.

The relative size of each limb segment varies greatly between species, however, all limbs have surrounding musculature capable of extending and flexing each of the major joints (Fischer and Blickhan, 2006). Using many of the kinematic techniques outlined in the previous section, investigators have reported the displacement of each limb segment of quadrupeds, such as dogs and horses, at various stages of the gait cycle, revealing that flexion occurs at the stifle and hock when the foot contacts the ground, whilst the hip is flexed at foot contact and continues to extend during the stance phase of gait (Goslow et al., 1981; Gregersen et al., 1998; Walter and Carrier, 2009).

The muscles that extend the hip, the adductors and hamstrings have long parallel fibres. Throughout the stance phase of gait, these muscles actively shorten and therefore reduce the hip angle suggesting there is very little capacity to store energy within these muscles (Alexander, 1984).

The extensors of the stifle, the quadriceps, absorb energy as the animal lands and dissipates much of this as heat, with only small amounts stored as elastic strain energy in the relatively short patellar ligament. The fibres of this muscle are a combination of long parallel fibres and short fibres arranged in a pennate pattern, consistent with a minor role in elastic energy storage (Alexander, 1984).

In contrast, the extensors of the hock, the m. gastrocnemius and m. superficial digital flexor, have short fibres arranged in pennate fashion and elongated tendons suggesting an important role in elastic energy storage and the biological spring mechanism of the hind limb (Alexander, 1984). These muscles insert on the tuber calcanei, which is well developed in most digitigrade and unguligrade species, therefore providing a mechanical advantage when extending the hock or resisting flexion. Furthermore, the m. gastrocnemius was recorded to lengthen by 9% during the stance phase, whilst actively contracting, as demonstrated by simultaneous electromyographic recordings, providing additional data to support eccentric contraction, in which energy is stored for eventual release later in the stride (Goslow et al., 1981). In non-repetitive motions, such as jumping, the ability of the extensors of the hock to act as elastic springs has also been demonstrated (Alexander, 1974) and it has been suggested that the majority of the elastic energy storage in many species occurs in the distal limb (Alexander, 1984; Gregersen et al., 1998), however, it is important to recognise that the energy is stored within both the tendons and muscles, of which the latter originate from more proximal in the limb.

When Alexander and others used the camel to further investigate the role of tendon elasticity in locomotion (Alexander et al., 1982), they discovered that the tri-segmented limb model was inadequate to explain their observations and calculations regarding tendon lengthening. They concluded that the pes could not be modelled as a rigid beam and motion at the intertarsal and tarsometatarsal joint allowed for additional tendon lengthening and must be taken into account during kinematic calculations. In fact, the flexion of the intertarsal and tarsometatarsal joints, resulting in dorsiflexion of the pes could clearly be observed on high speed film, and was measured as approximately 17 degrees of flexion by the authors. It is important to recognise that this figure included motion at both the intertarsal and tarsometatarsal joints and no attempt was made to further divide flexion into individual joints.

Studies involving mechanical loading of the donkey pes (Dimery and Alexander, 1985) and the human pes (1987) have demonstrated that elastic energy storage during dorsiflexion is possible in these species and further questions the accuracy of calculations made when the pes is modelled as a rigid body. Although simplification of complex anatomy into more basic models may be advantageous in some situations, there is the risk of introducing an additional source of error when rigid body assumptions are violated (Nester et al., 2010).

2.2.3 The importance of the pes in canine locomotion

Canine kinematic investigations have most frequently modelled the canine hind limb as a tri-segmented model (Fischer and Blickhan, 2006) and this has contributed to valuable descriptions of normal and abnormal canine gait (Colborne et al., 2011; Colborne et al., 2005; Fischer and Blickhan, 2006; Fu et al., 2010; Gregersen et al., 1998; Hottinger et al., 1996; Walter and Carrier, 2009). Commonly, the canine pes (not including the phalanges) is modelled as the rigid beam of a lever, which rotates around the trochlea of the talus (the fulcrum) and plays a vital role in force transmission through the segment (Devas, 1961; Pratt, 1935)

The canine pes in not comprised of a single or paired continuous bone that span from proximal to distal articular surfaces, as seen in other limb segments, but rather this limb segment consists of the seven tarsal bones, four metatarsals and phalanges (Evans et al., 2012). These bones are arranged into irregular rows, with the talus and calcaneus comprising the proximal row. These bones are firmly united by proximal and distal talocalcaneal ligaments, which span the tarsal canal (Gorse et al., 1990). The motion between these bones has been described only as exceedingly rigid (Gorse et al., 1990) with these two bones almost morticed together (Carmichael and Marshall, 2013)

The distal row consists of four small bones. Three of the four bones (the first, second and third tarsal bones), are all positioned side by side and separated from the proximal row by the central tarsal bone, which is termed the navicular bone in human anatomy. The larger fourth tarsal bone, equivalent to the cuboidal bone in human anatomy, completes the distal and middle rows laterally, spanning the height between the calcaneus and metatarsals (Evans et al., 2012). (figure 2.1)

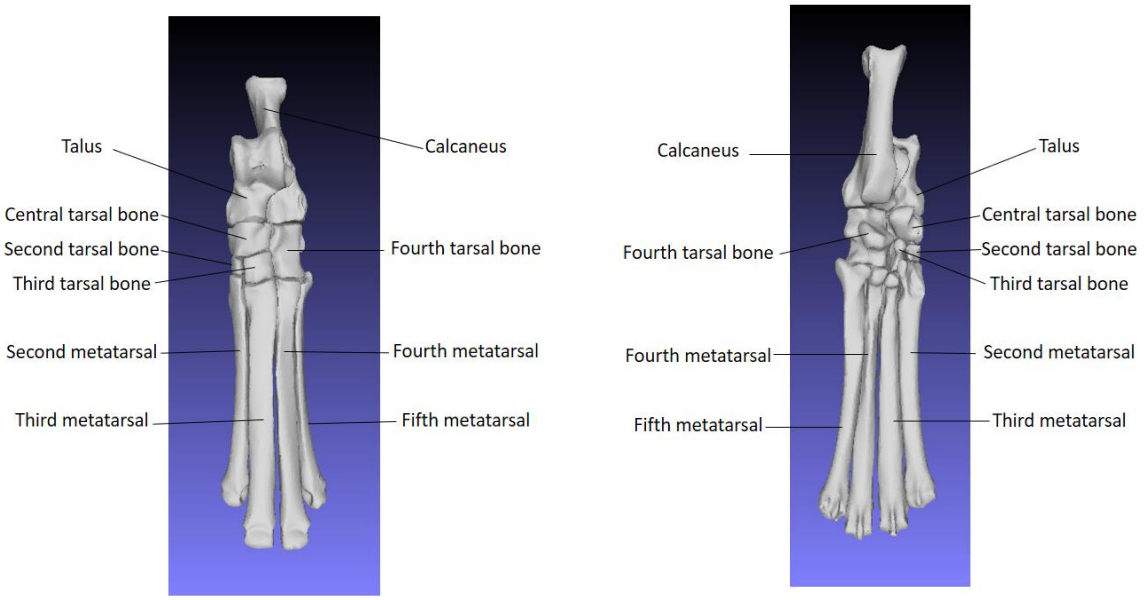

Figure 2-1: The bones of the tarsus are arranged in irregular rows as viewed from the dorsal surface (left) and plantar surface (right). The talus and calcaneous comprise the proximal row, whilst the distal row comprises the numbered tarsal bones. The larger fourth tarsal bone spans the distal and middle rows.

This complex arrangement of bones gives rise to a series of articulations within the pes (figure 2.2). The articulation between central tarsal bone and the talus is known as the talocentral joint, whilst the articulation between the calcaneus and fourth tarsal bone is known as the calcaneoquartal joint. Collectively, these two joints comprise the proximal intertarsal joint (Carmichael and Marshall, 2013). Recently, computed tomography has been used to further characterise the articulations of the tarsal bones (Galateanu et al., 2013) and demonstrated a consistent articulation between the plantar process of the central tarsal bone and a newly described articular process of the calcaneus, further emphasising the complexity of this series of articulations.

The series of articulations between the central tarsal bone and numbered tarsal bones distally is collectively known as the centrodistal joint and is bridged by the fourth tarsal bone laterally. The tarsometatarsal joint refers to the articulation of the numbered tarsal bones to their respective metatarsal bones (Evans et al., 2012).

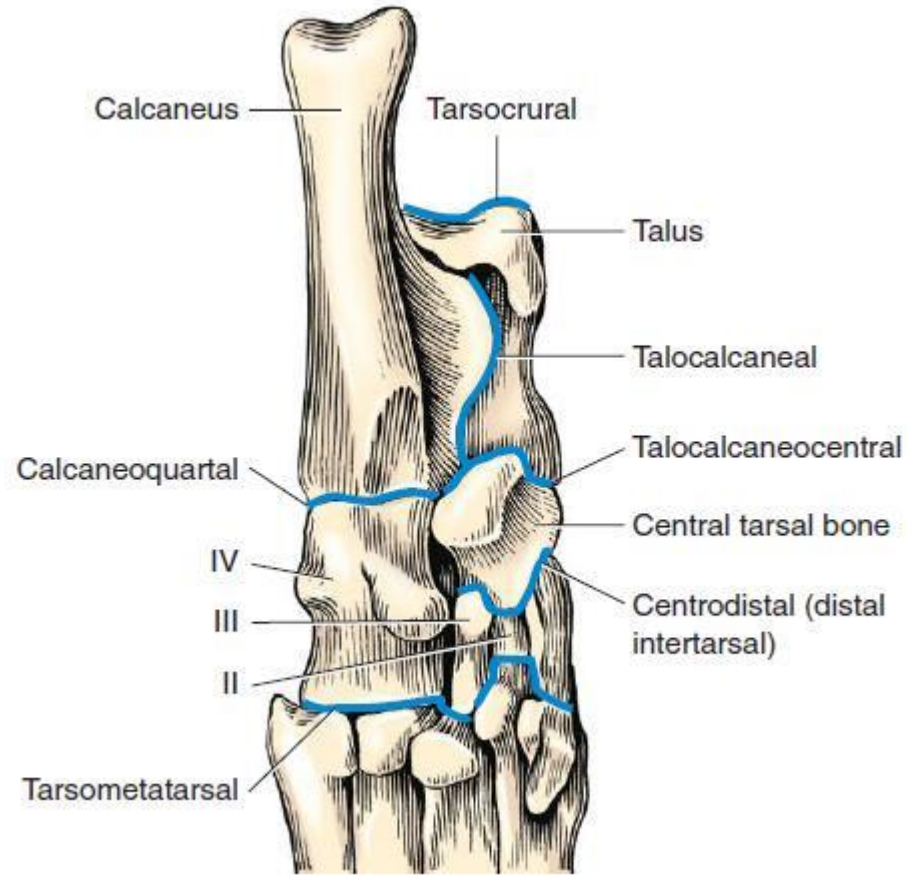

Figure 2-2: The tarsal joints, plantar aspect. IV fourth tarsal bone, III third tarsal bone, II second tarsal bone. From Evans HE, de Lahunta A, editor: Miller's anatomy of the dog, ed 3, Philadelphia, 1993, Saunders/Elsevier)

A vast array of dense connective tissue spans between the individual tarsal bones and adjacent bones and are responsible for imparting stability to this limb segment. The collateral ligaments of the high motion talocrural joint have been well described (Aron and Purinton, 1985a), with the function of each component identified through serial transection studies and subsequent assessment for stability (figure 2.3)

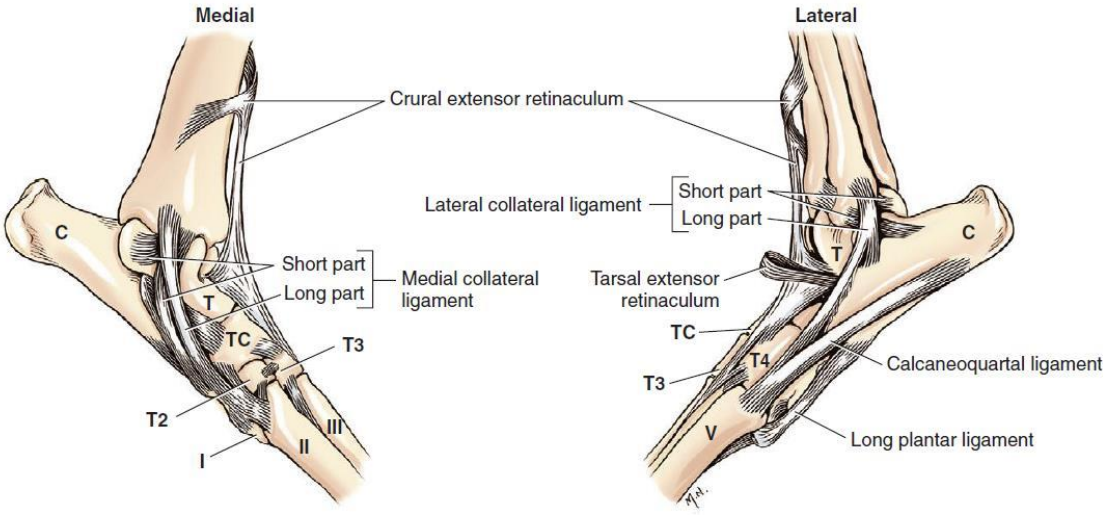

Figure 2-3: Medial and lateral ligaments of the tarsus. C, Calcaneus; T, Talus;T2,3,4, second, third, fourth tarsal bones; II to V, metatarsals. From Evans HE, de Lahunta A, editor: Miller's anatomy of the dog, ed 3, Philadelphia, 1993, Saunders/Elsevier)

A number of short ligaments connect the dorsal aspect of the individual tarsal bones and blends with the proximal transverse ligament of the tarsus, which serves to constrain the long digital extensor and cranial tibial muscles (Evans et al., 2012). On the plantar aspect of the pes, the ligamentous support is far more developed. The plantar ligament is divided into three major sections by some authors, whilst only two by others (figure 2.4)

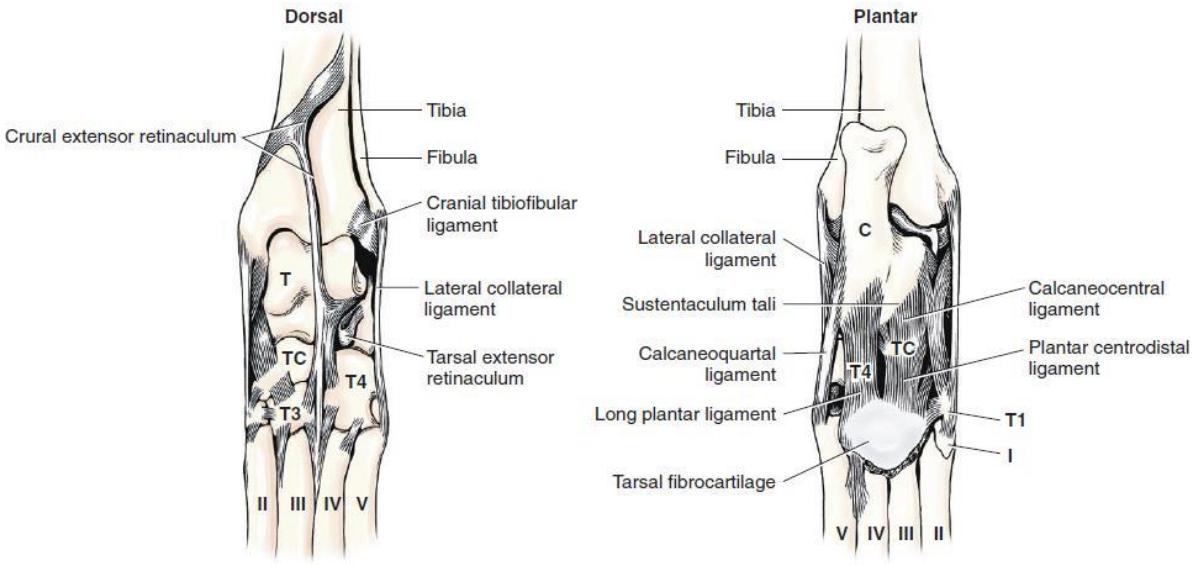

Figure 2-4: Dorsal and plantar ligaments of the tarsus. From Evans HE, de Lahunta A, editor: Miller's anatomy of the dog, ed 3, Philadelphia, 1993, Saunders/Elsevier)

The largest portion running from the plantar aspect of the calcaneus to the plantar process of the fourth tarsal bone, before continuing distally to insert on the thickened joint capsule of the tarsometatarsal joint, is known as the long plantar ligament (Evans et al., 2012) or middle plantar ligament (Carmichael and Marshall, 2013). On the medial aspect, another large ligament runs from the sustentaculum tali of the calcaneus to the plantar process of the central tarsal bone and is known as the calcaneocentral ligament (Evans et al., 2012) or medial plantar ligament (Carmichael and Marshall, 2013). The final component is a distinctive fibrous band, which has been termed the primarily tendinous muscle abductor digiti V by some authors (Arwedsson, 1954; Evans et al., 2012; Holt, 1974), whilst others have included this band as the third component of the plantar ligament, referring to it as the calcaneoquartal ligament (Evans et al., 2012) or the lateral plantar ligament (Carmichael and Marshall, 2013). I would suggest the nomenclature of Evans (2012) is more accurate as these terms are identified in the Nomina Anatomica Veterinaria (2012) and will therefore be used throughout this thesis.

The ability to identify the anatomical structures of the canine pes has been investigated using a number of imaging modalities including magnetic resonance imaging (Deruddere et al., 2014),

computed tomography (Deruddere et al., 2014; Galateanu et al., 2013) and sonography (Caine et al., 2009). The ability to accurately resolve and identify the bones of the canine tarsus are essential if imaging based kinematic measurements are to be employed as part of the study design.

Motion at the intertarsal and tarsometatarsal joints is well recognised in the dog (Evans et al., 2012), however, it has been widely ignored in many previous descriptions of canine gait (DeCamp et al., 1993; Fu et al., 2010; Walter and Carrier, 2009), leaving a substantial gap in our understanding of the role of the pes in the biological spring mechanism of the canine pelvic limb. This gap is one of the major motivations for this thesis, which aims to identify if dorsiflexion of the canine pes occurs during weight bearing, as in other species (Alexander et al., 1982; Dimery and Alexander, 1985; Ker et al., 1987) and characterise the kinematics of the canine tarsal bones which may facilitate any dorsiflexion.

Section 2.3: Pathological disruption of the canine pes

The biomechanical importance of the pes (not including the phalanges) as a "rigid" beam has been outlined in the previous section. The loss of integrity of this limb segment may occur after injury or disease that can affect any of the bones (Boudrieau et al., 1984a; Guilliard, 2010; Ost et al., 1987; Perry et al., 2017), ligaments (Allen et al., 1993; Barnes et al., 2013; Campbell et al., 1976; Holt, 1974) or tendons (Shani and Shahar, 2000; Worth et al., 2004) of the pes. A combination of ligamentous injury and fractures may also occur (Holt, 1974). The biomechanical implications of disruption will generally result in varying degrees of lameness, pain and dysfunction (Allen et al., 1993; Boudrieau et al., 1984a; Campbell et al., 1976).

The pathogenesis behind the conditions that result in loss of integrity of the pes varies widely. Some conditions, such as comminuted calcaneal fractures (Perry et al., 2017) and tarsometatarsal luxations (Fettig et al., 2002; Muir and Norris, 1999), are most commonly associated with major trauma whilst other conditions, such as proximal intertarsal luxations (Campbell et al., 1976) and transverse calcaneal fractures (Perry et al., 2017), are associated with no known trauma or more minor trauma. This likely represents two key mechanisms by which tissues are damaged; either a single supraphysiological force which exceeds the ultimate strength of tissues or a repetitive loading of tissue that produces gradual disruption of the tissues before fatigue failure occurs (George and Vashishth, 2005). Understanding the normal kinematics of the pes, as reviewed in the previous section, may provide valuable evidence to improve our understanding of the mechanisms behind both forms of failure but particularly those associated with fatigue failure. The link between stress fractures and different kinematic patterns has been shown previously in human runners (Dixon et al., 2006; Loudon and Reiman, 2012; Milner et al., 2010) and highlights the importance of kinematic investigations to improve our understanding of a number of disease processes across varying species.

2.3.1 Stress fractures and remodelling of the bones of the pes

Stress fractures most commonly affect the cortical bone of the diaphysis of long bones, such as the tibia (Bennell et al., 1996; Milgrom et al., 1985). However stress fractures may also affect the bones of the pes and have been reported in a number of species including humans (Bennell et al., 1996; Gross and Nunley, 2015; Pavlov et al., 1983), horses (Devas, 1967; Nunamaker et al., 1990) , cats (Cantatore and Clements, 2015; Perry et al., 2017) and dogs(Bergh et al., 2012; Boudrieau et al., 1984a).

Stress fractures are believed to be the result of an imbalance between bone damage due to an applied load and the body's ability to repair this damage (Warden et al., 2006). Microdamage has been shown to occur at loads well within the physiological range, and experimental data supports the hypothesis that microdamage stimulates osteonal remodelling (Burr et al., 1985). Although microdamage is often of little consequence as the body efficiently repairs this damage, certain extrinsic and intrinsic factors, may allow accumulation of microfractures, which may lead to complete fractures, known as stress fractures. (Warden et al., 2006).

Extrinsic factors are in the environment or external to the individual, including the type of activity and training patterns. Although stress fractures are associated with both high magnitude loads of short duration (sprinting) and low magnitude loads with high repetitions (endurance running), the site of stress fractures differ between these two different activities, reflecting the fact that stress fractures only occur at sites or repetitive mechanical loading. Sprinters exert greater force in their feet, increasing the incidence of tarsal and metatarsal fractures (Bennell et al., 1997), whilst endurance runners typically suffer from more proximal stress fractures (Bennell et al., 1996). Other extrinsic factors in humans include equipment and ground surfaces (Warden et al., 2006).

Intrinsic factors are those factors which influence how the individual responds to the applied load, including bone mass and size (Warden et al., 2005), with a small (less than two-fold) change in structural properties resulting in a greater than 100-fold increase in fatigue resistance.

Biomechanical factors are also considered intrinsic factors and have been associated with an increased incidence of stress fractures in humans. Although static measurements, such as longitudinal arch height have been shown to correlate with location of stress fractures in human runners (Simkin et al., 1989), it has been suggested that bone kinematics, measured by dynamic techniques, are more important as a risk factor for the development of stress fractures. In a cohort of military recruits, no difference in the incidence of metatarsal stress fractures was seen between groups based on static measurements of the foot, however, significant differences were seen between groups based on dynamic measurements of foot kinematics (Dixon et al., 2006).

A variety of stress fractures have been recognised in dogs (Boudrieau et al., 1984a; Gannon, 1972; Perry et al., 2017) and result in significant morbidity of the affected animals. Unsurprisingly, the most frequently affected canine breed is the greyhound, a canine athlete capable of attaining speeds of up to 72 kilometres per hour (Staaden, 1984), which subject their limbs to repetitive high magnitude loads during training and racing (Gannon, 1972). Stress fractures have been identified in a wide variety of bones including vertebrae, the acetabulum, long bones and the tarsal and metacarpal bones (Boudrieau et al., 1984a; Gannon, 1972; Wendelburg et al., 1988) and the pathophysiological mechanisms occurring in the dog are likely to mirror those in the human condition (Devas, 1961).

Like human athletes, the pes is the location of a large proportion of stress fractures (Gannon, 1972), reflecting the high loads experienced by this body segment. Although these fractures have been reported to affect a variety of different bones within the canine tarsus (Boudrieau et al., 1984a; Guilliard, 2007; Guilliard, 2010; Guilliard, 2000; Perry et al., 2017), stress fractures of the right central tarsal bone (Gannon, 1972), the equivalent to the human navicular bone (Devas, 1961), are most common.

The reason for this high incidence is unclear, however, it has been suggested that the central tarsal bone plays a critical “buttress” function within the pes, due to its central location, articulating with

all other tarsal bones (Evans et al., 2012; Galateanu et al., 2013). It has been assumed that the central tarsal bone is loaded in compression (Johnson et al., 2000) and is subjected to repetitive loads as the pes resists the bending moment that is applied during weight-bearing (Alexander, 1984). Bergh et al. (2012) used radiographs, computed tomography and histopathology to demonstrated that fractures of the central tarsal bones occur through sites of active remodelling, whilst Tomlin et al. (2000) used scanning electron microscopy of central tarsal bone fractures to show fractures occurred as the result of coalescing microdamage. Muir et al. (1999) also identified microdamage and remodelling histologically in a series of fractured central tarsal bones, further supporting the hypothesis that these are fatigue related stress fractures and damage is cumulative.

The relationship between biomechanical factors and the incidence of stress fractures is further strengthened when central tarsal bone fractures of racing greyhounds are examined. Greyhounds always run counter-clockwise around a circular or oval track, subjecting their limbs to asymmetrical loading patterns. The right central tarsal bone of racing greyhounds showed compaction of trabecular bone and increased bone mineral density compared to the left, demonstrating asymmetric adaptive remodelling occurs in racing dogs (Johnson et al., 2000). Fractures of the central tarsal bone occur through these regions of active remodelling (Bergh et al., 2012) with 96% of all central tarsal bone fractures occur on the right hand side (Boudrieau et al., 1984a). Although the adaptive changes and microdamage are typical of compression stress fractures, the kinematic patterns of the tarsal bones are yet to be characterised. Understanding tarsal bone kinematics may help identify kinematic patterns which are associated with a higher risk of development of stress fractures, as has been demonstrated in human studies (Dixon et al., 2006).

Stress fractures are also reported in other canine tarsal bones. Calcaneal fractures have been reported in racing greyhounds (Ost et al., 1987) and non-racing breeds of dogs (Perry et al., 2017). A comparison between the configurations in these two groups of dogs suggested that calcaneal fractures in racing greyhounds are more likely stress fractures, with a much higher incidence of

simple slab fractures and concurrent central tarsal bone fractures compared to non-racing dogs, which show a much higher incidence of mid body fractures, particularly with a comminuted configuration. Calcaneal fractures may also occur concurrently with central tarsal bone fractures. Here, it has been suggested that the central tarsal bone fracture occurs initially, exposing the calcaneus to altered loading patterns that result in calcaneal fractures (Ost et al., 1987). Calcaneal fractures are also reported in cats, with many cats showing simple transverse configurations and no known trauma, most consistent with stress fractures (Cantatore and Clements, 2015; Perry et al., 2017)

Fractures of the second, third and fourth tarsal bones are rare and most commonly associated with concurrent central tarsal bone fracture (Boudrieau et al., 1984a; Carmichael and Marshall, 2013). Guilliard (2010) reported 23 cases of third tarsal bone fractures in the greyhound, reporting clinical outcomes after treatment. Fragment removal was not recommended due to poor outcomes, presumably due to the loss of the buttress function, that is performed by all of the tarsal bones.

Fractures of the metatarsal bones have been reported in the racing greyhound (Gannon, 1972; guilliard, 2013) (Bellenger et al., 1981) and may also be related to fatigue failure with site specific asymmetric adaptive changes demonstrated in the meta bones of the racing greyhound (Johnson et al., 2001), consistent with asymmetric loading as discussed earlier.

2.3.2 Ligamentous injuries of the canine pes

Ligamentous damage within the pes has been reported in a wide variety of species including humans (Harris et al., 2017; Puthezhath et al., 2009), horses (Keller et al., 2015; McCormick and Watkins, 2014; O'neill, 2012), cats (Schmökel et al., 1994) and dogs (Holt, 1974).

In the dog, the tarsal ligaments span highly mobile joints such as the talocrural joint, but also joints that demonstrate little motion, such as the proximal intertarsal and centrodistal joints (Aron and Purinton, 1985a; Evans et al., 2012).

At the talocrural joint, ligaments complement the deeply contoured articular surfaces to restrain motion to a plane that is several degrees off the sagittal plane. A complex arrangement of ligaments ensures stability is maintained throughout the joint's entire range of motion (Aron and Purinton, 1985a).

Medially, the collateral ligament is comprised of a long component, which is taut in extension, a tibiocentral short component, which is taut in extension, and the tibiotalar short component, the largest component which is taut in flexion. Laterally, a similar arrangement is of three distinct bands is observed. The long component is taut in extension, whilst the calcaneofibular short component, which runs approximately perpendicular to the long component is taut in flexion. The third talofibular short component does not appear to change tension throughout the entire range of motion (Aron and Purinton, 1985a; Evans et al., 2012).

Ligaments that connect the individual tarsal bones have been described in the previous section and do not allow a large degree of motion across these joints, however, they play an essential role in allowing the pes to act as a lever that is capable of transmitting force through the limb segment (Devas, 1961; Pratt, 1935). Whilst compression occurs on the dorsal surface of the pes during weight bearing, structures on the plantar surface are placed under tension (Alexander, 1984), and this is

consistent with the relative size of the tarsal ligaments, which are well developed on the plantar surface and much less distinct on the dorsal surface (Evans et al., 2012).

Ligamentous injury to the canine pes most commonly is associated with major trauma and has the potential to affect any of the individual ligament.

Collateral ligament injury of the talocrural joint is generally associated with major trauma, such as road traffic accidents, and can affect any component of the ligament (Beever et al., 2016). Isolated injuries to the short lateral collateral components in six dogs have been reported (Sjöström and Håkanson, 1994) and required thorough palpation and radiographic evaluation to allow complete characterisation. The presence of small fragments by the lateral malleolus, suggests that many of these cases suffered avulsion injuries of the ligament. Due to the paucity of soft tissue coverage in the region, collateral ligaments may also be affected by shearing injuries, resulting in tissue loss and subsequent instability (Benson and Boudrieau, 2002; Diamond et al., 1999). Reconstruction techniques in these cases must consider the normal range of motion of this joint and also the different roles that each component of the ligament plays in maintaining stability (Aron and Purinton, 1985b; Holt, 1974)

Gorse et al. (1990) reported a series of 5 cases of talocalcaneal ligament rupture that resulted in talocalcaneal luxation. All dogs had experienced some known trauma to damage the proximal and distal talocalcaneal ligaments that the authors described in the anatomical component of their study. This luxation has also been reported by other authors (Holt, 1974; Hurter et al., 2004; Lawson, 1960), who similarly report major trauma as the cause of ligamentous injury.

Proximal intertarsal subluxation has been widely reported, with some authors reporting that it accounts for one third of all hock lesions diagnosed in their hospital population (Campbell et al., 1976). It represents instability at one of the two transverse joints of the pes, whose joints extend across the entire width of the pes. The proximal intertarsal joint comprises the combined talocentral joint and calcaneoquartal joints (Carmichael and Marshall, 2013), and is equivalent to the transverse

tarsal joint, also known as the mid tarsal joint or Chopart's joint in humans (Kelikian and Sarrafian, 2011). The second transverse joint of the canine pes is the tarsometatarsal joint, which includes the combined articulations of the metatarsal bones with their respective numbered tarsal bones (Evans et al., 2012). The centrodistal joint is an incomplete transverse joint as it is bridged laterally by the large fourth tarsal bone (Evans et al., 2012) and this was suggested by Muir and Norris (1999) as the reason that injury at this level is extremely uncommon. Currently only one report exists that describes lameness attributed to disease at this level (Guilliard, 2005).

Although their clinical presentation may be similar, there are a number of differences between the proximal intertarsal luxations and tarsometatarsal luxations. Perhaps the most significant of these is the fact that tarsometatarsal luxations are most commonly associated with major traumatic events (Campbell et al., 1976; Muir and Norris, 1999), often seen in other ligamentous injuries of the hock and pes, whilst proximal intertarsal subluxations are most commonly associated with minor or no known trauma (Allen et al., 1993; Campbell et al., 1976).

Proximal intertarsal luxation was first described by Lawson (1960), who described 5 cases that comprised of a mixed population of dogs, some with no known trauma and others who suffered known trauma such as a road traffic accident. Later, larger case series have been published and identified a marked breed predilection for Shetland sheepdogs and Collie breeds. Campbell et al. (1976) reported 44 cases of proximal intertarsal subluxation, of which 22 (50%) were Shetland sheepdogs and a further 10 were Collie and Collie X breeds. Females were overrepresented with an average age of onset of 7.8 years. Over 54.5% of dogs had no known history of trauma, 20.5% had minor trauma and the remaining 25% has known major trauma including dog bites and road traffic accidents. Allen et al. (1993) reported 39 proximal intertarsal luxations in 36 dogs, with 18 (50%) Shetland sheepdogs and a further 7 Collies or Collie crosses. Once again, minor trauma or no known trauma was commonly reported in the Shetland sheepdogs. Barnes et al. (2013) also identified a predilection for these breeds with Shetland sheepdog comprising 25 of 74 procedures and Collies

and Collie crosses comprising 27 or 74 procedures, however, these authors did not report the entire clinical history associated with these cases. Shetland sheepdogs and Collies appear consistently in smaller case reports (Dieterich, 1974; Fettig et al., 2002; Wilke et al., 2000).

Although some cases of proximal intertarsal luxation may be purely related to major trauma, the majority appear to be related to ligament degeneration. It remains unclear why there is an over-representation of Collies and Shetland sheepdogs in this population and although most authors state that that the loss of plantar support is required for proximal intertarsal luxation, Barnes et al (2013) identified that which specific components of the plantar ligament that must degenerate to result in subluxation remains unknown. Whilst some authors suggest that the primary joint instability occurs at the calcaneoquartal joint (Welch, 2003), others have recognised that the entire proximal intertarsal joint is commonly affected (Barnes et al., 2013).

Specific ligament degeneration has been previously investigated in the dog, with cranial cruciate ligament disease the most investigated. In these cases, degenerative changes and unsuccessful repair attempts have been demonstrated histopathologically (Comerford et al., 2011; Vasseur et al., 1985). Similar to the signalment of dogs suffering plantar ligament degeneration and proximal intertarsal luxation, dogs identified with cranial cruciate ligament rupture demonstrate a predilection for certain breeds (Duval et al., 1999; Whitehair et al., 1993; Witsberger et al., 2008), ages (Duval et al., 1999; Whitehair et al., 1993; Witsberger et al., 2008) and in some cases, sex and neuter status (Comerford et al., 2011; Duval et al., 1999; Whitehair et al., 1993; Witsberger et al., 2008).

In humans it has been shown that hormonal status may affect the incidence of non-contact anterior cruciate ligament rupture in women (Renstrom et al., 2008). In addition, different breeds of dogs have been shown to have marked variation in morphology of the proximal tibia (Vedrine et al., 2013; Wilke et al., 2002), which may have significant biomechanical impacts upon the cranial cruciate ligament (Guerrero et al., 2007; Inauen et al., 2009b), leading to an increased likelihood of rupture.

Although most of the proximal intertarsal injuries result in plantar ligament disruption, damage to the dorsal ligaments have also been reported (Voss et al., 2004).

Tarsometatarsal luxations also result in a plantigrade stance and may not be easily differentiated from intertarsal luxations from examination alone. These injuries are widely reported in the veterinary literature and are commonly the result of major trauma, such as road traffic accidents and getting the pes caught in a gate or fence whilst jumping (Campbell et al., 1976; Chow and Balfour, 2012; Dyce et al., 1998; Muir and Norris, 1999; Shani et al., 2006). This injury is the result of damage to the thickened joint capsule of the tarsometatarsal joints, known as the plantar fibrocartilage, which is the point of insertion of the plantar ligament. There may also be concurrent tarsal bone fractures (Dyce et al., 1998; Muir and Norris, 1999), which is unsurprising given the aetiology of this injury. Similar to proximal intertarsal luxation, most injuries affect the plantar structures of the tarsometatarsal joint, however, dorsal luxations are also reported (Dyce et al., 1998; Inauen et al., 2009a). The significance of this difference shall be discussed further in the following section, which will review repair techniques.

Section 2.4: Stabilisation techniques following disruption to the pes

Disruption of the pes, secondary to bone fracture, ligamentous injury or a combination of both will have significant effect of distal limb biomechanics, often resulting in debilitating lameness and pain. The literature reporting various repair techniques and outcomes will be reviewed in the following section.

2.4.1 Repair following fracture

2.4.1.1Calcaneal fractures

Fractures of the body of the calcaneus prevent normal force transmission from the common calcaneal tendon through the pes and are most commonly treated with surgical repair. The calcaneus experiences large bending forces and repair techniques must be able to combat these bending loads. Simple fractures have been successfully treated with a pin and tension band wire, whilst comminuted fractures generally require bridging fixation with bone plates and screws (Perry et al., 2017). Perry et al. (2017), reported fewer complications associated with plate fixation compared to pin and tension band wire repairs, however, the configuration of fractures differed between groups as is commonly seen in retrospective studies. Other authors have also suggested poorer clinical outcomes compared to racing greyhounds with calcaneal fractures (Ost et al., 1987).

2.4.1.2 Talar fractures

Fractures of the talus are rare and may affect any aspect of the bone. Articular fractures should aim to reconstruct the articular surface (Carmichael and Marshall, 2013), whilst good results have been achieved using a unilateral trans-articular external skeletal fixator in a small number of cats with fractures through the neck or head (McCartney and Carmichael, 2000)

2.4.1.3 Central tarsal bone fractures

As detailed in the previous section, the central tarsal bone is the most commonly fractured tarsal bone and these fractures are believed to be related to fatigue failure. Five patterns of central tarsal bone fracture have been recognised (figure2.5), with 75% type IV (dorsal and medial slab fractures) or type V (comminuted) (Boudrieau et al., 1984a).

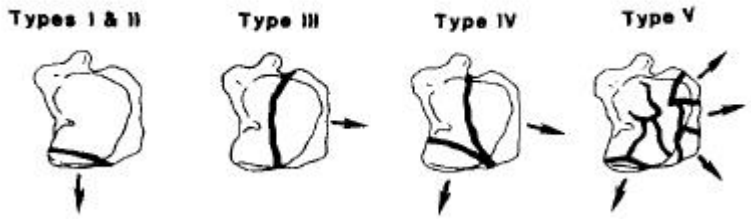

Figure 2-5: The five patterns of central tarsal bone fractures as described by Boudrieau et. al 1984a

Displaced fractures or fracture luxations (Guilliard, 2007) both result in collapse and hyperextension of the pes, due to the loss of the buttress function of the central tarsal bone, which may also lead to secondary fourth tarsal bone or calcaneal fractures. Reconstruction of the central tarsal bone is therefore desirable to re-establish the buttress role of the bone and hence integrity of the pes and also to maintain congruity of the articular surface. Lag screws are generally recommended to reconstruct the central tarsal bones following type I-IV fractures (Boudrieau et al., 1984b; Guilliard, 2007; Guilliard, 2000; Hudson and Pozzi, 2012), with good clinical results reported. Type V (comminuted) fractures cannot be accurately reconstructed and external coaptation is generally recommended at it subjectively produces acceptable clinical function, however, the chances of a return to racing are minimal (Carmichael and Marshall, 2013).

2.4.1.4 Numbered tarsal bone fractures

The principles of surgical repair of the numbered tarsal bone are very similar to those of the central tarsal bone with the numbered tarsal bones also playing a vital buttress function within the pes

(Carmichael and Marshall, 2013). Fractures of these bones are rare (Guilliard, 2010) and generally involve a dorsal slab fracture which can be reduced and stabilised with lag screws.

2.4.2 Repair following ligamentous injury or degeneration

In contrast to repairs of the talocrural joint, where repair techniques aim to preserve the original range of motion (Aron and Purinton, 1985b), repair techniques for instability of the more distal joints; talocalcaneal, proximal intertarsal and tarsometatarsal joints generally involve sacrificing any motion in favour of promoting a bony arthrodesis.

2.4.2.1 Talocalcaneal luxations.

Gorse et al (1990), reported 5 cases of talocalcaneal luxation secondary to rupture of the talocalcaneal ligaments. Three of the five cases were treated with a screw positioned from talus to calcaneus in a lag fashion. One of the two remaining dogs had the luxation stabilised by two figure-of-eight wires and the final case was treated external coaptation alone. All but one dog, which developed a post-operative infection had a good clinical outcome. A single case was reported by Lawson (1960), who used a similar technique but additionally debrided the articular surfaces between the two bones. In another case series, two of three dogs were treated with a single talocalcaneal lag screw, and one with coaptation alone producing satisfactory results (Campbell et al., 1976).

2.4.2.2 Proximal intertarsal luxations

Non-surgical management of proximal intertarsal luxations with rest and anti-inflammatories (Campbell et al., 1976; Dieterich, 1974) or external coaptation (Lawson, 1960) have produced poor clinical outcomes and are therefore not currently recommended.

Although it appears that most proximal intertarsal luxations affect both the talocentral and calcaneoquartal joint (Barnes et al., 2013), it has most commonly been recommended to provide stability across the calcaneoquartal joint alone (Allen et al., 1993; Campbell et al., 1976). Due to the lack of any biomechanical data to support this recommendation, it is likely that this practice is based on clinical outcomes from limited numbers of dogs in the previously reported case series.

Although debridement of articular cartilage is a common feature between previous reports, it is unclear as to what extent that the cartilage must be removed. Whilst it has been recommended to remove the articular cartilage of both the calcaneoquartal joint and talocentral joint by some authors (Dieterich, 1974; Lawson, 1960; Whittick, 1975), others have suggested this is unnecessary (Allen et al., 1993; Campbell et al., 1976).

Following debridement, rigid stabilisation must be provided across the calcaneoquartal joint to promote arthrodesis. Broadly speaking, stabilisation techniques fall into two categories; bone plate application and intramedullary techniques that utilise a pin or screw positioned through the longitudinal axis of the calcaneus and into the fourth tarsal bone. Tension band wires have been inconsistently applied in reported case series to help resist the bending load endured by the pes.

The earliest report of calcaneoquartal arthrodesis (Lawson, 1960) reports removal of articular cartilage from the opposing surfaces of the talus, calcaneus, central tarsal bone and fourth tarsal

bone with a Volkmann curette. A “reverse nailing” technique was described which involved drilling from the articular surface of the calcaneus in a proximal direction, before inserting a large screw from proximal to distal through the calcaneus and into the fourth tarsal bone. A good outcome was reported in all cases, except one case which died 11 days post operatively. A similar technique was used by (Campbell et al., 1976) in the majority of their cases, however, a screw length was chosen to deliberately engage the metatarsal bones distally, although it was noted that on many occasions the screw passed between these bones. A poorer outcome was seen in dogs who had the calcaneoquartal joint stabilised with a smooth pin and tension band wire. Screw failure was seen in two cases; breakage in one case where no attempt was made to remove articular cartilage and bending of a screw in another. This highlights the large bending forces that implants are subjected to.

In another large case series, Allen et al. (1993) utilised four techniques, including a single Steinmann pin alone, a laterally applied 2.7mm bone plate, a Sherman screw and tension band techniques, which were supported by either a Steinmann pin, Sherman screw, two Kirschner wires. The overall rate of successful arthrodesis was 85% and no significant difference was observed between all techniques, however, some groups had only one animal. This finding was in contrast to that of Campbell et al. (1976), however, like this study, implant failure was also recognised with breakage of two screws and one Steinmann pin. None of these cases were protected with a tension band wire, suggesting that a tension band wire may help combat some of the bending forces on the repaired limb. Loosening of implants were seen in 2 cases and calcaneal fractures reported in a further 2 cases. The clinical results, evaluated by client questionnaires, revealed 81 % of dogs were completely sound, whilst 19% showed a mild weightbearing lameness.

Subsequent case series commonly utilise bone plate fixation to stabilise the calcaneoquartal joint and may provide improved stability when compared to the pin and screw techniques, which cannot provide rotational stability to the same extent as plate fixation. Adequate stability is essential to

promote bone formation across the arthrodesis site, which will reduce the risk of cyclic failure of the implants. (Fettig et al., 2002; Roch et al., 2008; Scrimgeour et al., 2012; Théoret and Moens, 2007) all report the use of laterally applied bone plates which span across both the calcaneoquartal and tarsometatarsal joints. Application onto the lateral surface of the pes, results in the plate being loaded “on edge” as the pes acts as a lever (Devas, 1961). This significantly increases the area moment of inertia of the implant, reducing the risk of implant deformation.

Whilst (Fettig et al., 2002) recommended a minimum of three screws in the calcaneus and metatarsals when a hybrid plate was used, none of the other authors provided any recommendation regarding the configuration of plate stabilisation when attempting to achieve bony union across the calcaneoquartal joint. Examination of radiographic images from these papers, clearly identifies a lack of consistency across studies where lateral plates are applied. One case presented by (Fettig et al., 2002) shows no screws engaging the fourth tarsal bone, whilst another case by the same authors was performed with a single screw positioned in the fourth tarsal bone that also engaged the central tarsal bone on the medial aspect of the joint. The radiographic images of (Scrimgeour et al., 2012) demonstrate another variation, with two screws engaging the fourth tarsal bone. No comparison of these various configurations is currently available, however, it is likely that changes in plate and screw configuration may influence the biomechanical performance of the construct as seen in other scenarios (Field et al., 1999; Törnkvist et al., 1996). The construct configuration is likely influenced by a number of factors including patient size, plate size and design, underlying pathology and surgeon preference.

Comparison of clinical outcome following lateral plate repair of calcaneoquartal arthrodesis is difficult due to the variable outcome measures used by authors. Fettig et al. (2002) reported good outcomes in 4/4 cases and (Théoret and Moens, 2007) reported good outcomes in 2/2 cases based on owner assessment, whilst (Roch et al., 2008) evaluated complications, reporting major complications in only 1/11 cases treated with a lateral plate and this was related to sepsis, with no

cases showing implant or bone failure. (Scrimgeour et al., 2012) looked at return to work as a measure of successful surgery in a series of 14 working dogs with lateral plate repair of either proximal intertarsal luxation or tarsometatarsal luxation. In this case series, 50% of working dogs were able to return to full work duties, whilst 4/14 were able to perform most of their duties. The remaining 3 dogs were unable to return to work following surgery.

Another plating approach described to combat the bending load on the pes, is plantar plating (Wilke et al., 2000). Here, the plate is located on the biomechanically favourable tension surface of the bones and the authors report a good outcome in 3 dogs, one dog with objective force plate data that showed no difference in kinetic parameters between the affected and unaffected limb 7 months post operatively.

Recently, a large retrospective study (Barnes et al. 2013) was published with the objective to compare complications and outcomes of calcaneoquartal arthrodesis following one of three stabilisation techniques; laterally applied bone plate and a figure of eight tension band combined with either a pin or a screw.

This multicentre study reported 74 procedures, performed in 61 dogs with 58 procedures in the plate group, nine procedures in the pin group and seven procedures in the screw group. Consistent with previous reports (Allen et al., 1993; Campbell et al., 1976), implant failure was identified in both the pin and screw group with breakage, bending and loosening all identified, however, implant failure was also identified in the plating group, which has not been previously reported in case series of lateral plate fixation (Fettig et al., 2002; Roch et al., 2008; Théoret and Moens, 2007). In the study of Barnes et al. (2013), screw loosening was seen in five cases, four involving the fourth tarsal bone and one involving a screw positioned across multiple metatarsals. Metatarsal fractures (3 cases) and implant failure (2 cases) were also reported and previous unreported complications. This study represents the largest collection of cases of calcaneoquartal arthrodesis following non traumatic disruption of the plantar ligament in dogs to date and concluded that lateral plating was associated

with fewer complications compared to screw and pin techniques (Barnes et al., 2013). No attempt was made to evaluate variables related to the configuration of the implants, such as the number of plate screws used in each bone or the engagement of metatarsal bones in the pin and screws groups and therefore no recommendations regarding configuration could be provided.

Dorsal instability at the proximal intertarsal joint is less commonly reported than plantar instability in dogs (Campbell et al., 1976; Voss et al., 2004)and these two conditions differ biomechanically as dorsal luxations are likely to be reduced during weight bearing, whilst plantar luxations show increasing displacement. (Voss et al., 2004) report a case series of 10 dogs and 3 cats treated with dorsal splinting of the affected joints without debridement of articular cartilage to promote permanent arthrodesis. Locking plate systems were used in these cases, with good results in 12/13 cases. Joint fusion was identified in 3 cases and two cases suffered from implant breakage, but without affecting outcome.

2.4.2.3 Tarsometatarsal instability

Instability at the tarsometatarsal joint has been treated in a similar fashion to proximal intertarsal luxations, with removal of articular cartilage, application of autogenous cancellous bone graft and stabilisation with internal or external fixation to promote tarsometatarsal arthrodesis.

Campbell et al. (1976) suggested that better outcomes were achieved with lateral plate fixation compared to compression screwing, wiring and pin-casts, with many of these other techniques technical challenging to achieve. Good outcomes have been reported in a number of small case series that were stabilised with lateral plates in a similar fashion to proximal intertarsal luxations. Dyce et al. (1998) reported a good outcome in 11/11 procedures where a lateral plate was applied to a subluxated tarsometatarsal joint. Arthrodesis was promoted and achieved in all cases, with 9/11 procedures involving concurrent tarsal or metatarsal fractures. Similar results were reported by Muir and Norris (1999) who performed plate stabilisation of the tarsometatarsal joint subluxation in 8 dogs, 6 of which has concurrent fractures. No implant breakage was recorded. However, due to the

retrospective nature of these studies no attempt was made to standardise plate configuration making it difficult to provide any recommendations regarding the ideal plate size, screw number and screw length. As for calcaneoquartal arthrodesis, these is variable engagement of the fourth tarsal bone, with some cases receiving two screws in the fourth tarsal bone, whilst others received a single screw. Screw length also varied in these case series with variable engagement of the third or central tarsal bone on the medial aspect of the pes.

Chow and Balfour (2012) reported a series of 12 dogs and 2 cats that all achieved successful tarsometatarsal arthrodesis following removal of articular cartilage and stabilisation with 4 intramedullary pins driven from the individual metatarsal bones into the proximal and distal rows of tarsal bones. The authors suggest, that although the intramedullary pins violated the distal articular surface of the metatarsals, they provided the benefit of avoiding difficulty in skin closure, as may be seen with plate repairs. Pin migration and breakage were seen with single pins, however, the remaining 3 pins in each case remained intact and a successful arthrodesis was achieved.

External skeletal fixation has also been described as a method of fixation to achieve arthrodesis across the tarsometatarsal joint. Halling et al. (2004) described three cases of tarsometatarsal stabilisation performed with a circular external skeletal fixator with good results. The mean time before fixator removal was prolonged (16 weeks), however long term function was good in all cases. A single case report has described the use of an external skeletal fixator, to provide stabilisation across the tarsometatarsal joint without debridement of the articular surface, resulting in ankylosis across these joints. Although good long term clinical function was reported based on owner assessment, complications were experienced in all 4 cases.

Section 2.5 Purpose

From this review of the current literature, it is clear that the canine pes plays a vital role in locomotion and can be damaged through both injury or disease. Despite long recognising that motion does normally occur within the pes, facilitated by intertarsal bone movement, there is a lack of understanding regarding the role this motion may play in normal locomotion. Furthermore, no descriptions of the nature of intertarsal bone motion during weight bearing have been published. This may reflect the technical challenges posed by attempting to record small magnitudes of motion in overlapping cuboid bones that are moving at great speed.

Plantar ligament degeneration has been proposed as the underlying cause of proximal intertarsal subluxation in dogs and despite highly detailed anatomical descriptions of the components of plantar ligaments, the role these ligaments play in maintaining the integrity of the pes remains unknown. Furthermore, recommendations for surgical repair to re-establish the integrity of the pes following injury or disease are based on small, retrospective case series, which report a wide variety of surgical techniques and implants employed to re-establish force transmission through the canine pes.

These gaps in our collective knowledge have been the motivation for this thesis, which sets out to develop new approaches to measure tarsal bone kinematics in the dog, allowing insights into the cause of clinical conditions, such as proximal intertarsal subluxations, and facilitating evaluation of surgical procedures, which have been suggested as the most appropriate means of treating such conditions.

Chapter 3 A computed tomography-based technique for the measurement of canine tarsal bone kinematics

Chapter 3 represents work that has been published as

"Influence of Scan Resolution, Thresholding, and Reconstruction Algorithm on Computed Tomography-Based Kinematic Measurements" Christopher John Tan, William C. H. Parr, William R. Walsh, Mariano Makara and Kenneth A. Johnson. *J Biomech Eng* 139(10), 104503

doi: 10.1115/1.4037558

Abstract from published paper

Radiographic data, including CT and planar x-ray, are increasingly used for kinematic studies in humans and animals. There is a tendency towards using as high resolution imaging as possible. Higher resolution imaging is one factor (in conjunction with the reconstruction algorithm) which may increase the accuracy of reconstructed 3D surface models in representing true bone shape. However, to date no study has tested the effects of scan resolution, threshold and 3D model reconstruction algorithm on the accuracy of bone kinematic results. The present study uses a novel method to do this where canine tarsal bones were positioned on a radiolucent Lego™ board and scanned before and after undergoing known translations and/or rotations. The DICOM images were acquired using two different CT scanning resolutions and processed using three different segmentation threshold levels and three different reconstruction algorithms. Using one bone as the reference bone, an iterative closest point (ICP) algorithm was used to register bones to a global co-ordinate system and allow measurement of other bone kinematics in terms of translations and rotations in and around the x, y, z axes. The measured kinematics were compared to the 'known' kinematics, which were obtained from the Lego™ board's manufacturing standards and tolerances, to give accuracy error metrics for all bones. The results showed error in accuracy of measured kinematics was at sub voxel levels (less than 0.5mm). Despite altering the volume and surface area of the 3D bone models, variation in resolution, segmentation threshold and reconstruction algorithm had no significant influence upon the accuracy of the calculated tarsal bone kinematics.

3.1 Introduction

The field of kinematic analysis of bones has expanded in recent years with the advent of non-invasive, novel surface matching techniques. Biplanar fluoroscopy techniques, such as X-ray Reconstruction of Moving Morphology (XROMM) (Brainerd et al., 2010), can be used to calculate in-vivo kinematics with high degrees of accuracy. However, one limitation of 2D to 3D matching systems is combatting the challenges posed by complex joints, such as the wrist and ankle, where there is considerable overlapping of bones (Ito et al., 2015).

For these regions, multiple CT scans have been employed to calculate bone motions between 'static states', for example, at their extreme range of motion (Beimers et al., 2008; Pfaeffle et al., 2005), or before and after surgical intervention. Similar to biplanar fluoroscopy, non-invasive surface matching techniques can be employed to identify the positions of the bones in the different CT scans and hence, record their motion. Surface matching requires generation of 3D models of bones, which can be generated from the CT data using a number of different techniques and settings.

There is a tendency to acquire CT images at the highest possible resolution (Moore et al., 2015) to create highly accurate 3D models, which increases exposure to potentially damaging radiation by 30-50% (Nickoloff and Alderson, 2001).

To date, no study has evaluated the effects of different CT scanning protocols and 3D surface model reconstruction parameters on the accuracy of the kinematic results obtained from CT data. If kinematic accuracy is unaffected, then increasing scan resolution (to increase 3D bone reconstruction precision), with inherent increased radiation exposure, may be unwarranted. The following experiment aims to test if scan resolution and techniques used for generating 3D bone models will influence accuracy of kinematic calculations. It was hypothesised that the variations in scan resolution, threshold levels and reconstruction algorithm will have no significant influence on the accuracy of calculated kinematics when settings are consistent between scans.

3.2. Materials and methods

3.2.1 Specimens

11 canine tarsal bones with soft tissues removed were individually mounted onto plastic building bricks (Lego® brick, Lego, Billund, Denmark) with double sided padded mounting tape (scotch-mount, 3M, Pymble, Australia) and polypropylene adhesive film (ConTact, Pomona, CA). The dimensions of the building bricks were measured using calipers accurate to 0.02mm (Mitutoyo 530-122, Japan).

All brick-bone constructs were positioned onto a rigid, plastic board (Lego®, Billund, Denmark), which had two vertical plates attached perpendicularly to the board, and one another (figure 3.1a). This configuration permitted translation and rotation around and along each (x,y,z) axis. With a reported manufacturing tolerance of 5 microns (Corbet, 2008), this building block system can produce accurate and repeatable movements of building blocks.

3.2.2 Image acquisition

A CT scan of the board with 11 brick-bone constructs was performed using a 16 slice helical CT scanner (Philips Brilliance 16-slice CT scanner). The board was scanned at “high” resolution (120KVP, 117 mA, slice thickness 1mm, slice increment 0.5mm, , 512 X512 matrix, pixel size 0.36mm X 0.36mm) and again at “low” resolution (120KVP, 117 mA, slice thickness 2mm, slice increment 1mm, 512 X512 matrix, pixel size 0.77mm X 0.77mm). These scans were designated as “before” scans.

The brick bone constructs were re-arranged on the board (figure 3.1b). The right calcaneus (reference bone) was not moved. The right fourth tarsal bone (negative control) was removed from the board, then replaced in its identical location and orientation. The remaining 9 bones underwent a known translation, rotation or both together as outlined in table 3.1.

The board was rescanned again using both “high” and “low” resolution, designated as the “after” scans.

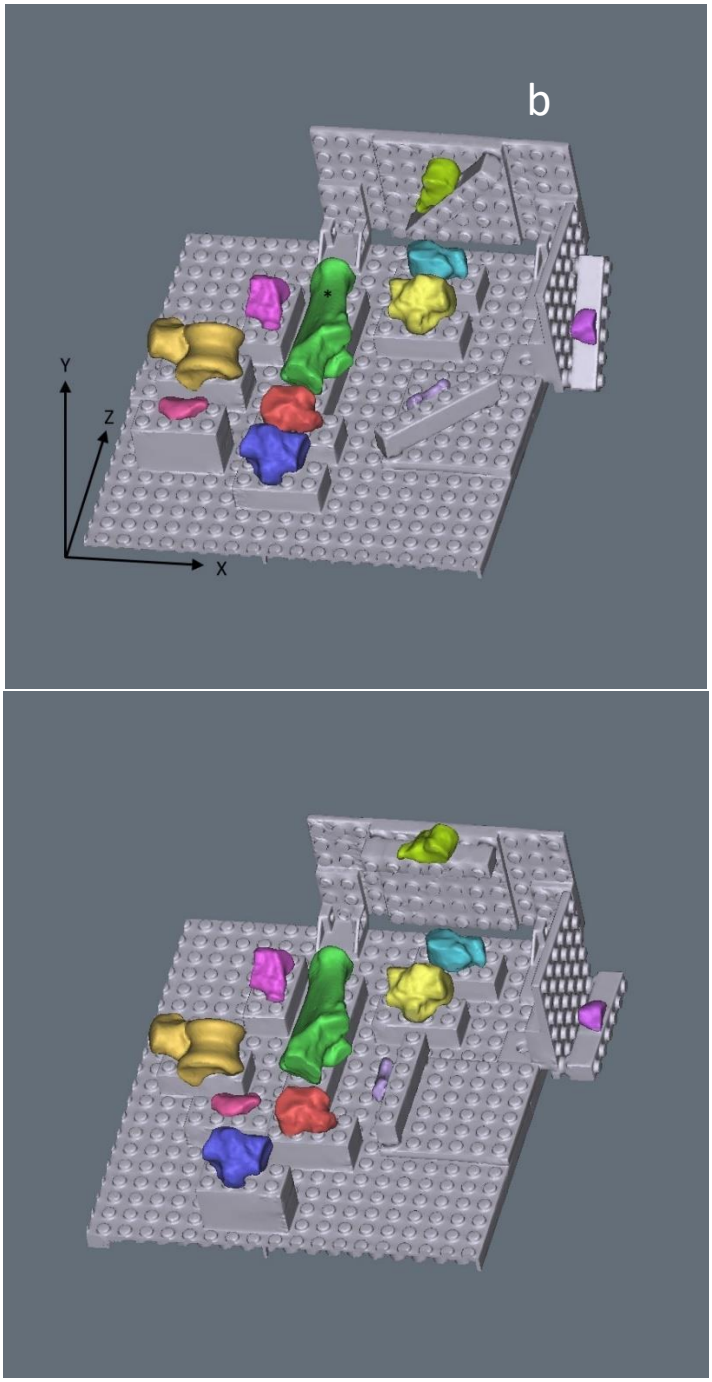

Figure 3-1: Position of the eleven bones during the “before” scans (a) and “after” scans (b). All motion is described relative to the reference bone, the calcaneus (*). The direction of motion is described relative to the global co-ordinate axes shown.

Table 3-1: Known magnitude and direction of the translation or rotation of each bone. CTB = central tarsal bone

Bone	Motion	Direction (axis)	Movement	Distance/angle
Right fourth tarsal bone	None			
Left CTB	Translation	X	1 stud across	8.00mm
Left Talus	Translation	Y	1 plate down	3.20mm
Right third tarsal bone	Translation	Z	1 stud across	8.00mm
Right CTB	Translation	X	1 stud across	8.00mm
	Translation	Y	1 plate up	3.20mm
	Translation	Z	1 stud across	8.00mm
Left fourth tarsal bone	Translation	X	1 stud across	8.00mm
	Translation	Y	1 brick up	9.60mm
	Translation	Z	2 studs across	16.00mm
Left first tarsal bone	Translation	X	2 studs across	16.00mm
	Translation	Y	1 brick up	9.60mm
	Translation	Z	1 stud across	8.00mm
Left second tarsal bone	Rotation	X		45 degrees
Right first tarsal bone	Rotation	Y		45 degrees
Left third tarsal bone	Rotation	Z		45 degrees

3.2.3 Segmentation and 3D surface model generation

DICOM images were imported to Mimics (version 17.0, Materialize, Belgium) and each bone segmented using three different Hounsfield unit (HU) threshold levels. Based on a previous pilot study, segmentation performed with 900HU as the threshold, produced a 3D bone model with a volume most similar to that of the actual bone, whilst a segmentation threshold of 500HU produced a 3D bone model with a smaller volume that the original bone a smaller representation. Segmentation with a 1300HU threshold, produced a 3D bone model with a larger volume than the original bone. For each threshold level, three 3D surface models were created using pre-defined marching cubes reconstruction algorithms: “high” accuracy, “optimal” accuracy, “optimal” accuracy with subsequent smoothing. The “high” accuracy setting applies a matrix reduction and applies 2 iterations of a 0.5 weighted 1st order Laplacian smoothing algorithm and 10 iterations of an advanced edge mesh reduction algorithm (tolerance = 0.05mm, edge angle = 10^{o}) to the 3D boundary mesh resulting from the interpolation of the segmented CT slices. The “optimal” accuracy setting applies no matrix reduction and 2 iterations of a 0.3 weighted 1st order Laplacian smoothing algorithm and 3 iterations of an advanced edge mesh reduction algorithm (tolerance = 0.0559mm, edge angle = 10^{o}). The third model was generated using the “optimal” mesh generation setting followed by application of 2 iterations of a 0.5 weighted 1st order Laplacian smoothing algorithm.

For each 3D surface model, the centre of mass, volume and surface area were recorded.

3.2.4 Initial alignment to a global co-ordinate system

A two-step alignment of ‘before’ and ‘after’ scans was performed prior to kinematic calculations. In the first step, “before” and “after” scans were manually aligned to the global co-ordinate system in 3-matic 8.0 (Materialize, Belgium) so that the edges of the Lego® board aligned with the X, Y and Z axes. In this regard, movement of the Lego® bricks between “before” and “after” scan positions occur along and around the axes of the global co-ordinate system.

3.2.5 Calculation of kinematics

For each bone, the movement between the “before” and “after” scan positions was determined 18 times by a single observer: once for every combination of the predictor variables (scan resolution, threshold level and smoothing protocol). Bone motion was reported in relation to a single reference bone (right calcaneus).

The second stage of alignment aligned the “after” scans with the “before” scans. This was performed using the open source program Meshlab (Cignoni et al., 2008). The right calcaneus from the “before” scan, the Lego board of which was aligned with the global coordinate system in the first step (described above), was set as the base mesh.

From the “after” scan, the surface meshes of the right calcaneus and the bone of interest were combined to form a single 3D “shell” of two parts (right calcaneus and the bone of interest).

An Iterative Closest Point (ICP) algorithm (Besl and McKay, 1992)was then used to superimpose the calcanei of the two scans. This step achieved two important objectives; 1) to align the two scans, minimising error due to movement of the reference bone between scans and 2) to align the scan to a meaningful reference coordinate system.

The position of the 3D surface model of the bone of interest from the “before” scan was then recorded as the “before” position. Again, using a rough manual alignment followed by an ICP alignment, the 3D surface model of the bone of interest was superimposed on the combined meshes of the “after” scan. The new position of the 3D surface model of the bone of interest was then saved as the “after” position. Using this method, the identical 3D surface model was recorded in both the “before” and “after” position allowing a transformation matrix, consisting of a translation matrix (mm moved in the global x,y,z coordinate system) and rotation matrix (rotations around the global coordinate system x, y, z axes) to be calculated (figure 3.2).

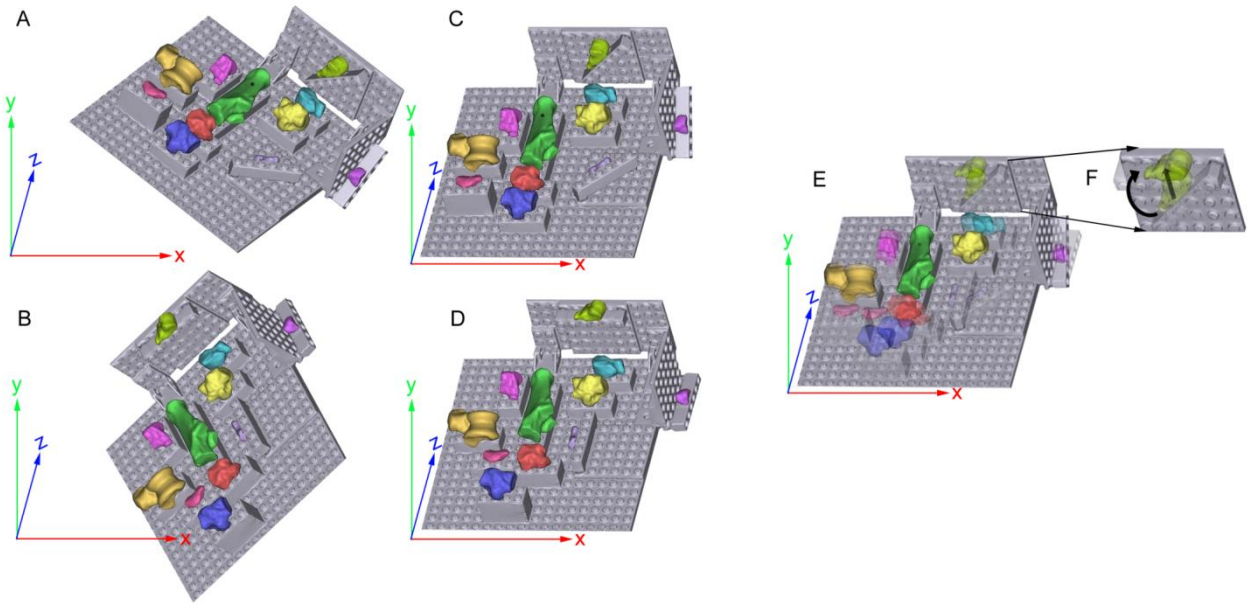

*Figure 3-2: workflow for the scan alignment and calculation of bone kinematics. Initial isosurface reconstructions of the lego boards with bones in the two positions are not aligned with the global coordinate system or one another (A and B). The first step is to align the "before" scan with the global coordinate system (C). The "after" scan is also roughly aligned with the global coordinate system (D). The second stage of alignment uses an ICP algorithm to minimise translational and rotational differences between the scans using the calcaneus (green bone with * shown) of the "before" scan as the fixed entity and superimposing the calcaneus in the "after" scan along to this. The remainder of the "after" lego board and bone models are moved with the "after" calcaneus, but do not influence the alignment (E). The "before" model for each bone is then aligned (again using ICP alignment) with the "after" position and saved separately from the "before" model in the "before" position (F). Thereby, the same 3D model is stored in both "before" and "after" positions.*

The translation matrix is calculated by calculating difference between the centroid (mean of all 3D coordinate points in the mesh) of "before" and "after" 3D surface model positions. The rotation matrix is calculated in two steps: 1) removing translational differences between the two models by centering both models at the global coordinate system x, y, z, 0, 0, 0 position and 2) using a Singular Value Decomposition algorithm (using the the QR algorithm with Given's rotations (Golub and Kahan, 1965))implemented in Mathematica (version 10.1, Wolfram, IL, USA) to calculate the rotation matrix that rotates the 3D surface model from "before" to "after" orientation. The rotation matrix was then decomposed into the rotations occurring around the global coordinate system x, y, z axes.

The error in kinematic measurement was calculated for each rotation and translation by subtracting the measured value (acquired from the transformation matrix decomposition) from the known value (calculated from the building brick dimensions in table 1).

3.2.6 Statistical analysis

All statistical analyses were performed using the commercially available statistical package Genstat (VSNi, Hemel Hempstead, UK). Descriptive data was performed for the measurement error, including maximum error, mean, median, and variance. Data were checked for normality using the Anderson-Darling test before further analysis. For each bone, a general mixed linear model was used to evaluate the effect of scan resolution (high/low), threshold level (500,900,1300HU), reconstruction algorithm (high/optimal/additional smoothing) and axis (x/y/z) on the outcome variables. The measured outcome variables were 3D surface model parameters (co-ordinates of the centre of mass, model volume and surface area) and the measurement error. Values of $p<0.05$ were considered significant. Rotations were known for all bones and included in the calculation of rotational error. For bones undergoing rotation, a translation would necessarily have occurred. The translation of the centre of mass of these bones between the “before” and “after” scans was calculated along the x, y and z axes, however, as the true magnitude of the translation could not be deduced before the scans, the three bones that underwent rotation were excluded from the calculation of translational error.

3.3. Results

3.3.1 Measurements of the Lego® brick and calculation of 'known' bone motions

The dimensions of a Lego® brick were measured (brick height 9.60mm, plate height 3.20mm and the distance between studs 8.00mm). Table 1 demonstrates the known motions of each bone in the study, based upon the measurements of the Lego® brick dimensions.

3.3.2 Influence of scan resolution, thresholding and smoothing on 3D surface model parameters

For each bone, there was no significant difference in the location of the centre of mass between 3D surface model models created using different scan resolution, threshold or smoothing protocols. In all bones, increasing the threshold level and increasing smoothing reduced both volume and surface area of the 3D surface model (figure 3.3).

3.3.3 Magnitude of error in calculated kinematics

For the control fourth tarsal bone, which was removed and replaced in the same location and orientation, the mean error in calculated translation was 0.02+/- 0.02mm, 0.03+/- 0.02mm and 0.04+/- 0.01mm along the x,y and z axes respectively. The mean error in calculated rotation was 0.04+/- 0.05^0, 0.05+/- 0.04^0 and 0.03+/- 0.03^0 around the x,y and z axes respectively

For all bones collectively, the mean error in calculated translation was 0.06+/- 0.06mm, 0.07+/- 0.06mm and 0.07+/- 0.06mm along the x,y and z axes respectively. The mean error in calculated rotation was 0.29+/- 0.36^0, 0.25+/- 0.35^0 and 0.32+/- 0.38^0 around the x,y and z axes respectively (Table 3.2).

Full results are available in Appendix A

Figure 3-3: Effect of scan resolution and smoothing on visual appearance of 3D surface model of canine calcaneus segmented with a threshold of 900HU. Top: 3D surface models generated from high resolution scans and "high" quality model generation (left), "optimal" quality model generation (centre) and "optimal" quality model generation and additional smoothing (right). Bottom: 3D surface models created from low resolution scans and "high" quality model generation (left), "optimal" quality model generation (centre) and "optimal" quality model generation and additional smoothing (right).

Table 3-2: Descriptive data for the calculated error in translation and rotation

	Translation error (mm)			Rotation error (degrees)		
	x	y	z	x	Y	Z
Number of measurements	126	126	126	180	180	180
Mean	0.06	0.07	0.07	0.29	0.25	0.32
Median	0.04	0.05	0.05	0.17	0.10	0.17
Maximum	0.27	0.25	0.27	2.44	1.48	2.22
Lower quartile	0.01	0.02	0.03	0.06	0.04	0.07
Upper quartile	0.09	0.10	0.11	0.38	0.27	0.35
Standard deviation	0.06	0.06	0.06	0.37	0.35	0.38
Variance	0.00	0.00	0.00	0.14	0.12	0.15

3.3.4 Influence of scan resolution, thresholding and reconstruction algorithm on kinematic accuracy

For each bone, there was no significant difference in kinematic accuracy between scans performed at low or high resolution. Similarly, segmentation threshold level had no significant effect on the accuracy of kinematic calculations for both high and low resolution scans. The three different reconstruction algorithms used to generate the 3D surface models had no significant influence of kinematic accuracy for either high or low resolution scans or any of the different segmentation threshold levels.

3.4 Discussion

The ICP (surface morphology based) registration method used in this study showed a high level of accuracy when measuring bone motion using a variety of canine tarsal bones. The results are comparable to previous studies (Crisco et al., 1999; Pfaeffle et al., 2005) although quantitative comparisons of results is difficult due to variations in the methods used and metrics reported. Accurate detection of small motions may be vitally important in the diagnosis of conditions such as joint instability and in the evaluation of post-operative range of motion, particularly in multiple level joints, such as the carpus and tarsus, where palpation and radiographs alone may be inadequate.

Higher scan resolutions, with reduced voxel size, may make subsequent bone segmentation simpler, but will increase the radiation exposure. Patel et al. demonstrated a nominal increase in error with increased pitch using tissue-based classification registration (Marai et al., 2006). The experiment performed in this chapter, using a 16-slice CT scanner and surface-based registration method, demonstrated no decrease in kinematic accuracy with lower resolution scanning, suggesting that a reduction in radiation exposure may be possible when measuring kinematics alone. However, when investigating kinematics in a conscious patient, the scan acquisition time (determined by number of slices the CT machine may obtain per revolution) may also play a significant role in kinematic accuracy as motion artefact may impact kinematic accuracy.

Formation of the 3D bone models from the multiple DICOM images produced from the CT scan involves segmentation of the bone of interest and generation of a surface, which is subsequently used for kinematic calculation. Segmentation can be performed by manual pixel selection but generally semi-automated segmentation is utilized to increase the efficiency of the process. Altering threshold segmentation levels had a significant influence on surface area and volume; however, it had no effect on the accuracy of measured rotations and translations, presumably as the effect of thresholding level is uniform across the entire surface of the bone (figure 3.4). When kinematics

alone are calculated, thresholding may be set at the level which allows most efficient segmentation of bone.

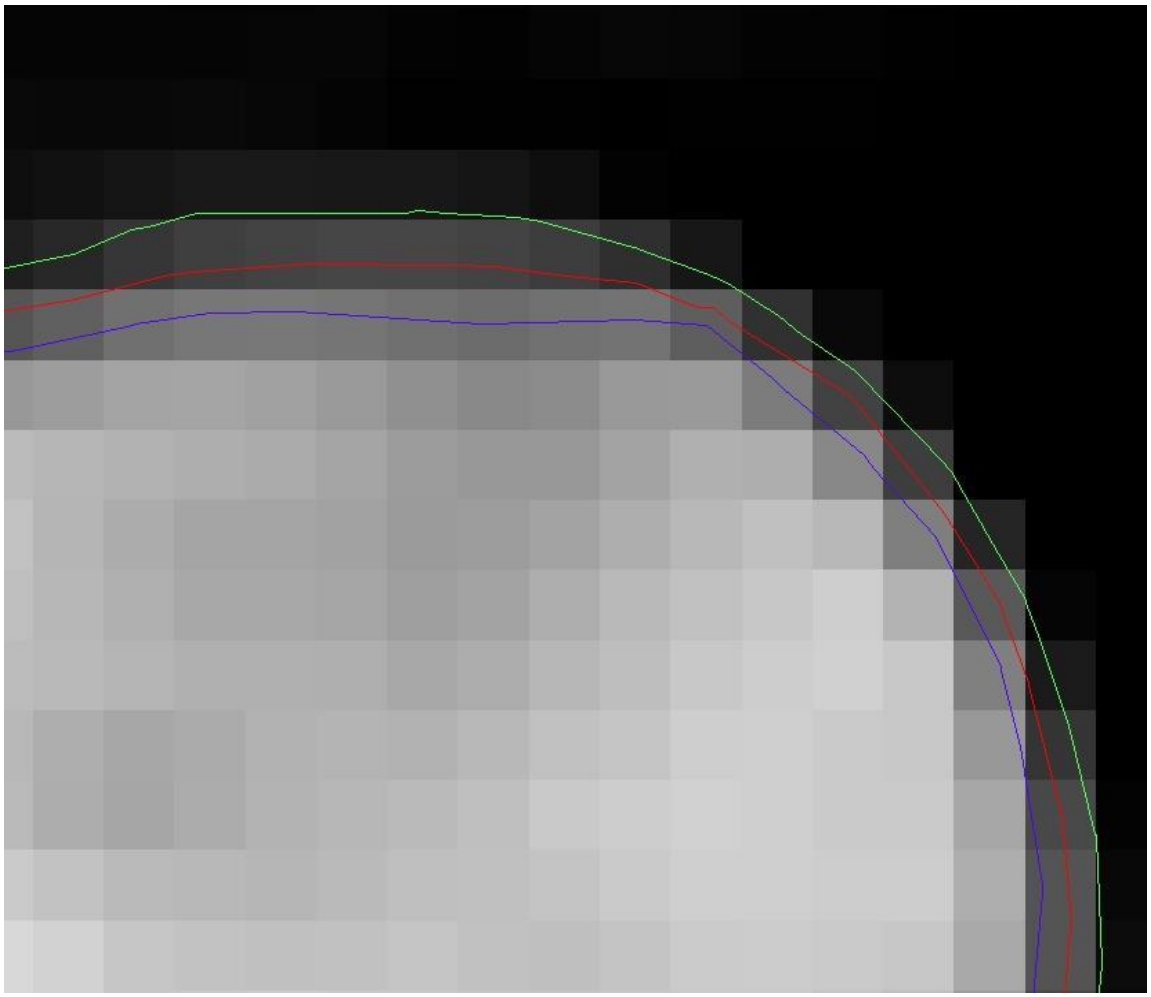

Figure 3-4: Effect of segmentation threshold level of surface generation of 3D bone model. The inner blue line represents the surface generated with a threshold setting of 1300HU, the red line represents thresholding at 900HU and the outer green line represents the surface generated at 500HU for a small portion of one of the bones used in the study. Changes in model volume and surface area will occur but there is equal effect across the entire bone surface.

Reconstruction algorithms that included additional smoothing reduced both surface area and volume of the bones in this study. The reconstruction algorithms with smoothing produce bone models that more closely resemble the actual bone specimen (figure 3.3); however, smoothing had no significant impact upon calculated bone motions. This finding suggests that reconstruction algorithms with additional smoothing following segmentation may be applied to produce more accurate visual representations, but is unnecessary in kinematic calculations. The elimination of smoothing from any protocol may produce a more time efficient method of kinematic calculation.

One limitation of this study is the use of bone specimens that are no longer in close proximity to each other and covered with soft tissues. Segmentation may have been more accurate and repeatable compared to in vivo studies, in which segmentation may prove challenging. However, it would be extremely difficult to perform accurate known bone motions, which are used as a "gold standard", in an ex vivo situation. It must also be recognized that these findings may only apply to this particular surface based method of kinematic measurement and must be validated against other methods, such as inertia based techniques. This study utilized canine tarsal bones, which display a generally globular geometry. Although it has been shown that obtaining accurate CT based kinematic data in globular bones is more challenging than elongated bones (Crisco et al., 1999), care must be taken when extrapolating these results to bones of different geometry. The techniques described here may also permit kinematic calculations on other tissues such as ocular and vascular tissues, however, further studies optimized for visualizing these particular tissues would be required to validate this technique. A lack of contrast between soft tissues may influence accuracy and any conclusion regarding soft tissue kinematics is beyond the scope of this present study.

These is also the potential for error introduced when the CT scans were aligned to our co-ordinate system. This alignment was performed visually and this step was introduced so motion could be described along the axes of the LEGO board and to reduce errors associated with inaccurate placement of the LEGO board on the CT gantry. Another source of inaccuracy may have originated

from variation in measurement between trials. Although not performed as part of this study, multiple measurement trials would help identify the magnitude of variability from variation in measurement between trials.

Although no significant difference was identified in regard to scan resolution, a power calculation was not performed and hence it is possible that the failure to identify any significant difference could be related to a type II error.

3.5 Conclusions

The findings of this study show that scan resolution, segmentation threshold level and the reconstruction algorithm used to generate 3D surface models have no significant ($p = 0.05$) influence on the magnitude of error in tarsal bone kinematics (rotations and translations). Lower resolution scanning is therefore recommended to reduce radiation exposure without compromising kinematic accuracy.

Chapter 4 Development of an ex vivo limb loading device

4.1 Chapter Introduction

Kinematic studies reveal the unique patterns of movement across different joints and improve our understanding of both normal and diseased conditions. A huge variety of measurement techniques and experimental designs have been reported. These techniques may be categorised based upon their level of tissue disruption. Whilst non-invasive techniques preserve the surrounding tissues, their usefulness may be limited by a lack of coupling between external marker motion and the motion of the underlying bone (Benoit et al., 2006; Kim et al., 2011). Additionally, variation in marker positioning can also influence kinematic measurements (Torres et al., 2011).

Imaging based techniques are non-invasive and directly measure bone motion, however, the subject must remain in the imaging field, which generally surrounds the patient.

Invasive techniques, such as the use of cortical pins, allow 3D tracking of bones in real time, but require a surgical procedure, which may alter the kinematic patterns through disruption of soft tissue structures (Lundgren et al., 2008). Additionally, the smaller tarsal bones, such as the cuneiforms (in humans) and numbered tarsal bones (in dogs) are difficult to instrument with invasive markers. Despite the relative larger size of the human tarsal bones, many are considered too small to instrument with pins (Wolf et al., 2008). Failure to measure motion of each bone will introduce kinematic errors due to violations of rigid body assumptions (Nester et al., 2010).

Kinematic studies can also be classified as dynamic, where continuous data is collected in real time, or static, where bone position may be recorded at certain points in time. Depending on the variable being measured, static studies have been shown to be as accurate as dynamic studies (Foumani et al., 2009).

Kinematic experiments can be performed in vivo or ex vivo using cadaveric specimens, each with their own limitations. The kinematics recorded *in vivo* are the result of both external forces (if applied) and internal forces (muscular contractions) and are considered the most representative of

true bone motions. Reproducing the muscular forces during cadaveric experiments is important as this has been shown to alter kinematic patterns (Foumani et al., 2010; Hamel et al., 2004; Sharkey and Hamel, 1998). The advantages of cadaveric specimens include the ability to perform additional procedures and correlate kinematic results with dissection of specimens.

In veterinary medicine, cadaveric limb loading jigs that replicate the major muscular forces acting on the stifle joint have greatly improved our understanding of stifle biomechanics and surgical interventions. The ideal limb loading jig should consistently reproduce the intended force on the limb, be re-usable and applicable to limbs of differing size and potentially even different species.

To allow for the further investigation of kinematics of the canine tarsal joint, a limb loading jig was designed to replicate both the internal and external forces exerted on the canine tarsal joint. Utilising the CT based kinematic measurement techniques described in the previous chapter, this jig could then be used to improve our understanding of normal motion and the pathophysiology of disease in the canine tarsal joint.

In this chapter, four sequential experiments detailing the development and the validation of the limb loading jig are reported.

4.2 Experiment 1: Initial concepts and jig design: phase 1

4.2.1 Introduction

Limb loading jigs have been developed to replicate muscular forces across the stifle of both dogs (Apelt et al., 2007; Hoffmann et al., 2011; Warzee et al., 2001)and cats (Kneifel et al., 2017). These limb presses apply a load to the femur and collapse of the specimen (by flexion of the stifle and hock) is counteracted by replication of the forces generated by the stifle extensors (quadriceps muscle) and hock extensors (gastrocnemius muscle).

In these limb presses, the quadriceps muscle is replaced with a spring that connects the patella and proximal femur, whilst a cable with turnbuckle connects the caudodistal femur to the tuber calcanei. The turnbuckle allows alteration to the length of the cable, which simulates the forces of the gastrocnemius muscle and hence allows alteration to the joint angles (Warzee et al., 2001).

One potential concern when replacing the natural insertion of the muscle with a bone tunnel or bone screw, is the alteration of the tensile force of the tendon. Altering the direction of pull may influence the motion of the bone and therefore alter kinematic measurements. To best replicate the force of a muscle on bone, some jig designs incorporate small motors that can be attached to the tendon of muscle and preserve the complex enthesis (Hamel et al., 2004; Sharkey and Hamel, 1998).

When investigating kinematics of the canine tarsal joint in cadaveric specimens during the stance phase, the effect of the tarsal extensors must be replicated. The tarsal joint is extended when a tensile force is exerted through the attachment of the common calcaneal tendon on the tuber calcanei. This tendon comprises the tendon of insertion of the gastrocnemius muscle, superficial digital flexor and the conjoined tendon of semitendinosus, gracillis and biceps femoris muscles (Evans et al., 2012).

As the gastrocnemius muscle contracts eccentrially during weight bearing and undergoes minimal change in length (Goslow et al., 1981), the aim of this experiment was to evaluate if the intact gastrocnemius muscle would maintain hock extension during axial loading of the tibia.

It was hypothesised that immobilisation of the stifle joint and preservation the gastrocnemius muscle would maintain tarsal extension during application of load to the tibia.

4.2.2 Materials and methods

A limb loading jig was constructed and comprised a proximal limb holding constraint, a base plate upon which the foot was positioned and a compression mechanism to simulate load bearing.

4.2.2.1 Limb preparation

All limbs were obtained from adult greyhounds euthanased for reasons unrelated to this study. Limbs were prepared by transection of the femur proximal to the insertion of the gastrocnemius muscle. Care was taken to preserve the insertion of the gastrocnemius and superficial digital flexor muscle. All other muscles proximal to the stifle were removed. Limbs were wrapped in saline soaked cloth and frozen at -20 degrees until use. Limbs were thawed at 4 degrees overnight prior to use.

A Steinmann pin (4.8 mm diameter) was positioned transarticularly across the stifle joint. With the stifle fully flexed, the pin was first driven proximally from the intercondylar notch to exit through the cranial cortex of the femur proximal to the trochlea. The stifle was then extended to approximately 135 degrees to simulate the mean stifle angle measured during the stance phase of a walk (Hottinger et al., 1996). The pin was then driven distally to engage the tibial condyle and cranial tibial cortex (figure 4.1).

Figure 4-1: Method of stifle immobilisation. The stifle was immobilised by a 4.8mm diameter Steinmann pin positioned transarticularly. The stifle was extended to approximately 135 degrees to simulate the stifle angle during the mid-stance phase of the walk. The medial collateral ligament (arrow) was used as a landmark to produce a consistent starting point for the second trans-tibial pin.

A second 4.8mm diameter pin, termed the trans-tibial pin, was driven through the proximal tibial metaphysis in a medial to lateral direction. The starting position of this pin was located approximately 5mm below (distal) to the proximal articular surface of the tibia and through the middle of the medial collateral ligament (figure 4.1). Insertion of a 25Ga needle through the medial collateral ligament facilitated accurate identification of this position.

The trans-tibial pin was used to apply a simulated weight bearing load to the limb using the loading mechanism of the jig.

4.2.2.2 Proximal restraint

To constrain the trans-tibial pin during loading, approximately one quarter the circumference of a 100mm diameter PVC pipe was removed longitudinally. Two longitudinal slots were then cut in the pipe to accommodate the trans-tibial pin (figure 4.2). The pipe was attached directly to the foot plate by a single wood screw.

4.2.2.3 Foot plate

The foot plate was constructed with a series of structural pine blocks attached to the PVC piping.

4.2.2.4 Loading mechanism

Two “tie down” straps were hooked over each end of the trans-tibial pin. To prevent slippage of the hooks off the ends of the pin, two external skeletal fixator clamps were placed on either end of the pin. The tie down straps were then connected behind the base plate by interlinking their hooks. The tie down straps use a ratchet mechanism to shorten and then maintain their length. The limb was compressed as the ratchets of the tie down straps were alternatively tightened (figure 4.2).

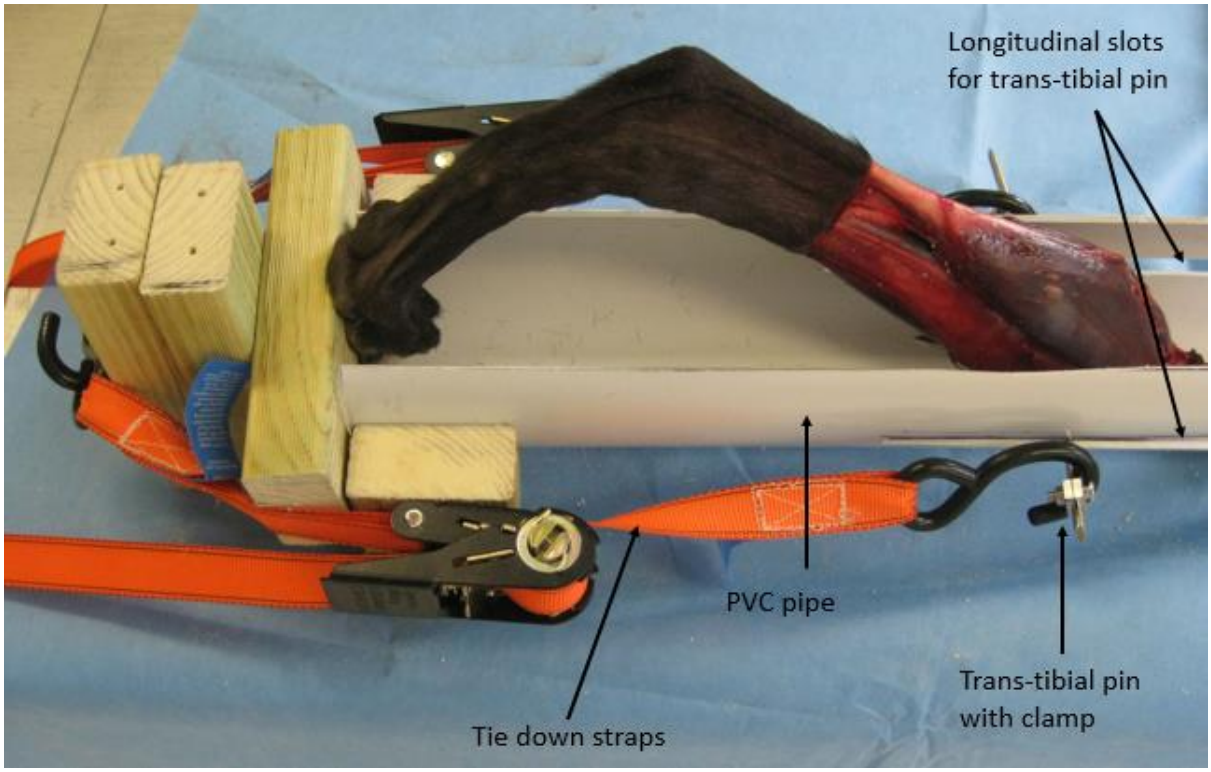

Figure 4-2: Configuration of the limb loading jig. Note the metallic ratchets of the tie down straps are at the level of the tarsal bones. As this would result in imaging artefact, the position of the ratchets was subsequently changed.

4.2.3 Results

Fixation of the stifle with a trans-articular pin was sufficient to create tension in the common calcaneal tendon and prevent collapse of the hock during loading (figure 4.3). There was palpable tension in the common calcaneal tendon and no visible disruption to the gastrocnemius muscle. The force exerted on the trans-tibial pin was sufficient to produce plastic deformation of the pin (figure 4.4).

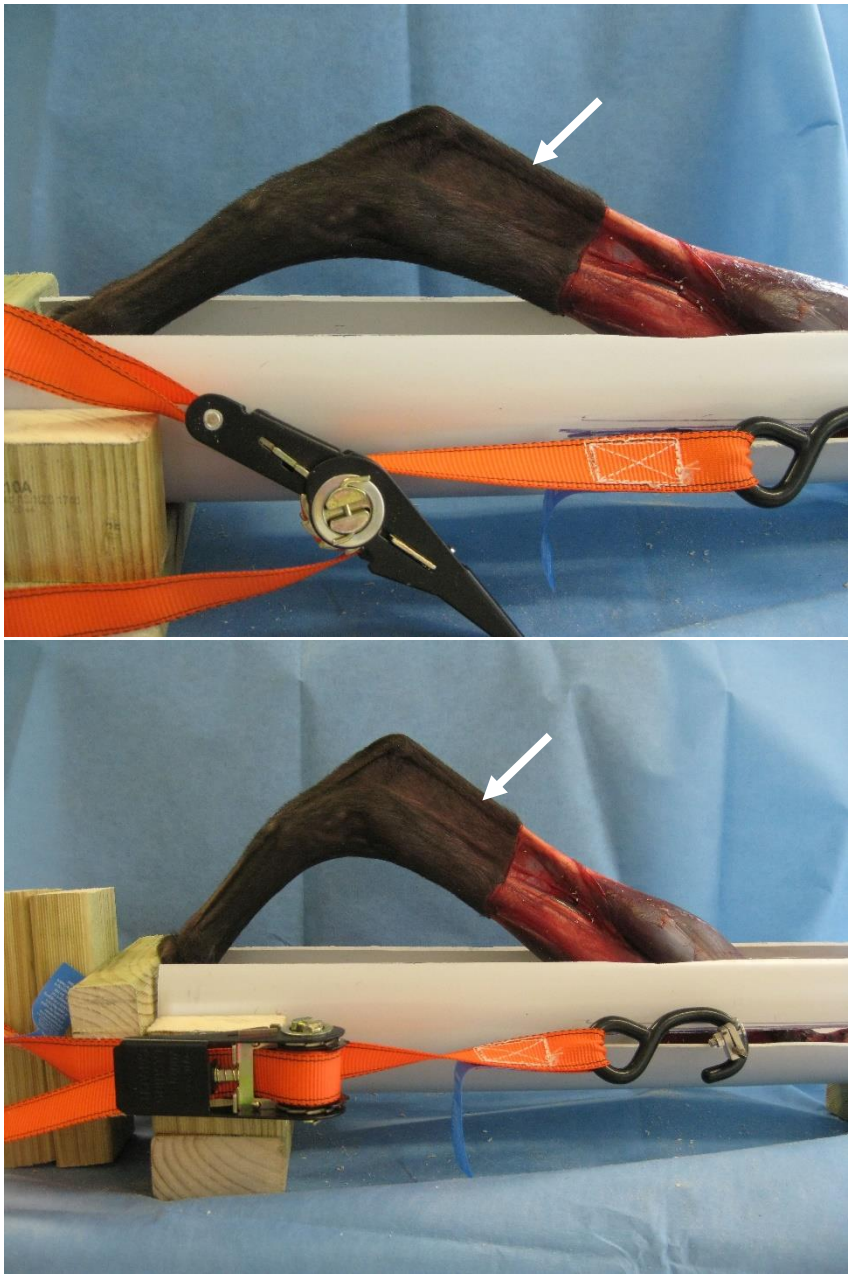

Figure 4-3: Top: the position of the canine hock without a load applied. Bottom: The position of the limb following tightening of the tie down straps. There is tension generated in the common calcaneal tendon (arrow) as it resists flexion of the hock.

Figure 4-4: View of the limb loading jig from the caudal aspect of the limb. The trans-tibial pin is seen to plastically deform (arrow). External skeletal fixator clamps (open arrows) were attached to the trans-tibial pin to prevent slippage of the strap hooks

The jig and attached limb then underwent computed tomography scans in an unloaded and loaded position.

The DICOM images were then imported into segmentation software (Mimics version 17.0, Materialize, Belgium) and no metallic artefacts were identified, suggesting that PVC and structural pine are materials suitable for construction of a radiolucent jig.

4.2.4 Discussion

The results of this experiment, demonstrate that immobilisation of the stifle joint and preservation of the gastrocnemius muscle and common calcaneal tendon was sufficient to passively restrict hock flexion when a compressive load was applied to the tibia, supporting the original hypothesis.

This finding is likely to reflect the strong connective tissue that surrounds the gastrocnemius muscle and also contributes to a significant internal framework that infiltrates around the pennate arrangement of the muscular fibres. The cadaveric gastrocnemius musculotendinous unit was able to resist high loads during passive stretching, although the tension was not measured in this pilot experiment.

During limb compression, bending forces were generated if the foot pads were not positioned directly in the line between the trans-tibial pin and the point where the tiedown straps were joined under the base plate. These bending forces resulted in separation of the PVC pipe and wooden base plate. This precarious balance was also noted in previous limb press devices (Hoffmann et al., 2011), which were subsequently modified by the addition of a caudal tensioner that allowed a wider range of joint angles to be studied. The delicate balance in this situation could be overcome with a more rigid frame to connect the base plate and proximal restraint. The addition of a restraint as suggested by others (Hoffmann et al., 2011) may alter the physiological loading pattern of the limb and was not considered as a solution for future jigs due to original aim of ensuring accurate representation of internal and external forces on the cadaveric limb.

The ratchet mechanism was also located at the level of the tarsal bones which would have created artefact if left unchanged (figure 4.3). The position of the ratchets was subsequently moved distal to the foot plate leaving only the tape webbing crossing the bones of interest (figure 4.4). Future jigs may overcome this problem by changing the loading mechanism from a tension generating mechanism, which naturally must span from foot plate to proximal restraint, to a compression

generating device This device could be positioned behind either the foot plate or proximal restrain, thereby avoiding the mechanism producing unwanted imaging artefact.

The trans-tibial pin was observed to plastically deform at higher loads (figure 4.4), which may reduce the ability to apply a clinically relevant load to the limb. The greater the distance between the tibia and the point where a force is applied, the greater the bending moment generated (Johnson and DeCamp, 1999). Future jigs would benefit from reducing the working length of the trans-tibial pin by applying the force as close to the tibia as possible. Other alternatives to prevent bending of the trans-tibial pin include increasing the pin dimeter, which will increase the area moment of inertia, a geometric measure which dictates a structure's ability to resist a bending load. Selecting a different material for use as the trans-tibial pin could potentially increase bending resistance. Amongst the commonly used materials for orthopaedic implants, 316L stainless steel has a high modulus of elasticity, about twice that of titanium alloys, with only cobalt chrome alloys having a higher modulus (Niinomi, 2002). Selecting highly cold worked metals will also increase resistance to bending. In contrast to orthopaedic wire, which is minimally cold worked and bone plates, which are moderately cold worked, intra-medullary nails are highly cold worked and therefore most resistant to bending (Johnson et al., 2005).

4.3 Experiment 2: Jig design phase 2

4.3.1 Introduction

The direction and magnitude of any bone movement is the result of tensile forces acting at tendinous insertions during muscular contraction, force from the adjacent bones and a restriction in movement from connective tissues such as ligaments and the joint capsule.

When cadaver based kinematic studies are performed, the force from adjacent bones and restriction in motion due to ligaments and the joint capsule are more readily reproduced. Re-creating muscular forces is more challenging. In our previous experiment, the stifle joint was immobilised and this was adequate to maintain tension in the intact gastrocnemius muscle and superficial digital flexor muscles, resisting hock flexion during loading of the tibia.

Preservation of the enthesis of the tuber calcanei allows replication of the natural complex tensile force on this bone, which is a major determinant of the kinematics of the calcaneus and neighbouring tarsal bones. The calcaneus exerts both a tensile force on adjacent bones (via strong ligamentous connections) and a compressive force (through compression of adjacent articular cartilage). This reproduction of internal forces within the tarsus is an important aspect of kinematic calculations in cadaveric specimens.

The aim of this experiment was to redesign the limb loading jig in order to address the problems associated with the previous jig, such as the balance of the limb and deformation of the apparatus. An additional aim was to create a jig that could replicate a range of external forces that best simulate a dog performing normal activity at high speeds. In galloping dogs, a ground reaction force of approximately 1.6 times body weight has been recorded (Walter and Carrier, 2007), which equates to approximately 560N in a 35kg dog

4.3.2 Materials and methods

4.3.2.1 Limb preparation

All limbs were obtained from adult dogs euthanased for reasons unrelated to this study. Limbs were prepared by transection of the femur proximal to the insertion of the gastrocnemius muscle. Care was taken to preserve the insertion of the gastrocnemius and superficial digital flexor muscle. All other muscles proximal to the stifle were removed. Limbs were wrapped in saline soaked cloth and frozen at -20 degrees until use. Limbs were thawed at 4 degrees overnight prior to use.

A Steinmann pin (4.8 mm diameter) was positioned transarticularly across the stifle joint (as described in experiment 4.1. With the stifle fully flexed, the pin was first driven proximally from the intercondylar notch to exit through the cranial cortex of the femur proximal to the trochlea. The stifle was then extended to approximately 135 degrees to simulate the mean stifle angle measured during the stance phase of a walk (Hottinger et al., 1996). The pin was then driven distally to engage the tibial condyle and cranial tibial cortex (figure 4.1).

4.3.2.2 Overview

The basic design of jig 2 was a radiolucent frame constructed from structural pine (cross sectional dimensions 70mm X 35mm). The frame was joined at either end with metallic wood screws that would be positioned proximal and distal to the limb and hence avoid imaging artefact in the region of interest. The frame was a rectangular prism which comprised 4 longitudinal “rails” that would house the proximal restraint (figure 4.5). Wood was selected as the construction material as it is an inexpensive, widely available construction material that is easy to work with and was shown to produce minimal radiographic artefact in the previous experiment. The construction of the jig was performed entirely by myself without the requirement for external manufacturing support. Perspex

was also considered as a manufacturing material but was considerably more expensive and more brittle, making it harder to work with.

Figure 4-5: The redesigned jig (jig2) with a frame that comprised 4 beams of structural pine and housed the proximal limb restraint and foot plate (not shown above). Wood was selected as the construction material as it was inexpensive, radiolucent and easy to work with. The open sides allow the operator to visualise the limb position from two orthogonal positions.

4.3.2.3 Proximal restraint

The proximal limb restraint originally comprised two L-shaped aluminium brackets that would secure the limb to a wooden disc positioned within the 4 "rails" of the frame (figure 4.6). The brackets were positioned centrally on the disc. Initial testing showed that brackets placed on a single disc were inadequate to prevent angulation of the limb (a problem in the previous experiment). This "delicate balance" has been identified in previous limb presses (Hoffmann et al., 2011). The addition of a second disc created a cylindrical shape to the proximal restraint (figures 4.5 and 4.7) thereby constraining the proximal device so only axial motion and rotation were permitted.

A 5mm bone tunnel was drilled from medial to lateral through the proximal tibial metaphysis. The tunnel was positioned approximately 5mm distal to the articular surface, which was identified with insertion of a series of 25Ga needles. The craniocaudal position of the tunnel was approximately half

way along the articular surface, with the midpoint of the medial collateral ligament providing the external landmark (figure 4.1). The tibia was then secured to the jig with a 6mm threaded bolt that engaged two aluminium brackets that were centred within the cylinder (figure 4.8)

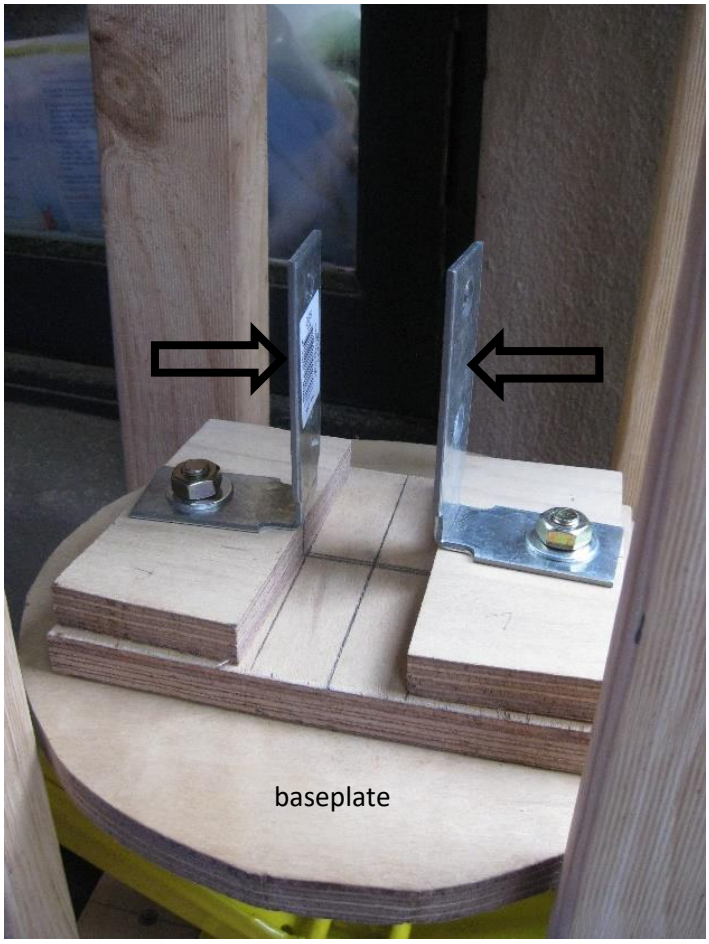

Figure 4-6 shows the location of the aluminium brackets (open arrows) on the baseplate. They have been positioned to centre the proximal tibia in the restraint. This image was taken during construction before a second circular disc was joined.

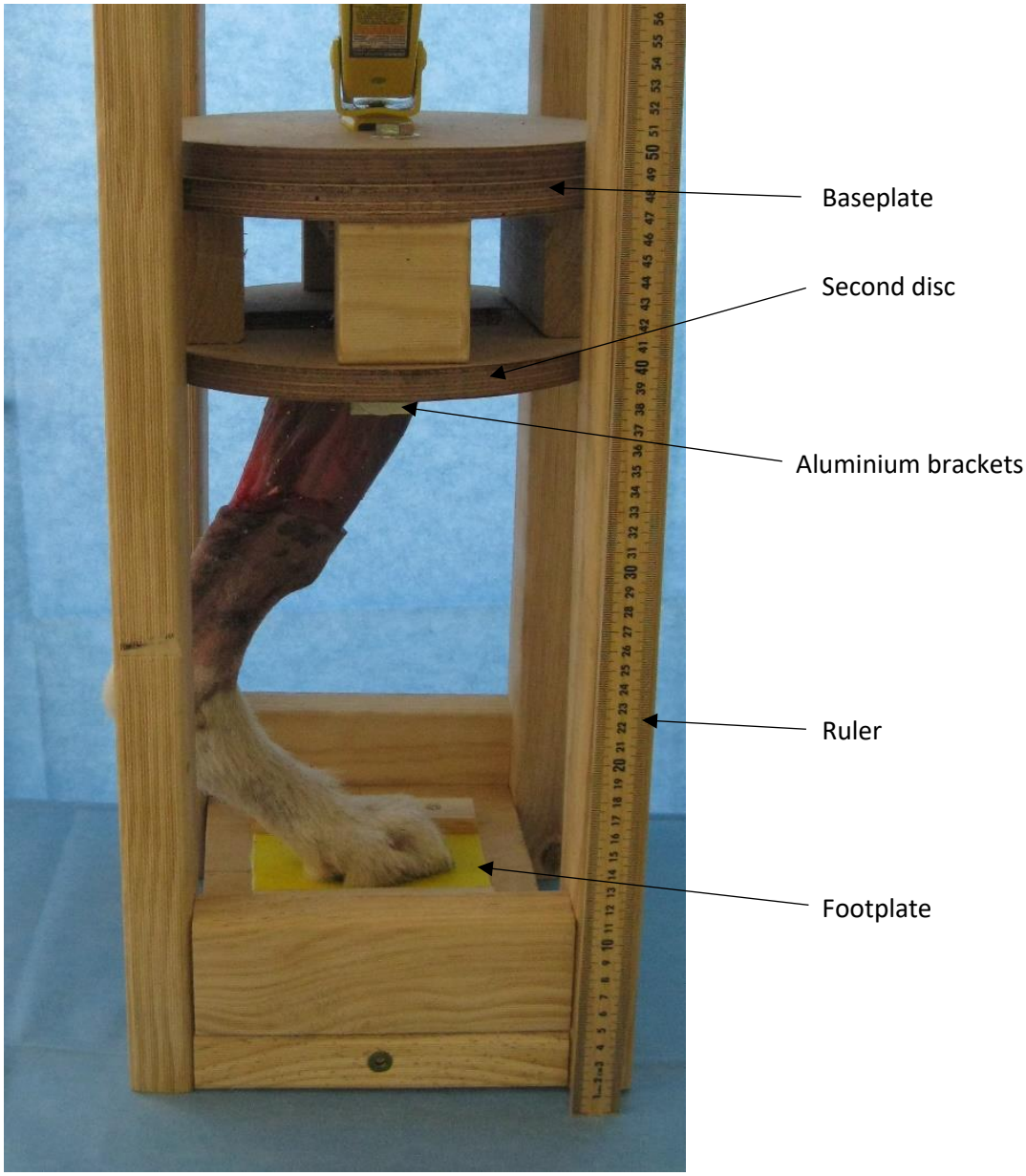

Figure 4-7: A limb loaded within the newly constructed jig (lateral view). The addition of a second disc produced the cylindrical shape of the proximal restraint, allowing linear translation and rotation. Linear displacement of the proximal restraint was measured using a wooden ruler.

Figure 4-8: Cranial view of the jig with limb loaded. The proximal tibia is secured to the jig with a 6mm threaded bolt positioned through a previously drilled bone tunnel (yellow arrow). The distance between the aluminium brackets was customised to decrease the distance between bracket and the limb. This would reduce bending forces on the trans-tibial pin.

4.3.2.4 Foot plate

The foot plate was a square of 12mm thick plywood with a centrally positioned non-slip surface. The foot was positioned centrally on the plate with the centre of the metatarsal pad placed over the centre point of the plate. The foot was not constrained on the foot plate.

The angle of the foot plate was altered in a medial to lateral direction to simulate a dog tilting during bend running. A series of wooden blocks were posited asymmetrically under the plate to produce a slope (figure 4.9) and the slope was recorded with a digital goniometer or protractor. Three different grades of sandpaper (P40, P80, P120) were tested and the maximal angle before foot slippage was recorded. Sandpaper grades complied with ISO 6344 standards and define the grit size used in each abrasive paper.

Figure 4-9: shows the slope created by placement of wooden blocks (open arrow) under the foot plate. The maximal angle was recorded before foot slippage

A torsional force was also applied with a spring-loaded tensioning device. The maximal force applied before slippage of the foot was also recorded

Figure 4-10: A rotation force was applied to identify the torque required for foot slippage. This value would also include frictional forces in the system and was quantified using a spring-loaded scale.

4.3.2.5 Loading mechanism

A scissor jack intended for automotive use (rated to 1500kg) was secured behind the proximal limb restraint and bolted to the jig frame. The jack was operated by turning a central threaded bolt with a handle and this would displace the limb restraint towards the foot plate, producing an axial load on the limb (figure 4.11).

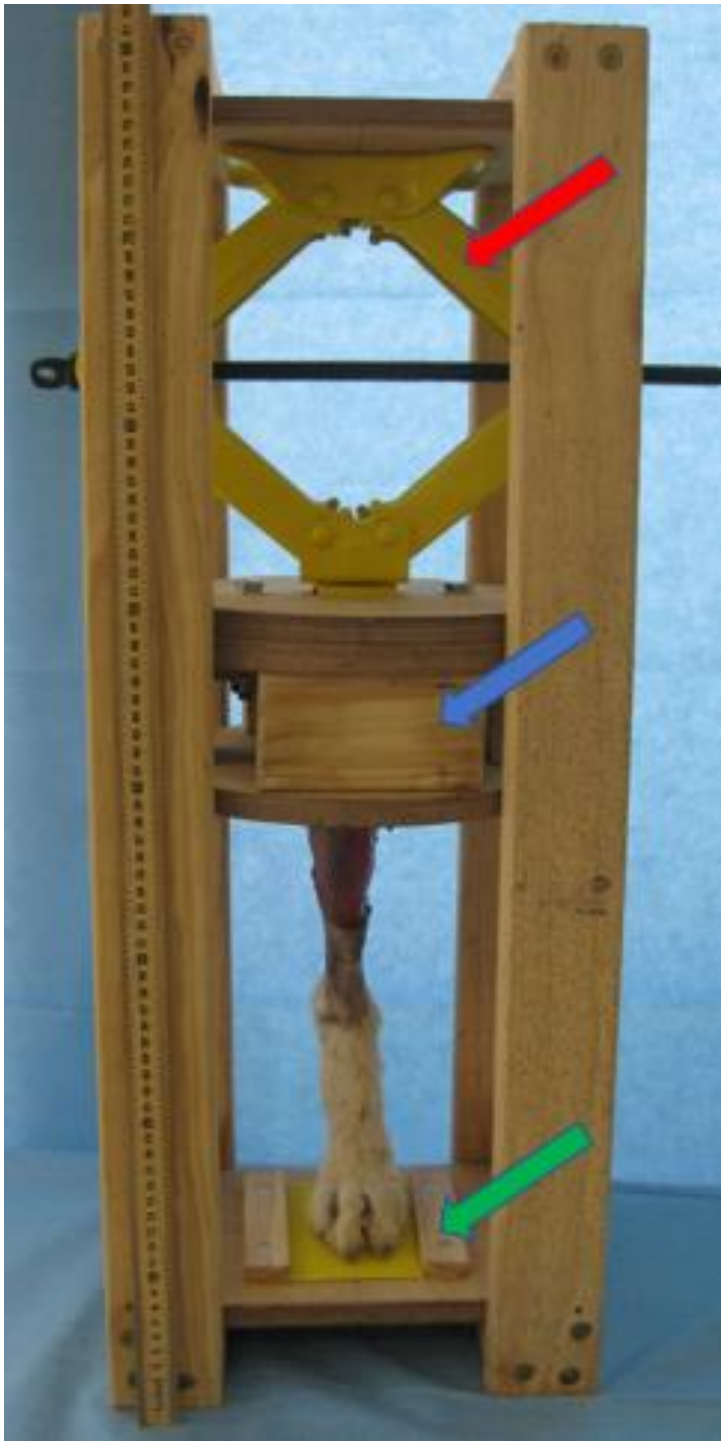

Figure 4-11 The limb loading mechanism (red arrow) comprised an automotive scissor jack and would linearly displace the proximal limb restraint (blue arrow) towards the foot plate (green arrow). The entire assembly is housed within a radiolucent frame.

4.3.3 Results

Rotation of the central thread of the scissor jack produced linear displacement on the proximal limb restraint and there was no angulation of the limb evident. As with the previous experiment, the intact gastrocnemius muscle maintained hock extension when the stifle was immobilised with a trans-articular pin. There was no evident of bending of the trans-tibial pin. There was no requirement to “delicately balance” the limb during loading as with the previous jig.

During insertion of the limb into the jig there was a tolerance between the holes in the brackets and the size of the trans-tibial pin which allowed the foot to be positioned centrally on the foot plate. However, when load was applied, the force on the trans-tibial pin was asymmetrical and this produced a lateral force, pushing the foot pads to one side. Figure 4.11 shows the foot pad not centrally located on the foot plate.

There was no difference in the angle of the plate before slippage between the 3 grades of sandpaper used. Slippage was not noted at 10, 20 or 30 degrees angulation for all 3 grades of sandpaper. Visual slippage occurred at 40 degrees for all grades of sandpaper. Slippage of the foot required approximately 6kg of load applied to the edge of the cylindrical frame. It was noted, however, that increased torque was required as axial load increased.

4.3.4 Discussion

The second jig overcame the major limitations of the previous jig, namely, plastic deformation of the trans-tibial pin and requirement for perfect “balance” to prevent angulation of the limb. During this experiment, additional factors which required modification, were also identified.

- **Inaccurate drilling of bone tunnel.**

In this experiment, the bone tunnel was not directed in a perfectly orthogonal plane. In the previous jig, this asymmetry was overcome by individual tensioning of a medial and lateral strap. However, with jig 2, the orientation of the bone tunnel influenced the position of the foot on the foot plate. The protocol was modified so that the limb was positioned into the proximal restraint before the bone tunnel was drilled. This ensured the foot was in the optimal central position. The start point of the bone tunnel was marked and a drill guide, which was attached to the restraint was developed (figure 4.12).

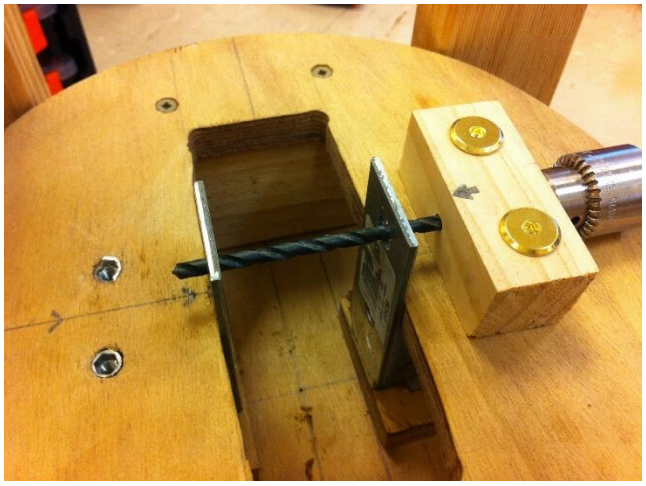

Figure 4-12: A removable drill guide was developed to ensure the bone tunnel was directed orthogonally across the proximal tibia and would pass through the holes in the brackets. The bone tunnel was drilled with the limb positioned in the jig and metatarsal pad centered on the foot plate.

- **Replication of angle of foot plate**

Positioning of wooden blocks under the footplate was convenient for the preliminary studies but was considered an unreliable means to consistently reproduce foot plate angles. A radiolucent foot plate constructed entirely of wood and plastic was developed at a set angle. The initial slope was set

to 30 degrees based on our pilot experiment with jig 2. A second flat foot plate was also constructed (figure 4.13)

Figure 4-13: shows the two foot plates. The centre of both the flat plate (behind) and sloped plate (front) are marked. The plastic screws and wooden strips allow the non slip surface to be firmly attached to the plate, without creating any imaging artifacts.

A subsequent experiment with a greyhound limb produced significantly different results with the maximal angle before slippage measured at 10 degrees. One potential reason for this breed variation is the highly adapted conformation of the greyhound which has resulted in smaller foot pads and less compliance compared to other breeds(Besancon et al., 2004). To account for this variation, a 10 degree sloping foot plate was developed (figure 4.14)

Figure 4-14: shows the flat (right) and 10 degree sloping foot plate(left). Both have a non-slip surface attached and the centre of the plate marked to facilitate foot placement

.

The foot plate was further refined by the introduction of a pivoting foot plate, that would allow alteration in slope without the need to remove the foot off the plate (which may introduce inaccuracy as the foot was replaced on the foot plate). Initially the angles were maintained by a series of pegs (figure 4.15). This system was replaced with the final design of footplate which was capable of an infinite number of slope angles. Alteration of the foot plate angle could be performed by turning two screws positioned under the plate (figure 4.16).

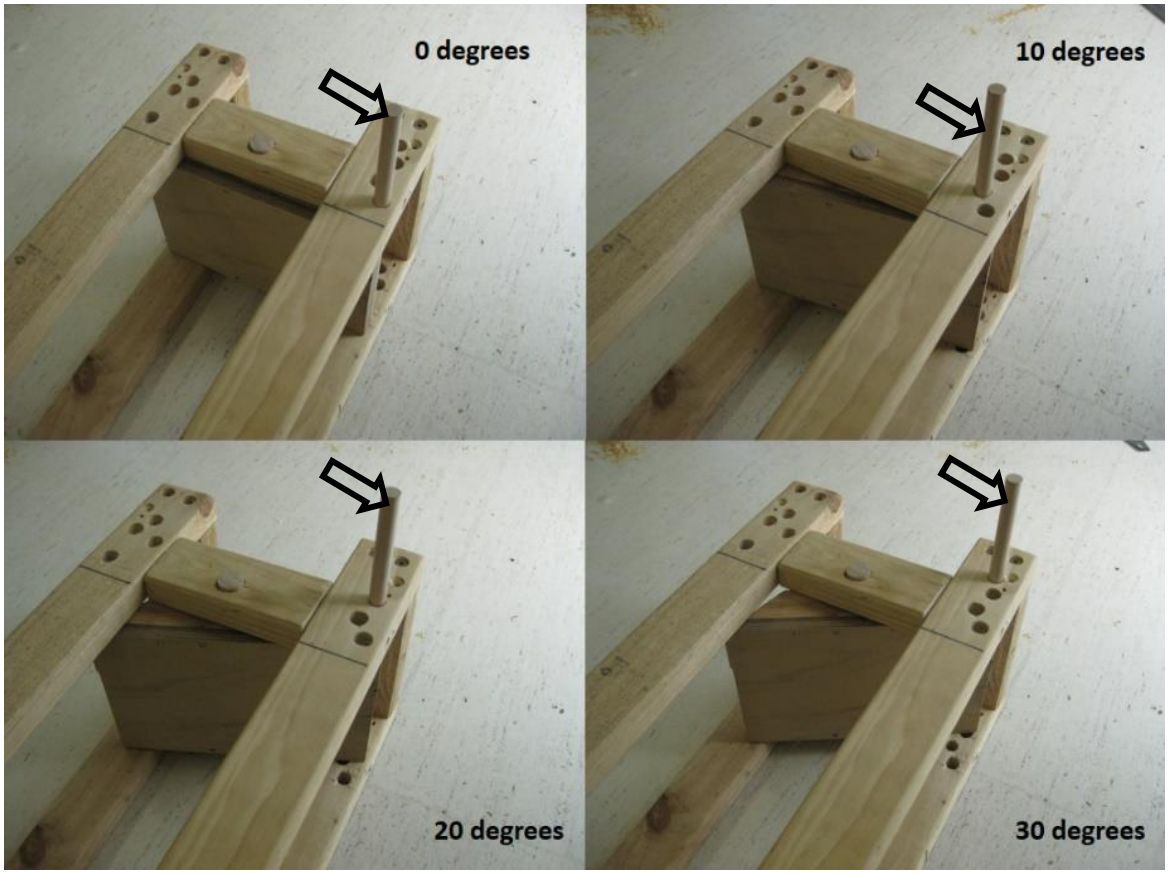

Figure 4-15: A pivoting foot plate allows angulation without having to remove and replace the foot. The position of the foot plate was maintained with pegs (open arrows)

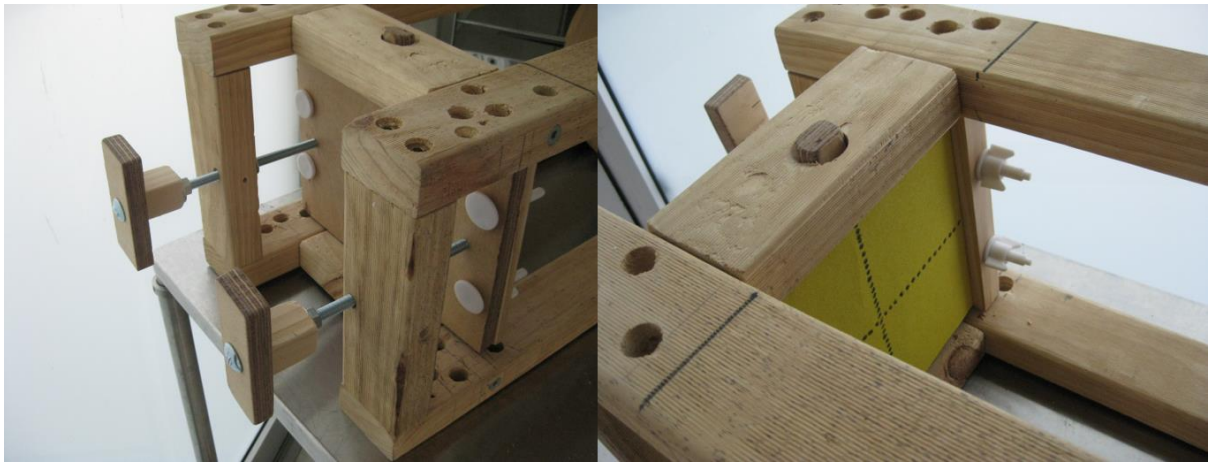

Figure 4-16: Left: the underside of the foot plate, which is held in place with two large bolts. These bolts can be adjusted to produce fine movements and hence infinite plate angles. Right: the top surface of the foot plate shows the non-slip surface with the centre of the plate marked.

- **Fixed stifle angle**

Immobilisation of the stifle was an efficient means to maintain to maintain tension in the gastrocnemius muscle and associated tendon. However, the stifle undergoes flexion during loading, particularly at faster gaits (Goslow et al., 1981; Gregersen et al., 1998; Hudson et al., 2012; Walter and Carrier, 2009). The proximal limb restrain was therefore modified to better reflect the natural motion of the stifle.

The limbs were prepared as for previous studies, however, the transarticular pin was not placed to rigidly immobilise the stifle. The limb was positioned in the jig and the trans-tibial bone tunnel drilled and a threaded bolt placed though the jig and bone tunnel to secure the bone to the proximal limb restraint. Flexion of the stifle was resisted by an acrylic block (Perspex, Lucite International, Lancashire, UK) positioned caudal to the transected femur (figure 4.17) This block could translate in a craniocaudal direction to allow the stifle angle to be altered. Moving the block cranially extended the stifle, while moving it caudally permitted a greater amount of flexion. The initial Perspex femoral block was secured to the proximal restraint with two bolts. Pilot experiments identified some caudal slippage of the femoral block during loading and subsequently a threaded bolt was positioned caudal

to the femoral block, which prevented slippage and could be used to easily adjust the level of stifle extension. In addition, the femoral block itself was replaced with a larger wooden block with a trough cut out to receive the cut end of the femur (figure 4.18)

Figure 4-17: shows a side view (left) and view from distal to proximal (right) of the redesigned proximal limb restraint. The femoral block (blue arrow) rests caudal to the proximal femur (Asterix). As the limb is loaded and gastrocnemius tensioned, a force pulling the femur caudally into flexion is created. The femoral block resists this force.

Figure 4-18: shows further modifications to the proximal limb restraint. The femoral block (blue arrow) positioned to resist stifle flexion is now larger and a bolt is positioned behind the block to prevent slippage of the block and permit easy alteration of femoral block position. A handle (open arrow) was secure to the end of the bolt to allow convenient adjustment to the craniocaudal position of the femoral block.

To evaluate if movement of the femoral block could alter the stifle angle, a greyhound cadaver limb was prepared as described earlier. To identify the longitudinal axis of the femur, a 3mm diameter pin was inserted from proximal to distal down the femoral medullary canal exciting distally through the joint. Approximately 10cm of pin was left protruding from the joint to allow identification of the axis. A 3mm diameter pin was inserted centrally in the distal tibia in a medial to lateral orientation to mark the craniocaudal midpoint of the distal tibia. This point would mark the centre of the tibia distally. The proximal trans-tibial pin was positioned just distal to the midpoint of the articular surface of the tibial condyles and consequently a line connecting the proximal trans-tibial pin with the distal tibial pin represented the tibial mechanical axis. The intersection of this line and the femoral axis represented the stifle angle.

The limb was loaded with the femoral block positioned in its most caudal position. Digital photographs were taken and the stifle angle measured using commercially available software (Image J, https://imagej.net/Welcome). Without moving the position of the proximal limb restrain in the jig, the femoral block was then moved to its most cranial position by turning the screw behind it. Digital photographs were acquired and the stifle angle measured again (figure 4.19).

The stifle was extended from 98.1 degrees to 111.9 degrees with a set hock angle. With the ability to alter stifle angle, the next experiment would validate the jig by comparing the stifle and hock angles of the cadaver with previously published in vivo kinematic data. The final jig design can be seen in figure 4.20.

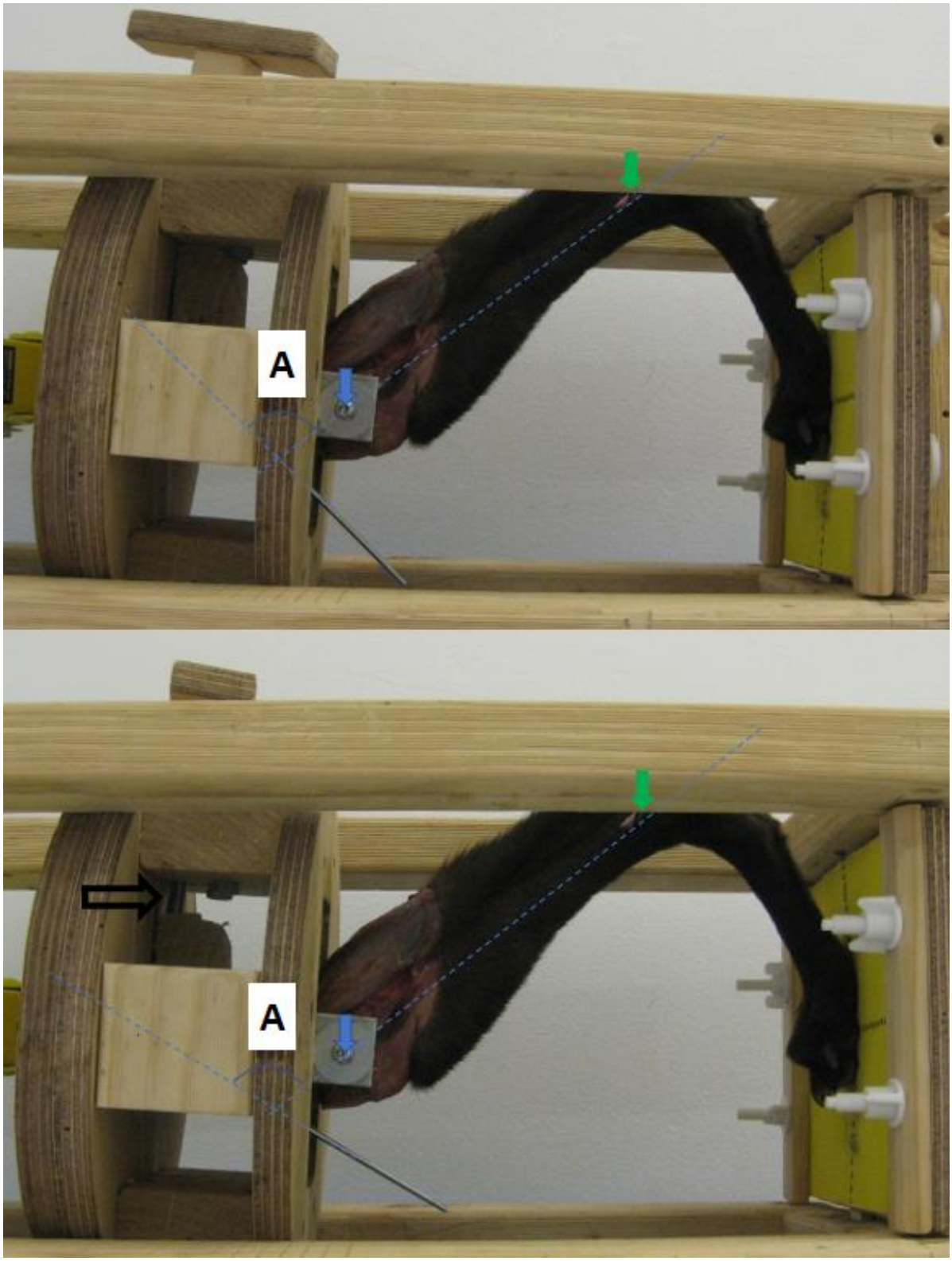

Figure 4-19: showing limb loaded with femoral block positioned caudally (top) and cranially (bottom). The femoral axis is identified from the protruding intramedullary pin, whilst the tibial axis is a line connecting the trans-tibial pin (blue arrow) with a second pin positioned centrally in the distal tibia (green arrow). The stifle angle is marked A. The bolt behind the femoral block is seen in the bottom image (open arrow) when the femoral block is advanced to its most cranial position. All angles were measured using an open source platform for scientific image analysis, Image J (https://imagej.net/Welcome)

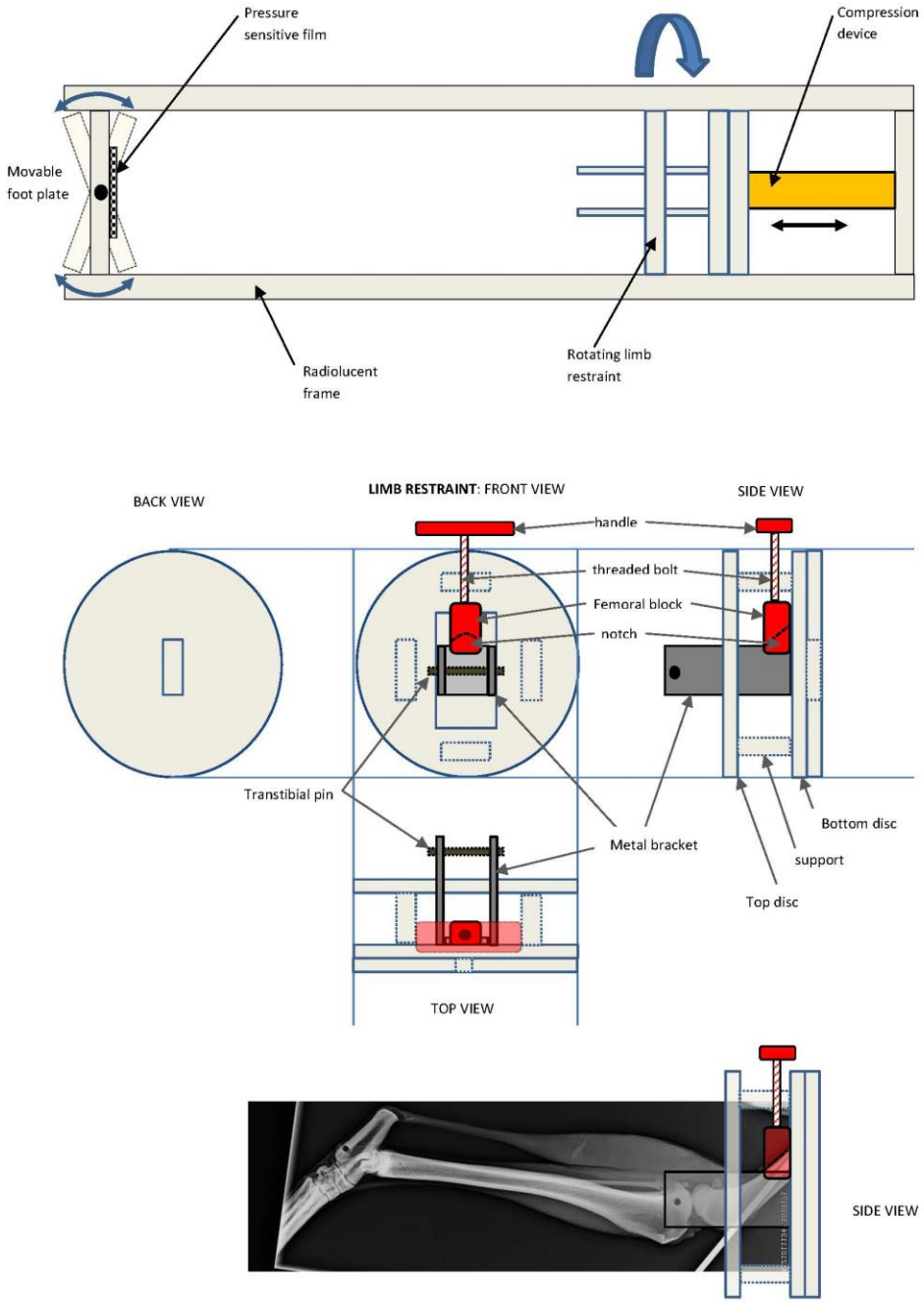

Figure 4-20: schematic of the final jig design, showing overhead view of the jig (top), orthogonal views of the proximal limb restrain (middle) and position of the limb within the jig (bottom).

4.4 Experiment 3: Replicating *in vivo* joint angles

4.4.1 Introduction

Replication of muscular forces are an important component of cadaveric kinematic studies as they are one of the major forces that determine bone motion. To most accurately reproduce the effects of muscle pull on bones, preservation of the enthesis of major insertions is important. In the previous experiment, a jig which utilises the intact gastrocnemius to recreate the natural pull of the common calcaneal tendon and load the canine tarsus in a physiological pattern was described.

To identify if the limb loading jig designed in experiment 2 could replicate the joint angles that have been previously identified during in vivo kinematic studies, incremental loading of canine limbs was performed and joint angles recorded. The hypothesis was that the relationship between hock and stifle angles in the limb loading jig would not differ significantly from previously published data recorded from in vivo kinematic studies. An additional aim of the study was to identify if the position of the femoral block would need to be adjusted during loading to replicate the coupled motion of the stifle and hock. The hypothesis was that the femoral block would not need to be moved during loading to replicate in vivo joint angles

4.4.2 Materials and Methods

4.4.2.1 Specimens

Two cadaveric pelvic limbs were obtained from two adult female greyhounds euthanised for reasons unrelated to this study. Only two limbs were used as testing was non-destructive in loading and repeated measurements were possible.

Limbs were prepared by transection of the femur proximal to the insertion of the gastrocnemius muscle. Care was taken to preserve the insertion of the gastrocnemius and superficial digital flexor muscle. All other muscles proximal to the stifle were removed. Limbs were wrapped in saline soaked

cloth to prevent tissue desiccation and frozen at -20 degrees until use. Limbs were thawed at 4 degrees overnight prior to use.

To identify the longitudinal axis of the femur, a 3mm diameter pin was inserted from proximal to distal down the femoral medullary canal exciting distally through the joint. Approximately 10cm of pin was left protruding from the joint to allow identification of the axis. A 3mm diameter pin was inserted centrally in the distal tibia in a medial to lateral orientation to mark the craniocaudal midpoint of the distal tibia. This point would mark the centre of the tibia distally. The proximal trans-tibial pin was positioned just distal to the midpoint of the articular surface of the tibial condyles and consequently a line connecting the proximal trans-tibial pin with the distal tibial pin represented the tibial mechanical axis. The intersection of this line and the femoral axis represented the stifle angle.

The dorsal cortical border of the metatarsals was used to represent the axis of the pes. The intersection of this line with the mechanical axis of the tibia produced the angle of the hock joint.

4.4.2.2 Mechanical loading

Limb 1 was initially loaded with the stifle in a more flexed position (femoral block caudally located). Incremental loading was performed and angles of the stifle and hock measured when the linear distance from the proximal restraint to the foot plate was 35cm, 33cm, 31cm and 29 cm. Digital photographs were obtained and the angles measured using commercial software with a measuring function (image J, (https://imagej.net))

The femoral block was then moved into the most cranial position (stifle extended) and stifle and hock angle measurements were repeated at the same linear displacement (figure 4.21). During incremental loading, there was no change to the position of the femoral block.

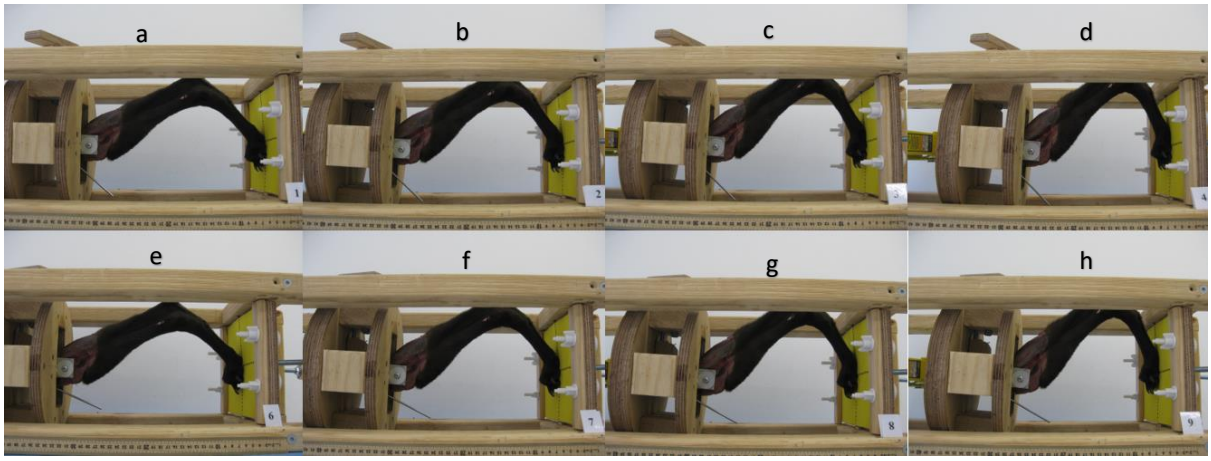

Figure 4-21: Incremental loading of limb 1 with the femoral block in different positions. The images along the top row were taken with the femoral block in the caudal (flexed stifle) position. The limb was initially in the unloaded position(a) and incrementally loaded (b,c) until the maximal load was applied (d). Similarly, sequential images were taken with the femoral block in the cranial (stifle extended) position. Unloaded(e), incremental loading (f,g) and maximal loading (h).

The foot plate was not angled and was therefore perpendicular to the limb. Pressure measurements were not recorded for this experiment

For each condition, the angle of the hock was plotted against the angle of the stifle to determine the correlation co-efficient and slope of the line

Limb 2 was incrementally loaded to predetermined angles of the hock (80, 90, 100, 110 and 120 degrees of extension). The hock angle was measured with a goniometer, whilst the stifle angles were measured from digital radiographs as for limb 1. Limb 2 was only loaded with the stifle in the extended position.

To compare the joint angles to previously reported *in vivo* measurements, a literature search was conducted to identify well designed studies with clear graphical representation of both hock and stifle angles during canine running. For these graphs, the hock angle and simultaneous stifle angle were plotted to identify the correlation co-efficient and slope of the line. Figure 4.22 shows how the angles were derived. Firstly, a line was digitally drawn across from a given hock angle (line 1). A

vertical line was dropped down at the point of intersection with the graph (line 2). When this line intersected with the line giving stifle angle, a horizontal line was drawn across to derive the stifle angle (line 3). In this example, a hock angle of 100 degrees produces a stifle angle of 115 degrees. At least four points were derived from each graph, with measurements taken for the most flexed hock position and then in 10 degree increments of hock angle.

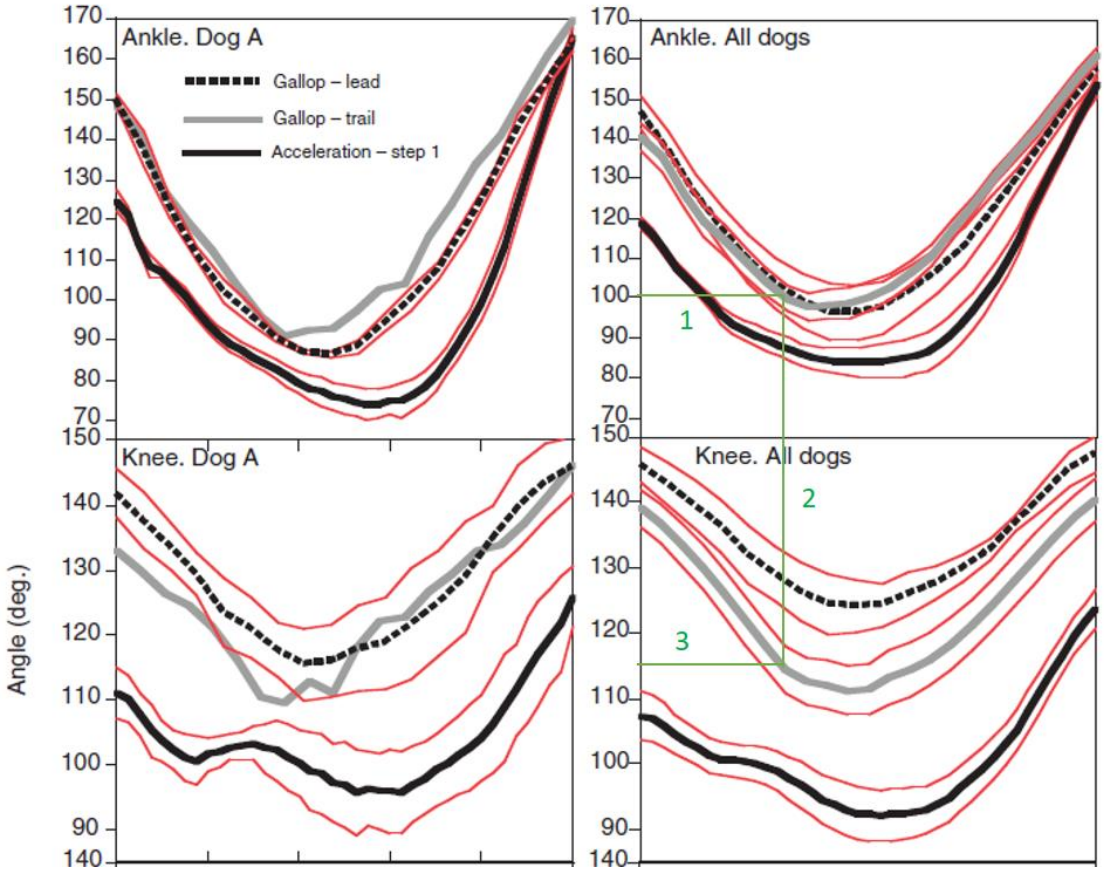

Figure 4-22: The simultaneous in vivo hock and stifle angles were obtained from previously published graphical data (Walter and Carrier, 2009). For a given hock angle (line 1), a vertical line (line2) was dropped to identify the simultaneous stifle angle (line 3).

4.4.3 Results

The joint angles for the stifle and hock of the cadaver limbs were recorded (Table 4.1). Limb 1 was incrementally loaded by linear distance from proximal restraint to foot plate whilst limb 2 was loaded to a set hock angle.

There was high correlation between stifle and hock angles (fig 4.23) for all cadaveric limbs.

Table 4-1: The hock and stifle angles of the two cadaver limbs in this study. Limb one was tested with the femoral block in a "stifle flexed" and "stifle extended" position. For all limbs, the reduction in hock angle that occurred during loading was also associated with a reduction in stifle angle

Limb	Limb 1				Limb 2	
stifle position	stifle flexed		stifle extended		stifle extended	
Joint	stifle angle	hock angle	stifle angle	hock angle	stifle angle	hock angle
angle (degrees)	111.1	112.96	139	114.33	140.7	120
	103.6	99.2	131.6	99.88	127.6	110
	100.8	89.7	125.5	90.2	123.5	100
	95.3	82.8	119.3	79.56	118.6	90
					115.0	80

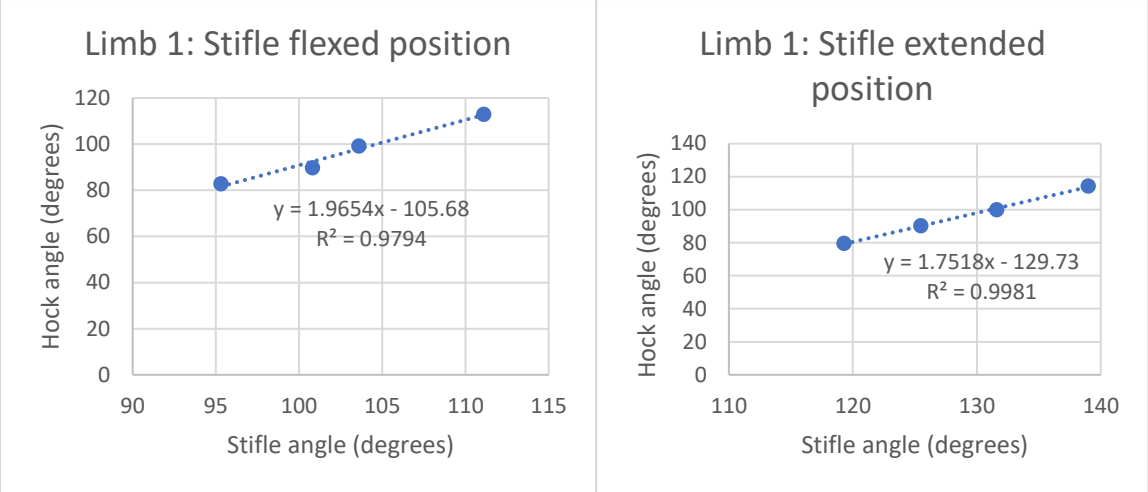

Figure 4-23: The correlation of stifle and hock angles for limb one with the stifle in a flexed (left) or extended(right) position. A trendline and value for correlation are seen, along with the slope of the line.

Two studies with clear graphs that would allow us to plot stifle vs hock angles were identified (Walter and Carrier 2009, Gregersen et al. 1998). An example of a graph is seen below (Fig 4.24) and a summary table comparing the results from the cadaver study to previously published in vivo results (table 4.2)

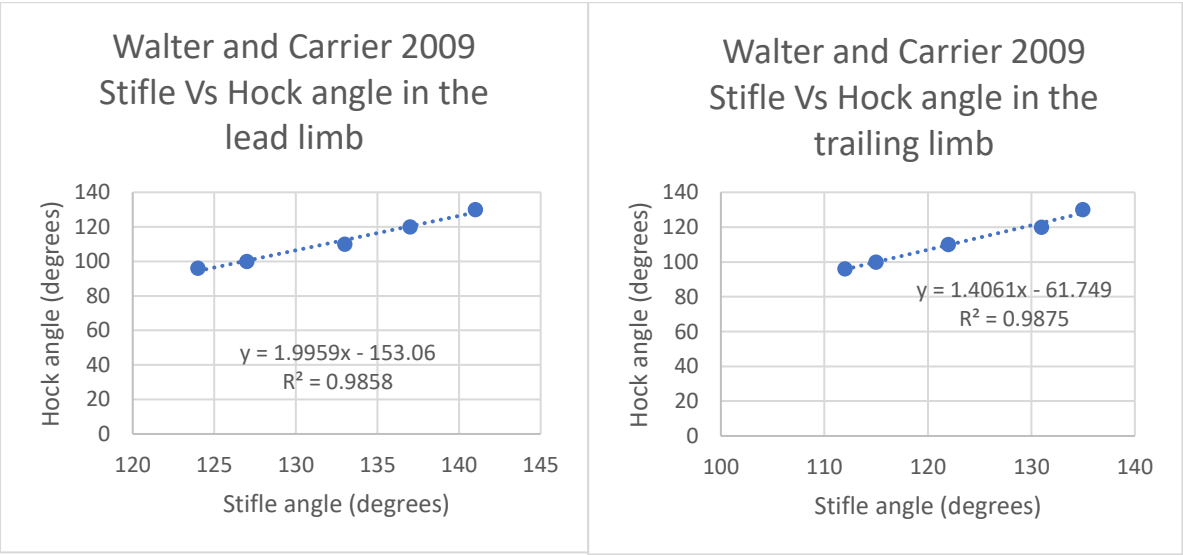

Figure 4-24: Plotted stifle and hock angles for the lead hind leg (left) and trailing leg (right) from Walter and Carrier (2009)

Table 4-2: The correlation co-efficient and slope from the cadavers used in this experiment and three previous in vivo kinematic studies when stifle and hock angle are plotted against each other. A correlation coefficient of 1 represents a perfect linear relationship, whilst 0 represents random data. All limbs in the above table show a near perfect linear relationship between stifle and hock angles. The coupling ratio represents the slope of the trendline. A coupling ratio of 1 means that for every one degree of stifle flexion, one degree of hock flexion occurs. A coupling ratio of 2 means that for every one degree of stifle flexion, two degrees of hock flexion occurs.

study	correlation co-efficient	Coupling ratio
Limb 1: stifle flexed position	0.9794	1.965
Limb 1: stifle extended position	0.9981	1.752
Limb 2: Stifle extended position	0.9191	1.521
Walter and Carrier 2009: Dog A lead leg	0.9934	1.996
Walter and Carrier 2009: Dog A trailing leg	0.9987	1.406
Gregerson 1998	0.9946	2.783

In vivo studies, show a very high correlation between stifle and hock angles in galloping dogs. The slope of the trendlines ranges from 1.406 to 2.783, meaning that for every 1 degree of stifle flexion there is 1.406 to 2.783 degrees of hock flexion. The cadavers loaded in our jig also showed a very high correlation, with R^2 values all >0.9 and slope ranging from 1.521 to 1.965, which is within the range from the in vivo studies. The values from Gregerson (1998) are obtained from non weight bearing limbs in comparison to the loaded limbs from Walter and Carrier (2009).

4.4.4 Discussion

The results of this study demonstrate that the angles of the stifle and hock in our cadaver limb loading jig are highly correlated, with every 1 degree of stifle flexion producing between 1.521 and 1.965 degrees of tarsal flexion. The coupled motion of the stifle and hock was also identified in previously published in vivo studies, where 1 degree of stifle flexion produced between 1.406 and 2.783 of tarsal flexion (Walter and Carrier 2009, Gregersen et al. 1998). The results from the cadaveric limbs fall within the ranges previously recorded in vivo, therefore supporting the hypothesis that the limb loading jig being evaluated is capable of replicating in vivo joint angles.

The position of the femoral block did influence the relationship between stifle and hock angles but this relationship (slope of the line when stifle angle and hock angle are plotted against each other) remained within the limits of previous in vivo testing, suggesting either position would be appropriate for replicating in vivo joint angles.

Coupling of stifle and hock flexion has been previously described with 1 degree of stifle flexion resulting in 0.72 degrees of hock flexion (Gregersen et al., 1998). That is, a change in stifle angle produces a smaller change in hock angle. This is in contrast to the present cadaveric study and in vivo measurements, where the change in stifle angle produced a greater change in hock angle. This can be explained by the measurement techniques used in both studies. Gregerson et al (1998) measured these angles in non-weight bearing limbs, whilst our measurements and those from in vivo studies were measured during loading of the limb. Elasticity in the gastrocnemius tendon allows an increased degree of hock flexion during load bearing as is considered the most likely reason for these discrepancies.

The length of the gastrocnemius increases during the stance phase by up to 10% (Goslow et al., 1981) despite activation of the muscle. The muscle fibre length and pennate arrangement of the gastrocnemius suggest this muscle undergoes isometric contraction and comprises part of the biological spring mechanism of the limb.

In this experiment, the force exerted by the foot pads on the foot plate was not recorded, which would have allowed correlation between limb angles and applied force, further validating the use of this device.

Although this limb loading device accurately replicates the coupled motion of the stifle and hock, further studies that measure the force exerted by the foot are required before the jig can be validated as accurately replicating the biomechanics of the distal limb.

4.5 Experiment 4: Replication of joint forces

4.5.1 Introduction

During force-displacement studies, the investigator may choose to load to a set displacement (and measure force) or alternatively load to a predetermined force (and measure displacement). In the previous experiment, displacement of the limb segments, and subsequent joint angles were recorded, however, the force exerted on the limb was not measured. To investigate if the force exerted on the foot plate is within physiological limits for a given displacement, the jig was modified to allow quantification of the force the paw exerts on the foot plate. The angle of flexion of the hock when loaded to a predetermined force on the foot plate is reported in the following experiment.

4.5.2 Materials and Methods

To enable the measurement of force transmitted through the limb, pressure sensitive film (Film code 5076-350. Tekscan, South Boston, MA, USA) was positioned under the non-slip surface of the foot plate. The film was calibrated to measure force in newtons. The readout produced a real-time pattern of loading of the foot pads and the peak force measured (figure 4.25).

10 paired canine cadaver hind limbs from adult greyhounds euthanised for reasons unrelated to this study were obtained. They were prepared and positioned into the limb loading jig as described for the previous experiment.

The limbs were loaded until the peak vertical force reached 600N, which is approximately 1.7 X body weight for an average greyhound. This value was selected based on recordings of peak vertical force of the hind limbs of a galloping dog. (Walter and Carrier, 2007; Walter and Carrier, 2009)

The jig and attached limb were then scanned in a computed tomography scanner (Philips Brilliance 16-slice CT scanner)(120KVP, 117 mA, slice thickness 1mm, slice increment 0.5mm, 512 X512matrix).

The DICOM images imported into commercially available software (Mimics 17.0, Materialize, Belgium)

From sagittal images, the angle of hock flexion was recorded. A line was drawn between the tibial tuberosity and the centre of the talus. A second line connected the centre of the talus to the metatarsophalyngeal joint. The intersection of these lines gave the joint angle (fig 4.26). These landmarks do not represent the mechanical long axis of the bones but correlate with the position of skin markers used in previous kinematic studies.

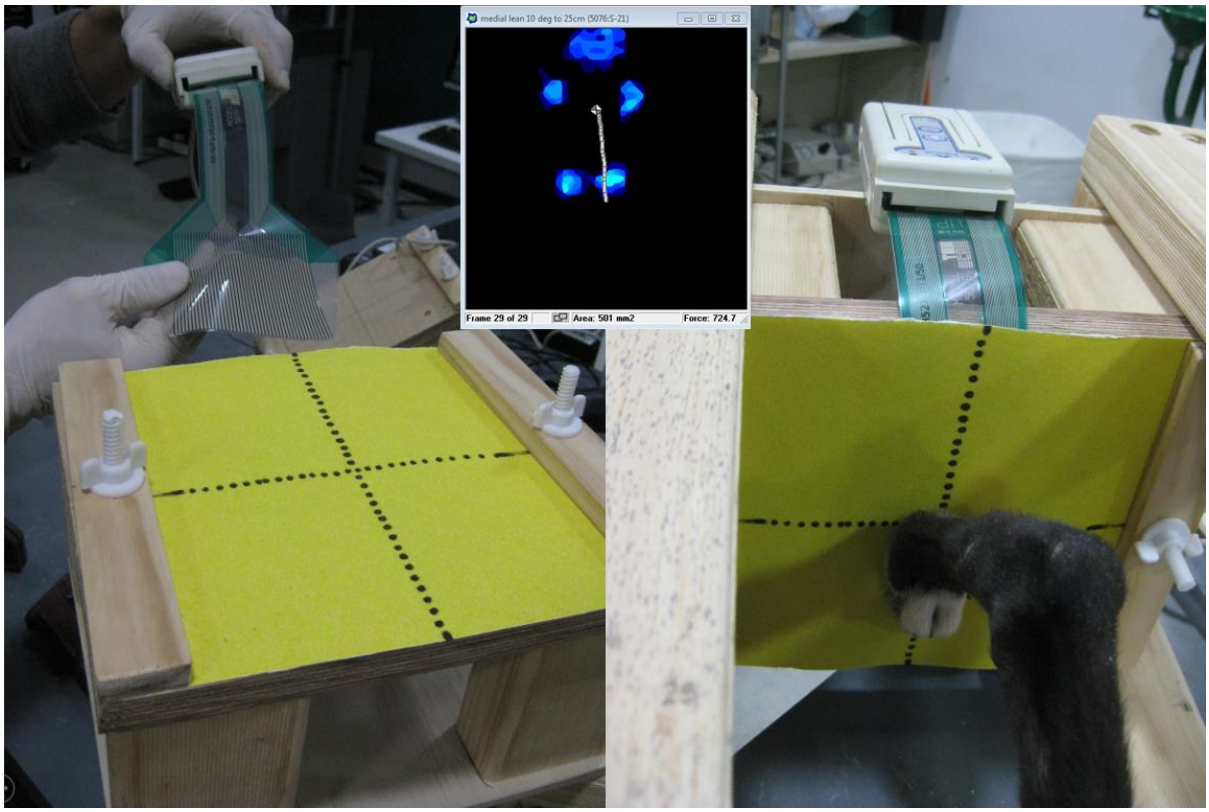

Figure 4-25: The pressure sensitive film being positioned under the non-slip surface (left). The foot was centred on the foot plate (right) and a digital pressure distribution pattern produced (inset). This film allowed real time recording of force exerted as well as the distribution of load through the digital and metatarsal pads. Additionally, the centre of force distribution is also recorded and was shown to move caudally during limb loading.

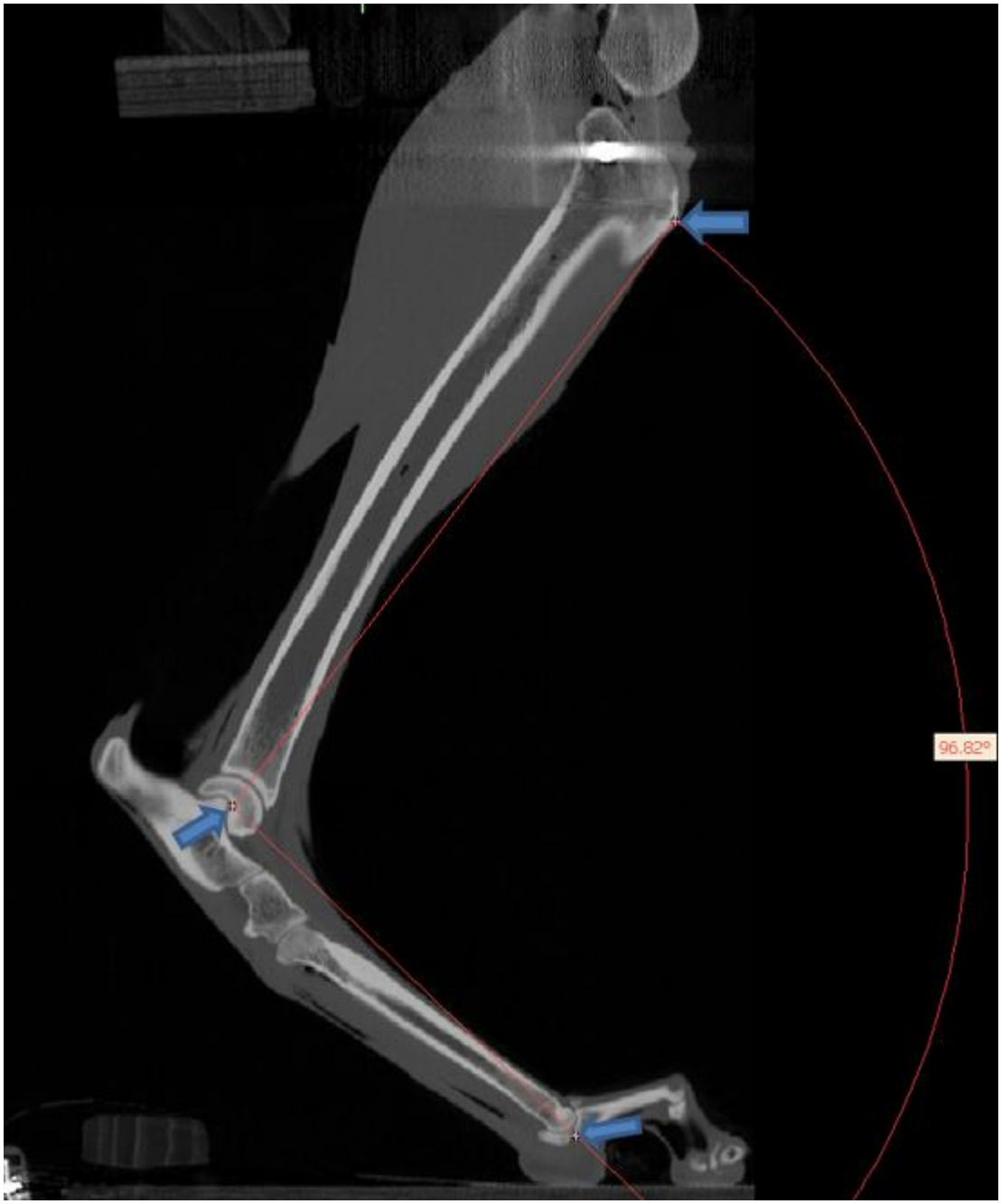

Figure 4-26: The measurement of the hock angle. The tibial axis was a line connecting the tibial tuberosity(top arrow) and centre of the talus(middle arrow), whilst the axis of the pes was a line joining the centre of the talus with metatarsophalyngeal joint (bottom arrow). In this example the angle measures 96.82 degrees.

4.5.3 Results

The mean angle and hock flexion was 101.0 ± 7.33 degrees when 600N was recorded on the pressure sensitive film. The results of the individual limbs can be seen in table 4.3

Table 4-3 hock angle of the 10 specimens when a peak vertical force of 600N was recorded. The mean hock angle of 101 degrees is similar to in vivo measurements from previous investigations which simultaneously recorded ground reaction force and joint angles using skin markers (Walter and Carrier, 2007)

Specimen number	**hock angle (degrees)**
1	95.87
2	101.97
3	96.25
4	96.61
5	89.59
6	96.82
7	114.7
8	107.44
9	105.37
10	105.37
mean	**101.00**
SD	**7.33**

4.5.4 Discussion

A mean hock angle of 101 ± 7.33 degrees was recorded when the ground reaction force of approximately 1.7 X body weight was applied. This finding is consistent with the minimum angle of hock flexion (96 ± 8.8 for the lead hind limb and 97 ± 3.8 for the trailing hind limb) recorded in vivo, which simultaneously produced a peak vertical force of 1.64 ± 0.11 X body weight in the galloping dog(Walter and Carrier, 2009). These findings support the hypothesis that the limb loading jig can produce a hock flexion angle and ground reaction force similar to those recording from the in vivo galloping dog.

The ground reaction force(GRF) is dependent on a tensile force being applied to the tuber calcanei. (fig 4.27) The magnitude of the GRF will increase if tensile forces acting on the calcaneus increase and conversely, the GRF will decrease if the tensile force decreases.

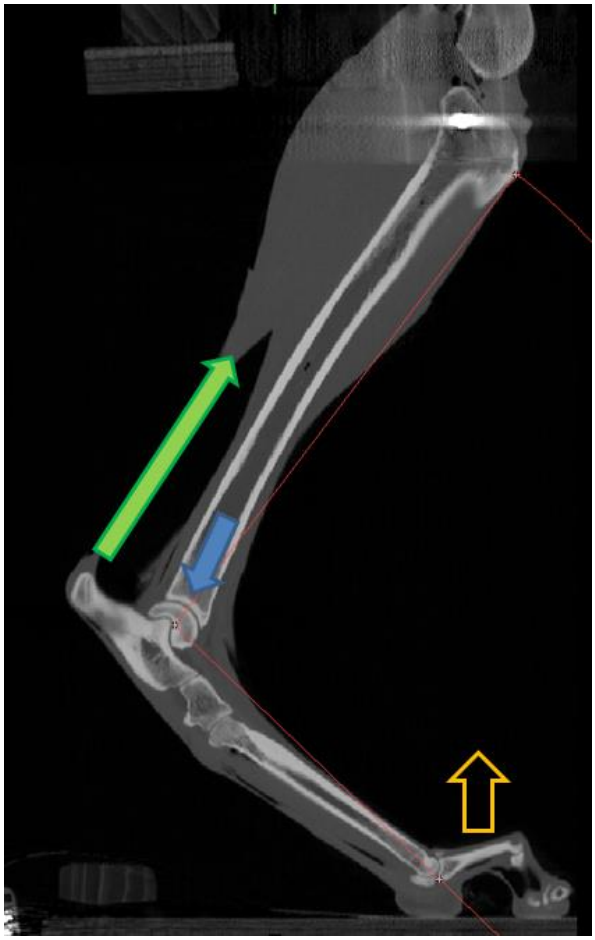

Figure 4-27: shows the forces acting on the canine pes. The pes will rotate about the centre of the talus, which is loaded by the animal's body weight (blue arrow). A tensile force produced by the gastrocnemius (green arrow) will produce a proportional ground reaction force that can be measured using the pressure sensitive film (open yellow arrow)

In the limb loading jig, designed to simulate both internal and external forces across the tarsus, the tensile force acting on the tuber calcanei is produced by the intact gastrocnemius. Despite no active contraction of the muscle in the cadaver specimen, this muscle is still able to generate a tensile fore on the calcaneus when the stifle is prevented from flexing. The m. gastrocnemius is covered in thick tendinous leaves and is infiltrated by tendinous strands(Evans et al., 2012). Previous investigations of the canine gastrocnemius suggest that is a major contributor to the biological spring of the hind limb, with a high tendon length change: muscle fascicle length, indicating a reliance on passive length change (tendon elongation) rather than active muscle shortening (Williams et al., 2009). In vivo studies report a lengthening of the gastrocnemius of 9% during the first stages of the stance phase, followed by a 10% shortening at take-off , suggesting that active contraction of the muscle is most important in the final stages of the stance phase (Goslow et al., 1981).

Accurately reproducing the stifle and hock angles during loading is likely to result in a close approximation of the tensile force within the gastrocnemius muscle and tendon that occur during galloping. This in turn, has produced a ground reaction force that is comparable to measurements made in galloping dogs.

This limb loading jig can accurately reproduce the displacement of limb segments during loading (measured by stifle and hock angles) and accurately reproduced the major internal and external forces exerted on the tarsus, including replication of the major muscular forces exerted during weight bearing at high speeds. These findings suggest that this limb loading jig would be able to accurately reproduce in vivo tarsal kinematics for a dog running at high speeds. However, it must be recognised that the rate of loading in this jig occurs slowly in contrast to in vivo conditions where the stance phase may be a short as 0.2 seconds during trotting. As tissues of the musculoskeletal system are viscoelastic, this is, will demonstrate different material properties dependant on the rate of loading, any difference in loading rate may influence any potential results.

4. 6 Chapter discussion

A radiolucent limb loading jig that can replicate the coupled motion of the hock and stifle as observed in in vivo studies (Goslow et al., 1981; Gregersen et al., 1998; Walter and Carrier, 2009) and the internal and external forces that are exerted on the canine tarsus during high speed running was designed, constructed and further refined as part of this thesis.

This jig was designed with the purpose of investigating canine tarsal bone kinematics using non-invasive CT based kinematic measurements. Prior to construction, a number of key capabilities that would be required from such a device were identified.

Firstly, the jig would have to be constructed of radiolucent material in the areas where metal artefact may interfere with identifying the cortical contours of the tarsal bones. This jig was constructed primarily with pine which has a radiographic density of -456 Hounsfield Units (HU) (Lee, 2010), which is well below the density of water (0HU) and bone (greater than700 HU) (Fat et al., 2012). During processing of the DICOM images, the only artefacts were created by the metal brackets used to restrain the proximal limb. No artefacts were identified at the level of the tarsal bones.

Secondly, the jig was designed to approximate in vivo loads and permit kinematic measurements with minimal disruption to the tissues. All cadaver limbs were frozen before use and dehydration was prevented by wrapping limbs in saline soaked cloth. Previous studies have suggested that the material properties of connective tissue are minimally affected by the freezing process (Moon et al., 2006; Woo et al., 1986).

Maintaining the soft tissue structures that surround joints is important for accurate recreation of forces when using cadaver models as the ligaments and joint capsule act as natural passive restraints to limit motion. The loading jig described in this chapter required no dissection distal to the mid tibia for loading or kinematic measurements, allowing preservation of all periarticular structures.

Recreation of muscular force is essential when studying kinematics in cadaver models as the magnitude and direction of muscular tensile forces determine the displacement of bone, in conjunction with the limiting effects of ligaments, joint capsule and congruent bone contours. The canine tarsal bones have few direct muscular attachments. The common calcaneal tendon inserts upon the tuber calcanei and comprises the tendons of the superficial digital flexor muscle, gastrocnemius muscle and conjoined tendon of gracillis, semitendinosis and biceps femoris. In this model, preservation of the superficial digital flexor and gastrocnemius muscles allowed accurate recreation of tensile force (experiment 4.4). Both these muscles show a high tendon length change: muscle fascicle length, indicating a reliance on passive length change (tendon elongation) rather than active muscle shortening(Williams et al., 2009).

The other muscle with direct insertion on the tarsal bones is the cranial tibial muscle, a flexor of the hock that is not active during mid stance and hence no attempt was made to replicate the force produced by this muscle. Other tarsal flexors include the fibularis longus and fibularis brevis which are both active in the swing phase of gait (Wentink, 1976) but not active during the stance phase.

The quadratus plantae muscle is considered an insignificant muscle running from the lateral tuberosity of the calcaneus to the deep digital flexor tendon (Evans et al., 2012).

The extensor digitorum brevis has its origin on the dorsal part of the calcaneus and runs distally. This small muscle extends the digits and is not considered active during the stance phase(Evans et al., 2012) and hence, no attempt was made to replicate its effect.

The adductor digit V is a small, mainly tendinous muscle that runs from the lateral aspect of the tuber calcanei to insert of the base of metatarsal V (Evans et al., 2012). This mainly tendinous band was preserved allowing replication of the passive effects of the muscle.

The gastrocnemius spans across two joints and couples the motion of the stifle and hock joints. The relationship between stifle and hock flexion differs between the passive range of motion (without

weight bearing load) and load bearing scenarios. Whilst one degree of stifle flexion results in less than 1 degree of hock flexion in the non-load bearing state, one degree of stifle flexion during load bearing produces greater than one degree of flexion at the hock joint. This finding may be partially explained by the elongation in the gastrocnemius muscle which has been previously reported (Alexander, 2002), but another possible explanation is dorsiflexion of the pes. In other species, up to 17 degrees of dorsiflexion was observed at the intertarsal and tarsometatarsal joints. It is likely that both factors are responsible for the observed changes in stifle and hock coupling.

The initial limb loading jig design relied upon immobilisation of the stifle joint and prevented simultaneous flexion of the stifle and hock as seen in in in vivo kinematic studies. Following modification of the proximal limb restraint, the coupled motion of the stifle and hock that has been identified in vivo, was reproduced.

Limitations:

This series of experiments represents the evolution of the limb loading device, which developed rapidly following each experiment. Therefore, large numbers of replicates were not performed for every step as obvious flaws were identified and rectified. All testing was non-destructive and so allowed for repeated measures to be performed on single specimens. However, there is the possibility of changes to the material properties of the limb with repeated loading due to tissue creep, which may not be recoverable in cadaveric tissue, and has the potential to influence results. The load exerted on the force plate as the limb was repeatedly loaded and unloaded to the same position in the jig was measured and noted that after 1-2 cycles, there was no change in force recorded for the following measurements. Although this data is not reported here, it was used to develop the pre-conditioning protocol that was used in later experiments.

The data from the cadaveric specimen was only compared to in vivo data from a limited number of dogs from previous studies (Gregersen et al., 1998; Walter and Carrier, 2009). These studies were selected as they provided clear graphical representation that allowed us to derive simultaneous hock

and stifle angles from in vivo experiments. Other studies (Goslow et al., 1981), also represent similar graphical data but the image resolution was not of a suitable standard to reliable derive the required data. It is important to acknowledge that small errors are possible when deriving numerical data from published graphical representations rather than the original data set.

Validation of this jig could also include instrumenting tendons and ligaments, such as the common calcaneal tendon and plantar ligament, with strain gauges allowing comparisons to be made to the in vivo scenario. Similarly, direct measurement of forces across the individual joints could have been performed with pressure sensitive film and used as another validation measure. This was not performed in this series of experiments for two reasons; firstly, it would involve performing a series of in vivo experiments as there is no published data recording the strain in these tissues for canine limbs or force across articular surfaces during high speed running in the dog. Secondly, instrumentation with strain gauges and pressure sensitive films would require further dissection of the pes, which may alter the kinematic patterns of the bones being investigated. Rather, the resultant force on the ground, measurement of elongation of the gastrocnemius muscle and joint angles were used as in vivo data was available for these parameters to allow a comparison to be made and measurements could be recorded without disrupting tissues, such as the tendons, ligaments and joint capsules, which all play a role in determining bone kinematics. However, it is acknowledged that direct measurement of internal forces in the cadaveric limb and comparison to in vivo data would provide further validation of this jig and its ability to replicate all relevant forces for the weight bearing limb.

Conclusion

The results of the experiments performed in this chapter suggest the limb loading jig can accurately replicate the displacement of limb segments and produce ground reaction force comparable to in vivo kinetic and kinematic studies. As most of the forces on the tarsal bones are passive, derived from the forces from adjacent bones, the joint capsule and ligaments, the ability of this jig to

accurately replicate the internal forces of the tarsus without dissection of the distal limb makes it a valuable device for the study of tarsal bone kinematics.

The overall design of this jig may also make it suitable for investigating bone kinematics in the canine forelimb and in the limbs of other digitigrade species. Modifications to the proximal limb restrain may be required but the development of a range of proximal limb restraints may increase the versatility of this jig and scope for kinematic investigations.

Chapter 5 : Characterisation of canine tarsal bone kinematics identifies the functional units of the canine foot

5.1 Introduction

The limbs of trotting, galloping or hopping terrestrial mammals can be considered as biological springs, storing kinetic and potential energy as elastic strain during the first half of the stance phase, then releasing this energy as the animal propels itself upwards and forwards during the second half on the stance phase of gait (Alexander and Bennet-Clark, 1977). It has been suggested that this mechanism may conserve up to 50% of the energy that would otherwise be required did this mechanism not exist (Alexander and Vernon, 1975; Cavagna et al., 1964).

The mechanism that facilitates energy storage is complex and remains only partially characterized in most species. It involves a highly specific anatomical arrangement of tissues with varying mechanical properties and will naturally vary between animals with different conformation and gait.

Amongst legged terrestrial animals, the dog (Canine Familiaris) is a supreme athlete capable of both great speed and endurance (Poole and Erickson, 2011). In this species, the majority of energy storage in the hind limb occurs below the stifle due to the specific arrangement of tissues with differing mechanical properties (Alexander, 1984; Gregersen et al., 1998). In common with other species, the larger muscles of the thigh have long muscle fibres and short tendons (Williams et al., 2008), which facilitates active muscle shortening but limits their able to store elastic strain (Alexander, 1984). In contrast, the muscles of the crus display short fibres in a pennate arrangement with elongated tendons; an arrangement which facilitates elastic strain storage (Alexander, 1984; Alexander and Bennet-Clark, 1977). Active muscle shortening does not appear to contribute significantly to generating elastic strain in elongated tendons, but rather a change in joint angle leads to stretching of these tendons. This is observed at the hock, when flexion of this joint during the stance phase results in elongation of the gastrocnemius muscle, the primary extensor of the hock. The gastrocnemius muscle and tendon, will lengthen by up to 9% during eccentric contraction during the stance phase (Goslow et al., 1981), allowing storage of significant amount of elastic strain energy. In addition, hock flexion will also result in lengthening of the digital flexor tendons as they

pass along the caudal aspect of the joint, further facilitating the storage of elastic stain energy in the distal limb.

Elastic deformation of the pes has been documented in a number of species including man (Ker et al., 1987) and camels (Alexander et al., 1982) and is believed to further contribute to elastic energy storage in the limb. In camels, up to 17 degrees of dorsiflexion occurred at the intertarsal and tarsometatarsal joints and this motion allowed greater elongation of flexor tendons and hence, energy storage (Alexander et al., 1982). In the human foot, the flattening of the longitudinal arch stretches connective tissue of the foot and has been shown to store about half the elastic strain that can is stored in the Achilles tendon, further improving locomotor efficiency (Ker et al., 1987).

The canine pes is commonly modelled as a rigid structure in kinematic studies (Fischer and Blickhan, 2006; Fu et al., 2010; Gregersen et al., 1998; Hottinger et al., 1996; Walter and Carrier, 2009), which allows application of the laws of rigid body mechanics and generates clinical useful information regarding gait (Colborne et al., 2005; Colborne et al., 2006). However, the canine pes comprises 7 tarsal bones (talus, calcaneus, central, fourth, third, second and first tarsal bones) four metatarsals and the phalanges (figure 5.1). Palpable motion is recognised at the intertarsal and tarsometatarsal joints, with these joints described as low motion joints (Gorse et al., 1990) and exceedingly rigid (Evans et al., 2012). The magnitude, direction and significance of intertarsal bone motion is currently unknown, however, it can be hypothesised that intertarsal bone motion facilitates dorsiflexion of the pes during locomotion, which may enhance the ability to store elastic strain energy in structures such as the digital flexor tendons and plantar ligaments.

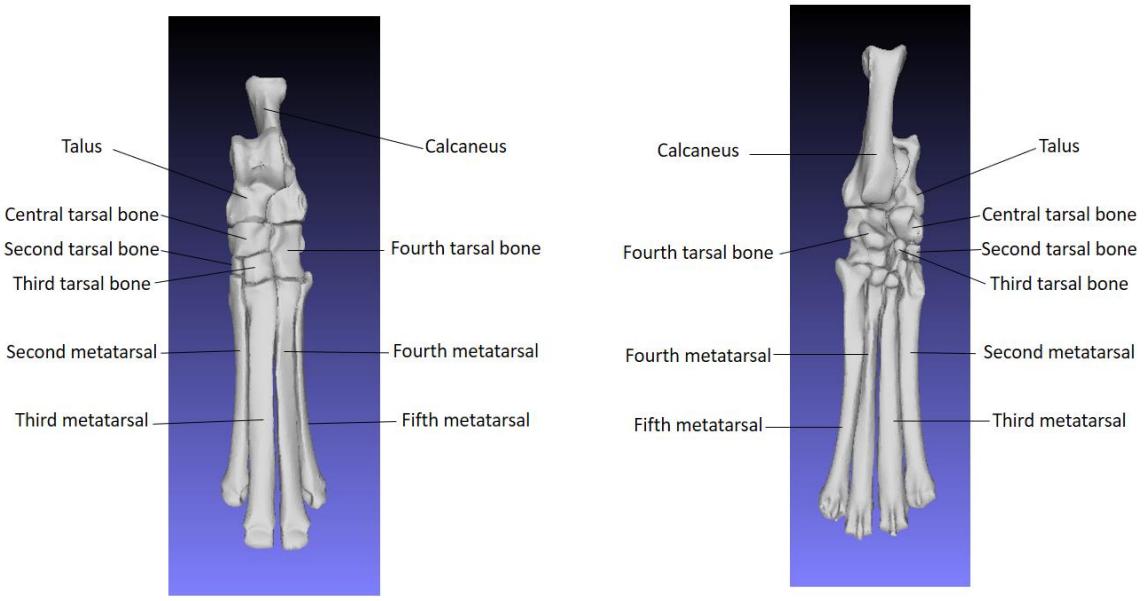

Figure 5-1: The bones of the canine pes. The dorsal view (left) and plantar view (right) showing the bones of the canine pes. The first tarsal bone and phalanges are not shown in the images as the kinematics of these bones were not included as part of the study.

To determine if intertarsal bone motion facilitates dorsiflexion of the canine pes during locomotion, a novel cadaver limb loading device was developed, which could replicate the internal and external forces exerted on the canine limb during running (described in chapter 4). Given the high speed and rapid gait cycle of the galloping dog, in vivo testing was considered unsafe for charactering tarsal bone kinematics at maximal speeds. Computed tomography based kinematic measurement techniques have been previously used to quantify motion of canine tarsal bones and are accurate to within 0.06mm in translation and 0.3 degrees in rotation (Tan et al., 2017). This technique allowed quantification of tarsal bone motion without any disruption to the soft tissues, which are essential in the constraint and guiding of bone motion (Leardini et al., 1999; Sennwald et al., 1993).

The aims of this study were to:

- Characterise the motion of each canine tarsal bone within a 3-dimensional, anatomically based reference frame
- Describe how intertarsal bone motion may contribute to elastic deformation of the pes, quantifying the contribution of motion within the pes to overall hock flexion
- Identify if any co-ordinated pattern of intertarsal bone motion occurs by identifying both rigid functional units and highly correlated, kinematically coupled movements.

The first hypothesis was that tarsal bone motions does not occur simply in the sagittal plane and more complex out of plane motions are also involved for each bone. The second hypothesis to be tested was that dorsiflexion of the pes occurs during weight bearing making an overall contribution to hock flexion. The final hypothesis was that within the tarsal and metatarsal bones, there will be pairs of bones that move in unison allowing us to consider them as a rigid functional unit.

5.2 Materials and methods

5.2.1 Specimens

Ten hind limbs were obtained from five adult greyhounds, euthanised for reasons unrelated to this study. Limbs were disarticulated at the coxofemoral joint and frozen at -20^{0}C until testing. 24 hours prior to testing, limbs were thawed within a 4^{0}C refrigerator. To facilitate the positioning of the limbs within a custom-built radiolucent loading jig, all thigh muscles were removed, with the quadriceps muscles transected through the patellar ligament and all other muscles transected distally at their musculotendinous junction. The origins of the gastrocnemius and superficial digital flexor muscles on the supracondylar tubercle of the femur were carefully preserved. All four femorotibial ligaments were preserved. The femur was transected approximately 8 cm from the distal end of the bone.

Paired specimens were selected to allow comparison of left to right sided differences in kinematics, as racing greyhounds always run counter-clockwise around a circular track and have been shown to undergo asymmetrical skeletal remodelling as a result (Johnson et al., 2000; Johnson et al., 2001). The racing history of the specimens were unknown. Five cadavers of the same sex and breed, showing very similar conformation were tested to provide a representative sample of this breed consistent with previous kinematics reports from human foot kinematics (Arndt et al., 2007; Fassbind et al., 2011; Wolf et al., 2007; Wolf et al., 2008).

5.2.2 Limb loading jig

All limbs were loaded into a custom designed jig (figures 5.2 and 5.3) developed as part of this study. The limb was secured to the support arms of the jig by placement of a 6mm diameter threaded bolt through a previously drilled 5mm diameter bone tunnel in the proximal tibia. The tibial bone tunnels were initiated at a point 5mm distal to the articular surface and midway along the cranio-caudal width of the medial collateral ligament. The support arms of the jig, and attached tibia, could be

displaced towards a foot plate via a scissor jack. The geometric centre of the foot plate, which was covered in a non-slip surface (P80 sandpaper) was measured and marked with a permanent marker. Care was taken to position the metatarsal pad directly over this point. The force exerted on the foot plate by the paw was measured using a pressure sensitive film (Film code 5076-350. Tekscan, South Boston, MA, USA) positioned under the non-slip surface.

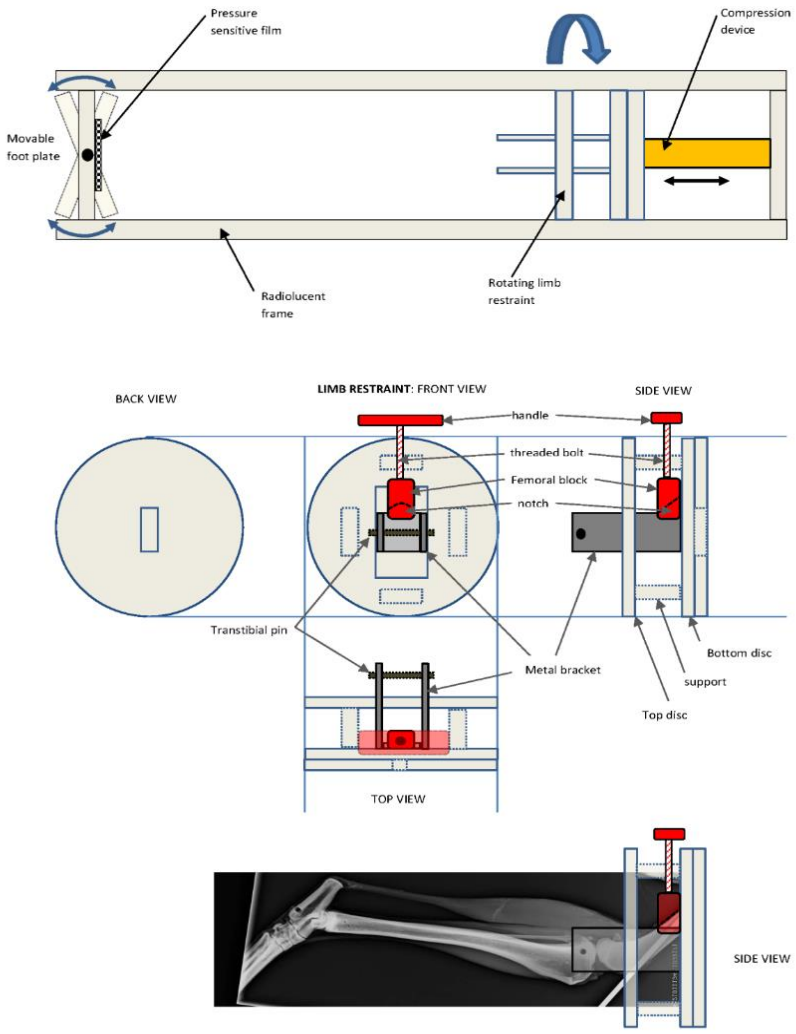

Figure 5-2: The design of a radiolucent limb loading jig designed for use in this study. The limb is secured to the jig by a trans-tibial pin (bolt) and stifle flexion is prevented by the femoral block. An intact gastrocnemius muscle produces tension in the common calcaneal tendon when loaded and replicates the major muscular force during weight bearing.

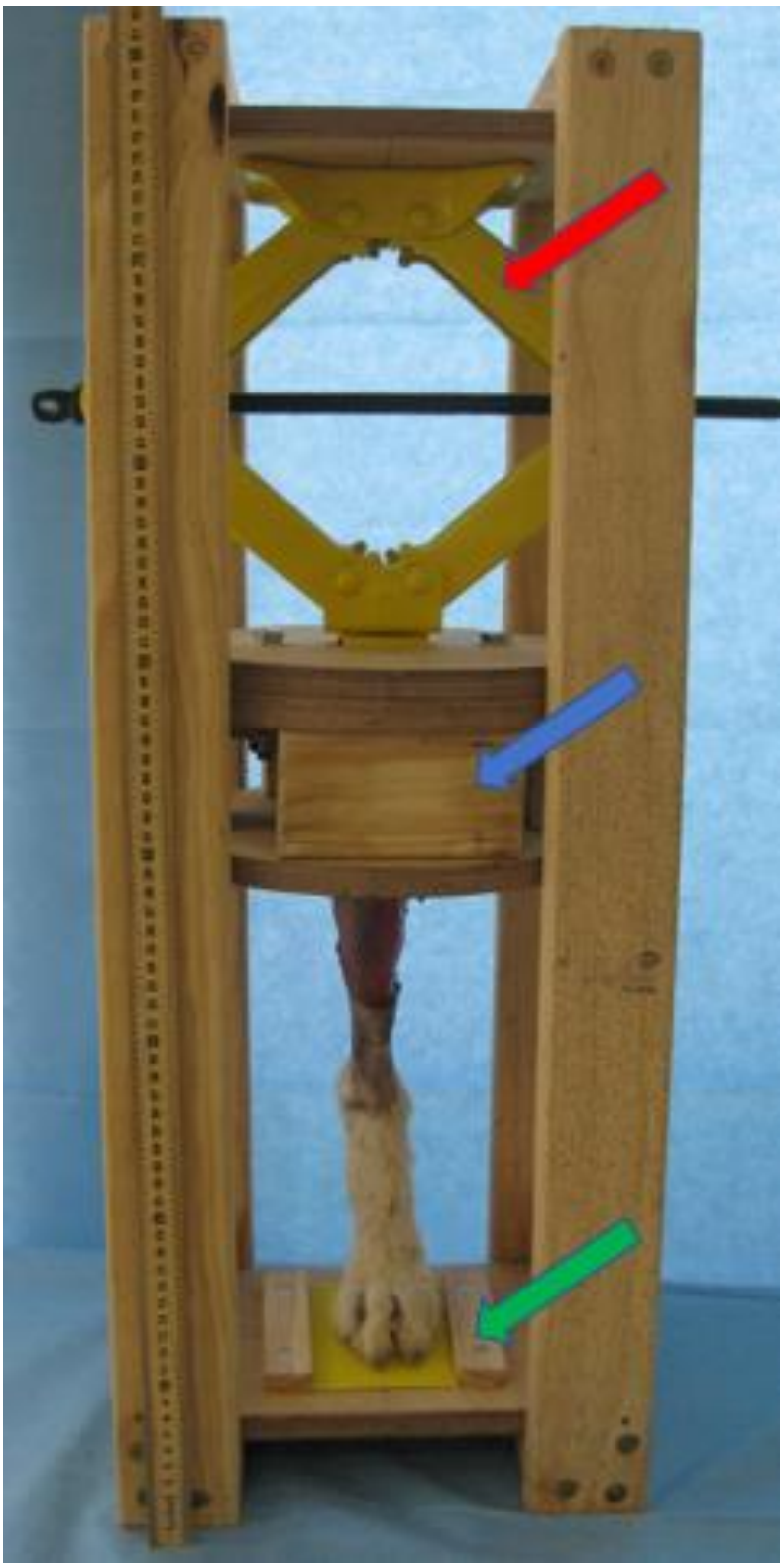

Figure 5-3: The jig comprises a proximal limb restraint (blue arrow) and a non-slip foot plate (green arrow). An axial load can be applied to the limb with a compression device (scissor jack) (red arrow)

To maintain tension within the gastrocnemius and superficial digital flexor muscles during loading, the stifle was maintained in extension by placement of a support block caudal to the femur. The support block was rigidly attached to, and hence moved in conjunction, with the support arms.

In the previous chapter (chapter 4), the limb loading jig was shown to be able to replicate the angles of the hock and stifle previously reported in galloping dogs in vivo (Walter and Carrier, 2009)

5.2.3 Computed tomography imaging

Prior to testing, the stifle and tarsal joints were manually flexed and extended and preconditioned in the jig to a force of 600N, measured on the pressure sensitive film positioned under the paw, over five cycles.

Following preconditioning, each limb (still positioned within the jig) was scanned three times using a 16 slice helical CT scanner (Philips Brilliance 16-slice CT scanner). The scanning parameters (120KVP, 117 mA, slice thickness 1mm, slice increment 0.5mm, 512 X512 matrix), resulted in a pixel size of 0.36mm X 0.36mm. The first scan involved the limb positioned in an “unloaded” position. A fiberglass mould was used to standardize the angle of flexion at the hock joint during the first scan. The second scan was performed following loading of the limb until a force of 600N was recorded on the foot plate and was termed the “load to force” scan. This force represents approximately 1.7X body weight of a 35kg dog, which has been previously recorded in vivo, using force plates (Walter and Carrier, 2007; Walter and Carrier, 2009). The linear distance was recorded between the foot plate and the limb restrain device for all specimens. The final scan was performed following loading of the limb to a hock flexion angle of 90 degrees, and termed the “load to displacement” scan. Like the “unloaded” scan, a fiberglass mould was used to standardize the position of the limb between specimens. This angle was chosen after viewing slow motion video of a galloping greyhound. The force exerted on the footplate during this scan was recorded along with the linear distance between the limb restrain device and foot plate.

5.2.4 Bone segmentation

All DICOM images were imported to Mimics 17.0 (Materialize, Belgium) and an accelerated segmentation tool (CT bone segmentation tool), which combined the functionality of thresholding, region growing, editing and 3D calculation was used to semi-automate the segmentation of the tibia, fibula, talus, calcaneus, central tarsal bone, second, third and fourth tarsal bones and metatarsal bones two to five. The 3-dimensional stereolithograph (STL) images of each bone were exported using the "optimal" STL export setting, which applies no matrix reduction but applies 2 iterations of smoothing and triangle reduction. Additional smoothing using 3 iterations of a 0.5 smoothing factor was applied.

5.2.5 Alignment to anatomically based reference axes

All bones from the "unloaded" scans were then aligned to a global co-ordinate system using commercially available software (3-matic 8.0, Materialize, Belgium), which allowed comparison of motion between specimens and description of kinematic motions in anatomically meaningful planes.

The reference axes were based upon anatomical landmarks of the pes. The dorsal plane was determined by using the dorsal cortical border of the third metatarsal bone, whilst the sagittal plane was positioned such that the third and fourth metatarsals were bisected. The transverse plane was calculated as the plane perpendicular to the two previously defined planes (figure 5.4). Motion along the X axis represented proximal or distal translation, whist motion along the y axis represented medial or lateral translation. Motion along the z axis referred to a dorsal or ventral translation. Rotation around the x axis represented internal or external rotation, rotation around the y axis represented dorsiflexion or plantarflexion and rotation around the z axis represented valgus or varus angulation (figure 5.5).

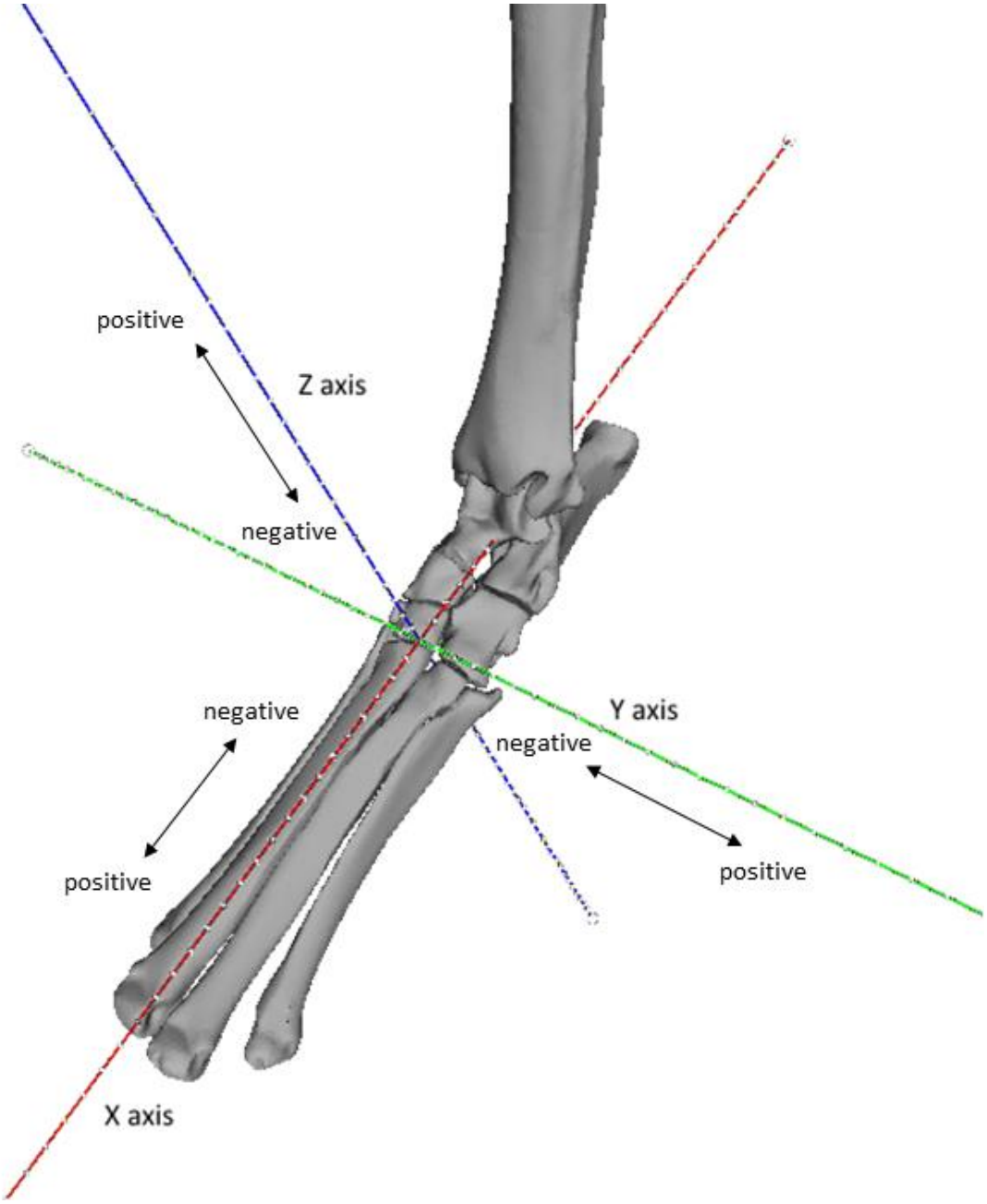

Figure 5-4: showing the three reference axes. Positive and negative values are reported indicating the direction of the translation along the axes. For translation along the Y axis, calculations have been adjusted so positive translations always indicate a medial direction for both left and right limbs. No adjustment is required for translation along the other axes.

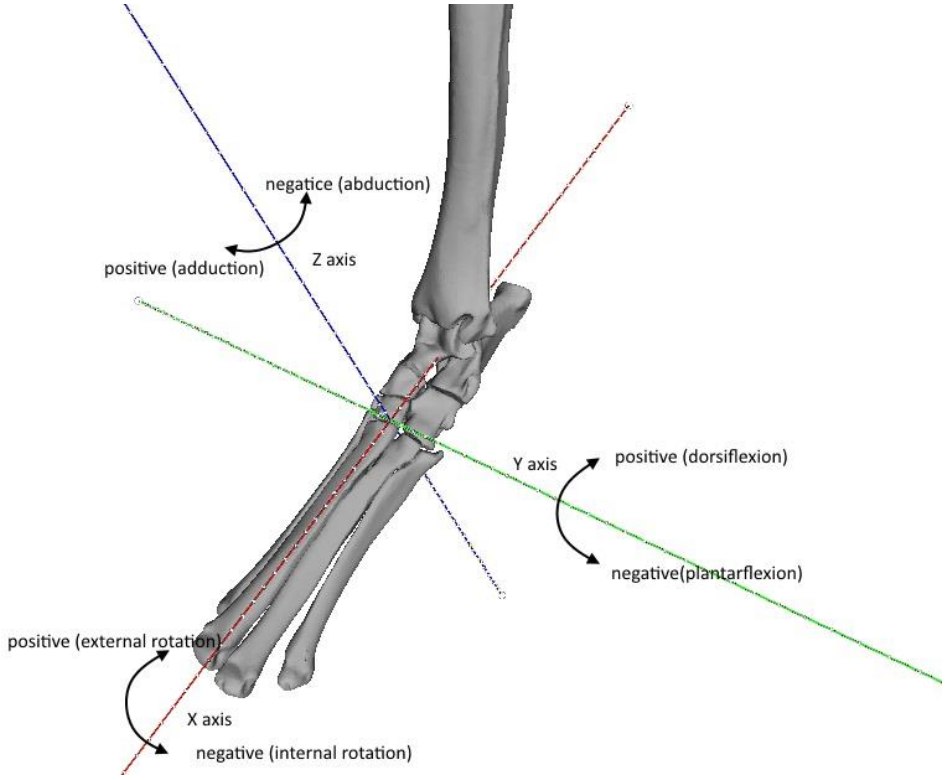

Figure 5-5: showing the three reference axes. Positive and negative values are reported indicating the direction of the rotations around the axes. For rotations around the X axis, calculations have been adjusted so positive values translate to an external rotation for both left and right limbs. For rotations around the Z axis, calculations have been adjusted so positive values translate to adduction for both left and right limbs No adjustment is required for rotations around the Y axis.

5.2.6 Calculation of kinematics

The STLs of the tibia, tarsal bones (talus, calcaneus, central tarsal bone, second, third and fourth tarsal bones) and four metatarsal bones from both the “load to force” and “load to displacement” scans were merged to form a single STL.

Using an open source meshing program (Meshlab) (Cignoni et al., 2011), the aligned talus from the “unloaded” scan was set as the base mesh, with all bone motions reported relative to this reference bone. An Iterative Closest Point (ICP) algorithm (Besl and McKay, 1992) was used to superimpose the aligned talus from the “unloaded” scan (reference bone) and the talus of the joined bones from the loaded scans.

Once the joined bones from the loaded scans were aligned, the position of the tibia, tarsal bones (with the exception of the first tarsal bone) and 4 metatarsals were then recorded in both the “load to force” and “load to displacement” positions. Briefly, the STL of each bone from the unloaded scan were superimposed onto the joined bones using the ICP algorithm. This resulted in each individual bone STL being recorded in an “unloaded” position, a “load to force” position and a “load to displacement” position relative to the talus.

A 4X4 transformation matrix was obtained for the motion of each bone from the “unloaded” to the “load to force” and “load to displacement” positions and decoded to yield the motion in 6 degrees of freedom (3 translations along the X, Y and Z axes and 3 rotations around the X, Y and Z axes) using a custom code (Mathematica, Wolfram, IL, USA) detailed in Appendix B

An overview of the sequential steps involved in calculating kinematics is shown in figure 5.6.

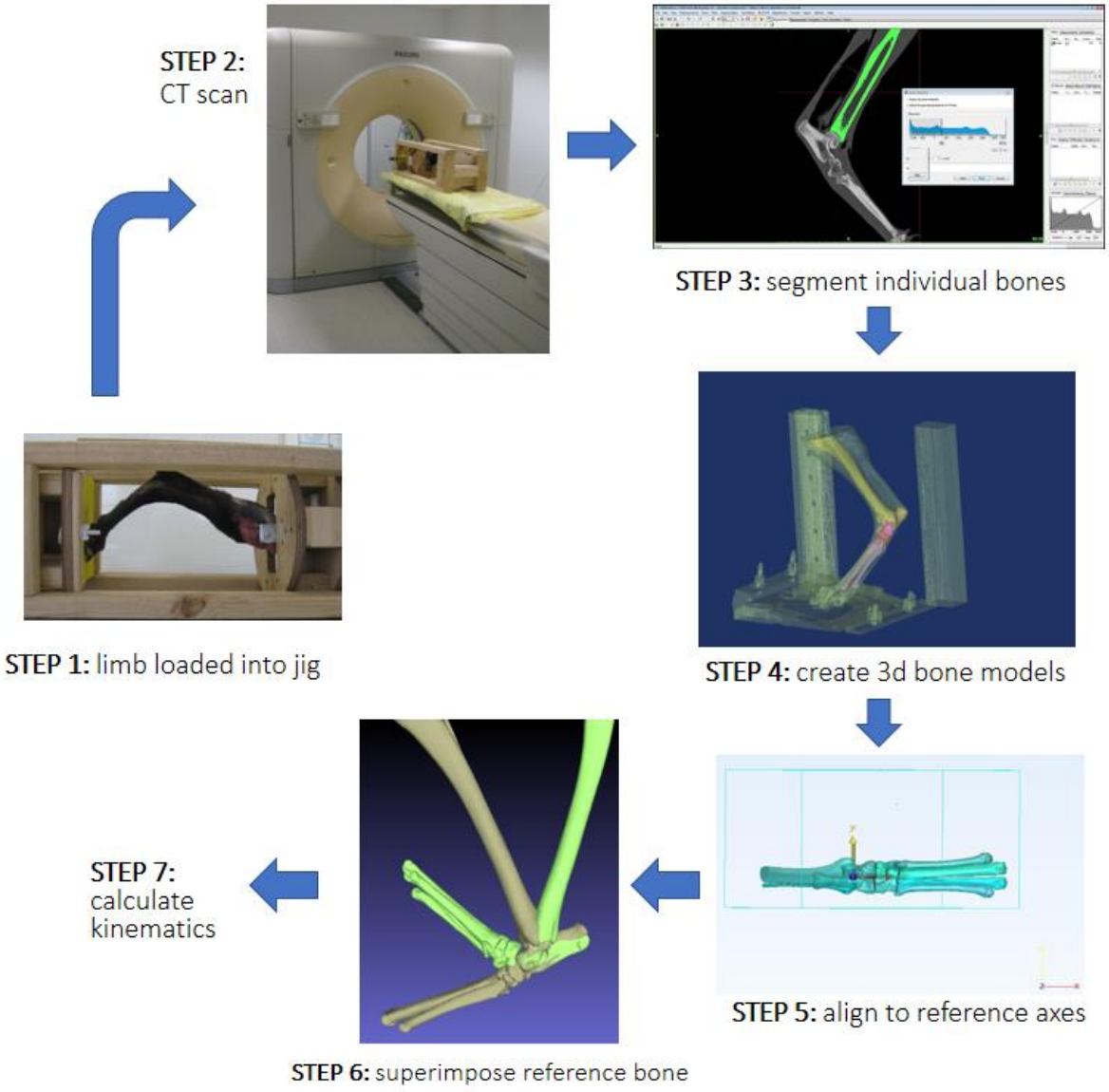

Figure 5-6: Shows the sequential steps involved in kinematic calculations. Following positioning in the limb loading jib (step 1), limbs undergo CT scanning (step 2) allowing the DICOM images to be exported to a computer where scans are segmented (step 3) based on Hounsfield units. From the segmented scans, 3 dimensional sterolithographic bone models are created (step 4) and aligned to anatomical reference axes (step 5). The reference bone of two scans are superimposed (step 6) allowing the motion of each bone from one scan to the next to be calculated (step 7)

5.2.7 Description of bone motion

As an alternative to reporting in 6 degrees of freedom, rigid body transformations can be reported as a single summative rotation around a helical axis. This single rotation was termed total rotation.

The magnitude of rotation around and orientation of the helical axis was calculated for each bone based upon previously published calculations (Panjabi, 1979; Spoor and Veldpaus, 1980; Woltring et al., 1985) and processed using coding in commercially available software (Mathematica, Wolfram, IL, USA). The orientation and position of the axis was reported as a point (x,y,z co-ordinates) and three vectors. In order to calculate how well aligned the helical axes of two bones were, the angle between these two axes in 3D space (alignment angle) was calculated using the following formula:

$$\text{Alignment angle (AA) (degrees)} = A\cos((x_1 \times x_2)+(y_1 \times y_2)+(z_1 \times z_2)) \times 180/\pi$$

Equation 5.1: Calculation of the alignment angle

Where,

x_1= x vector component of helical axis of bone 1

x_2 = x vector component of helical axis of bone 2

y_1= y vector component of helical axis of bone 1

y_2 = y vector component of helical axis of bone 2

z_1= z vector component of helical axis of bone 1

z_2 = z vector component of helical axis of bone 2

5.2.8 Kinematics relative to the sagittal plane

To calculate the contribution each joint made to the overall motion in the sagittal plane, only rotation around the Y axis was considered. The limb was divided into two kinematic chains; the medial column, which comprised the talus, central, third tarsal bone and third metatarsal and the lateral column, which comprised the calcaneus, fourth tarsal bone and fourth metatarsal bone. The relative contribution of each joint in the chain to sagittal plane potation was compared between the two loading patterns.

In order to compare the orientation of the helical axis of multiple bones in one analysis, the angle between the helical axis and the y axis of our co-ordinate system was calculated for each bone. As rotation around the y axis occurs in the sagittal plane, this angle represents the deviation in rotation away from the sagittal plane. This angle was termed the sagittal deviation angle (SDA) and was calculated using equation 5.2.

Sagittal deviation angle (degrees)= Acos (y vector component) X $180/\pi$

Equation 5.2: was used to calculate the sagittal deviation angle

5.2.9 Statistical analysis

All statistical analyses were performed using the commercially available statistical package Genstat (VSNi, Hemel Hempstead, UK). Descriptive data was performed for translations and rotations about the anatomically based axis, the magnitude of rotation around the helical axis and the orientation of the helical axis in relation to the sagittal plane. A paired t-test was used to compare hock angles between load to force and load to displacement. Similarly, a paired t-test was used to compare load recorded on the foot plate for both loading positions. All data was checked for normality using the Anderson-Darling test before further analysis. To compare the SDA, a general mixed linear model was used to evaluate the effect of bone, cadaver (dog 1-5), side (left or right limb) and loading pattern (load to force or load to displacement) on the SDA. Values of $p<0.05$ were considered significant.

A general linear model was also used to evaluate the effect of cadaver and side on the magnitude of rotation around the helical axis. As the magnitude would be expected to vary depending on load condition, one model was created for each load condition. To identify if any kinematic coupling existed, the magnitude of rotation for each pair was plotted using Excel (Microsoft, Redmond, Washington, USA) to yield a correlation coefficient (R^2) and kinematic coupling ratio (slope of the trendline).

A paired t-test was used to compare the relative contribution of each joint in the chain to sagittal plane rotation for both patterns of loading.

5.3 Results

5.3.1 Description of tarsal bone kinematics in 3 dimensions:

5.3.1.1 Six degrees of freedom descriptions

All bones demonstrated translation and rotation relative to the reference bone (talus). A summary of these motions along and around each reference axis is provided for load to force (table 5.1) and load to displacement (table 5.2).

Table 5-1: The mean motion of the tibia, tarsal bones and metatarsal bones following application of a standard (600N) load. The data is provided as a series of three translations and three rotations along and around the previously described reference axes. All motion is relative to the reference bone, the talus. From this table it is clear that there is motion about all three axes and not only about the sagittal plane. CTB = central tarsal bone, TB = tarsal bone, MT= metatarsal bone

Load to force (600N)		translation along (mm)			rotation around (degrees)		
		x axis	y axis	z axis	x axis	y axis	z axis
Tibia	mean	19.98	1.66	10.47	0.72	-15.62	1.52
	SD	5.13	1.66	1.69	1.08	2.01	0.77
Calcaneus	mean	0.21	0.24	0.08	-1.37	1.13	-0.40
	SD	0.13	0.07	0.08	0.80	0.72	0.25
CTB	mean	0.15	0.39	0.54	-1.35	2.18	-0.40
	SD	0.09	0.13	0.21	0.64	1.01	0.26
Fourth TB	mean	0.22	0.62	1.03	-1.50	2.55	-0.83
	SD	0.13	0.19	0.42	0.59	1.17	0.19
Third TB	mean	0.14	0.64	1.14	-0.89	3.25	-0.80
	SD	0.09	0.19	0.43	0.63	1.19	0.26
Second TB	mean	0.22	0.63	0.98	-0.89	3.74	-1.05
	SD	0.10	0.19	0.40	0.70	1.57	0.76
MT II	mean	0.28	1.72	4.48	0.45	5.45	-1.37
	SD	0.13	0.42	1.31	0.47	1.48	0.39
MT III	mean	-0.17	1.71	5.30	0.55	5.94	-1.10
	SD	0.10	0.45	1.60	0.66	1.60	0.41
MT IV	mean	-0.23	1.84	5.36	-1.47	6.13	-1.58
	SD	0.11	0.47	1.70	1.30	1.63	0.47
MT V	mean	0.05	1.87	5.37	-1.39	6.08	-1.48
	SD	0.10	0.50	1.66	1.45	1.54	0.46

Table 5-2: The mean motion of the tibia, tarsal bones and metatarsal bones following loading to a predetermined displacement (load to displacement). The data is provided as a series of three translations and three rotations along and around the previously described reference axes. All motion is relative to the reference bone, the talus. From this table it is clear that there is motion about all three axes and not only about the sagittal plane. CTB = central tarsal bone, TB = tarsal bone, MT= metatarsal bone

Load to displacement		translation along (mm)			rotation around (degrees)		
		x axis	y axis	z axis	x axis	y axis	z axis
Tibia	mean	37.82	2.85	15.14	1.93	-28.60	3.14
	SD	5.25	2.78	3.54	1.97	3.30	1.61
Calcaneus	mean	0.42	0.40	0.14	-2.71	2.05	-0.76
	SD	0.29	0.09	0.18	1.46	1.49	0.45
CTB	mean	0.22	0.80	1.03	-1.92	4.56	-1.18
	SD	0.16	0.22	0.45	0.78	2.08	0.51
Fourth TB	mean	0.35	1.14	1.85	-2.07	4.75	-1.51
	SD	0.22	0.32	0.86	0.74	2.32	0.32
Third TB	mean	0.15	1.22	2.13	-1.12	5.99	-1.72
	SD	0.16	0.32	0.94	0.70	2.30	0.63
Second TB	mean	0.32	1.20	1.91	-1.40	5.81	-0.98
	SD	0.17	0.32	0.90	0.93	2.51	1.92
MT II	mean	0.09	2.92	8.84	1.83	10.84	-2.03
	SD	0.33	0.71	2.92	1.15	3.12	0.64
MT III	mean	-0.85	3.20	10.22	1.71	11.62	-2.10
	SD	0.50	0.80	3.30	0.88	3.11	0.71
MT IV	mean	-0.90	3.43	10.00	-1.97	11.54	-3.11
	SD	0.48	0.78	3.28	1.49	3.00	0.76
MT V	mean	-0.32	3.47	9.78	-1.93	11.11	-3.01
	SD	0.28	0.71	2.92	1.63	2.63	0.67

5.3.1.2 Description as a single rotation around helical axis

When expressed as total rotation around the helical axis, there were significant differences between the magnitude of rotation for different bones but no significant effect of side (p=0.183 for load to force, p=0.390 for load to displacement) or dog (p=0.093 for load to force, p=0.144 for load to displacement).

For both load conditions the tibia showed the greatest total rotation and was significantly different to all other bones. The was no difference in total rotation between the four metatarsal bones and the second, third and fourth tarsal bone for each load condition (figure 5.7)

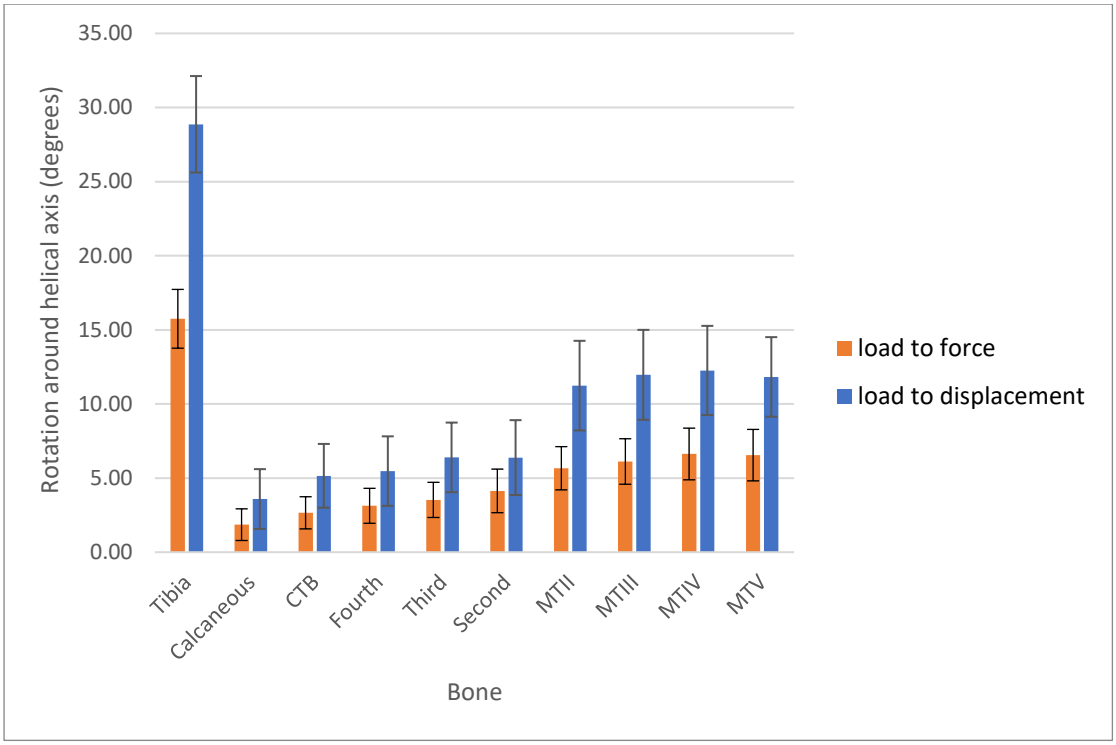

Figure 5-7: The total rotation of each bone around it's own helical axis for both loading conditions. Each bone underwent greater rotation when loaded to displacement rather that to 600N of force. There was greatest motion at the talocrural joint, followed by the tarsometatarsal joint with the least motion observed between the tarsal bones themselves. CTB = central tarsal bone, Fourth = fourth tarsal bone, Third = third tarsal bone, Second = second tarsal bone, MT = metatarsal

The calcaneus and central tarsal bones showed no difference in total rotation compared to the numbered tarsal bones, with the exception of the calcaneus, which rotated significantly less than the second tarsal bone in the load to displacement scan.

The orientation of the helical axis of each bone was oblique to the reference co-ordinate axis was located remotely to the bone itself in all cases other than the calcaneus (figures 5.8 and 5.9) The vectors for each axis are available in Appendix C

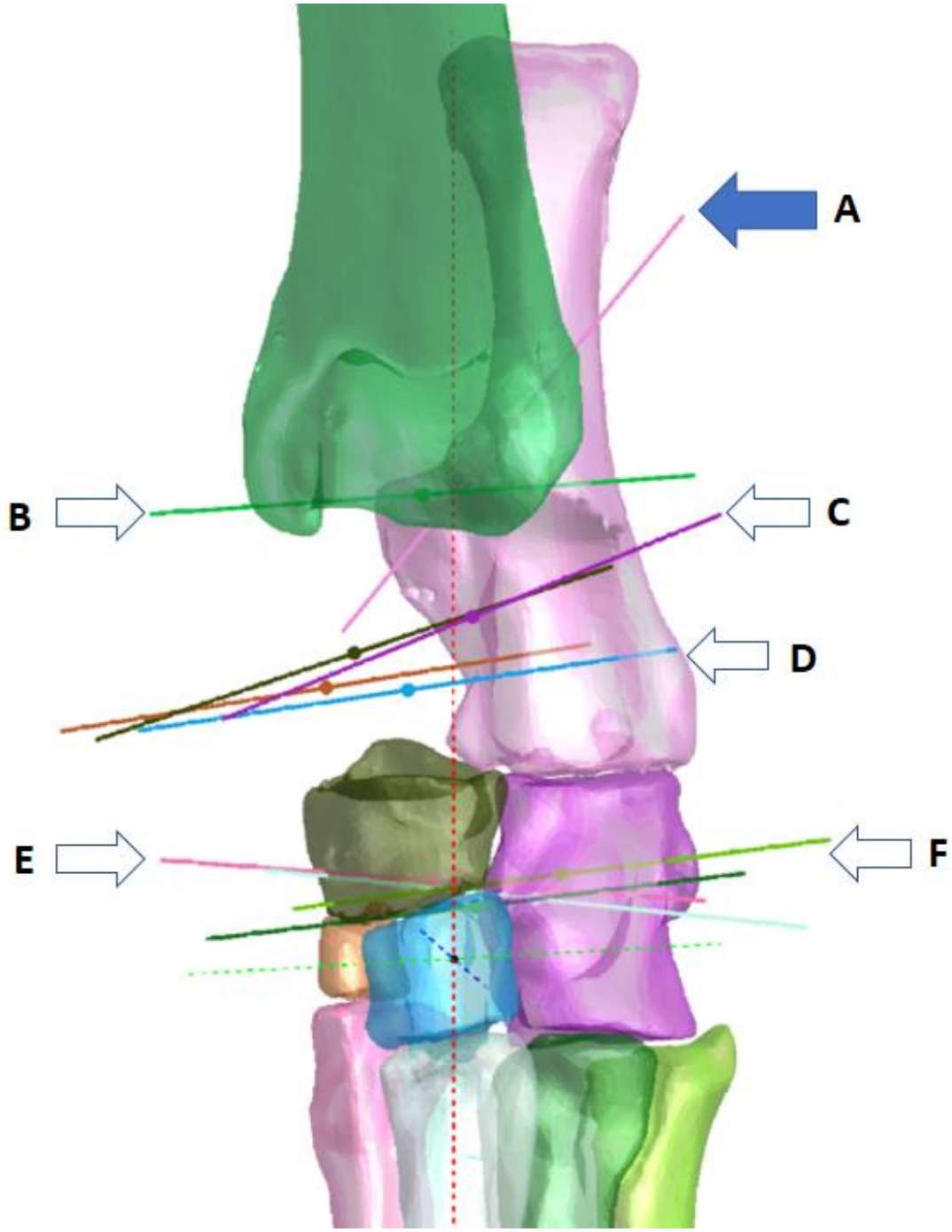

Figure 5-8: The helical axes of the tarsal bones, metatarsals and tibia for Dog 1 (dorsal view). The calcaneus moves around an obliquely orientated axis(A), whilst the tibia rotates around a helical axis (B) almost parallel to the y-axis. The helical axes of the CTB (black) and fourth tarsal bone (purple) are very similar (arrow C). The helical axes of the second tarsal (brown) and third tarsal (blue) are also similar (arrow D). The helical axes of MTII and MTIII (arrow E) are very similar whilst the helical axes of MTIV and MTIV (arrow F) are similar.

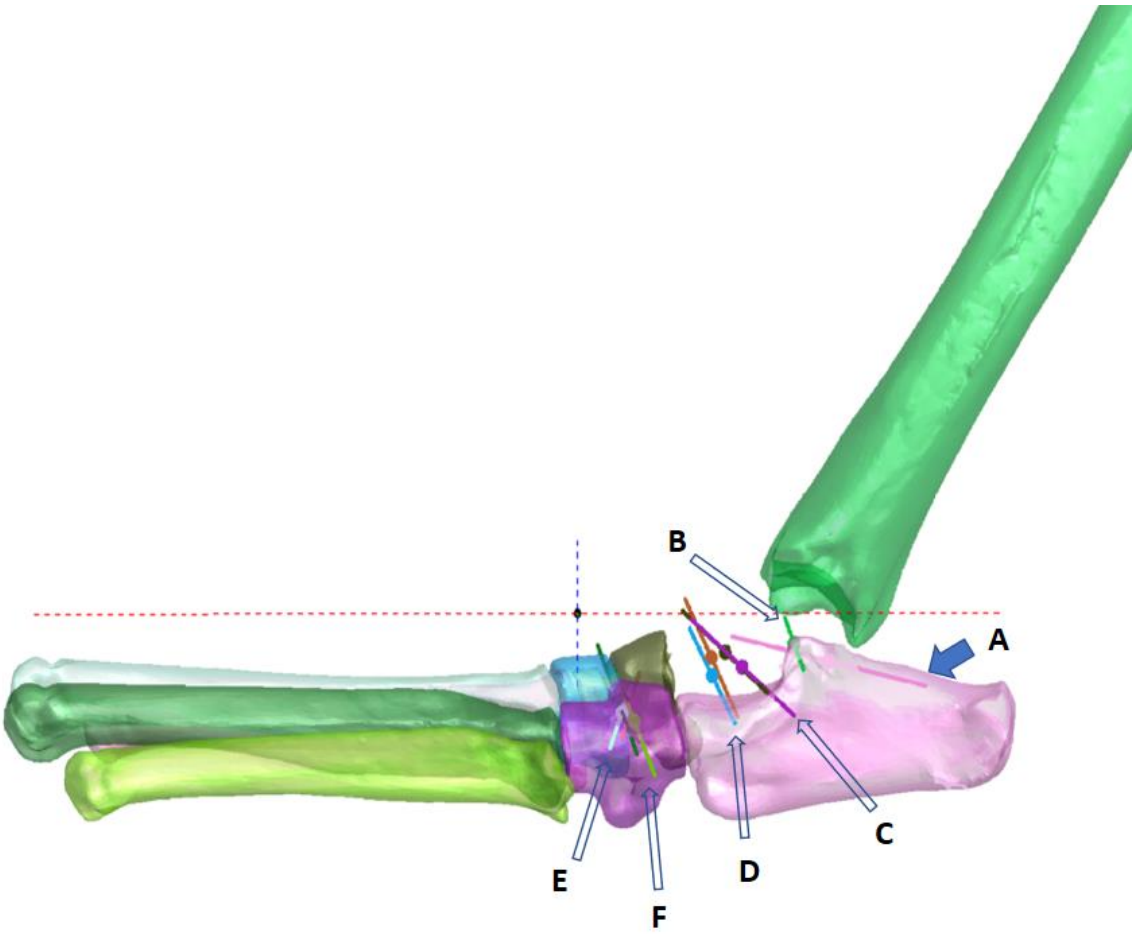

Figure 5-9: The helical axes of the tarsal bones, metatarsals and tibia for Dog 1 (lateral views). The calcaneus moves around an obliquely orientated axis(A), whilst the tibia rotates around a helical axis (B) almost parallel to the y-axis. The helical axes of the CTB (black) and fourth tarsal bone (purple) are very similar (arrow C). The helical axes of the second tarsal (brown) and third tarsal (blue) are also similar (arrow D). The helical axes of MTII and MTIII (arrow E) are very similar whilst the helical axes of MTIV and MTIV (arrow F) are similar.

5.3.2 Kinematic coupling

The degree of rotation of the tibia showed poor correlation with the degree of rotation of any of the other bones, however many of the tarsal and metatarsal bones showed a very high level of kinematic coupling based on the magnitude of rotation about the helical axis.

When loaded to force, 7/45 pairings produced a correlation co-efficient (R^2) > 0.9, 12/45 produced an R^2 value between 0.8 and 0.9, 15/45 produced an R^2 value between 0.5 and 0.8 and the remaining 11 pairs (of which 9 included the tibia) produced an R^2 value less than 0.5 (table 5.3)

Table 5-3: Shows a pairwise comparison for all bones investigated when a standard force was applied (load to force). Pairs with the highest correlation coefficient (>0.9) are shown in green, whilst coefficients of 0.8-0.9 are shown in yellow and 0.6-0.8 in yellow. If <0.6, there is no colour coding. A perfect correlation of 1 indicated a perfect linear relationship between the total rotation of a pair of bones.

	Tibia		Calcaneous		CTB		Fourth TB		Third TB		Second TB		MTII		MTIII		MTIV	
	Correlation coefficient (R^2)	coupling ratio	Correlation coefficient (R^2)	coupling ratio	Correlation coefficient (R^2)	coupling ratio	Correlation coefficient (R^2)	coupling ratio	Correlation coefficient (R^2)	coupling ratio	Correlation coefficient (R^2)	coupling ratio	Correlation coefficient (R^2)	coupling ratio	Correlation coefficient (R^2)	coupling ratio	Correlation coefficient (R^2)	coupling ratio
Calcaneous	0.04	-0.10																
CTB	0.00	0.01	0.92	0.97														
Fourth TB	0.01	0.04	0.94	1.07	0.93	1.05												
Third TB	0.00	0.04	0.87	1.03	0.83	0.99	0.86	0.93										
Second TB	0.02	0.24	0.64	1.10	0.53	0.99	0.50	0.88	0.69	1.03								
MTII	0.00	0.00	0.85	1.26	0.78	1.19	0.81	1.11	0.94	1.19	0.70	0.83						
MTIII	0.00	0.03	0.87	1.34	0.85	1.30	0.87	1.21	0.95	1.26	0.62	0.82	0.98	1.04				
MTIV	0.04	0.18	0.78	1.44	0.80	1.44	0.88	1.39	0.79	1.31	0.29	0.64	0.78	1.06	0.87	1.06		
MTV	0.10	0.28	0.66	1.32	0.75	1.39	0.80	1.31	0.72	1.24	0.20	0.53	0.69	0.99	0.78	1.00	0.97	0.98

When loaded to displacement, 17/45 pairings produced a correlation co-efficient (R^2) > 0.9, 10/45 produced an R^2 value between 0.8 and 0.9, 7/45 produced an R^2 value between 0.5 and 0.8 and the remaining 11 pairs (of which 9 included the tibia) produced an R^2 value less than 0.5 (table 5.4)

Table 5-4: Shows a pairwise comparison for all bones investigated when loaded to displacement. Pairs with the highest correlation coefficient (>0.9) are shown in green, whilst coefficients of 0.8-0.9 are shown in yellow and 0.6-0.8 in yellow. If <0.6, there is no colour coding. A perfect correlation of 1 indicated a perfect linear relationship between the total rotation of a pair of bones. Compared to table 5.3, there is a general increase in correlation coefficients of each pair

	Tibia		Calcaneous		CTB		Fourth TB		Third TB		Second TB		MTII		MTIII		MTIV	
	Correlation coefficient (R^2)	coupling ratio	Correlation coefficient (R^2)	coupling ratio	Correlation coefficient (R^2)	coupling ratio	Correlation coefficient (R^2)	coupling ratio	Correlation coefficient (R^2)	coupling ratio	Correlation coefficient (R^2)	coupling ratio	Correlation coefficient (R^2)	coupling ratio	Correlation coefficient (R^2)	coupling ratio	Correlation coefficient (R^2)	coupling ratio
Calcaneous	0.07	-0.17																
CTB	0.09	-0.20	0.99	1.06														
Fourth TB	0.06	-0.18	0.98	1.15	0.98	1.08												
Third TB	0.13	-0.26	0.97	1.15	0.97	1.07	0.95	0.98										
Second TB	0.13	-0.28	0.70	1.05	0.71	0.99	0.63	0.85	0.71	0.91								
MTII	0.02	-0.12	0.91	1.43	0.85	1.30	0.89	1.21	0.90	1.22	0.66	0.97						
MTIII	0.02	-0.13	0.92	1.44	0.88	1.32	0.91	1.23	0.92	1.24	0.63	0.96	0.99	1.00				
MTIV	0.01	-0.10	0.91	1.42	0.88	1.31	0.93	1.24	0.88	1.20	0.4462	0.80	0.89	0.94	0.92	0.95		
MTV	0.00	0.00	0.85	1.23	0.84	1.14	0.90	1.09	0.79	1.02	0.3702	0.65	0.81	0.80	0.85	0.82	0.97	0.88

The most highly correlated pairs produced a near perfect linear relationship and included the calcaneus and the CTB (R^2 = 0.9855), the calcaneus and fourth tarsal bone (R^2 = 0.9834), the CTB and fourth tarsal bone (R^2 = 0.9821) (figure 5.10).

Distally, the second metatarsal (MTII) and third metatarsal (MTIII) showed very high correlation (R^2 = 0.987), whilst the forth metatarsal (MTIV) and fifth metatarsal (MTV) also showed a very high correlation (R^2 = 0.972)

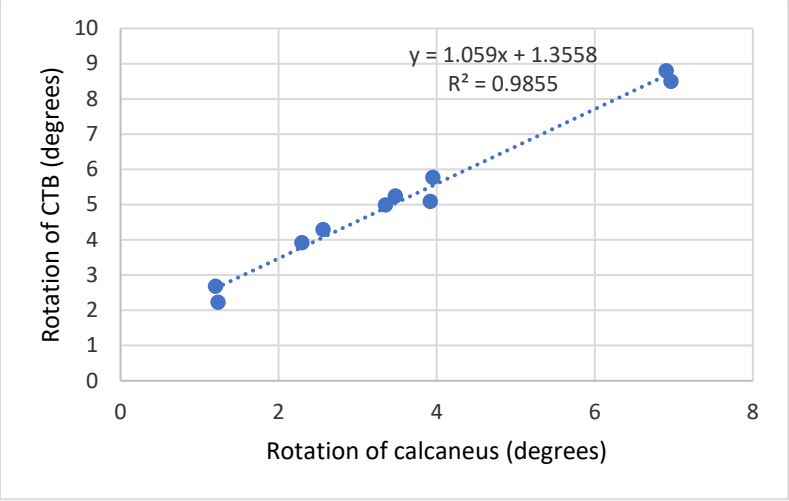

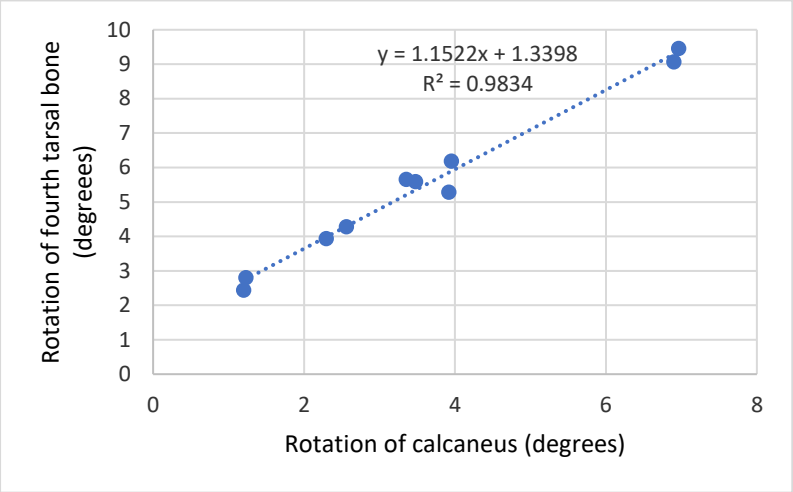

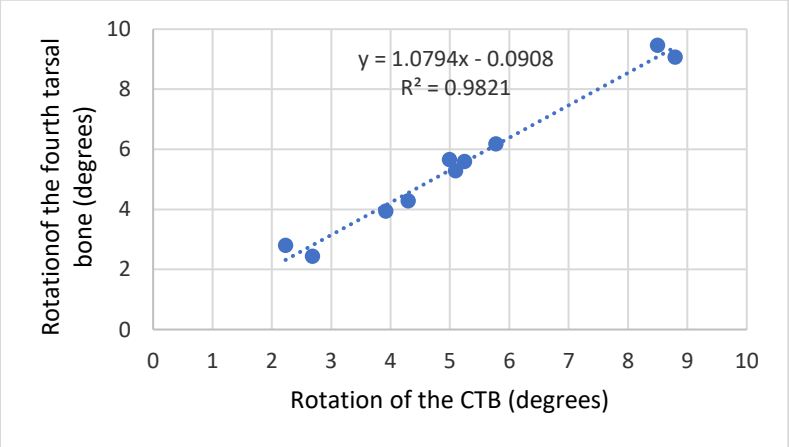

Figure 5-10: plotting magnitude of rotation of a kinematic pair to derive a correlation coefficient and coupling ratio. CTB and calcaneus (top), Fourth tarsal and calcaneus (middle) and Fourth tarsal and CTB (bottom) all showed very high levels of kinematic coupling

A high correlation allows prediction of motion at one joint based on the measured motion at another joint. The kinematic coupling ratios for each pair are given in tables 5.3 and 5.4

The alignment angle formed between adjacent bones are reported (table 5.5). The bones that showed the most similar orientation of their helical axes and therefore the smallest alignment angle were the CTB and fourth tarsal bone, MTII and MTIII and MTIV and MTV. Compared to the well aligned helical axis of their other neighbouring bone, MTIII and MTIV showed a mean AA of 19.5^0 (load to force) and 19.8^0 (load to displacement) to each other.

Table 5-5: The alignment angle for selected pairs of adjacent bones. The alignment angle is the angle formed between the helical axes of a pair of bones, meaning that the smaller this angle, the more closely the bones rotate together.

		Alignment angle (mean ± SD) (degrees)	
kinematic pair		load to force	load to displacement
MTIV	MTV	2.7 ± 2.4	2.2 ± 2.3
MTII	MTIII	4.8 ± 2.6	3.5 ± 1.8
CTB	Fourth	9.6 ± 5.5	5.6 ± 2.4
Second	Third	10.2 ± 4.0	16.0 ± 15.3
CTB	Third	18.4 ± 9.8	12.8 ± 4.2
Fourth	MTIV	19.1 ± 6.7	14.4 ± 5.2
MTIII	MTIV	19.5 ± 8.1	19.8 ± 6.0
Calcaneus	CTB	20.1 ± 8.0	33.7 ± 16.5
Calcaneus	Fourth	20.3 ± 11.6	32.4 ± 16.1
Third	MTIII	21.7 ± 7.8	20.1 ± 3.0

5.3.3. Description of tarsal bone kinematics relative to the sagittal plane

Within the lateral kinematic chain (calcaneus, fourth tarsal bone and MTIV), the calcaneus contributed 10.2 ± 4.8% and 9.7 ± 5.4% of sagittal plane rotation (for load to force and load to displacement respectively). The fourth tarsal bone contributed 25.0 ± 3.8% and 24.9 ± 3.5% respectively, whilst the MTIV contributed 64.9 ± 8.3% and 65.4 ± 8.8% respectively. There was no significant difference between the contribution each joint made between the two loading patterns. The relative contribution for the individual limbs can be seen in figure 5.11.

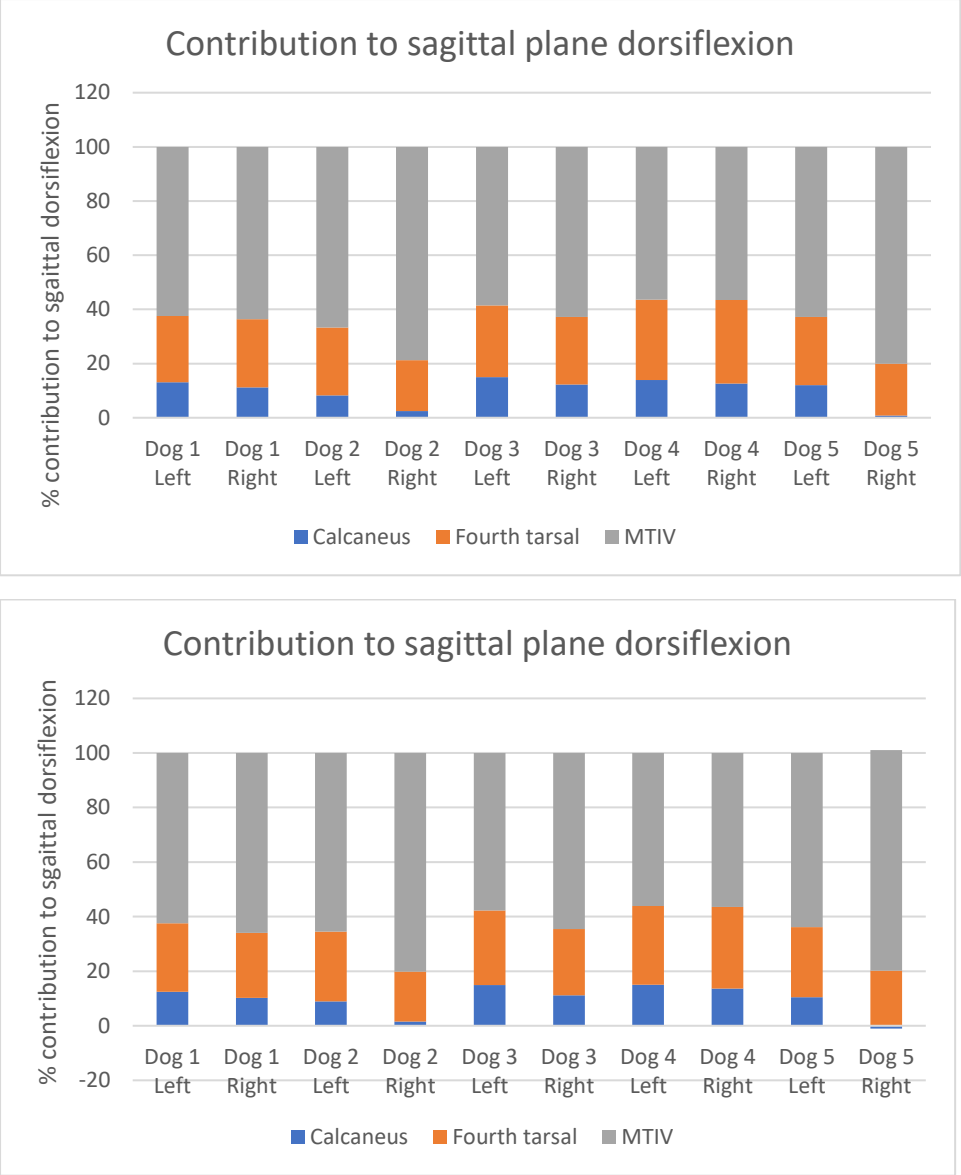

Figure 5-11: The relative contribution of each bone of the lateral kinematic chain to total sagittal plane dorsiflexion for the 5 pairs of limbs. There was no difference in the mean values for each bone between load to force (top) and load to displacement (bottom). Whilst three of the dogs (1,3 and 4) appear very symmetrical, two dogs (2 and 5) have a reduced contribution from the talocalcaneal joint in the right limb which may be related to adaptations related to previous racing. MTIV = fourth metatarsal bone

For the medial chain (CTB, third tarsal bone and MTIII) the CTB contributed 18.2 ± 4.9% and 19.8 ± 3.2% (for load to force and load to displacement respectively). The third tarsal bone contributed 28.3 ± 2.5% and 26.6 ± 1.9% respectively, whilst the MTIII contributed 53.5 ± 5.7% and 53.5 ± 5.0% respectively. There was no significant difference between the relative contributions of each bone at the two patterns of loading (figure 5.12)

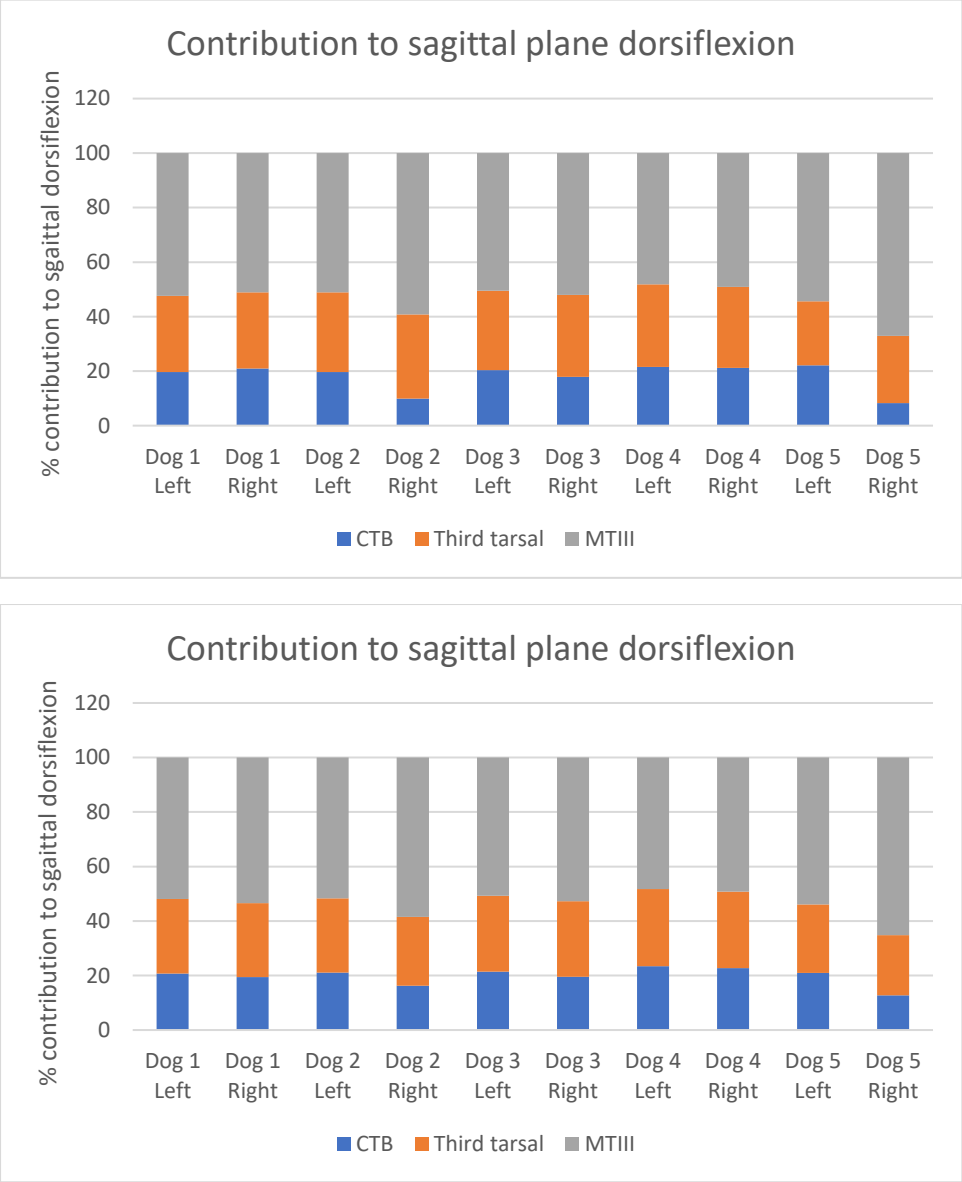

Figure 5-12: the relative contribution of each bone of the medial kinematic chain to total sagittal plane dorsiflexion for the 5 pairs of limbs. There was no difference in the mean values for each bone between load to force (top) and load to displacement (bottom). CTB = central tarsal bone, MTIII = third metatarsal bone.

There was no significant effect of dog (p=0.283), side (p=0.812) or degree of loading (p=0.743) on orientation of the helical axis relative to the sagittal plane (SDA) for each bone, suggesting that the helical axis is well preserved between individuals and symmetrical within individuals. The orientation of the axis also remained constant at both positions measured in this study. There was significant variability when comparing the SDA of the individual tarsal bones, metatarsal bones and tibia (figure 5.13) The calcaneus showed the greatest SDA (mean 57.5^0 ± SD 14.3^0) and was significantly different to the helical axis of all other bones except the CTB (32.9^0 ± 9.3^0) fourth tarsal bones (34.5^0 ± 8.4^0). The SDA of the tibia showed the least deviation from motion from the sagittal plane and was significantly different from all other bones.

The bones with the smallest SDA, the tibia and metatarsals, also demonstrated the greatest magnitude of rotation, whilst the bone with the largest SDA showed the least total rotation.

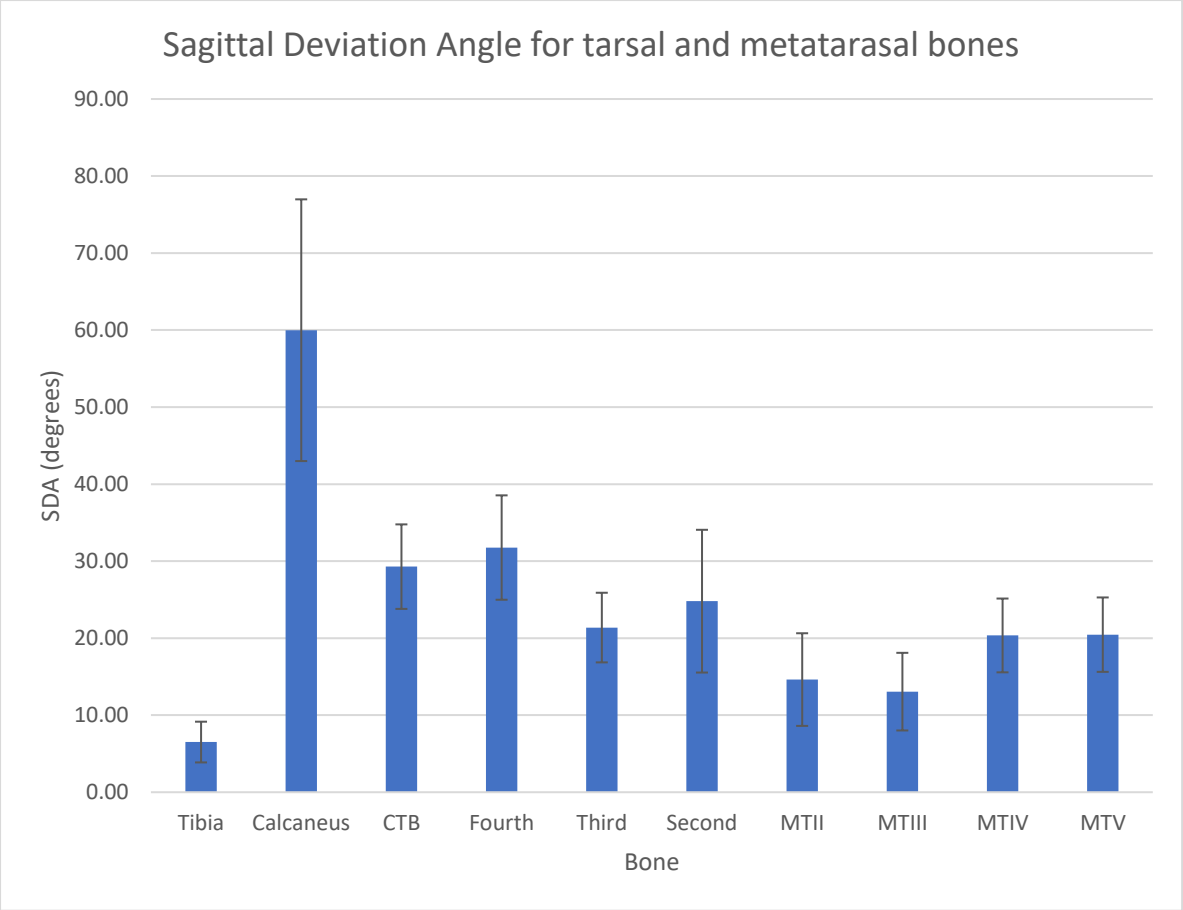

Figure 5-13: The sagittal plane deviation angle (SDA) for each of the bones. This angle is measured between the helical axis and the y-axis. As rotation around the y-axis occurs in the sagittal plane, the SDA represents deviation in the rotation of the bone away from the sagittal plane. Error bars represent one SD. From this graph it can be seen that the high motion talocrural joint acts primarily in the sagittal plane, whilst many of the tarsal bones rotate around an oblique helical axis that is not closely aligned with sagittal plane rotation. . CTB = central tarsal bone, Fourth = fourth tarsal bone, Third = third tarsal bone, Second = second tarsal bone, MT = metatarsal

5.4 Discussion

The complex and highly coupled kinematics of the canine tarsal bones have been characterised using a newly validated limb loading jig and accurate, non-invasive measurement technique. The findings of this experiment support the first hypothesis that individual tarsal bone motion occurs out of the sagittal plane. The data also confirms that dorsiflexion of the pes occurs during loading of the hind limb, supporting our second hypothesis, and this motion is facilitated by a highly coupled kinematic chain that extends from the talus to the metatarsal bones. The identification of rigid functional units within the pes, supports the third hypothesis that some bones move almost in perfect unison and may allow development of more simplified models of the canine pes.

5.4.1 Contribution of the tarsal joints to hock flexion

Motion at all tarsal and metatarsal joints was identified, meaning each articulation contributed to the overall motion of the distal limb. The talocrural joint has been reported to contribute 90% of the overall motion in the hock (Carmichael and Marshall, 2013) and although the results of this experiment found this joint contributed the majority of sagittal plane dorsiflexion, the tarsal and tarsometatarsal joints contributed a mean of 27.6% and 28.9% of total sagittal plane dorsiflexion when loaded to force and displacement respectively. This translated into a mean of 11.4^0 and 22.2^0 degrees of sagittal plane dorsiflexion when loaded to force and displacement respectively. If the pes is considered as a rigid body, and the hock modelled as a simple gingylmus, as in many kinematic studies (Fu et al., 2010; Headrick et al., 2014b; Hottinger et al., 1996), inaccuracies will result. Small but potentially significant motions at the intertarsal and tarsometatarsal joints will be overlooked, whilst movement will be incorrectly attributed to adjacent joints, and may impact upon derived calculations such as power and work.

The contribution of intertarsal and tarsometatarsal joints to dorsiflexion of the pes in any species remains widely unknown. In the running camel, approximately 17 degrees of dorsiflexion was attributed to dorsiflexion at the proximal intertarsal and tarsometatarsal joints (Alexander et al., 1982) and this motion was a vital component of the energy storage mechanism in this species, allowing increased energy storage in flexor tendons. In the greyhound, the gastrocnemius, superficial and deep digital flexor muscles all demonstrate a high tendon length change: muscle fascicle length, indicating a reliance on passive length change (tendon elongation) rather than active muscle shortening for function (Williams et al., 2009). It may be suggested that dorsiflexion of the canine pes allows greater elongation and hence energy storage within the digital flexor tendons as seen in other species (Alexander et al., 1982; Alexander, 1984; Vereecke and Aerts, 2008). Dorsiflexion of the pes may also allow storage of elastic energy within the passive structures of the foot. Up to 17% of the elastic energy storage in the human leg is believed to be stored within the plantar aponeurosis, spring ligament and long and short plantar ligaments (Ker et al., 1987).

5.4.2 Patterns of tarsal bone kinematics

The orientation of the helical axis of each bone was identified and the magnitude of rotation was reported, revealing a consistent pattern of motion between all dogs. The helical axis represents the 3D axis around which a bone rotates and is commonly used in kinematic investigations (Beimers et al., 2008; Kirby, 2000; Sennwald et al., 1993). Sennwald et al. (1993) suggested that complex motions may not be completely characterized by use of a single helical axis. For example, if a bone translates then subsequently rotates, it would be best characterized by identifying one helical axis that describes the initial translation and another that characterizes the latter rotation. Results of this chapter revealed that the helical axes did not show significant differences in position between the two loading patterns suggesting that the canine tarsal bones continue to rotate around a very similar helical axis throughout their motion. With the exception of the calcaneus, the position of the helical axis of each bone that was investigated was remote to the bone itself, implying a gliding pattern of

motion. This can result in significant movement through translation despite only limited rotation (Sennwald et al., 1993).

The tarsal and tarsometatarsal joints show high levels of kinematic coupling, defined as intersegment co-ordination (Wilken et al., 2011) resulting in a distinct pattern of movement that allows the pes to function as a unit. The orientation of the helical axes of the tarsal bones all run from a proximal, lateral and caudal position in a distal, medial and cranial direction.

5.4.2.1 The calcaneus

The helical axis of the calcaneus shows the greatest obliquity, producing more internal rotation than dorsiflexion during loading. As the only tarsal bone with the helical axis located within the bone itself, the calcaneus undergoes little translation. The orientation and position of this axis is consistent with the oblique, compromise helical axis reported in man, where foot inversion and eversion plays an important role in foot function (Beimers et al., 2008) and in a wide variety of other species (Lewis, 1980) suggesting the helical axis of the calcaneus is well preserved across species despite great differences in the pattern of locomotion.

5.4.2.2 The bones of the mid foot

The helical axes around which the CTB and fourth tarsal bone rotate are well aligned, with an alignment angle of less than 10 degrees. Like the calcaneus, their oblique axes results in dorsiflexion coupled with internal rotation, however, due to the decreased obliquity of the helical axis compared to the calcaneus, both the CTB and fourth tarsal bone show greater a greater dorsiflexion component than internal rotation component. The magnitude of rotation of these bones about their helical axis are highly kinematically coupled to each other and to that of the calcaneus. Despite being spanned by the fourth tarsal bone, motion was consistently identified at the centro-distal joint. Rotating around a similar oblique helical axis, the second and third tarsal bones also demonstrate internal rotation coupled with dorsiflexion. However, as the SDA is less than for the calcaneus, CTB

and fourth tarsal bone, the dorsiflexion component of rotation is the major component with significantly less internal rotation. These bones may play a major role in facilitating the differing, but complementary motions of the metatarsal bones as discussed below.

5.4.2.3 Metatarsal bones

There was high kinematic coupling of the magnitude of rotation of MTIV and MTV and these bones displayed well aligned helical axes. Similar to the other tarsal bones, dorsiflexion of these joints was coupled with slight internal rotation. MTII and MTIII demonstrated tight coupling and well aligned helical axes, however, these bones displayed an external rotation coupled with dorsiflexion. This change in direction of rotation on either side of the midline of the pes results in a flattening of the natural arc of the metatarsals in the transverse plane. This may act to further increase elastic storage in the foot, being returned during the take-off phase of gait. Additionally, the internal rotation of the lateral metatarsals and external rotation of the medial metatarsals may facilitate equalization of pressure on all digital foot pads despite an internal rotation of the more proximal aspect of the pes.

Apart from the common calcaneal tendon insertion, there are no muscular attachments of significance on the tarsal bones that are active during the stance phase (Evans et al., 2012; Goslow et al., 1981) and therefore the motion of these bones is the result of the direct force from adjacent bones and the limiting effects of ligaments and the joint capsule. A similar situation is reported in the human wrist, where the bones of the proximal carpal row will self-align as they move towards extremes of motion (Sennwald et al., 1993). The increased kinematic coupling seen at higher loads in this experiment, support the fact that bones of the tarsus self-align during loading, taking position as dictated by adjacent joint surfaces and limited by the vast array of ligaments that attach to the tarsal and adjacent bones (Aron and Purinton, 1985a; Evans et al., 2012; Gorse et al., 1990). Ligaments have been shown to possess non-linear viscoelastic properties (Attarian et al., 1985; Crary et al., 2003; Funk et al., 2000), becoming stiffer as the load increases and further restricting bone motion

at the limits of motion. The increased coupling demonstrated at higher loads in our study is an example of the effect of this biomechanical property. However, as ligaments act as elastic tissues within their functional range, it is possible that the well-developed plantar ligaments in the canine foot may also contribute to energy storage as the pes dorsiflexes.

Divergence of the helical axis of adjacent bones has been proposed as one mechanism that may "lock" bones into position at extremes of motion, providing a more rigid level off which to propel. This has been described in the human mid-foot (Blackwood et al., 2005) (Okita et al., 2014). However, it is observed that there is no obvious divergence amongst the helical axes of the tarsal bones but rather a gradual transition in obliquity from the most oblique axis of the calcaneus, to the most distal tarsometatarsal joints, which show very little divergence from sagittal plane dorsiflexion. This anatomical arrangement makes a locking mechanism unlikely in the dog. Furthermore, the positioning of the helical axes remote from the bone creates a gliding motion at the flat or spheroidal articular surfaces with no obvious end point created by the bone shape alone. This arrangement would be biomechanically advantageous to a limb that acts as a biological spring, limiting motion by the elastic potential of ligaments and tendons rather than compressive forces of adjacent bones which would produce a more abrupt end-point.

During take-off from the stance phase, the pes undergoes an external rotation coupled with plantarflexion (foot inversion), which has been demonstrated in the human foot after heel lift (Kirby, 2000). It has been proposed that this external rotation brings the fourth tarsal bone into a more plantar position, whilst the CTB takes a more lateral and dorsal position, producing a more vertical alignment of the proximal intertarsal joint which provides a more rigid lever from which to push off. There are obvious differences between the human and canine foot during the early stance phase, where the plantigrade human foot undergoes a heel strike followed by a flat foot phase in contrast to the dog which remains digitigrade. However, the pattern of motion after heel lift in the human is

likely to be similar to the take-off phase in the canine foot and our findings of coupled external rotation with plantarflexion are consistent to that of human kinematic foot studies.

5.4.3 A simplified model of the canine foot

By quantifying the motion of each tarsal bone in a series of canine cadavers, bones that consistently move a similar magnitude around a similarly orientated axis were identified. Depending on the aspect of motion being studied, small movements between bones may be significant, whilst in other situations, the pes may be simplified into a smaller number of functional units. A number of bones that were investigated as part of this experiment may be considered as functional units, therefore simplifying future kinematic studies, particularly those involving instrumentation of bones. The medial two metatarsal bones (MTII and MTIII) showed a very similar magnitude of rotation around their helical axes, which were also aligned in a similar orientation in 3D space. These two bones were the only bones to undergo external rotation during dorsiflexion and were also highly kinematically coupled. Therefore, it may be suggested that these two bones could be considered as a rigid functional unit. Similarly, the lateral two metatarsals (MTIV and MTV) also showed a very similar magnitude of rotation about closely orientated axes and could be considered as a rigid functional unit. The medial and lateral metatarsals provide easily identifiable and palpable landmarks that can be visualized throughout gait if markers are used. The CTB and fourth tarsal bones can also be considered to form a mid-foot rigid function unit in the canine tarsus as they meet the same criteria as the metatarsal units. Despite a high kinematic coupling with the calcaneus, the CTB and fourth tarsal bones rotate about a very different helical axis and so although these three bones work in synchrony, they cannot be considered to form one rigid functional unit. Kinematic coupling between the tibia and any of the tarsal bones was not identified. This may be because no coupling exists or because our limb loading jig did not replicate the forward motion of the tibia as it moves over the planted foot during the gait cycle.

A simplified model of the tarsal and metatarsal bones may allow motion to be attributed more appropriately to the talocrural joint and the individual intertarsal and tarsometatarsal joints. This may be particularly important in in vivo studies, where identification of all individual tarsal bones may be challenging. The high kinematic coupling between the tarsal bones mean that instrumentation of each bone may not be required and that if motion between two adjacent or potentially non-adjacent bones can be accurately measured in a given plane, then the 3D motion at other joints may be able to be accurately derived.

5.4.4 Study limitations

The major limitation with any cadaveric kinematic study is the need to accurately replicate the forces that result in bone displacement. This has been achieved previously with the use of motors attached to tendons in walking models. One of the key features of these jigs is that they preserve the natural insertion of the tendon onto bone, the enthesis. This ensures the tensile force on the bone is accurately reproduced. The experimental design used in this chapter preserved both the gastrocnemius muscle and superficial digital flexor muscle as they spanned between the caudodistal aspect of the femur and calcaneus. The gastrocnemius muscle, in particular, is covered in a strong fascial sheath and the short pennate fibres are infiltrated throughout with connective tissue. During loading, the simultaneous stifle and hock angles recorded in a galloping dog were able to be replicated. This required some lengthening of the gastrocnemius muscle, which occurred in our specimens and has also been recorded in vivo in the galloping dog (Goslow et al., 1981). Furthermore, the ground reaction force that results from tension in the common calcaneal tendon was similar between our specimens and GRFs measured in galloping dogs for a given hock angle. Therefore, it is suggested that the jig used in this experiment can accurately replicate the tensile force in the common calcaneal tendon in a cadaveric specimen.

The only other muscular insertions on the canine tarsal bones belong to flexors of the hock (Cranial tibial muscle, fibularis longus muscle and fibularis brevis muscle), which are not active during the initial stance phase and very small muscles, such as the quadratus plantae, which are generally considered insignificant. Therefore, this experimental design replicates the relevant muscle forces during the stance phase of gait. It must also be recognised that although there may be no other muscular insertions, there are a number of tendons that run across the tarsal bones and these may also influence kinematics. From this experiment, which did not replicate all muscular forces, we cannot speculate on the effect that these tendons may have had on tarsal kinematics.

There are intrinsic muscles of the pes that may influence motion but these are generally considered as digital flexors. As no attempts were made to replicate natural forces acting on the phalangeal bones, the motion of these bones was not recorded.

In this experiment, only one breed, the greyhound, was investigated as this breed is of consistent size and conformation and would minimize inter-specimen variation. Care must be taken when extrapolation these finding to other breeds, which may have differences in the degree of motion and direction of motion of each bone. Greyhounds have undergone intense selection and display significant anatomical and functional differences when compared to other breeds (Williams et al., 2008). They are highly adapted for high speed locomotion and demonstrate a different distribution of power across the hind limb joints when compared to Labradors (Colborne et al., 2005). Their narrow and slender feet are another adaptation for speed, resulting in a different pattern of force distribution through the pads when compared to a Labrador Retriever (Besancon et al., 2004). Based upon palpation of dogs of several different breeds, it is possible that other breeds may show greater tarsal movement and future studies comparing breeds would be of great value. The greyhounds used in this study have an unknown history but it is likely that they have been involved with training and racing. Always racing counter-clockwise around an oval track leads to asymmetrical tarsal and metatarsal bone adaptive remodelling (Johnson et al., 2000; Johnson et al., 2001) and this fact may

influence tarsal bone kinematics. A paired limb design was chosen to address this potential confounding factor and side was included as a factor in our statistical model, which demonstrated there was no significant effect of side on tarsal bone kinematics.

The results reported in this chapter must also be interpreted in the light of the earlier experiments of chapter 3, which detail the accuracy of the measurement technique employed. It is possible that some of the small motions detected, particularly in the x axis, may reflect “noise” or alternatively very small potions associated with compression of articular cartilage.

5.5 Conclusions

Far from a rigid structure, the canine pes undergoes elastic deformation during weight bearing, facilitating storage of energy as elastic strain and increasing the efficiency of locomotion. The dorsiflexion of the pes involves highly coupled motions at adjacent and non-adjacent joints, with each bone rotating about its unique helical axis. The most rotation occurs in joints where rotation is more closely aligned with the sagittal plane of the foot, whilst the most highly constrained joints demonstrate more oblique helical axes. The pes shows abduction and internal rotation during dorsiflexion and adduction and external rotation during plantarflexion at take-off.

Chapter 6 : The plantar ligament: Role in tarsal bone kinematics and force transmission

6.1 Introduction

Proximal intertarsal luxation or subluxation of the canine tarsus results in a debilitating lameness that will not resolve without surgical intervention (Campbell et al., 1976; Dieterich, 1974; Lawson, 1960). There are numerous reports of this condition (Allen et al., 1993; Barnes et al., 2013; Dieterich, 1974; Fettig et al., 2002; Lawson, 1960; Wilke et al., 2000) with some reporting that proximal intertarsal luxation is the most commonly encountered lesion of the canine hock in their hospital population, accounting for 35% of all hock lesions (Campbell et al., 1976). Damage or degeneration of the plantar ligamentous support has been suggested as the underlying cause of proximal intertarsal subluxation (Allen et al., 1993; Barnes et al., 2013; Campbell et al., 1976; Lawson, 1960), however, further characterisation of which components of the complex plantar ligamentous support are damaged to permit subluxation have not been reported (Barnes et al., 2013).

The tarsal ligaments connect all aspects of the tarsal bones but are most significant on the plantar surface, resisting the dorsiflexion of the pes during weight bearing (Carmichael and Marshall, 2013). The canine plantar ligament has been previously described as having three components (Barnes et al., 2013; Evans et al., 2012). The most lateral component, termed the calcaneoquartal ligament (Evans et al., 2012) is also known as the lateral plantar ligament (Carmichael and Marshall, 2013) and forms a small but distinct band running from the plantarolateral aspect of the tuber calcanei to the head of the fifth metatarsal and fourth tarsal bone. The long plantar ligament, also termed the middle plantar ligament (Carmichael and Marshall, 2013) is significantly larger, and its parallel fibres run from the plantar aspect of the distal calcaneus to the thick fibrocartilage of the tarsometataral joint capsule, inserting on the plantar process of the fourth tarsal bone as they pass over it (Evans et al., 2012). The most medial component of the plantar ligament is known as the calcaneocentral ligament or medial plantar ligament (Carmichael and Marshall, 2013), which runs from the plantar aspect of the sustentaculum tali to the plantar process of the central tarsal bone. The fibres continue

distally as the plantar centrodistal ligament, which also inserts upon the thick fibrocartilage of the tarsometatarsal joint capsule (Campbell et al., 1976; Evans et al., 2012).

The work of the previous chapter in this thesis demonstrates that motion occurs between all tarsal bones during loading, making important contributions to overall hock flexion. However, it remains unclear what role the various components of the plantar ligament play in tarsal bone kinematics in the normal limb and what components of the plantar ligaments must be damaged to allow proximal intertarsal subluxation.

Stability across the proximal intertarsal joint is essential for allowing the pes to act as the rigid beam of a lever, rotating about the trochlea of the talus, which acts as the fulcrum (Pratt, 1935) (Ker et al., 1987). The tensile force exerted on the tuber calcanei by the common calcaneal tendon allows generation of a ground reaction force at the paw when the integrity of the pes is maintained. Conversely, when the integrity of the pes is lost, as in proximal intertarsal subluxation, force transmission through the pes, which permits generation of a ground reaction force, is also presumably reduced (figure 6.1).

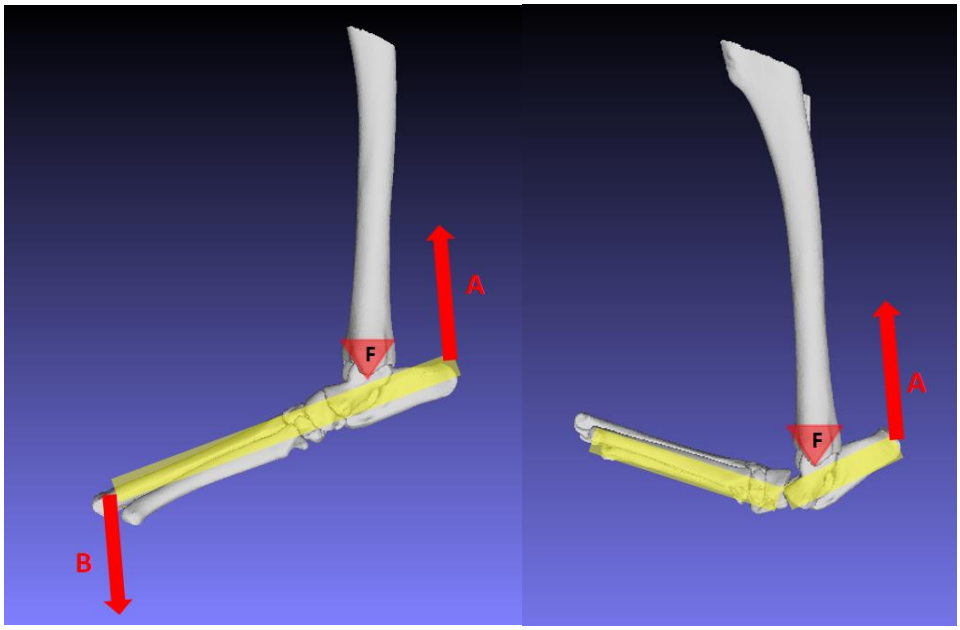

Figure 6-1: Left: the intact pes acts as a lever arm in the distal limb, rotating around a fulcrum (the trochlea of the talus). A tensile force (A) exerted by the common calcaneal tendon, creates a ground reaction force (B), which was measured using pressure sensitive film. Right: if the integrity of the pes is lost as seen in proximal intertarsal luxations, then the tensile force (A) cannot generate a ground reaction force.

To determine the role each component of the plantar ligament plays in tarsal bone kinematics and force transmission through the pes, serial transection of the plantar ligament was performed in cadaveric specimens and bone motions measured using CT based kinematic measurements. The aim of this study was to characterise tarsal bone kinematics and measure force transmission in the intact canine cadaver foot, following transection of the medial aspect of the plantar ligament (calcaneocentral ligament), the lateral aspect of the plantar ligament (long plantar ligament) and following transection of both of the major components of the plantar ligament. The null hypothesis was that partial or full transection of the plantar ligament would produce no difference in tarsal bone kinematics and force transmission through the pes when compared to the intact canine pes. The calcaneoquartal ligament has been previously described as the third component of the plantar ligament, but was not included in the transection model due to its lateral position that is unlikely resist dorsiflexion of the pes and its relatively insignificant size compared to the other components of the plantar ligament. Furthermore, despite being described as a component of the planter ligament, this thin band actually represent an entirely tendinous muscle (m. abductor digiti V).

6.2 Materials and methods

6.2.1 Specimens

Ten paired hind limbs (from 5 dogs) were used for this study. These limbs were all obtained from skeletally mature greyhounds, euthanised for reasons unrelated to this study. Limbs were disarticulated and wrapped in cloth moistened with saline and frozen at-20^{0}C until testing. The paired nature of this study allows for a reduction in sample size. Note, the sample size in this portion of the thesis is also consistent with similar human clinical studies (Arndt et al., 2007; Fassbind et al., 2011; Wolf et al., 2007).

6.2.2 Study design

For each dog, one limb from each pair was allocated to the "lateral transection" group, whilst the other limb was allocated to the "medial transection" group (figure 6.2). To ensure equal group sizes, alternation was used to allocate limbs to a particular group.

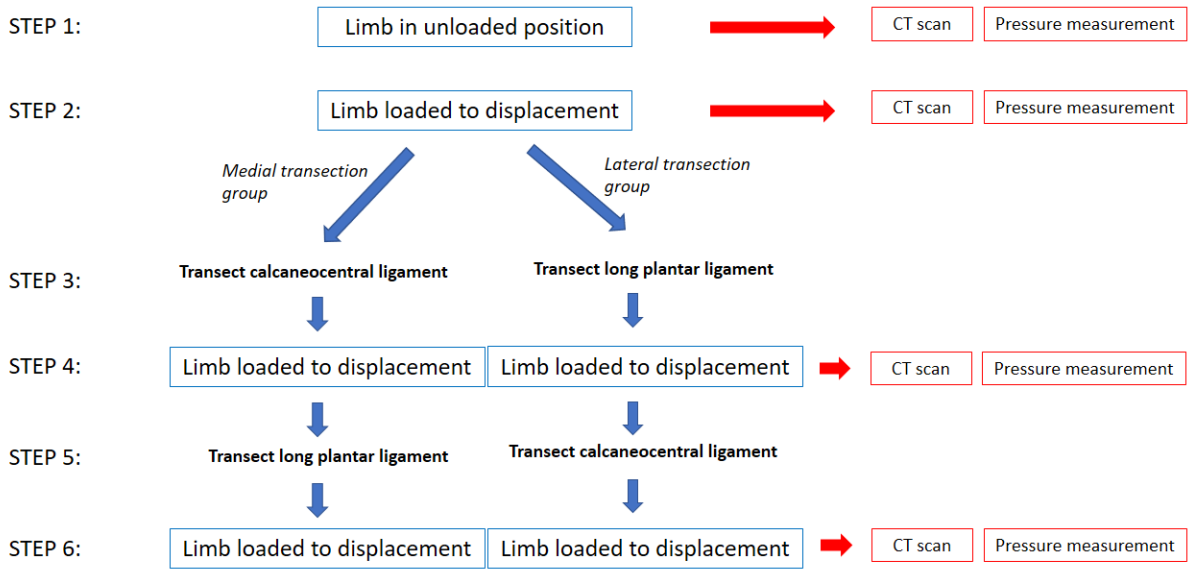

Figure 6-2: shows the overview of study design. One limb of each pair was allocated to the medial transection group whilst the other was allocated to the lateral mtransection group. Each limb was scanned in an unloaded position (step1), loaded position (step 2) , following partial transection of the plantar ligament (step 4) and finally after complete transection of the plantar ligament (step 6)

6.2.3 Limb loading

All limbs were prepared as previously described and loaded into a custom loading jig (described in chapter 4). Prior to testing, the samples were thawed to room temperature and remained hydarated with saline to avoid any drying artefact. The stifle and tarsal joints were manually flexed and extended and preconditioned in the jig to a force of 600N, measured on the pressure sensitive film (Film code 5076-350. Tekscan, South Boston, MA, USA) positioned under the paw and cycled for five repetitions (as described in Chapter 5). This force represents the approximate ground reaction force measured from galloping dogs of similar size dogs, recorded from in vivo kinetic investigations (Walter and Carrier, 2007) and has been discussed in the previous chapters of this thesis.

6.2.4 Computed tomographic scanning

All limbs were scanned using a 16-slice helical CT scanner (Philips Brilliance 16-slice CT scanner) with scanning parameters (120KVP, 117 mA, slice thickness 1mm, slice increment 0.5mm, 512 X512 matrix). Each limb was initially scanned in an “unloaded” position. A previously designed fiberglass mould (described in Chapter 5) was used to standardize the angle of flexion at the hock joint during the first scan. The second scan was performed in a “loaded” position, defined as the point where the metatarsals were perpendicular to the mechanical axis of the tibia. A second fibreglass mould was again used to identify this position. The maximum force exerted by the paw on the foot plate was recorded for each position using pressure sensitive film (Film code 5076-350. Tekscan, South Boston, MA, USA). The position of the proximal limb restrain in relation to the foot plate was also recorded for each limb in the unloaded and loaded position.

6.2.5 Plantar ligament transection

The skin over the pes was then removed and the tendons of the superficial and deep digital flexors were displaced from their synovial sheaths to expose the long plantar ligament, running from the caudodistal aspect of the calcaneus to the plantar process of the fourth tarsal bone, and the more medially located calcaneocentral ligament, running from the sustentaculum tali of the calcaneus to the plantar process of the central tarsal bone (figure 6.3).

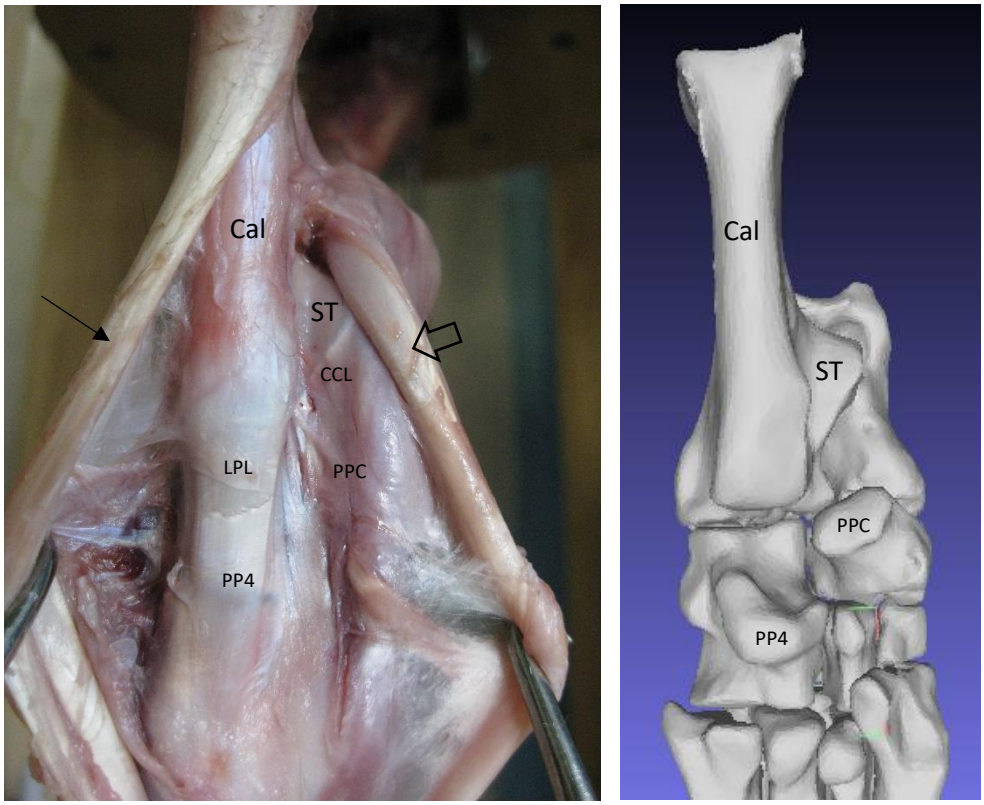

Figure 6-3: The plantar aspect of the pes with the tendons of the superficial digital flexor (arrow) and deep digital flexors (open arrow) retracted.

Cal= calcaneus, ST = sustentaculum tali, PP4 = plantar process of 4th tarsal bone, PPC = plantar process of the central tarsal bone, LPL = long plantar ligament, CCL = calcaneocentral ligament

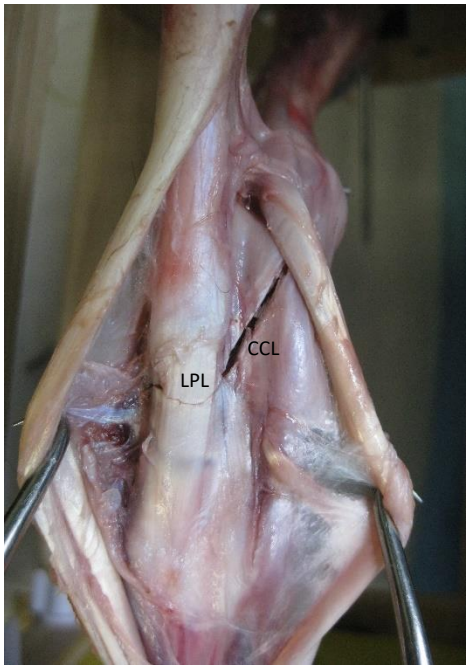

Figure 6-4: The appearance of the specimen following complete transection of both the long plantar ligament (LPL) and the calcaneocental ligament (CCL)

For limbs in the "lateral transection" group, the long plantar ligament was completely transected and the tendons of the superficial and deep digital flexors were returned to their original position. Each limb was then reloaded so the proximal limb restraint was in the same position as during the "loaded" scan. The limbs were then scanned again using the identical parameters to the previous scans. The force exerted by the paw was recorded using the pressure sensitive film as described in chapters 4 and 5. For dogs allocated to the "medial transection" group, the calcaneocentral ligament was completely transected before reloading the limb to the previously recorded loaded position. As for the lateral transection group, these limbs were then CT scanned and the maximal pressure exerted by the paw was recorded.

Finally, the calcaneocentral ligament was transected for limbs in the lateral transection group, completing the transection of the entire plantar ligament (figure 6.4). Likewise, the long plantar ligament was transected for dogs in the "medial transection" group completing the full transection of the plantar ligament. Following complete transection of the plantar ligament, all limbs were scanned again and the force on the foot plate recorded as previously described.

6.2.6 Calculation of kinematics

A previously validated CT based technique for measuring canine tarsal bone kinematics (Tan et al., 2017), previously outlined in chapters 3 and 5 was used. Briefly, a 3D bone model was generated for the calcaneus, talus, fourth, third and second tarsal bones, central tarsal bone and metatarsal bones II, III, IV and V for every scan. The bones were then aligned to an anatomically based co-ordinate system that would allow motions to be described using conventional descriptors. Rotation around the y axis represented dorsiflexion and plantarflexion, rotation around the x axis represented internal and external rotation, whilst rotation around the z axis represented either valgus or varus angulation (figure 6.5). The position of each bone was recorded in an unloaded position, a loaded position, a position after transection of the medial or lateral portion of the plantar ligament and a position following full transection of the plantar ligament. The displacement of each bone relative to its unloaded position was reported for each condition (loaded, partial transection and full transection). Bone displacement was described using 6 degrees of freedom (3 translations along the co-ordinate axes and 3 rotations around the same axes). As in the previous chapters, individual bone motion was also reported as a total summative rotation (total rotation) around a single axis, which was termed the helical axis of rotation.

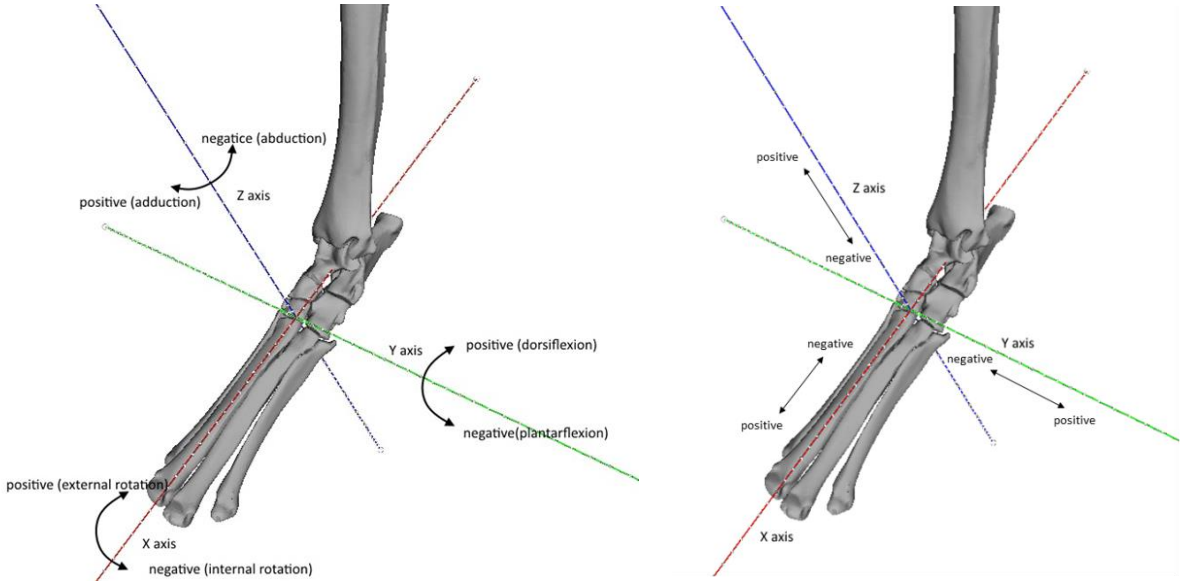

Figure 6-5: The three reference axes around which all motions are described. Left: *Positive and negative values are reported indicating the direction of the rotations around the axes. For rotations around the X axis, calculations have been adjusted so positive values translate to an external rotation for both left and right limbs. For rotations around the Z axis, calculations have been adjusted so positive values translate to adduction for both left and right limbs No adjustment is required for rotations around the Y axis.* Right: *Positive and negative values are reported indicating the direction of the translation along the axes. For translation along the Y axis, calculations have been adjusted so positive translations always indicate a medial direction for both left and right limbs. No adjustment is required for translation along the other axes.*

6.2.7 Data analysis

The two groups (medial and lateral transection) were compared for two different conditions (intact and following sectioning of the plantar ligament). Initially, the groups were compared following application of a load to the intact limbs. A paired t-test was used to compare the force exerted on the footplate, hock angle and the motion of individual bones between groups using Excel (Microsoft, Redmond, Washington, USA). The two groups were again compared using the same parameters following complete transection of the plantar ligament.

6.2.7.1 Investigating the effect of transection of the calcaneocentral or long plantar ligament

Within each group, comparisons were made between the intact limb and the limb following partial plantar ligament transection using a paired t-test performed in Excel (Microsoft, Redmond, Washington, USA). Limbs were compared based upon force exerted on the footplate and the total rotation of each individual bone. The change in helical axis orientation of each bone following partial ligament transection was calculated using the following formula:

Change in angle (degrees) = A cos ((x_1 X x_2)+(y_1 X y_2)+(z_1 X z_2)) X 180/π

Equation 6.1: was used to quantify the change in helical axis following ligament transection. Where,

x_1= x vector component of helical axis of the bone before transection

x_2 = x vector component of helical axis of the bone after transection

y_1= y vector component of helical axis of the bone before transection

y_2 = y vector component of helical axis of the bone after transection

z_1= z vector component of helical axis of the bone before transection

z_2 = z vector component of helical axis of the bone after transection

The effect of partial ligament transection on the kinematic pairs associated with the proximal intertarsal joint was investigated. The Pearson's correlation co-efficient and coupling ratio of each pair before and after partial transection were reported. In addition, the change in alignment angle between each kinematic pairing was reported. The alignment angle is the angle between the helical

axis of one bone in the kinematic pair and the helical axis of the other bone in the pair and was calculated using the following equation:

Alignment angle (AA) (degrees) = A cos ((x_1 X x_2)+(y_1 X y_2)+(z_1 X z_2)) X 180/π

Equation 6.2: Calculation of the alignment angle

Where,

x_1= x vector component of helical axis of bone 1

x_2 = x vector component of helical axis of bone 2

y_1= y vector component of helical axis of bone 1

y_2 = y vector component of helical axis of bone 2

z_1= z vector component of helical axis of bone 1

z_2 = z vector component of helical axis of bone 2

Kinematic pairs with a low alignment angle therefore move in the same direction during loading.

6.3 Results

6.3.1 Comparison of groups before transection

There were 5 limbs assigned to each group. The mean force recorded on the footplate for the medial transection group (1013±155N, mean ± SD) was not different to the force recorded from the lateral transection group (1055±140N) (p= 0.44).

The mean hock angle recorded for the intact limb of the medial transection group (85.5 ± 3.2 degrees, mean ± SD) was not different to hock angle recorded for the intact limb of the lateral transection group (87.9 ± 2.9 degrees) (p= 0.1)

For all limbs, each bone underwent rotations around and translations along each of the 3 reference axes. There was no difference in rotation or translation of any bone along or around any of the axes between groups. Similarly, there was no difference in the total rotation of any bone between groups. The three vectors defining the helical axis of each bone were not different between the two groups (tables 6.1 and 6.2).

*Table 6-1: motion of each bone following application of a load to the intact limb **(medial transection group).** Rotations and translations can be seen to occur along and around all three reference axes. CTB = central tarsal bone, TB = tarsal bone, MT = metatarsal bone, SD = standard deviation.*

Medial transection group: Intact limb		translation along (mm)			rotation around (degrees)			total rotation (degrees)
		x axis	y axis	z axis	x axis	y axis	z axis	
Tibia	mean	38.45	2.72	15.08	1.91	-28.23	2.80	28.51
	SD	5.17	3.41	3.99	2.45	2.95	2.13	2.87
Calcaneus	mean	0.45	0.43	0.13	-2.90	2.28	-0.82	3.90
	SD	0.28	0.08	0.18	1.56	1.46	0.47	2.05
CTB	mean	0.22	0.84	1.08	-2.07	4.80	-1.21	5.46
	SD	0.14	0.23	0.44	0.90	2.04	0.59	2.07
Fourth TB	mean	0.37	1.20	1.96	-2.13	5.07	-1.50	5.79
	SD	0.20	0.30	0.85	0.80	2.53	0.30	2.51
Third TB	mean	0.15	1.27	2.21	-1.19	6.17	-1.66	6.59
	SD	0.17	0.34	0.93	0.77	2.33	0.61	2.29
Second TB	mean	0.32	1.24	1.96	-2.04	6.08	-0.39	6.88
	SD	0.16	0.30	0.88	0.86	2.07	2.56	2.00
MT II	mean	0.01	2.94	9.12	1.78	11.18	-1.95	11.52
	SD	0.47	0.63	3.17	0.77	3.44	0.47	3.29
MT III	mean	-0.92	3.18	10.49	1.41	11.86	-2.01	12.13
	SD	0.67	0.81	3.43	0.63	3.30	0.70	3.20
MT IV	mean	-0.96	3.35	10.34	-2.08	11.82	-2.87	12.52
	SD	0.65	0.83	3.43	1.67	3.15	0.93	3.06
MT V	mean	-0.31	3.43	10.15	-1.90	11.43	-2.85	12.14
	SD	0.39	0.71	3.06	2.10	2.77	0.79	2.76

*Table 6-2: motion of each bone following application of a load to the intact limb **(lateral transection group).** Rotations and translations can be seen to occur along and around all three reference axes. CTB = central tarsal bone, TB = tarsal bone, MT = metatarsal bone, SD = standard deviation.*

Lateral transection group: Intact limb		translation along (mm)			rotation around (degrees)			total rotation (degrees)
		x axis	y axis	z axis	x axis	y axis	z axis	
Tibia	mean	37.20	2.98	15.20	1.95	-28.98	3.49	29.23
	SD	5.86	2.40	3.51	1.65	3.94	0.99	3.90
Calcaneus	mean	0.38	0.37	0.15	-2.52	1.81	-0.71	3.27
	SD	0.34	0.10	0.20	1.50	1.65	0.48	2.17
CTB	mean	0.22	0.76	0.98	-1.77	4.32	-1.14	4.85
	SD	0.19	0.23	0.50	0.71	2.33	0.48	2.43
Fourth TB	mean	0.32	1.09	1.73	-2.01	4.44	-1.51	5.15
	SD	0.26	0.36	0.95	0.75	2.33	0.37	2.41
Third TB	mean	0.15	1.18	2.04	-1.06	5.81	-1.77	6.20
	SD	0.17	0.33	1.05	0.70	2.53	0.72	2.66
Second TB	mean	0.32	1.16	1.85	-0.77	5.54	-1.57	5.89
	SD	0.20	0.36	1.02	0.42	3.11	0.92	3.12
MT II	mean	0.17	2.89	8.56	1.89	10.50	-2.11	10.96
	SD	0.04	0.85	2.99	1.53	3.13	0.82	3.09
MT III	mean	-0.78	3.21	9.95	2.01	11.39	-2.20	11.80
	SD	0.29	0.89	3.54	1.05	3.27	0.78	3.22
MT IV	mean	-0.85	3.50	9.67	-1.85	11.26	-3.34	12.00
	SD	0.29	0.82	3.49	1.46	3.18	0.55	3.29
MT V	mean	-0.33	3.50	9.41	-1.96	10.78	-3.18	11.51
	SD	0.15	0.79	3.08	1.27	2.76	0.55	2.89

6.3.2 Effect of Medial (Calcaneocentral ligament) transection

6.3.2.1 Force exerted on the footplate

Following transection of the calcaneocentral ligament, the force measured on the footplate reduced in all cases (mean 978.4N ± SD 150.3N) when the proximal limb restrain was returned to the identical position for the intact scan. This reduction was significantly different (p=0.02) to the intact foot and represented a mean reduction in force of 3.4 % (table 6.3)

Table 6-3: Force measured on the footplate for the intact foot, following partial transection and following complete transection for the medial transection group (top) and lateral transection group (bottom)

dog	side	Intact limb		following calcaneocentral ligament transection		following complete plantar ligament transection	
		Force (N)	hock angle (deg)	Force (N)	% change	Force (N)	% change
1	L	1210	83.4	1175	-2.9	50	-95.9
2	R	940	83.9	905	-3.7	54	-94.3
3	L	830	82.3	790	-4.8	2	-99.8
4	R	1135	87.8	1077	-5.1	6	-99.5
5	L	950	89.9	945	-0.5	6	-99.4
mean		**1013**	**85.5**	**978.4**	**-3.4**	**23.6**	**-97.7**
SD		**155.3**	**3.2**	**150.3**	**1.8**	**26.0**	**2.5**

dog	side	Intact limb		following long plantar ligament transection		following complete plantar ligament transection	
		Force (N)	hock angle (deg)	Forc e (N)	% change	Force (N)	% change
1	R	1125	88.0	1070	-4.9	40	-96.4
2	L	900	86.8	737	-18.1	22	-97.6
3	R	910	84.4	750	-17.6	14	-98.5
4	L	1197	92.3	900	-24.8	7	-99.4
5	R	1145	88.1	960	-16.2	18	-98.4
mean		**1055.4**	**87.9**	**883.4**	**-16.3**	**20.2**	**-98.1**
SD		**139.8**	**2.9**	**141.6**	**7.2**	**12.4**	**1.1**

6.3.2.2 Total rotation

For all bones investigated, both a total rotation and 6 degrees of freedom motion was recorded following transection of the calcaneocentral ligament (table 6.4)

Table 6-4: Motion of each bone following application of a load to the limb after transection of the calcaneocentral ligament (medial transection group). Rotations and translations can be seen to occur along and around all three reference axes. CTB = central tarsal bone, TB = tarsal bone, MT = metatarsal bone, SD = standard deviation.

Medial transection group: Following calcaneocentral ligament transection		translation (mm)			rotation (degrees)			total rotation around helical axis (degrees)
		x axis	y axis	z axis	x axis	y axis	z axis	
Tibia	mean	36.68	2.99	14.71	2.08	-26.98	2.97	27.28
	SD	5.20	3.24	3.76	2.27	3.00	1.96	2.94
Calcaneus	mean	0.55	0.56	0.10	-3.43	3.15	-0.66	4.80
	SD	0.28	0.13	0.18	1.57	1.36	0.35	2.02
CTB	mean	0.32	1.09	1.53	-1.03	6.88	-2.20	7.46
	SD	0.24	0.32	0.44	0.91	2.46	1.01	2.29
Fourth TB	mean	0.46	1.41	2.40	-1.09	6.29	-1.89	6.78
	SD	0.24	0.33	0.82	0.97	2.61	0.38	2.50
Third TB	mean	0.22	1.60	2.91	-0.10	7.89	-2.54	8.39
	SD	0.23	0.44	0.96	0.91	2.38	0.88	2.24
Second TB	mean	0.32	1.70	2.53	-4.20	5.63	-3.54	11.44
	SD	0.33	0.45	1.11	7.26	5.12	4.81	4.03
MT II	mean	-0.04	3.84	11.34	3.16	13.30	-2.95	13.98
	SD	0.59	0.84	3.45	0.98	3.78	0.62	3.58
MT III	mean	-1.17	4.27	12.63	2.92	13.78	-3.06	14.40
	SD	0.86	0.97	3.69	0.89	3.66	0.76	3.52
MT IV	mean	-1.17	4.34	12.08	-0.64	13.45	-3.93	14.22
	SD	0.80	0.89	3.51	2.27	3.32	0.93	3.26
MT V	mean	-0.44	4.29	11.74	-0.69	13.08	-3.92	13.93
	SD	0.50	0.65	3.12	2.67	2.97	0.74	2.87

When the total rotation of each bone following transection was compared to the motion in the intact foot, all tarsal and metatarsal bones showed a significantly greater rotation following transection of the calcaneocentral ligament. Conversely, the tibial rotation was reduced in all dogs following calcaneocentral ligament transection (fig 6.6)

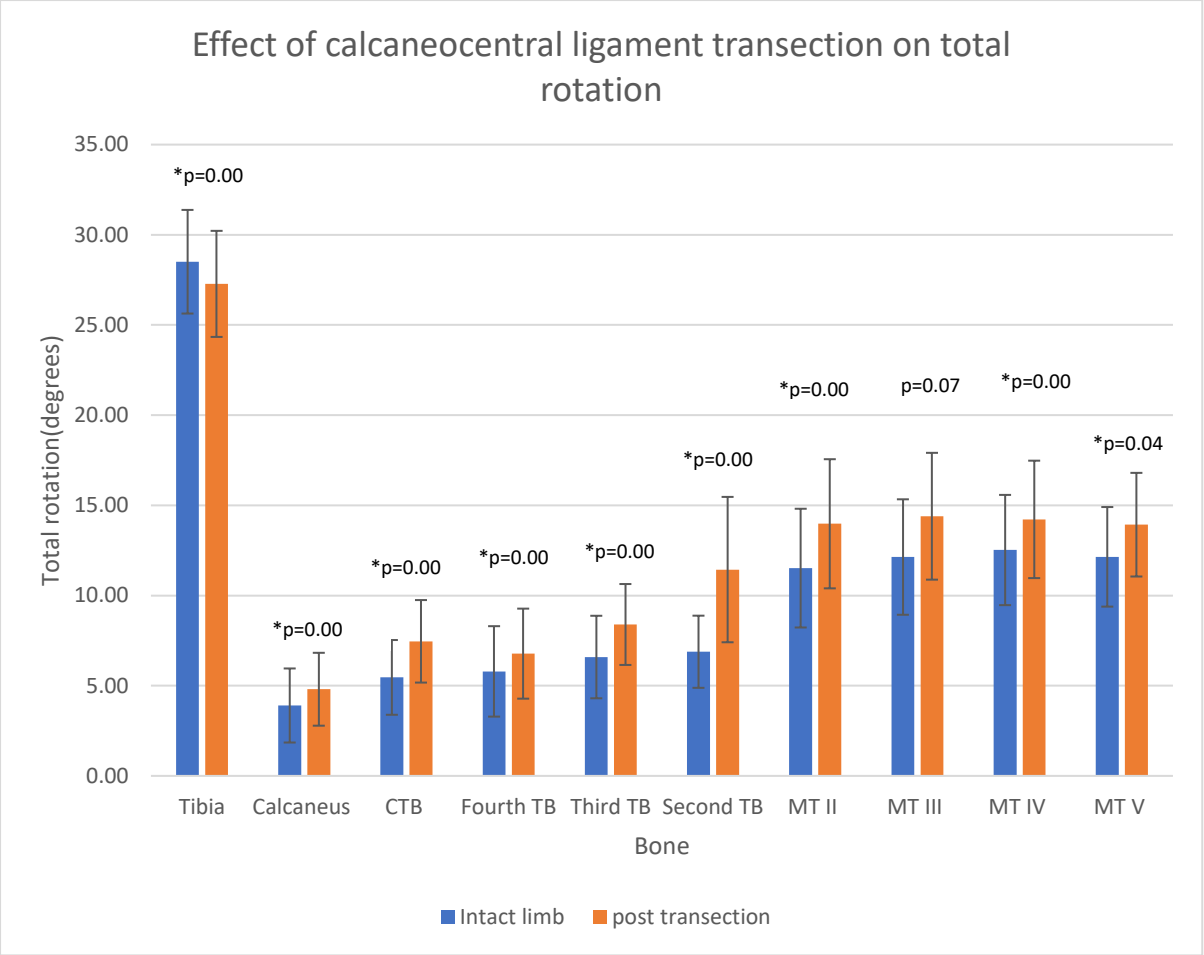

Figure 6-6: Comparison of total rotation of each bone before and after calcaneocentral ligament transection. For all tarsal and metatarsal bones, there is a significant increase in the magnitude of rotation following transection of the calcaneocentral ligament, suggesting the calcaneocentral ligament plays an important role in stability across the entire proximal intertarsal joint. Error bars represent one standard deviation. CTB = central tarsal bone, TB = tarsal bone, MT = metatarsal bone. denotes significant difference (p-value)*

6.3.2.3 Helical axis orientation

A change in helical axis occurred for all bones following calcaneocentral ligament transection. The helical axis of the calcaneus shifted by a mean of 10.11 degrees, whilst the central tarsal bone's helical axis changed by a mean of 14.38 degrees. In contrast, the helical axis of the tibia showed little change (0.78 ± 0.35 degrees; mean ± SD) after calcaneocentral ligament transection. (Table 6.5)

Table 6-5: Change in helical axis for each bone following transection of the calcaneocentral ligament (medial transection group) and long plantar ligament (lateral transection group). CTB = central tarsal bone, TB = tarsal bone, MT = metatarsal bone, SD = standard deviation.

		change in helical axis (degrees)	
		following calcaneocentral ligament transection	following long plantar ligament transection
Tibia	mean	0.8	2.8
	SD	0.3	0.8
Calcaneus	mean	10.1	16.5
	SD	10.6	16.5
CTB	mean	14.4	11.3
	SD	3.3	9.2
Fourth TB	mean	13.5	16.3
	SD	6.4	12.3
Third TB	mean	9.1	9.8
	SD	2.2	7.1
Second TB	mean	38.4	25.6
	SD	38.2	14.2
MT II	mean	4.1	12.3
	SD	0.5	6.6
MT III	mean	5.0	11.6
	SD	1.2	4.7
MT IV	mean	7.0	11.6
	SD	2.3	2.0
MT V	mean	6.1	12.3
	SD	2.6	4.5

6.3.2.4 Kinematic pairs of the proximal intertarsal joint

The kinematic pairs evaluated were the calcaneus and central tarsal bone, the calcaneus and fourth tarsal bone and the central tarsal bone and 4th tarsal bone.

The strong linear kinematic coupling between total rotation of the calcaneus and central tarsal bone (R^2 = 0.99 in the intact limb) remained high following calcaneocentral ligament transection (R^2 = 0.93) and this was similarly seen the calcaneus/fourth tarsal bone pairing and the Central/fourth tarsal bone pairing (table 6.6).

The alignment angle(AA) between the helical axis of the calcaneus and central tarsal bone was significantly different (p=0.047) between the intact limb (AA= 31.46 ± 17.25 degrees) and the limb following calcaneocentral ligament transection (38.64 ± 12.39 degrees). A significant difference (p=0.004) was also seen in the alignment axis of the calcaneus and fourth tarsal bone between conditions. The partial transection produced no significant difference in the AA of the central and fourth tarsal bones (p=0.24) (table 6.6).

Table 6-6: Comparison of the alignment axis, coupling ration and correlation coefficient for three pairs of bones associated with the PIT joint in the intact limbs, following partial transection and following complete transection of the plantar ligament. The small values of the alignment angle for the CTB and fourth tarsal bone pairing suggest that these bones always rotate around a very similar axis for all conditions consistent with a functional rigid unit.

CTB = central tarsal bone, 4th = fourth tarsal bone

Pair of bones	condition											
	Intact limb			Following calcaneocentral ligament transection			Following long plantar ligament transection			following complete transection of plantar ligament		
	correlation coefficient (R^2)	coupling ratio	alignment angle of helical axes (degrees)	correlation coefficient (R^2)	coupling ratio	alignment angle of helical axes (degrees)	correlation coefficient (R^2)	coupling ratio	alignment angle of helical axes (degrees)	correlation coefficient (R^2)	coupling ratio	alignment angle of helical axes (degrees)
Calcaneus and CTB	0.99	1.06	33.7	0.93	1.09	38.64	0.98	1.09	43.96	0.03	0.41	55.22
Calcaneus and 4th	0.98	1.15	32.45	0.97	1.22	37.61	0.99	1.13	50.83	0.04	0.46	56.24
CTB and 4th	0.98	1.08	5.62	0.97	1.07	4.01	0.99	1.02	8.48	0.98	0.91	2.22

6.3.3 Effect of Lateral (Long plantar ligament) transection

6.3.3.1 Force exerted on the footplate

Following transection of the long plantar ligament, the force measured on the footplate reduced in all cases (mean 883.4N; SD 141.6N) when the proximal limb restrain was returned to the identical position for the intact scan. This reduction was significantly different (p=0.01) to the intact foot and represented a mean reduction in force of 16.3 % (table 6.3)

6.3.3.2 Total rotation

For all bones investigated, both a total rotation and 6 degrees of freedom motion was recorded following transection of the long plantar ligament (table 6.7).

Table 6-7: Motion of each bone following application of a load to the limb after transection of the long plantar ligament (lateral transection group). CTB = central tarsal bone, TB = tarsal bone, MT = metatarsal bone, SD = standard deviation.

Lateral transection group: Following long plantar ligament transection		translation (mm)			rotation (degrees)			total rotation around helical axis (degrees)
		x axis	y axis	z axis	x axis	y axis	z axis	
Tibia	mean	34.09	2.82	14.67	1.75	-26.75	3.06	26.97
	SD	5.88	1.96	3.18	1.42	4.10	0.94	4.08
Calcaneus	mean	0.43	0.22	0.05	-2.20	1.45	-0.95	2.93
	SD	0.30	0.06	0.15	1.64	1.68	0.55	2.26
CTB	mean	0.29	1.05	1.40	-1.98	6.23	-1.89	6.86
	SD	0.14	0.21	0.48	0.81	2.38	0.46	2.50
Fourth TB	mean	0.69	1.40	2.66	-1.69	9.29	-2.31	9.85
	SD	0.19	0.36	1.00	1.45	2.50	0.72	2.55
Third TB	mean	0.25	1.51	3.10	-1.55	8.32	-2.32	8.83
	SD	0.13	0.32	1.02	0.88	2.34	0.73	2.50
Second TB	mean	0.48	1.52	2.76	-2.05	8.59	-0.93	9.12
	SD	0.16	0.30	1.00	0.77	2.41	2.22	2.50
MT II	mean	0.14	3.19	11.26	0.40	13.00	-1.89	13.26
	SD	0.23	0.86	2.83	1.72	2.80	0.84	2.75
MT III	mean	-1.06	3.42	13.22	-0.15	14.10	-2.00	14.32
	SD	0.44	0.83	3.36	1.38	2.97	0.68	2.96
MT IV	mean	-1.24	3.85	13.78	-4.36	14.95	-3.23	16.04
	SD	0.50	0.72	3.38	1.15	2.84	0.27	2.89
MT V	mean	-0.50	4.16	13.99	-4.14	15.02	-3.32	16.05
	SD	0.39	0.77	3.01	0.97	2.55	0.42	2.67

Following transection of the long plantar ligament, there was a significant decrease in rotation of the tibia and a significant increase in rotation of all other bones, with the exception of the calcaneus, which showed no significant difference in rotation to the intact foot (figure 6.7)

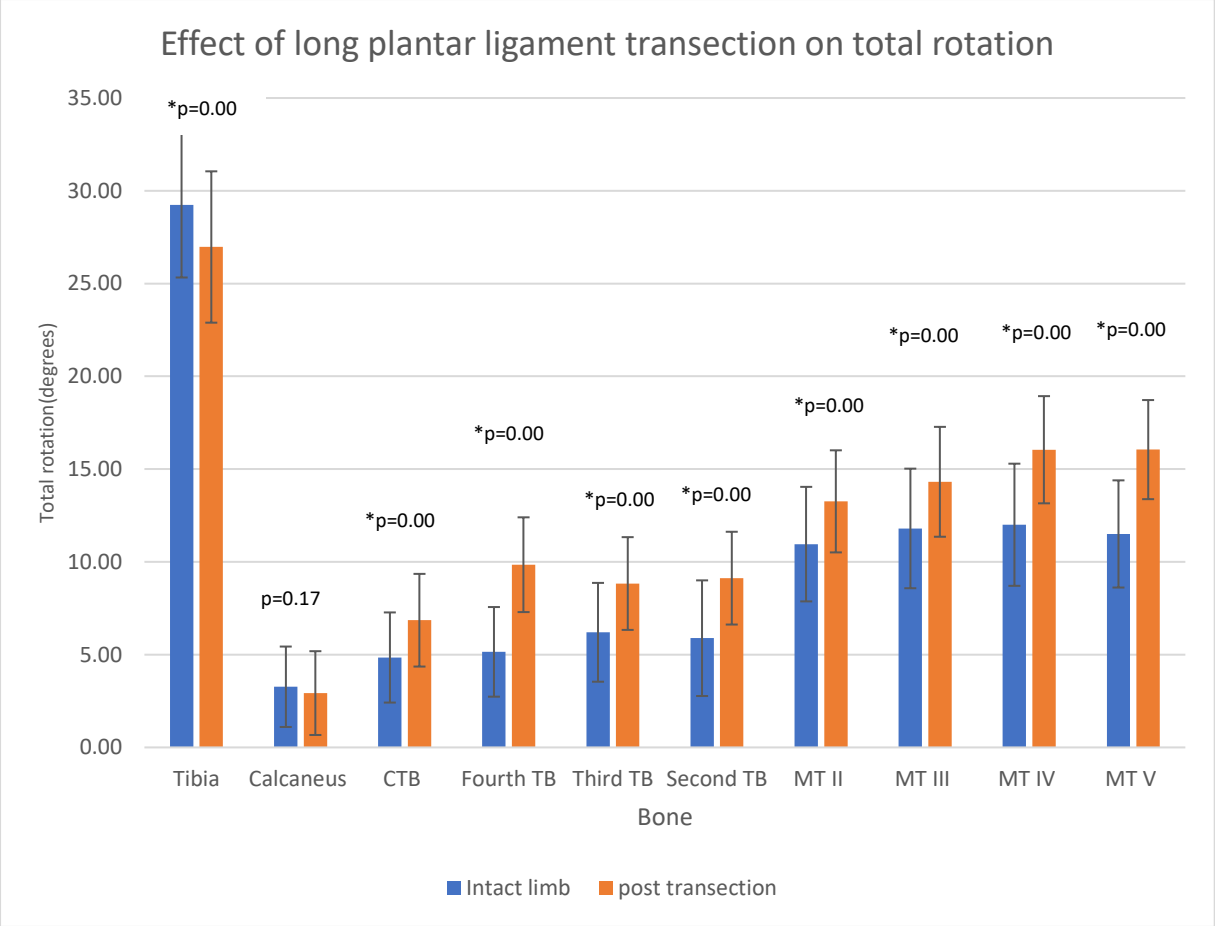

*Figure 6-7: Comparison of total rotation of each bone before and after long plantar ligament transection. For all tarsal and metatarsal bones, there is a significant increase in the magnitude of rotation following transection of the long plantar ligament, suggesting the long plantar ligament plays an important role in stability across the entire proximal intertarsal joint. Error bars denote one standard deviation. CTB = central tarsal bone, TB = tarsal bone, MT = metatarsal bone. * denotes significant difference (p-value)*

6.3.3.3 Helical axis orientation

As with the medial transection group, a change in the helical axis around which each bone rotated occurred for all bones following long plantar ligament transection (table 6.5)

6.3.3.4 Kinematic pairs of the proximal intertarsal joint

The strong linear kinematic coupling between total rotation of the calcaneus and central tarsal bone (R^2 = 0.99 in the intact limb) remained high following transection of the long plantar ligament (R^2 = 0.98) and this was similarly seen the calcaneus/fourth tarsal bone pairing and the Central/fourth tarsal bone pairing (table 6.6).

The alignment angle between the helical axis of the calcaneus and central tarsal bone increased between the intact limb (AA= 35.96 ± 17.49 degrees) and the limb following transection of the long plantar ligament (43.96 ± 22.44 degrees) was not significantly different (p=0.06). A significant difference (p=0.01) was seen in the alignment axis of the calcaneus and fourth tarsal bone between conditions. The partial transection produced no significant difference in the AA of the central and fourth tarsal bones (p=0.16) (table 6.6).

6.4 Effect of complete plantar ligament transection

For all bones investigated, both a total rotation and 6 degrees of freedom motion was recorded following transection of the entire plantar ligament (calcaneocentral and long plantar ligaments) (table 6.8)

Table 6-8: Motion of each bone following application of a load to the limb after transection of the entire plantar ligament (both transection groups). Rotations and translations can be seen to occur along and around all three reference axes. CTB = central tarsal bone, TB = tarsal bone, MT = metatarsal bone, SD = standard deviation.

All limbs: Following complete transection of plantar ligament		translation along (mm)			rotation around (degrees)			total rotation around helical axis (degrees)
		x axis	y axis	z axis	x axis	y axis	z axis	
Tibia	mean	-12.14	-4.63	-10.21	-0.39	10.57	-3.94	11.40
	SD	5.71	2.21	3.95	0.54	3.93	1.48	3.92
Calcaneus	mean	1.55	0.33	-1.04	-7.28	10.41	-0.88	12.92
	SD	0.52	0.40	0.34	1.74	2.09	1.43	2.36
CTB	mean	-3.70	3.08	13.47	63.30	63.24	-50.03	78.89
	SD	1.25	0.97	0.66	14.17	3.12	13.71	6.05
Fourth TB	mean	-1.19	2.64	17.78	60.53	60.15	-48.22	76.61
	SD	1.65	1.38	1.23	11.25	3.50	11.02	5.56
Third TB	mean	-9.59	6.03	22.50	58.02	61.91	-46.35	76.22
	SD	1.72	1.47	0.89	12.86	3.27	12.31	5.90
Second TB	mean	-9.80	6.26	24.19	58.72	62.48	-46.23	76.71
	SD	2.15	1.57	1.16	11.87	3.24	12.52	5.27
MT II	mean	-33.39	18.42	62.19	54.50	61.07	-42.83	73.65
	SD	5.17	4.29	3.07	12.07	3.79	11.69	5.96
MT III	mean	-39.69	20.58	62.68	52.78	60.97	-42.67	74.32
	SD	5.77	4.29	2.98	12.05	3.79	11.84	5.89
MT IV	mean	-31.87	17.25	54.77	44.68	55.08	-37.50	73.41
	SD	12.27	6.53	17.19	17.95	17.14	15.44	5.63
MT V	mean	-30.34	17.83	60.32	53.29	60.43	-45.96	73.99
	SD	5.41	4.37	3.69	11.07	3.68	11.18	5.70

Following complete transection of the plantar ligament, luxation of the proximal intertarsal joint was observed in all cases (fig 6.8). This did not occur in any of the cases following either calcaneocentral or long plantar ligament transection alone (figure 6.9)

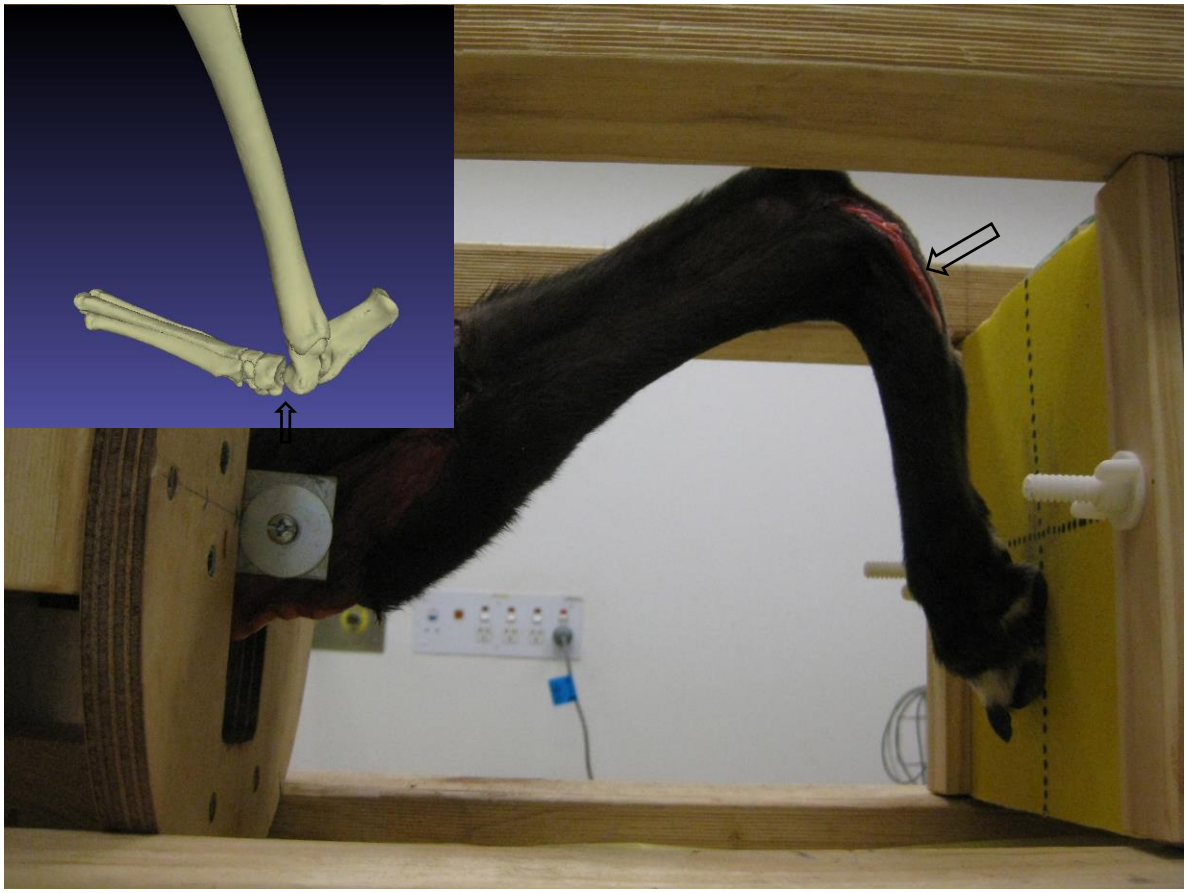

Figure 6-8: A proximal intertarsal luxation (arrow) occurred in all specimens with complete plantar ligament transection following application of a load. Inset: the reconstructed CT scan of a specimen following compete plantar ligament transection.

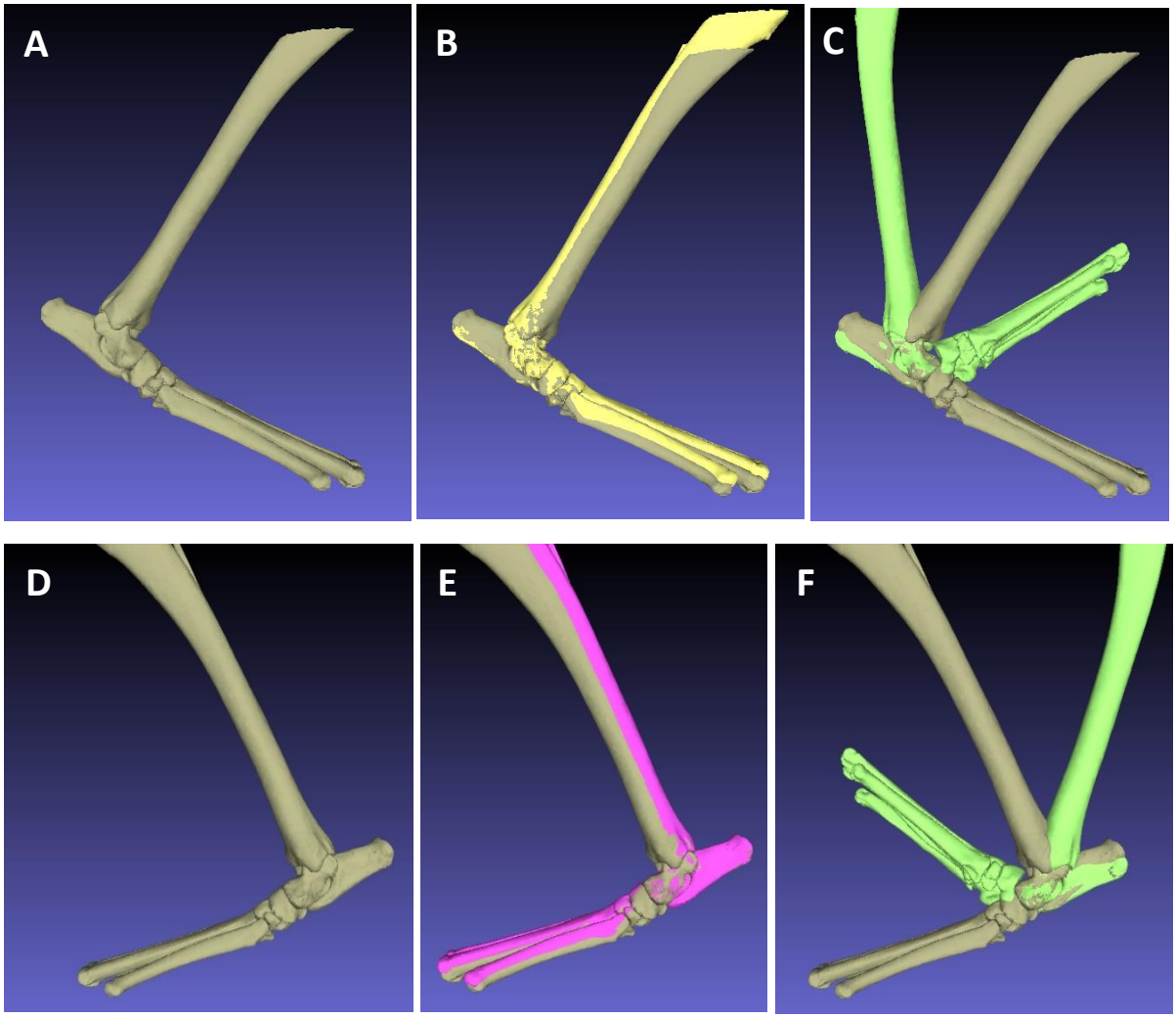

Figure 6-9: Effects of ligament transection on bone position. Top row: The position of bones of the pes of for a dog in the medial transection group before transection (A), after transection of the calcaneocentral ligament (yellow bones, B) and after complete plantar ligament transection (green bones, C). Bottom row: The position of bones of the pes of for a dog in the lateral transection group before transection (D), after transection of the long plantar ligament (pink bones, E) and after complete plantar ligament transection (green bones, F). Note the speckled appearance of the talus in the superimposed examples as this represents the reference bone that all other motion is described.

The mean force recorded on the footplate for dogs after complete plantar ligament transection was 23.6N (± SD 26.0N), representing a mean reduction in force of 97.7% for the medial transection group and 22.2N (± 12.4N), representing a mean reduction in force of 98.0% for the lateral transection group (table 6.3).

The mean CTB rotation increased from 5.2 degrees to 78.9 degrees following plantar ligament transection and the mean rotation of the fourth tarsal bone increased from 5.5 degrees to 76.6 degrees following complete plantar ligament transection (figure 6.10).

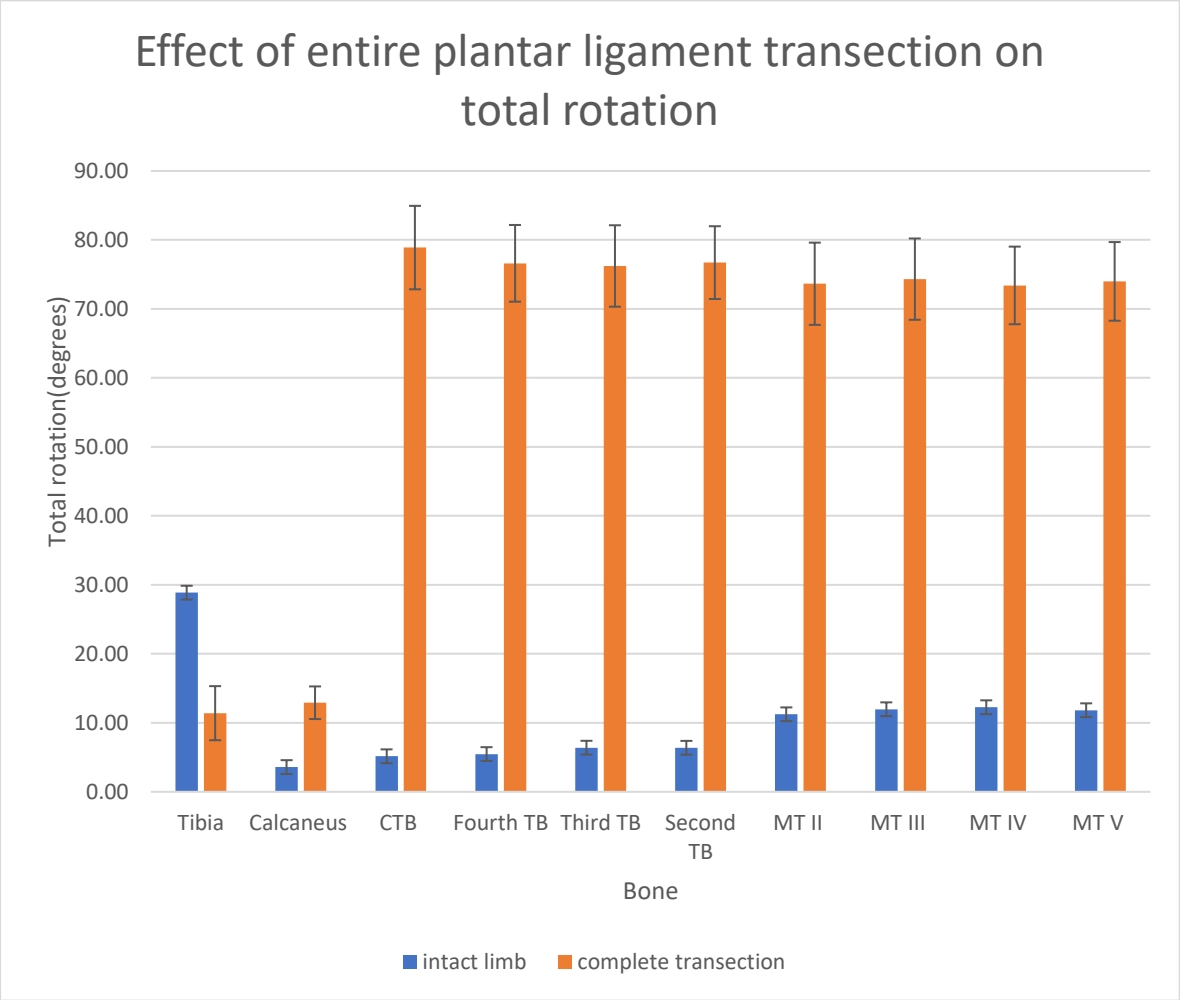

Figure 6-10: Total rotation of each bone before and after complete plantar ligament transection. The was significant increases in the magnitude of rotation in all bones distal to the proximal intertarsal joint consistent with the observed subluxation. CTB = central tarsal bone, TB = tarsal bone, MT = metatarsal bone.

Kinematic coupling was lost for the calcaneus and central tarsal bone ($R^2 = 0.03$) and for the calcaneus and fourth tarsal bone ($R^2 = 0.04$), whilst the strong linear relationship was maintained between the central and fourth tarsal bones ($R^2 = 0.98$) (table 6.6).

6.4 Discussion

To date, the role of plantar ligament in maintaining the stability within the pes has received little attention and most descriptions are based upon anatomical assumptions. The results of this chapter have identified that the plantar ligament is the only ligamentous structure that prevents subluxation of the proximal intertarsal joint during weight bearing. Furthermore, the results demonstrate that in this cadaveric model of ligamentous injury, loss of either the long plantar or calcaneocentral ligament alone does not produce proximal intertarsal subluxation and still allows continued force transmission through this limb segment, although at reduced levels.

6.4.1 Anatomy of the plantar ligament

The anatomical appearance of the plantar ligament was consistent with previous descriptions (Evans et al., 2012) (Arwedsson, 1954) (Carmichael and Marshall, 2013) (Holt, 1974), being comprised of two main parts, the calcaneocentral and long plantar ligaments, and a third smaller but distinctive fibrous band arising from the caudolateral aspect of the calcaneus to insert with the m. peroneus brevis on the head of the fifth metatarsal bone (figure 6.11). This distinctive fibrous band has been termed the primarily tendinous muscle abductor digiti V by some authors (Arwedsson, 1954; Evans et al., 2012; Holt, 1974), whilst others have included this band as the third component of the plantar ligament, referring to it as the calcaneoquartal ligament (Evans et al., 2012) or the lateral plantar ligament (Carmichael and Marshall, 2013).

Figure 6-11: Lateral aspect of dissected specimen of canine tarsus. The fibrous band (arrow) running from the calcaneus to the head of the fifth metatarsal (open arrow) which has been termed both the m. abductor digiti V and the calcaneoquartal ligament (as part of the plantar ligament)

6.4.2 Role of the plantar ligament in tarsal bone kinematics

The results from this chapter allow rejection of the null hypothesis, that partial or full transection of the plantar ligament would produce no difference in tarsal bone kinematics. Although this chapter represents the first report of kinematics following plantar ligament transection in the dog, these results are similar to previous investigations of both the human foot (Ker et al., 1987) and donkey pes (Dimery and Alexander, 1985), in that increased displacement was noted following sequential ligamentous transection. However, in contrast to these previous studies, the displacement of individual tarsal bones was recorded in this chapter's experiment following sequential transmission, allowing greater characterisation of the effect on each individual bone.

As the central and fourth tarsal bones have no direct muscular attachments(Evans et al., 2012), it is perhaps not surprising that an increase in rotation was seen following ligament transection, since ligaments, along with the joint surface shape, provide the major restraints to bone motion (Sennwald et al., 1993). However, the findings of this chapter also revealed significant changes in both the magnitude of total rotation and orientation of the helical axis of all bones and not just those associated with the proximal intertarsal joints. The bones of the pes form a kinematic chain both along the longitudinal axis of the foot and across it. Changes in the motion of one bone had a significant effect on all bones further suggesting that the pes works as a single co-ordinated limb segment, consistent with the results of the previous chapter.

Tarsal bone motions are particularly dependant on the movement of adjacent bones, which directly influence the compressive forces across articular surfaces and the tensile forces produced by ligamentous attachments. In the human foot, arthrodesis of any of the joints of the triple joint complex (the subtalar, talonavicular, and calcaneocuboid joints) limits the motion of the remaining, unfused joints (Astion et al., 1997) highlighting the interdependence of tarsal bone motions. Although the same experiments have not been repeated in dogs, the finding of this present study suggest that there is also an interdependence of tarsal bone motion. Injuries or interventions that alter motion at one intertarsal joint are likely to affect surrounding joints of the pes by altering the magnitude of rotation of a bone or altering the helical axis around which that bone rotates.

Following transection of the long plantar ligament, excessive rotation of the central tarsal bone and fourth tarsal bone (termed the midfoot functional unit in the previous chapter) is prevented by the calcaneocentral component of the plantar ligament and remaining joint capsule. Although the magnitude of rotation of the midfoot unit is increased, excessive rotation of the fourth tarsal bone is prevented despite complete loss of the plantar attachment to the proximal bone, the calcaneus. For this to occur, the strong ligamentous attachments between the central and fourth tarsal bones must remain intact.

Similarly, following transection of the calcaneocentral ligament, subluxation of the central tarsal bone was prevented by its strong attachments to the fourth tarsal bone and surrounding joint capsule.

6.4.3 Role of the plantar ligament in energy storage and transmission

In the previous chapter, the elastic dorsiflexion of the canine pes was suggested as a means of storing and transmitting energy within the limb segment. This has been demonstrated in other species including humans and equids (Dimery and Alexander, 1985; Ker et al., 1987).

The findings of this chapter suggest all aspects of the plantar ligament contribute to the transmission of force through the canine pes. Partial transection of different aspects of the ligament produced a significant reduction in force that could be transmitted through the pes, however, subluxation or luxation did not occur until the entire plantar ligament was transected (figure 6.7), suggesting that disruption to both the long plantar ligament and calcaneocentral ligament are required before proximal intertarsal subluxation occurs, supporting previous suggestions (Allen et al., 1993; Barnes et al., 2013; Campbell et al., 1976; Lawson, 1960). Proximal intertarsal subluxation was possible despite the presence of an intact tendinous abductor digiti V (also termed lateral plantar ligament or calcaneoquartal ligament), suggesting that it contributes little to stability across these joints.

This chapter represents the first known kinematic study of the canine pes and comparisons can only be made to kinematic investigations involving different species, which often exhibit significant variation in anatomy and stance. The bones of the plantigrade human foot were shown to store less elastic energy following transection of the long and short plantar ligaments and calcaneonavicular (spring) ligament (which runs in a similar direction to the calcaneocentral ligament) (Ker et al., 1987). Similar to the findings of this chapter, subluxation did not occur after transection of only components of the plantar ligamentous support. A sequential transection of tendons of the pes of

the donkey demonstrated a reduced ability to store elastic energy in the pes, however, transection of plantar ligaments was not performed (Dimery and Alexander, 1985).

The paired study design of this chapter allowed direct comparison between the role of the long plantar ligament and the calcaneocentral plantar ligament in force transmission through the pes. The loss of the integrity of long plantar ligament results in a greater loss in force transmission compared to the loss of integrity of the calcaneocentral ligament, suggesting the former plays a greater role in force transmission within the pes. This information may be important when attempting to re-establish integrity of the pes following proximal intertarsal subluxation. Previous clinical reports suggest that stabilisation of the calcaneoquartal joint alone may be adequate despite subluxation of the talocentral joint, which occurs concurrently during proximal intertarsal subluxation (Allen et al., 1993; Barnes et al., 2013; Campbell et al., 1976; Lawson, 1960)

6.4.5 Clinical importance

The clinical importance of these findings relates to conditions whereby the integrity of the plantar ligament is lost, either through trauma or degenerative processes. Proximal intertarsal (PIT) joint subluxation in well described and breeds such as Shetland sheepdogs and Collies are over-represented (Allen et al., 1993; Barnes et al., 2013; Campbell et al., 1976; Fettig et al., 2002). In many cases, degeneration of the plantar ligament is suspected, and many animals experience an insidious onset without a history of major trauma (Campbell et al., 1976). The ability to redirect force through the pes following the loss of approximately 50% of the plantar ligament, as demonstrated in this chapter's experiments, means affected animals can still transmit force through the pes and weight bear until late in the disease process. This may explain the periosteal reaction commonly identified

on the plantar aspect of the calcaneus (Barnes et al., 2013), the result of increased load experienced by remaining intact fibres of the plantar ligament.

The PIT joint comprises both the calcaneoquartal joint and talocentral joint. The present study showed that for subluxation or luxation to occur at this joint, both the long plantar ligament and the calcaneocentral components of the plantar ligament must be lost. Isolated subluxation of the talocentral or calcaneoquartal joints was not observed in the present study.

Following disruption to the plantar ligament and subsequent PIT subluxation, surgical repair is recommended and a number of different techniques have been described (Barnes et al., 2013). Successful techniques must overcome the dorsiflexion of the pes and most commonly involve arthrodesis of the calcaneoquartal joint alone. However, this procedure does not address the instability of the medial aspect of the proximal intertarsal joint, the talocentral joint. During calcaneoquartal arthrodesis, generally no attempt is made to stabilise the central tarsal bone but rather to rigidly stabilise the calcaneus and fourth tarsal bone to allow a permanent bony union to occur. The findings that central tarsal bone rotation can be limited solely by its firm attachment to the fourth tarsal bone would support the use of calcaneoquartal arthrodesis as an appropriate treatment for proximal intertarsal luxation provided the ligamentous attachments between the central and fourth tarsal bone remain intact.

6.4.6 Study limitations

The use of cadaveric specimens to study bone kinematics and force transmission has several advantages, such as the ability to perform procedures and apply standardised forces, however, it also has several limitations which much be considered before translating the findings to the clinical situation. As there is no active contraction of any muscles, this cadaver loading jig relies upon fibrous tissue throughout and around each muscle to produce appropriate forces. Previous studies have

identified that muscles such as the gastrocnemius, superficial digital flexor and deep digital flexor have short pennate fibres and a high tendon length change:muscle fascicle length (TLC : MFL) ratio, meaning that active shortening as not a major component of their function (Williams et al., 2008). Tension in these three muscles was created as flexion of the hock occurred. Both the digital flexors pass caudal to the hock and will elongate during loading in the jig and hence tension can be maintained in these muscles. However, this tension could not be controlled in the present study, nor adjusted to replicate the tension in these tendons during in vivo locomotion. This is an important component to both force transmission and bone kinematics. The pressure sensitive film records force on a series of pressure sensors and the records the peak force over the entire film. Pull from the digital flexors will increase the load recorded from each digital pad and will influence the peak recorded value. Only the peak value was recorded, however, future studies may consider recording the value exerted by each digital pad to further characterise force transmission through this body segment as had been performed in in vivo studies (Besancon et al., 2004). Whilst the superficial digital flexor tendon runs directly over the long plantar ligament, the deep digital flexor runs in a groove directly overlying the sustentaculum tali and the calcaneocentral ligament. Tension in these ligaments may therefore contribute to restraining individual tarsal bone motion. Based on the present study design, where the plantar ligament ligaments underwent transection and digital flexor tendons remained intact, it is impossible to describe the contribution the flexor tendons make to both force transmission and individual bone kinematics. However, it can be stated that intact digital flexors are insufficient to maintain integrity of the pes once the plantar ligament is lost. Examination of the tendons at the level whereby they pass over the tarsal bones revealed no gross evidence of thickened fibrocartilage, which is often found in other tendons where they are exposed to significant compressive forces (Benjamin et al., 2006). This would suggest that they are unlikely to play a major role in tarsal kinematics.

Another limitation of this study is that partial transection is unlikely to accurately represent the clinical scenario of ligament degeneration. As where partial transection disturbs a localised

collection of fibres, naturally occurring degeneration of the ligament is likely to be more diffuse. Natural degeneration may also result in changing properties of the ligament in regard to compliance and modulus if elasticity. Change in the material properties of ligaments is well described, with factors such as age (Thornton et al., 2015), sex (Chandrashekar et al., 2006; Romani et al., 2010) and exercise (LaCroix et al., 2013) significantly affecting these properties. Attempts were made to limit these affects in this study by selecting only female greyhounds, however, the age, clinical and racing history of these dogs was unknown and may have influenced the outcomes. Furthermore, the small changes recorded in the position of the tarsal bones are likely to represent the effect of transection of the ligament in addition to any change in position that resulted from loading, then unloading the limb (to allow transection) and then reloading of the limb. It is unknown if all bones will return to the same position each time a load is applied, removed and reapplied and this fact must be considered in the interpretation of the results. Further studies could be performed to explore the consistency of tarsal bone position following unloading and reloading of the limb in this cadaveric model.

6.5 Conclusions

The plantar ligament plays an important role in the structural integrity of the pes and loss of any component affects its performance. Following disruption, force transmitted through the pes may be redirected, however, this will influence the pattern of bone motion due to the dependence of motion of each bone on motion at adjacent joints. This support the findings of the previous chapter that suggest the canine pes functions as a co-ordinated unit and must be considered as a single structure rather than a series of separate joints. For subluxation of the proximal intertarsal joint to occur, both the calcaneocentral and long plantar ligaments must be disrupted.

Chapter 7 : Lateral plating to restore integrity of the canine pes following proximal intertarsal luxation

7.1 Introduction

Disruption of the integrity of the canine pes may involve damage to either bones or ligaments. Fractures of the calcaneus (Ost et al., 1987; Perry et al., 2017) and central tarsal bone (Boudrieau et al., 1984a; Guilliard, 2000) are most commonly reported, whilst ligamentous damage occurs most frequently at the proximal intertarsal joint or the tarsometatarsal joints (Campbell et al., 1976; Fettig et al., 2002). Both these joints are compound joints (figure 7.1); the proximal intertarsal joint is comprised of the talocentral and calcaneoquartal joints, whilst the tarsometatarsal joint is comprised of the articulations of each metatarsal bone with its respective numbered tarsal bone (Evans et al., 2012).

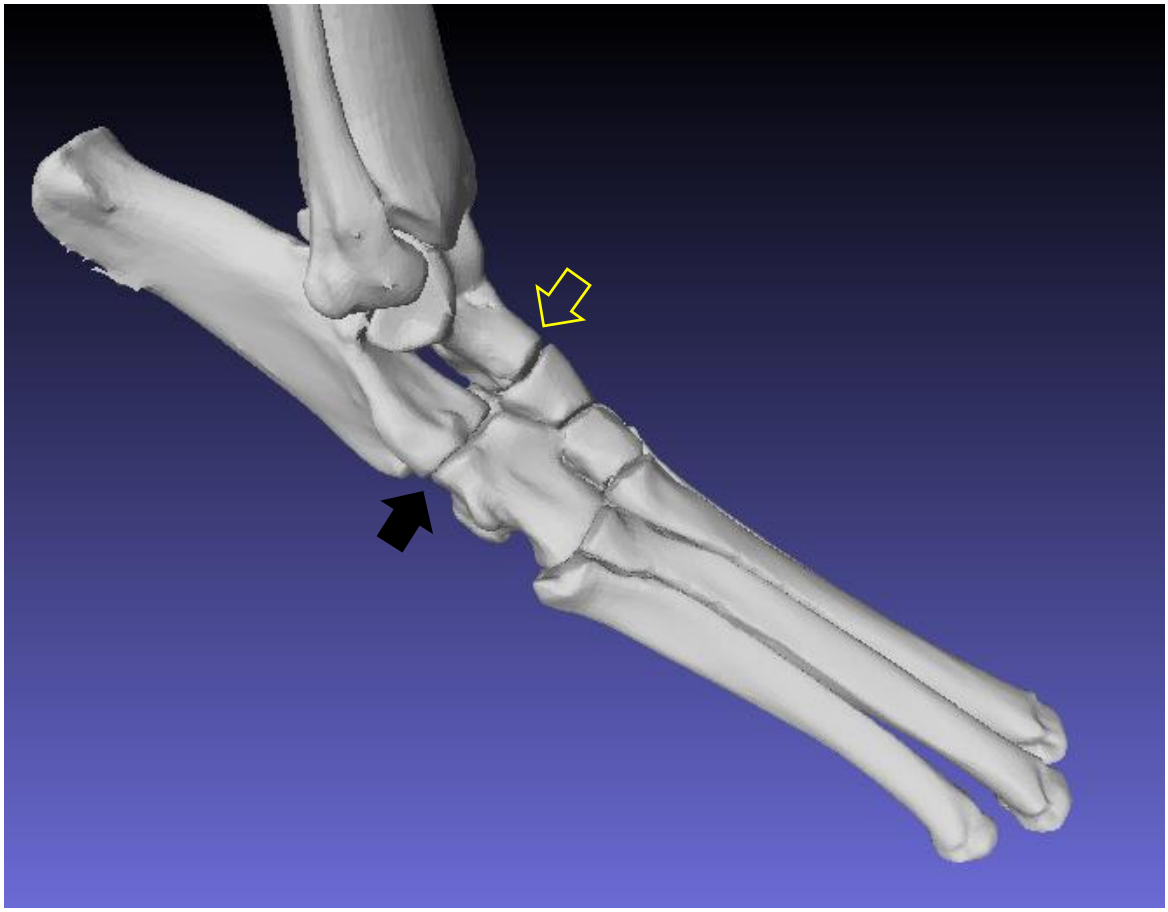

Figure 7-1: The bones of the canine pes. The proximal intertarsal joint is a compound joint that is comprised of the talocentral joint (open yellow arrow) and calcaneoquartal joint (solid black arrow). Craniolateral view.

Strong soft tissue structures surround these joints to produce only limited motion, allowing the pes to act as an effective lever in the distal limb. Damage to any of these supporting structures can have a significant detrimental effect on locomotion.

Due to their location on the dorsal, compression surface of the pes, disruption to the dorsal ligaments of the pes results in less compromise to the integrity of the pes during weight bearing and surgical stabilisation is generally successful (Inauen et al., 2009a; Voss et al., 2004). In contrast, disruption to any aspect of the plantar supporting structures, will have a major impact on the structural integrity of the pes. Damage to the plantar support allows tarsometatarsal subluxation or luxation (Arwedsson, 1954; Chow and Balfour, 2012; Dyce et al., 1998; Fettig et al., 2002; Muir and Norris, 1999) or proximal intertarsal joint subluxation or luxation (Allen et al., 1993; Barnes et al., 2013; Campbell et al., 1976; Fettig et al., 2002), depending of the level of injury. Damage to the plantar ligament has been suggested as the cause of proximal intertarsal subluxation in dogs (Barnes et al., 2013; Campbell et al., 1976)(figure 7.2).

Figure 7-2: The mediolateral radiographic projection of the distal limb of a dog with proximal intertarsal subluxation. Note the cranial and dorsal displacement of the central and fourth tarsal bones in relation to the talus and calcaneus. The arrow indicates the level of the proximal intertarsal joint.

Conservative management of these conditions generally results in poor clinical outcomes and arthrodesis of affected joints is recommended to re-establish the structural integrity of the pes and allow effective weight bearing (Allen et al., 1993; Campbell et al., 1976).

For the proximal intertarsal joint, a variety of surgical techniques have been described to re-establish function, with no clear consensus on the ideal technique. Whilst it has been recommended to remove the articular cartilage of both the calcaneoquartal joint and talocentral joint (Dieterich, 1974; Whittick, 1975), others have suggested this is unnecessary (Allen et al., 1993; Campbell et al., 1976). Similarly, stabilisation of the calcaneoquartal joint alone has been suggested to provide adequate function, whilst others have raised concerns about leaving the talocentral joint unsupported (Wilke et al., 2000), suggesting additional stabilisation may be beneficial.

There have been a wide variety of calcaneoquartal stabilisation techniques reported, including a single Steinmann pin, multiple Kirschner wires, rush pins or a lag screw inserted through the calcaneus into the fourth tarsal bone and potentially further distal, with or without a plantar tension

band wire. (Allen et al., 1993; Campbell et al., 1976; Dieterich, 1974). Other reported techniques include ventral plating (Wilke et al., 2000), lateral plating(Campbell et al., 1976; Fettig et al., 2002) extending from calcaneus to metatarsals, external skeletal fixation and pins and cast (Campbell et al., 1976). Complication rates of 41-47% (Allen et al., 1993; Barnes et al., 2013) suggest that the optimal fixation technique has not been established, however, a recent study regarding complications following calcaneoquartal arthrodesis suggested lateral plate fixation was associated with few complications when compared to pin and tension band wire techniques and was suggested as the favoured technique (Barnes et al., 2013). A variety of plates have been used for this procedure, including dynamic compression plates, hybrid plates, cuttable plates and limited contact plates (Fettig et al., 2002; Scrimgeour et al., 2012; Théoret and Moens, 2007). Currently, there is no data available comparing the performance of the different plates and the ideal configuration of the construct, regarding screw numbers and the bones which they should engage.

To determine if lateral plating that engages the calcaneus, fourth tarsal bone and metatarsals could adequately re-establish force transmission through the pes, a lateral plate repair in 10 canine cadaveric limbs was performed. These limbs had all previously undergone complete transection of the plantar ligament, which had resulted in a proximal intertarsal luxation. The experimental hypothesis was that stabilisation of the calcaneoquartal joint would restore the integrity of the pes, allowing force transmission comparable to the intact limb. The aim was to characterise the motion of the individual tarsal bones after lateral plate repair of a proximal intertarsal luxation and compare these motions to the intact limb when the same load was applied to the limbs.

7.2 Materials and methods

7.2.1 Specimens

Ten paired hind limbs (from 5 dogs) were used for this study. Briefly, these limbs were all obtained from skeletally mature greyhounds, euthanised for reasons unrelated to this study. Limbs were disarticulated and wrapped in cloth moistened with saline to prevent tissue dehydration and frozen at-20^{0}C until testing. 24 hours prior to testing, limbs were thawed within a 4^{0}C refrigerator.

7.2.2 Limb loading

All limbs were prepared as previously described and loaded into a custom loading jig (as described in chapter 4). Prior to testing, the stifle and tarsal joints were manually flexed and extended and then preconditioned in the jig to a force of 600N, measured on the pressure sensitive film positioned under the paw (Film code 5076-350. Tekscan, South Boston, MA, USA), over five cycles (as described in Chapter 5).

7.2.3 Study design

The overview of the study design is shown in figure 7.3. Briefly, each limb underwent CT scanning when intact (in an unloaded position and following application of a 600N load) and again after complete plantar ligament transection and repair with lateral bone plate and screws (in an unloaded position and following application of a 600N load).

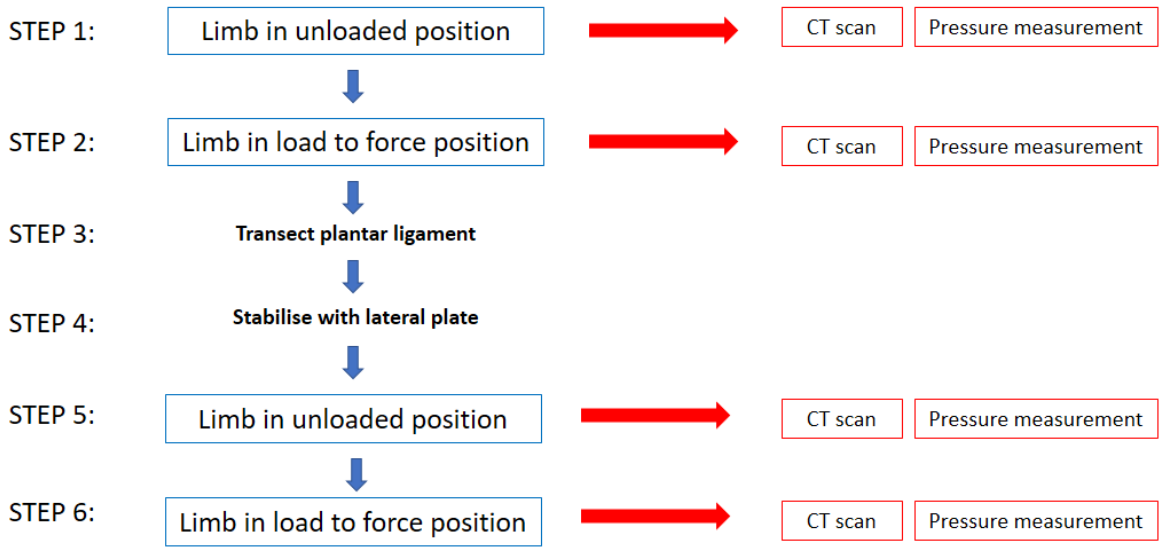

Figure 7-3: The overview of the study design in this experiment. Each limb is scanned at two time points; firstly, the intact the limb is scanned in an unloaded position and following application of a 600N force. The second scans are performed after complete transection of the plantar ligament and repair with a lateral bone plate and screws. Each limb is once again scanned in an unloaded position and following application of a 600N force.

7.2.4 Computed tomography scanning of the intact limb

All limbs had been used in the previous experiment and had undergone a CT scan (Philips Brilliance 16-slice CT scanner. Scanning parameters: 120KVP, 117 mA, slice thickness 1mm, slice increment 0.5mm, 512 X512 matrix) in an unloaded position and following application of a 600N load in the custom designed limb loading jig.

The distance from the proximal limb restraint to the foot plate, termed linear displacement (figure 7.4) was recorded for the unloaded position and the load to force (600N) position. The motion of the tibia, tarsal and metatarsal bones were calculated relative to the reference bone, the talus (as previously described in chapters 3 and 4). Motions were recorded both as a series of 3 translations and 3 rotations and as a total rotation about a single helical axis.

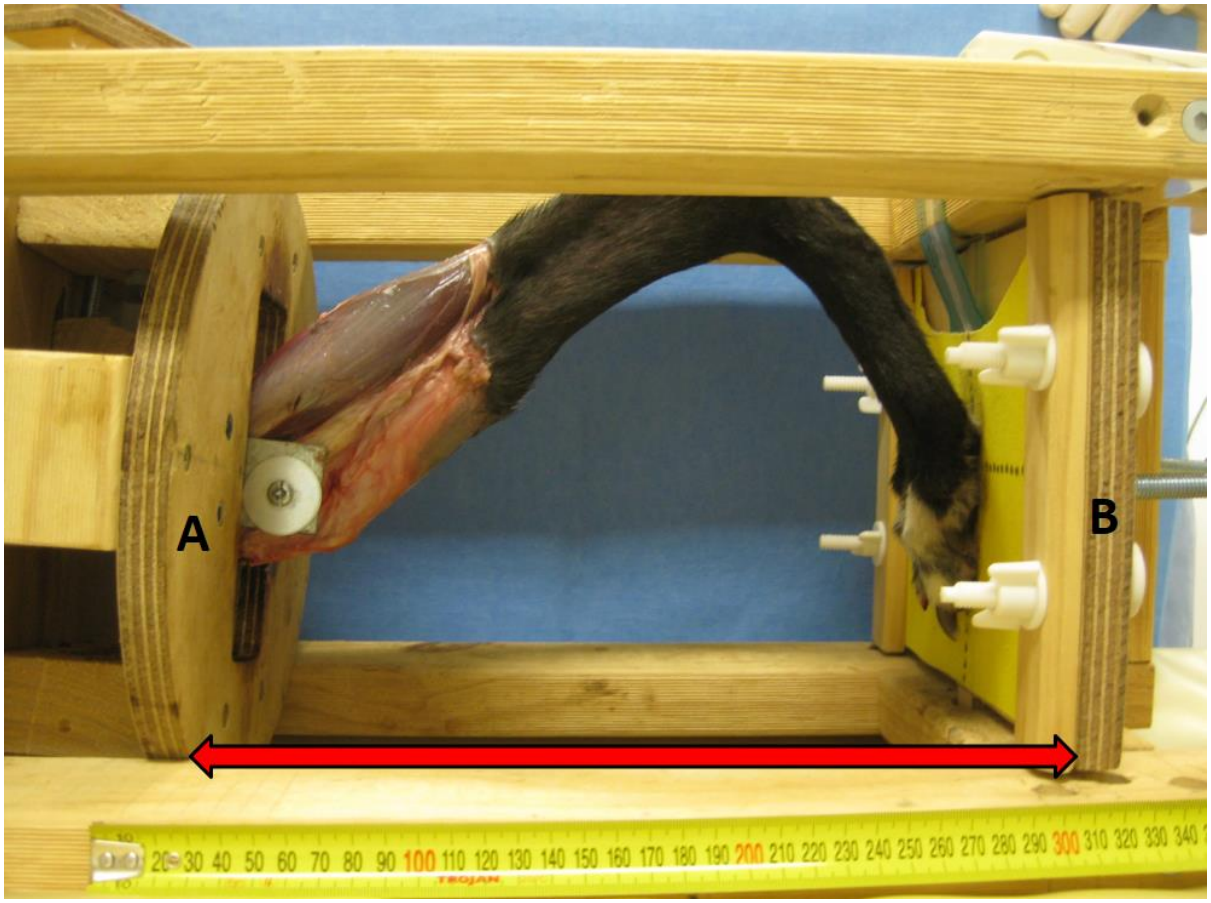

Figure 7-4: The limb in the custom designed limb loading jig. The linear displacement (red arrow) was the distance measured from the disc of the proximal limb restraint (A) to the top of the foot plate (B). Measurements were made with a measuring tape as shown in the image.

7.2.5 Ligament transection

All limbs then underwent complete transection of the plantar ligament, comprising the long plantar ligament and the calcaneocentral ligament using a scalpel blade (as described in chapter 6). Complete luxation of the proximal intertarsal joint was observed in all specimens following application of a load (figure 6.8).

7.2.6 Surgical repair with laterally applied bone plate

The limbs were then removed from the limb loading jig and a 2.7mm titanium locking compression plate (DePuy Synthes, Paoli, PA) was applied to the lateral aspect of the calcaneus, fourth tarsal bone and metatarsals. Prior to application, the lateral aspect of the calcaneoquartal and tarsometatarsal joint capsules were removed with a scalpel blade and a high-speed burr was used to remove the head of MTV, creating a relatively flat surface over the lateral aspect of the pes. If required, the plate was contoured to ensure maximal contact between the plate and the underlying bone using bending irons (DePuy Synthes, Paoli, PA). A 2mm drill bit attached to a high-speed drill (Ryobi, Fuchu, Hiroshima Prefecture, Japan) was used to create bone tunnels for the insertion of 2.7mm titanium self-tapping screws (DePuy Synthes, Paoli, PA). A 2.7mm universal drill guide (DePuy Synthes, Paoli, PA) was used to position the holes in the neutral position of the combi-holes. 4 screws were placed in the calcaneus, 2 in the fourth tarsal bone and 4 in the metatarsals (figure 7.5).

The most proximal 2 screws in the metatarsals were inserted with the aim to engage either 3 or 4 metatarsals, whilst the distal most two were inserted to engage only MTV. There was no standardisation of insertional torque of the screws, but each were inserted by an experienced surgeon to a point that was considered appropriate for application of a bone plate. Screw length was

determined using a depth gauge with the aim of engaging only calcaneus and fourth tarsal bones proximally. Articular cartilage was not removed in any case.

7.2.7 Computed tomography scanning of the repaired limb

Following bone plate application, each limb was repositioned in the limb loading jig using the same proximal trans-tibial bone tunnel and scanned once again in an unloaded position and the linear displacement recorded. The protocol for the CT scan remained identical to the previous scans (Scanning parameters: 120KVP, 117 mA, slice thickness 1mm, slice increment 0.5mm, 512 X512 matrix)

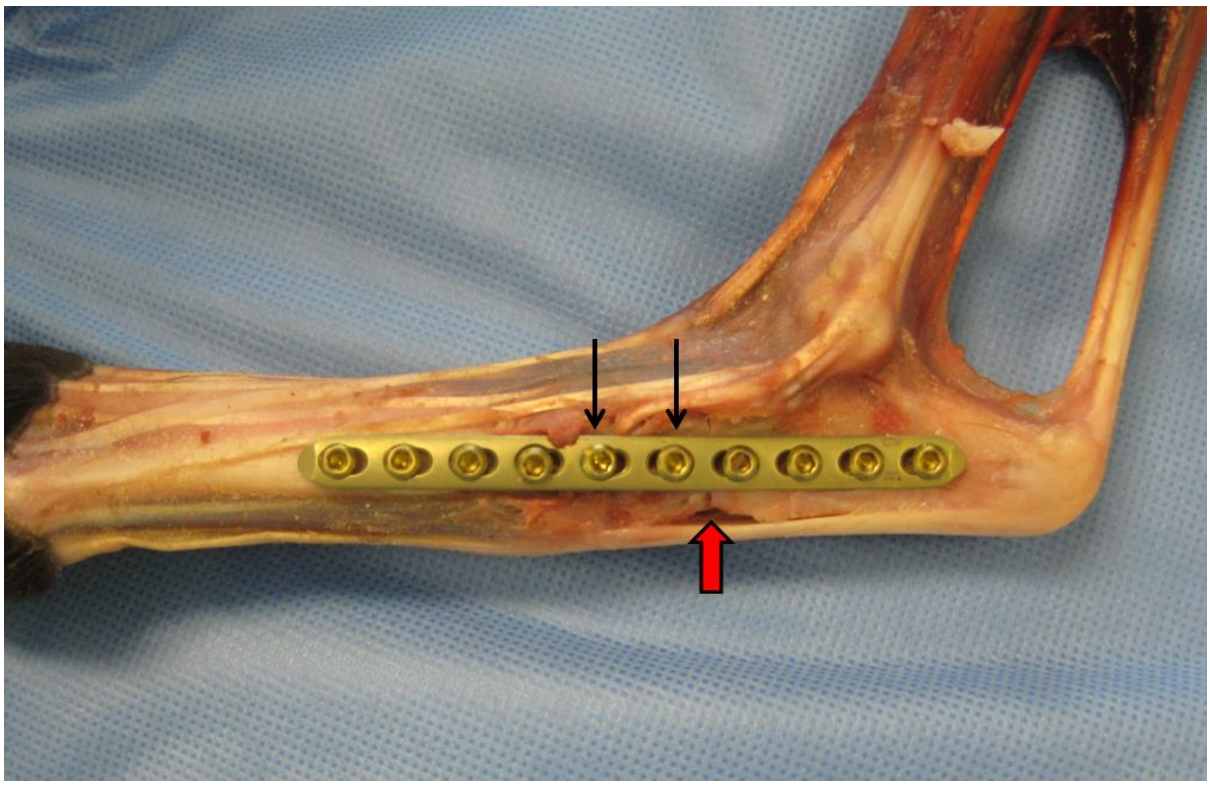

Figure 7-5: The 2.7mm titanium locking compression plate applied to the lateral aspect of the pes. The site of plantar ligament transection (red arrow) marks the proximal intertarsal joint. The four most proximal screws are placed in the calcaneus, the central 2 screws (black arrows) are positioned within the 4th tarsal bones, whilst the distal 4 screws engage metatarsal bones.

An axial load was then applied to each limb until a peak load of 600N was recorded on the pressure sensitive film of the foot plate. The linear displacement was recorded, and the limb within the loading jig underwent another CT scan using the identical settings.

7.2.8 Image processing and kinematic calculations

As for the previous chapters, the DICOM imaged were exported to Mimics 17.0 (Materialize, Belgium) where 3D models of each bone were created using the semi-automated techniques detailed in the previous chapters. The position of each screw was recorded as the number of cortices it engaged. If a screw partially engaged the edge of the cortical bone, this was classified as a single cortex (figure 7.6). Once again, all bones were aligned to the previously described reference axis using 3-matic 8.0 (Materialize, Belgium).

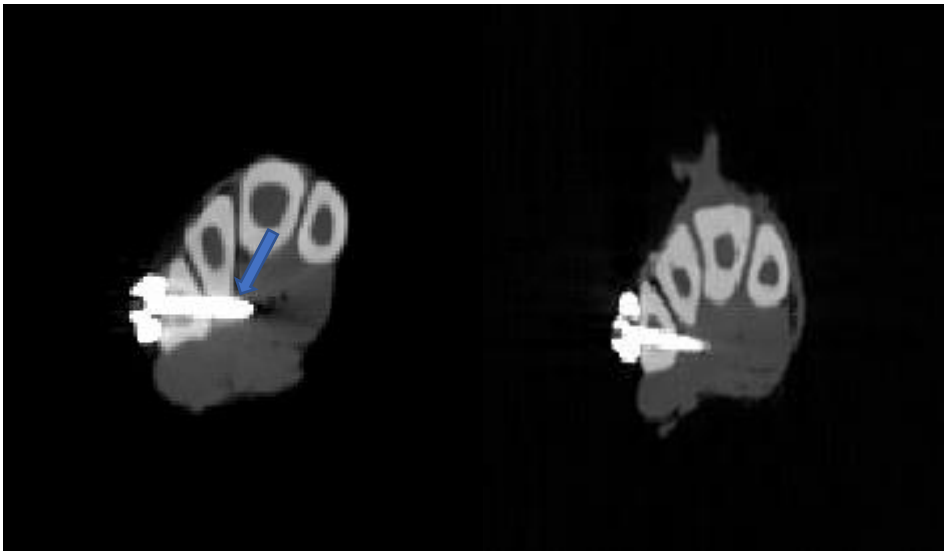

Figure 7-6: Examples of screw position from dogs in this experiment. Left: Bicortical engagement of the fifth metatarsal and partial engagement of the caudal cortex of the fourth metatarsal (arrow). This was classified as engaging three cortices. Right: Bicortical engagement of the fifth metatarsal without engagement of the fourth metatarsal. This was classified as engaging 2 cortices.

The motion of the tibia, tarsal and metatarsal bones were calculated relative the talus (reference bone) and the total rotation and helical axis were calculated as described in the previous chapters.

Kinematic coupling between the previously identified rigid functional units (Central tarsal bone/fourth tarsal bone, MTII/MTIII and MTIV/MTV), pairs of bones that cross the proximal intertarsal joint (calcaneus/central tarsal bone and calcaneus/fourth tarsal bone) and pairs of bones that were attached to the bone plate (calcaneus/fourth tarsal bone, calcaneus/ MTV and fourth tarsal bone/MTV) was examined. For each pair, the co-efficient of variation, coupling ratio and alignment angle was calculated as previously described.

7.2.9 Statistics

A two-tailed paired t-test was used to compare the linear displacement of the intact limb and the repaired limb when a force of 600N was recorded on the force plate using Excel (Microsoft, Redmond, Washington, USA). $p < 0.05$ was considered significant.

The total rotation for each individual bone was compared between intact and repaired conditions using a two-tailed paired t-test with Excel (Microsoft, Redmond, Washington, USA). $p < 0.05$ considered significant.

7.3 Results

All limbs had 4 screws placed in the calcaneus and none of these screws engaged any aspect of the talus. All limbs had 2 screws placed in the fourth tarsal bone and although some of the bone tunnels entered the central tarsal bone, none of the screws engaged the central tarsal bone. There was greater variability in the position of the 4 metatarsal screws. The two most proximal metatarsal screws engaged a median of 6 cortices each (range 3-7), whilst the two distal metatarsal screws engaged a median of 3 cortices (range 2-3) (table 7.1)

Table 7-1: The number of cortices engaged by each screw in all specimens. Screws are numbered from proximal to distal. None of the calcaneal screws (numbers 1-4) engaged the talus and similarly none of the fourth tarsal bone screws (numbers 5-6) engaged the central tarsal bone or third tarsal bones. There was more variability within the metatarsal screws (numbers 7-10) in terms of the number of cortices engaged. L = left limb, R = right limb.

bone	screw number	dog number (side)									
		1L	1R	2L	2R	3L	3R	4L	4R	5L	5R
calcaneus	1	2	2	2	2	2	2	2	2	2	2
	2	2	2	2	2	2	2	2	2	2	2
	3	2	2	2	2	2	2	2	2	2	2
	4	2	2	2	2	2	2	2	2	2	2
fourth tarsal bone	5	2	2	2	2	2	2	2	2	2	2
	6	2	2	2	2	2	2	2	2	2	2
metatarsals	7	6	6	6	6	6	6	5	6	6	7
	8	6	3	6	7	7	3	6	3	6	3
	9	3	3	3	3	3	3	3	2	3	2
	10	3	3	3	3	3	2	2	2	2	2

The linear displacement and pressure on the foot plate was recorded for the intact and repaired limbs in both then unloaded and loaded position (table 7.2). There was no difference in linear displacement between the intact and repaired limbs when a load of 600N was recorded on the foot plate. ($p = 0.94$)

Table 7-2: The force and linear displacement for each limb recorded during the unloaded and loaded scans before transection and after lateral plate repair of a proximal intertarsal luxation. L = left, R = right, st dev = standard deviation.

dog	side	Intact limb				Repaired limb			
		unloaded		load to 600N		unloaded		load to 600N	
		force (N)	linear displacement (cm)	force (N)	linear displacement (cm)	force (N)	linear displacement (cm)	force (N)	linear displacement (cm)
1	L	150.0	34.5	600.0	31.0	112.0	36.0	600.0	33.5
1	R	94.0	35.0	600.0	32.0	110.0	36.0	600.0	33.0
2	L	100.0	35.8	600.0	32.3	54.0	37.6	600.0	32.5
2	R	70.0	36.6	600.0	32.5	64.0	37.7	600.0	32.6
3	L	33.0	35.9	600.0	30.4	34.0	35.8	600.0	30.4
3	R	34.0	35.5	600.0	31.2	35.0	36.5	600.0	31.3
4	L	25.0	38.0	600.0	34.7	64.0	38.3	600.0	34.3
4	R	20.0	38.0	600.0	34.5	50.0	38.7	600.0	33.9
5	L	29.0	38.9	600.0	34.3	34.0	38.9	600.0	33.0
5	R	34.0	38.9	600.0	34.9	30.0	38.9	600.0	33.0
mean		**58.9**	**36.7**	**600.0**	**32.8**	**58.7**	**37.4**	**600.0**	**32.8**
st dev		**43.2**	**1.6**	**0.0**	**1.7**	**30.2**	**1.3**	**0.0**	**1.2**

For the intact limb, all tarsal and metatarsal bones underwent motion relative to the talus following application of a 600N load (table 7.3). Similarly, all tarsal and metatarsal bones underwent motion relative to the talus after the same load was applied to the repaired limbs (table 7.4).

Table 7-3: The 3 rotations and 3 translations of each bone recorded after application of a 600N load to the intact limb in the loading jig. The total (summative) rotation of each bone is also reported. CTB = central tarsal bone, TB = tarsal bone, MT = metatarsal bone, SD = standard deviation.

All limbs: Load to force (600N) for intact limbs		translation along (mm)			rotation around (degrees)			total rotation (degrees)
		x axis	y axis	z axis	x axis	y axis	z axis	
Tibia	mean	19.98	1.66	10.47	0.72	-15.62	1.52	15.75
	SD	5.13	1.66	1.69	1.08	2.01	0.77	**1.98**
Calcaneus	mean	0.21	0.24	0.08	-1.37	1.13	-0.40	1.86
	SD	0.13	0.07	0.08	0.80	0.72	0.25	**1.07**
CTB	mean	0.15	0.39	0.54	-1.35	2.18	-0.40	2.66
	SD	0.09	0.13	0.21	0.64	1.01	0.26	**1.09**
Fourth TB	mean	0.22	0.62	1.03	-1.50	2.55	-0.83	3.13
	SD	0.13	0.19	0.42	0.59	1.17	0.19	**1.18**
Third TB	mean	0.14	0.64	1.14	-0.89	3.25	-0.80	3.53
	SD	0.09	0.19	0.43	0.63	1.19	0.26	**1.19**
Second TB	mean	0.22	0.63	0.98	-0.89	3.74	-1.05	4.14
	SD	0.10	0.19	0.40	0.70	1.57	0.76	**1.47**
MT II	mean	0.28	1.72	4.48	0.45	5.45	-1.37	5.66
	SD	0.13	0.42	1.31	0.47	1.48	0.39	**1.46**
MT III	mean	-0.17	1.71	5.30	0.55	5.94	-1.10	6.12
	SD	0.10	0.45	1.60	0.66	1.60	0.41	**1.53**
MT IV	mean	-0.23	1.84	5.36	-1.47	6.13	-1.58	6.63
	SD	0.11	0.47	1.70	1.30	1.63	0.47	**1.74**
MT V	mean	0.05	1.87	5.37	-1.39	6.08	-1.48	6.55
	SD	0.10	0.50	1.66	1.45	1.54	0.46	**1.74**

Table 7-4: The 3 rotations and 3 translations of each bone recorded after application of a 600N load to the repaired limb in the loading jig. The total (summative) rotation of each bone is also reported. CTB = central tarsal bone, TB = tarsal bone, MT = metatarsal bone, SD = standard deviation.

All limbs: Following lateral plate repair		translation along (mm)			rotation around (degrees)			total rotation around helical axis (degrees)
		x axis	y axis	z axis	x axis	y axis	z axis	
Tibia	mean	23.17	2.30	12.62	1.20	-18.11	1.90	18.30
	SD	6.88	2.48	2.41	1.59	3.25	1.11	3.28
Calcaneus	mean	0.24	0.34	0.27	-2.01	0.63	-0.94	2.70
	SD	0.16	0.13	0.16	0.48	1.48	0.83	0.93
CTB	mean	0.06	0.69	0.85	-1.25	3.02	-0.42	3.59
	SD	0.15	0.30	0.36	0.98	1.66	1.05	1.62
Fourth TB	mean	0.18	0.94	1.40	-0.78	2.99	-0.87	3.52
	SD	0.20	0.48	0.70	1.07	1.60	0.85	1.49
Third TB	mean	0.02	0.92	1.52	-0.98	3.69	-0.87	4.16
	SD	0.18	0.47	0.65	1.05	1.69	0.92	1.67
Second TB	mean	0.02	0.90	1.20	-2.76	2.78	0.30	5.68
	SD	0.32	0.47	0.71	7.25	2.10	1.77	6.45
MT II	mean	0.02	2.04	4.47	0.21	4.50	-1.65	5.09
	SD	0.33	1.10	1.88	0.88	1.97	0.91	1.89
MT III	mean	-0.41	1.85	5.04	0.66	4.70	-1.02	4.97
	SD	0.41	1.08	2.27	1.02	2.15	0.79	1.89
MT IV	mean	-0.21	1.68	4.62	-0.10	4.07	-0.77	4.44
	SD	0.35	1.06	2.33	1.07	1.97	0.77	1.68
MT V	mean	0.20	1.57	4.27	0.53	3.67	-0.54	4.10
	SD	0.27	1.11	2.30	1.22	1.79	0.69	1.45

The calcaneus ($p = 0.049$) showed a significantly increase in total rotation in the repaired limb compared to the intact limb, whilst both MTIV ($p = 0.001$) and MTV ($p = 0.0001$) both showed significantly less total rotation in the repaired limb compared to the intact limb.

All other bones showed no significant different between repaired and intact limbs. However, the CTB ($p = 0.067$) showed a trend towards a significant increase in total rotation between repaired and intact limbs, whilst the MTIII ($p = 0.055$) showed a trend towards a significant decrease in total rotation between repaired and intact limbs (figure 7.7).

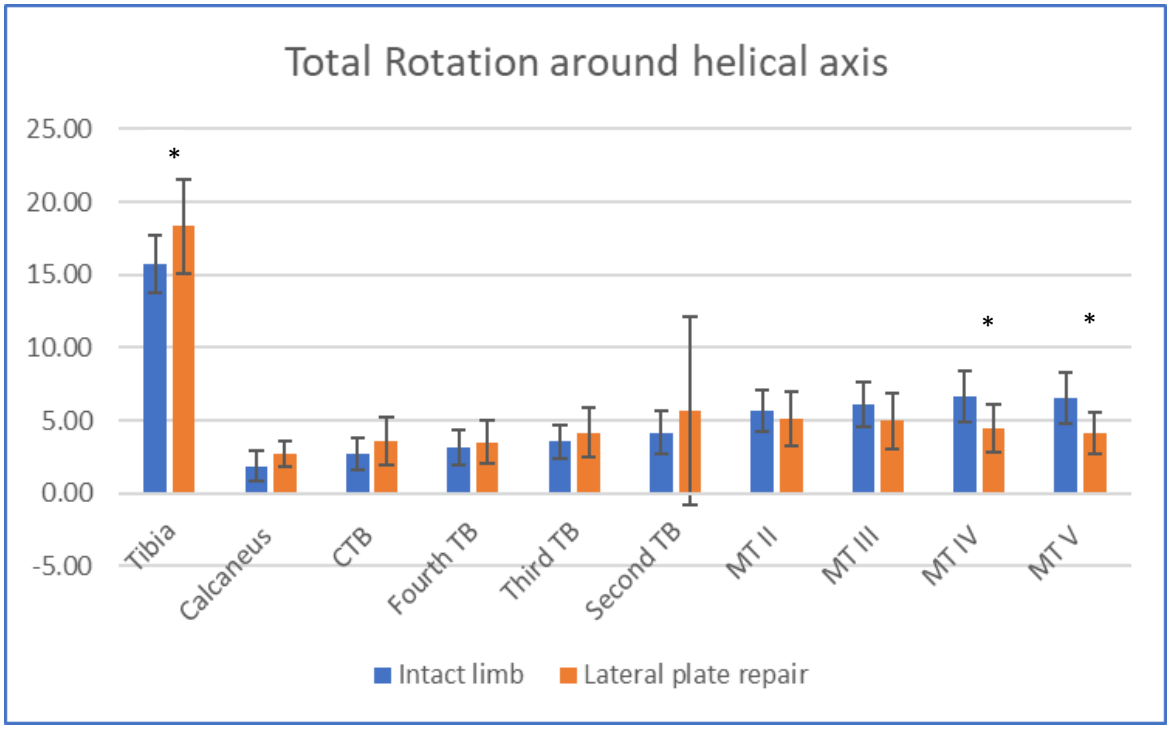

Figure 7-7: The total rotation of each bone for the intact limb and the repaired limb. Lateral plate repair reduced rotation in all metatarsal bones, but significantly for the two lateral digits, which were closest to the plate. No significant difference in rotation was seen in all other tarsal bones. CTB = central tarsal bone. TB = tarsal bone, MT = metatarsal bone.

** denotes a significant difference between intact and repaired conditions for that bone. Error bars are one standard deviation*

The kinematic coupling of the bones that cross the proximal intertarsal joint was not restored following application of a lateral bone plate. The angle between the helical axis of both bones (alignment angle) was similarly not restored after plate repair (table 7.5).

In contrast, the kinematic coupling of the previously identified functional units remained high after repair. However, the alignment angle increased significantly in all pairs following plate repair, demonstrating that their rotations became more divergent after plate repair (table 7.5).

For the bones that were attached to the lateral bone plate, there was an increase in kinematic coupling of these pairs with the exception of the calcaneus/fourth tarsal bone pairing. However, the

rotation of these pairs was not around a similarly orientated as demonstrated by the large alignment angle values.

Table 7-5: The correlation coefficient, coupling ratio and alignment angle for pairs of tarsal or metatarsal bones. The top rows are pairs of bones that cross the proximal intertarsal joint. The middle, shaded rows and the previously identified rigid functional units, whilst the bottom shaded pairs are pairs that are attached to the bone plate. There was a loss of coupling (decreased correlation co-efficient) for bones across the proximal intertarsal joint following repair and a significant difference in alignment angle for most pairs of bones.

** denotes significant difference between intact limb and repaired limb. CTB= central tarsal bone, 4^{th} = fourth tarsal bone, MT = metatarsal*

Pair of bones	Intact limb			Following repair		
	correlation coefficient (R^2)	coupling ratio	alignment angle of helical axes (degrees)	correlation coefficient (R^2)	coupling ratio	alignment angle of helical axes (degrees)
Calcaneus and CTB	0.92	0.97	20.1 ± 8.0	0.34	1.02	44.1 ± 14.6*
Calcaneus and 4th	0.94	1.07	20.3 ± 11.6	0.54	1.18	57.0 ± 29.5*
CTB and 4th	0.93	1.04	9.6 ± 5.5	0.92	0.88	16.6 ± 7.4*
MTII and MTIII	0.98	1.04	4.8 ± 2.6	0.98	0.99	13.1 ± 6.4*
MTIV and MTV	0.97	0.98	2.7 ± 2.4	0.87	0.81	13.1 ± 11.3*
Calcaneus and 4th	0.94	1.07	20.3 ± 11.6	0.54	1.18	57.0 ± 29.5*
Calcaneus and MTV	0.66	1.32	40.2 ± 15.2	0.76	1.36	78.4 ± 29.9*
4th tarsal and MTV	0.80	1.32	20.5 ± 8.9	0.90	0.92	22.4 ± 10.6

7.4 Discussion

The findings of this study demonstrate that the application of a lateral bone plate to the calcaneus, fourth tarsal bone and metatarsals is able to re-establish force transmission through the pes following proximal intertarsal luxation. It suggests that stabilisation of the medial column (the talus, central tarsal bone, third tarsal and third metatarsal) is not required to allow the pes to act effectively as a lever in the distal limb, providing additional data that may help resolve the open question of what is the most appropriate surgical technique to treat proximal intertarsal subluxation in the dog.

In the canine limb, there is no substantial ligamentous connection between the plantar aspect of the talus and central tarsal bone. Rather, the plantar support for the central tarsal bone, runs from its plantar process to the large medial projection of the calcaneus, the sustentaculum tali. (Evans et al., 2012). This arrangement allows the tensile force on the tuber calcanei to be transferred to both the medial and lateral aspect of the pes through the central and fourth tarsal bone respectively (Arwedsson, 1954). By stabilising the fourth tarsal bone with the calcaneus, the central tarsal bone motion is limited indirectly through its tight coupling with the fourth tarsal bone, which was demonstrated in chapter 5. This finding is also in agreement with the work in chapter 6, where transection of the calcaneocentral ligament resulted in only mild increases in central tarsal bone motion due to its strong attachment to the fourth tarsal bone.

Configuration of surgical stabilisation

In clinical practice, a major question that remains unresolved is what is the optimal surgical technique to re-establish force transmission through the pes following proximal intertarsal luxation. Numerous different implants and configurations of implants have been reported in the treatment of clinical cases (Allen et al., 1993; Campbell et al., 1976; Fettig et al., 2002; Roch et al., 2008;

Scrimgeour et al., 2012; Wilke et al., 2000) with a retrospective comparison of techniques reporting fewer complications with lateral plating compared to pin or screw and tension band (Barnes et al., 2013). However, a comparison of techniques should ensure that there is standardisation of implant configuration within techniques as this may influence biomechanical performance and clinical outcome. For example, in cases of pin and screw fixation (with or without a tension band) there is variable extension of the pin or screw into the metatarsal bones in reported case series (Allen et al., 1993; Barnes et al., 2013; Scrimgeour et al., 2012). Although implants crossing the tarsometatarsal joints may influence the stability of the repair by immobilising the tarsometatarsal joint in addition to the calcaneoquartal joint, the effect of placing implants across the tarsometatarsal joint is yet to be evaluated as a factor which may influence the incidence of complications, biomechanical performance and clinical outcome. Additionally, it is important to consider complications related to inappropriate application of fixation techniques. In the study of Barnes et al. 2013, there were cases of pin and tension band wire application to comminuted fractures, which is an example of inappropriate case selection and may influence complication rates.

In contrast to pin and screw-based repairs, all published reports of plate stabilisation across the proximal intertarsal joint span the tarsometatarsal joints to include the metatarsal bones. However, within plated repairs, there is little standardisation with a number of different plate designs used with varying screw configurations (Barnes et al., 2013; Fettig et al., 2002; Roch et al., 2008; Scrimgeour et al., 2012; Théoret and Moens, 2007).

The pes experiences large bending moments during loading (Alexander, 1974; Alexander, 1984) and surgical repair of proximal intertarsal subluxations must counteract these moments until complete bony union is achieved. Implant failure is a common complication of repair due to high magnitudes of repetitive loads. A laterally positioned bone plate is loaded on edge, towards its greatest dimension (Dyce et al., 1998). This substantially increases its moment of inertia, which resists the bending moment. The 2.7mm plate used in this experiment has a width of 7.5mm and a thickness of

2.6mm, producing a secondary area moment of inertia (AMI) of 91.4mm^4 when loaded on edge (compared to an AMI of 10.99mm^4 if loaded towards its narrowest dimension). This particular plate was selected as it allowed appropriate screw size selection in the metatarsal bones and allowed two screws to be positioned in the fourth tarsal bone. Although a larger 3.5mm plate would have further increased the secondary AMI, it would result in the metatarsal screws exceeding the recommend bone:screw diameter (Johnson et al., 2005). A hybrid plate which accepts different size screws in the proximal and distal fragments would have been a suitable alternative and has been used successfully in clinical cases (Fettig et al., 2002), however, this plate is currently only available in stainless steel. Newly developed intertarsal arthrodesis plates are also available and have been developed with appropriate lengths for engaging the calcaneus and metatarsals. Previous experience with stainless steel plates revealed increased CT artefacts compared to titanium plates, due to the higher x-ray attenuation coefficient of steel (Lee et al., 2007). Titanium plates were selected in preference to 316L stainless steel as the use of stainless steel plates may have prevented accurate segmentation of each individual tarsal bone. As a surface matching algorithm (Besl and McKay, 1992) was used to calculate the motion of each bone, accurate segmentation is critical to produce accurate kinematic results (Tan et al., 2017).

One important consideration when interpreting these findings is the differing material properties of titanium and stainless steel. The modulus of elasticity of titanium is approximately half that of steel, resulting in twice as much deformation for the same applied load (Niinomi, 1998). During testing, no obvious visual deformation of the titanium plates was observed, however, small motions were identified between the bones that were attached to the plate suggesting some deformation of the plate had occurred or alternatively, some motion occurred between the screws and the plate. This means that the reported motions include any contribution made due to deformation of the plate or motion between the screw heads and the plate. As all limbs were of similar size and all plates and screws were of the identical material and dimensions, the variation across specimens was

minimised. However, these results cannot be directly translated to surgical repairs performed with 316L stainless steel plates or plates of different size or design.

There is an opportunity to engage the central tarsal bone and third tarsal bone by placing longer screws through the fourth tarsal bone (Dyce et al., 1998; Fettig et al., 2002). In doing so, these screws may further help stabilise the central tarsal bone in relation to the calcaneus. However, there is also a potential risk of screw loosening when placed across a low motion joint, as the repeated motion may "toggle" the screw loose. Of 58 calcaneoquartal arthrodeses performed using laterally applied plates, 5 cases required screw removal due to loosening. Four of the five cases involved the screw in the fourth tarsal bone, whilst the remaining loose screw was positioned across multiple metatarsal bones (Barnes et al., 2013). It was not reported whether or not these screws also engaged the central or third tarsal bones. Loosening appears to be the more common mode of failure of the screw in the fourth tarsal bone as bending or breakage of this screw was not reported (Barnes et al., 2013) During triple pelvis osteotomy procedures, cortical screws that penetrated through the ilium and crossed the low motion sacro-iliac joint before engaging the sacrum were shown to have an increased likelihood of loosening when compared to screws that did not cross the joint (Doornink et al., 2006). Future studies may choose to include this additional variable of central tarsal bone engagement to identify if this provides additional stability to the construct. However, to determine its effect on construct longevity, a cyclic loading model would be recommended.

The results of this chapter suggest that central tarsal bone engagement may not be required since force transmission was restored with engagement of the fourth tarsal bone alone. The force applied to cadaveric limbs in this study (600N) represents approximately 1.6 times the body weight for an adult greyhound, which is the maximum recorded load for a galloping dog (Walter and Carrier, 2007; Walter and Carrier, 2009). This is likely to exceed the maximal force applied to limb in the post-operative recovery period, when exercise restriction is recommended (Roch et al., 2008). If force transmission can be restored through redirection of tensile forces through alternate ligamentous

pathways for these magnitudes, then gaining additional rigidity through central tarsal bone engagement may not be required, however, cyclic testing would be required to verify this assumption.

The decision not to engage the central tarsal bone would also be based on the assumption that the ligamentous support between the central and fourth tarsal bones remains intact. Based on the preoperative radiographs, it may be beneficial to engage the central tarsal bone if there is any suggestion of ligament failure between the central and fourth tarsal bones, as demonstrated by an alteration in the joint space.

Depending on the hole spacing in the selected plate, it may not be possible to achieve the placement of two screws in the fourth tarsal bone, and hence achieve rotational stability, making engagement of the metatarsals more desirable. The 2.7mm plate used in this study allowed for the safe placement of two screws in the fourth tarsal bone providing rotational stability. However, this configuration of two non-locking cortical screws would not provide adequate fixation for clinical use based upon current AO principles of fixation, which suggest a minimum of 6 cortices in each fragment (Johnson et al., 2005). For this reason, the length of plate was selected to allow for engagement of the metatarsal bones.

From the data in this chapter, it is therefore not possible to draw conclusions about restoring force transmission by stabilisation of the calcaneoquartal joint alone (as the tarsometatarsal joints were included in the surgical repair. Indeed, if this was possible in a clinical setting, preservation of motion at the tarsometatarsal joints may have additional benefits in preserving the natural elasticity of the pes, allowing for energy absorption following the impact of the paw on the ground and storage of elastic strain energy throughout the stance phase of gait. Alternatively, the increased lever arm created by a fused calcaneus and fourth tarsal bone may place additional strain on the tarsometatarsal joint, leading to injury or premature degeneration, however, this has not been

reported when a pin and tension band wire alone was used to stabilise the calcaneoquartal joint in isolation (Allen et al., 1993; Barnes et al., 2013; Campbell et al., 1976)

The evolution of locking bone plates in recent years, may in fact, allow adequate plate stabilisation of the calcaneoquartal joint without involvement of the tarsometatarsal joints. These plates, in which the screw heads rigidly engage the plate hole, create an angle stable construct that does not rely upon compression of the plate to the underlying bone for stability (Egol et al., 2004; Niemeyer and Sudkamp, 2006; Wagner, 2003). It has been suggested that two screws in each bone fragment produces adequate stability (Niemeyer and Sudkamp, 2006) and this may allow for adequate stabilisation of the fourth tarsal bone with the calcaneus. The use of these plates in treatment of proximal intertarsal instability warrants further investigation and particularly, the effect of preserving the tarsometatarsal joints.

The clinical outcome following calcaneoquartal arthrodesis as generally reported to be good based upon owner assessment and this is commonly attributed to the low magnitude of motion that normally exists at this joint (Allen et al., 1993; Fettig et al., 2002). However, only 50% of working dogs could return to full activity following partial tarsal arthrodesis (Scrimgeour et al., 2012) and significant asymmetry was identified in the only study of calcaneoquartal arthrodesis that utilised objective force plate data, despite no clinically detectable lameness (Wilke et al., 2000). One possible cause for the poorer outcomes may be disruption of the elastic dorsiflexion mechanism of the pes, which cushions impact and conserves energy (Alexander, 1984). This disruption may be unavoidable during repair of proximal intertarsal subluxation but must be a consideration when providing owners with a prognosis following surgical repair.

Another possible cause for ongoing lameness may be due to the immobilisation of neighbouring joints and subsequent ankylosis, which has been observed in joints that have not been debrided (Campbell et al., 1976; McLennan, 2007). Ankylosis, the pathological fusion of a joint, may be responsible for ongoing morbidity and is the likely fate of the tarsometatarsal joints when a lateral

plate engages the metatarsal bones. This may further support the investigation of calcaneoquartal stabilisation without metatarsal involvement. It is unclear from the literature, if debriding multiple joint spaces results in a more stable pes and ultimately improved clinical function.

In the previous chapter, the helical axis of the fourth and central tarsal bones were identified and were located remote to each bone in all cases. This means that translation of the central and fourth tarsal bones occurs at the articular surface. It is unclear if the motion of these bones would differ if articular cartilage debridement was performed prior to plate application. The effect of packing with cancellous bone graft and producing interfragmentary compression, as would be performed clinically, also remains unknown and care must be taken when extrapolating these findings to the clinical setting (Barnes et al., 2013; Roch et al., 2008). Articular debridement was not performed in this experiment to prevent the introduction of additional variables including the degree of debridement of each surface and total volume, fragment size and porosity of any autogenous cancellous bone graft.

The effect of lateral plate repair of a proximal intertarsal luxation had significant effects on the highly coupled and co-ordinated motions of the tarsal and metatarsal bones. Plate repair could not restore the normal kinematic coupling across the proximal intertarsal joint, as reported in chapter 5, and this likely reflects the different material properties of the plate compared to the plantar ligament and the different location and pattern of loading. The plate was also seen to alter the helical axis of the previously identified functional units. Although the correlation co-efficient remained high for these pairs, the redirection of force through the plate (rather than the plantar ligament) altered the orientation of their helical axis. This once again demonstrates the reliance of each tarsal bone on the motion of neighbouring bones for both its magnitude and orientation of rotation (Sennwald et al., 1993). Interestingly, even bones rigidly attached to the bone plate did not share a common axis of rotation as may be expected if they were to function as a single unit. Deformation of the plate during loading is one possible explanation and this may not simply occur in

the sagittal plane. The lateral plate is eccentrically located on the pes and during loading it is likely to have to counter both dorsiflexion of the pes and rotation of the pes. The oblique helical axis identified for MTV suggests that the plate may have deformed by torsion. The previous experiments of this thesis identified that internal rotation and dorsiflexion occur concurrently during limb loading and this would have exposed the plate to both on edge and rotational forces. The effect of this degree of deformation on the progression of bony fusion across an arthrodesis site is beyond the scope of this chapter but future studies may investigate if plate size, design and screw purchase may influence the degree of individual tarsal and metatarsal bone motion after limb loading.

A decrease in the correlation coefficient of the calcaneus and fourth tarsal bone was also observed following plate application. This finding may be somewhat surprising given that both bones are now attached to the plate, however, it may reflect the interdependent nature of intertarsal bone motion whereby fusion of one joint may affect the kinematics of the adjacent joints (Astion et al., 1997).

Limitations

This study has a number of limitations that must be acknowledged for the contribution they may have made to the overall results. Firstly, the majority of proximal intertarsal luxations present with evidence of remodelling changes consistent with their insidious onset (Campbell et al., 1976). These changes were not present in the normal limbs that were studied in this experiment. Sharp transection of a normal plantar ligament is unlikely to accurately reflect the clinical presentation of proximal intertarsal luxation. Periarticular osteophytosis and fibrosis may influence the kinematics of individual tarsal bones and could not be replicated in our model of proximal intertarsal subluxation.

As discussed in previous chapters, the use of cadaveric limbs requires active replication of all relevant muscle forces. The major forces on the tarsal bones can be replicated by this limb loading jig, however, not all muscular forces, particularly those of the interosseous muscles on the pes, were replicated and this fact must be considered when interpreting these results.

The lateral plate repair restored the integrity of the pes as the lever arm, which allows force to be transmitted through the distal limb (Alexander, 1984). However, our loading was applied as a single, non-destructive load that does not represent the repetitive loads that would be experienced by the pes during the period until a bony union is achieved. It is unknown if the configuration used in this experiment would provide adequate stability over time and therefore, the suggestion that engagement of the fourth tarsal bone alone is adequate must be applied with caution. Future studies may investigate the effect of plate configuration, including the number of screws used in each bone and the number of bones that are engaged by each screw, on cyclic loading of the pes repaired with a lateral plate.

The method of loading that was utilised in the present study, relies upon the integrity of the intact gastrocnemius muscle and superficial digital flexor tendon. It is unknown if these structures would survive cyclic testing and continue to produce the appropriate internal forces on the tarsal bones. Previous limb loading jigs (Warzee et al., 2001) have replicated the pull of the gastrocnemius with a wire and turnbuckle which may be one modification to our loading protocol that may support cyclic fatigue testing. The proximal limb restrain could be easily reproduced to be compatible with the attenuator of a sevohydraulic materials testing machine. This approach was not used in this kinematic study as it was believed that the intact gastrocnemius insertion would most accurately replicate the in vivo force on the tuber calcanei and was adequate for the small number of cycles used in these experiments.

When comparing the absolute motion of bones, one critical factor is the starting position for each bone. In the intact limb, it has been suggested that there is some free-play between bones when a load is not applied. To minimise the chance of any free-play, it was ensured all limbs had a small amount of force recorded on the foot plate, however, when ligaments are not taught, other forces, such as gravity, will influence bone position.

The application of a non-locking bone plate would also alter the starting position of each bone, as recorded in the unloaded scan as bones are pulled up towards the plate during screw tightening. Accurate contouring of the plate will reduce this effect, but absolutely perfect contouring is unrealistic in any clinical situation and will have subtle effects on bone position. Both plate contouring and burring of the lateral head of MTV were carefully performed to minimise this effect. A second unloaded scan was performed after repair and used as the start position for the loaded repaired limb rather than using the position of each bone in the unloaded scan of the intact limb.

7.5 Conclusions

The findings outlined in this chapter have identified that, following complete plantar ligament transection, application of a lateral bone plate and screws that engage the calcaneus, fourth tarsal bone and metatarsals will contribute to the redirection of force through the pes, which allows it to act effectively as a lever arm. Although, no assumptions can be made about maintaining stability over time, the repaired pes could generate a ground reaction force that was no different to that generated by the intact foot at similar displacements.

Chapter 8 : Thesis conclusions

The common practice of modelling the canine pes as a rigid limb segment, despite the well-recognised ability to produce motion at the intertarsal joints during clinical examination, provided one of the major motivations of this thesis. With no published descriptions of canine tarsal bone kinematics, there is limited understanding regarding the nature of movement within the pes during locomotion and how these motions may be implicated in fatigue fractures of the tarsal bones and degeneration of the plantar ligament. Describing the nature of tarsal bone motion may also be an important consideration when planning and evaluating surgical repairs of the canine pes.

Thus, the major aims of this thesis were i) to develop a technique to allow quantification of tarsal bone kinematics based on computed tomography imaging (chapters 3 and 4) and ii) application of this technique to normal cadaveric limbs (chapter 5), following sequential transection of the plantar ligament (chapter 6) and following lateral plate stabilisation (chapter7). The most important contributions of this thesis are summarised in the following paragraphs.

8.1 Major contributions

Chapter 3 detailed the computed tomography based kinematic techniques used throughout this thesis, revealing that segmentation threshold, reconstruction algorithm and scan resolution did not significantly influence kinematic accuracy. This means segmentation thresholds and reconstruction algorithms can be set at the most convenient settings which may lead to improvements in the efficiency of kinematic processing. Perhaps most significantly, was the finding that a reduction in radiation exposure, achieved by decreasing scan resolution, will not reduce kinematic accuracy. Although of little consequence in cadaveric investigations, this result may be of great importance in in vivo studies using human patients. In this chapter, the techniques described were shown to be highly accurate for identifying motion within canine tarsal bones, making them suitable for application in the following chapters.

Chapter 4 reports the design features and principles behind development of a cadaveric limb loading jig. Although the jig described in this chapter was optimised for loading of the pelvic limb of the dog, many of the principles and features could also be applied to both the canine pectoral limb or limbs of other species. Features such as the femoral block permit accurate replication of in vivo joint angles and can be easily installed into any future loading jig. This jig could also be used in future studies, investigating the effect of both ligament damage and fractures of the pes, whilst also providing insights into how various repair techniques restore the normal pattern of bone motion.

Chapter 5 provides the first description of the motion that each individual tarsal bone undergoes during weight bearing. The results reveal that although the majority of motion occurs at the talocrural joint as has been previously described, the collective motion at the intertarsal and tarsometatarsal joints contribute significantly (up to 28.9 %) to sagittal plane flexion. This dorsiflexion of the pes may be a significant component to the "biological springs" of canine pelvic limbs. Each bone demonstrated a unique helical axis, about which it rotates, with varying degrees of obliquity to the anatomical reference planes. The direction and magnitude of these motions may be applied to future investigations into the repetitive loading and potential fatigue failure of commonly injured tarsal bones, such as the right central tarsal bone. From the results of this study, a simplified model of the canine pes was proposed based on identification of rigid functional units within the canine pes. This may simplify kinematic measurements in all future studies that acknowledge intertarsal motion rather than modelling the pes as a single rigid segment.

Chapter 6 investigated the effect of partial plantar ligament transection on tarsal bone kinematics, providing an insight into the role played by various components of the plantar ligament during weight bearing. The results contribute to our understanding of the unanswered question of which components of the plantar ligament are damaged to allow proximal intertarsal luxation, suggesting that total loss of the plantar ligament is required to produce a proximal intertarsal luxation. The strong ligamentous attachments between the talus and calcaneus, as well as the central and fourth

tarsal bones were responsible for maintaining the integrity of the pes despite partial transection of the plantar ligament. These strong attachments would be further investigated in chapter 7.

Chapter 7 evaluated the effect of a lateral plate repair on tarsal bone kinematics and restoration of the integrity of the pes following proximal intertarsal luxation. The results show that a bone plate engaging the calcaneus, fourth tarsal bone and metatarsals was sufficient to restore force transmission through the pes in static testing. This finding provides important new insights into the configuration of laterally applied bone plates which can be applied in a variety of configurations. Whilst some repairs utilise long screws to engage the central, third and second tarsal bones, the results of this chapter suggest that it may be unnecessary and may even lead to premature loosening, due to the observed motion between all tarsal bones, despite application of the bone plate.

8.2 Future directions

Acknowledging the important contributions made by intertarsal bone motions is the first step to revealing the true importance of the pes in animal locomotion. Validation of the kinematic results in this thesis against in vivo studies will be an important step despite the technical challenges involved, however, as biplanar fluoroscopy and 2D-3D matching techniques continue to evolve, it becomes increasingly feasible. Once validated, the limb loading jig could be used to investigate other anatomical structures within the pes and the effect of a variety of surgical interventions or repairs. The capability to produce angulation of the foot plate and rotational forces within the limb will allow a more complete evaluation of the limb in future studies.

Another interesting research possibility would be to compare of the kinematics of the pes in a variety of species, such as the kangaroo or wallaby, which have previously been identified as animals which have a high dependence on elastic energy stores in the distal limb.

The work presented in this thesis also suggests that future kinematic studies should consider increasing the number of markers placed on the pes to better reflect the non-rigid nature of the pes. The highly consistent contributions made by each joint suggest the pes could be modelled as a three-segment model when viewed from the lateral aspect, comprising the calcaneus, the fourth tarsal bone and the fifth metatarsal bone.

The computed tomography based kinematic techniques outlined in this thesis also have potential applications in the clinical assessment of patients and evaluation of surgical interventions. CT scans performed with and without an applied load or in 2 extremes of motion could be used to characterise the normal range of motion in a variety of joints and may help in the diagnosis of instability or ligament damage. Furthermore, scans performed before and after a surgical treatment could be used to evaluate the success of the procedure.

References

Agostinho, F., Rahal, S. C., Miqueleto, N., Verdugo, M., Inamassu, L. and El-Warrak, A. (2011). Kinematic analysis of Labrador Retrievers and Rottweilers trotting on a treadmill. *Veterinary and Comparative Orthopaedics and Traumatology* **24**, 185-191.

Alexander, R. (1974). The mechanics of jumping by a dog (Canis familiaris). *Journal of Zoology* **173**, 549-573.

Alexander, R., Maloiy, G., Ker, R., Jayes, A. and Warui, C. (1982). The role of tendon elasticity in the locomotion of the camel (Camelus dromedarius). *Journal of Zoology* **198**, 293-313.

Alexander, R. and Vernon, A. (1975). The mechanics of hopping by kangaroos (Macropodidae). *Journal of Zoology* **177**, 265-303.

Alexander, R. M. (1984). Elastic energy stores in running vertebrates. *American Zoologist* **24**, 85-94.

Alexander, R. M. (2002). Tendon elasticity and muscle function. *Comparative Biochemistry and Physiology Part A: Molecular & Integrative Physiology* **133**, 1001-1011.

Alexander, R. M. (2005). Mechanics of animal movement. *Current Biology* **15**, R616-R619.

Alexander, R. M. and Bennet-Clark, H. (1977). Storage of elastic strain energy in muscle and other tissues. *Nature* **265**, 114-117.

Allen, M., Dyce, J. and Houlton, J. (1993). Calcaneoquartal arthrodesis in the dog. *Journal of Small Animal Practice* **34**, 205-210.

Anderson, F. C. and Pandy, M. G. (2001). Static and dynamic optimization solutions for gait are practically equivalent. *Journal of Biomechanics* **34**, 153-161.

Apelt, D., Kowaleski, M. P. and Boudrieau, R. J. (2007). Effect of tibial tuberosity advancement on cranial tibial subluxation in canine cranial cruciate-deficient stifle joints: an in vitro experimental study. *Veterinary Surgery* **36**, 170-177.

Nussbaum, M. C. (1978). Aristotle's De motu animalium: text with translation, commentary, and interpretive essays. Princeton, N.J: Princeton University Press.

Arndt, A., Wolf, P., Liu, A., Nester, C., Stacoff, A., Jones, R., Lundgren, P. and Lundberg, A. (2007). Intrinsic foot kinematics measured in vivo during the stance phase of slow running. *Journal of Biomechanics* **40**, 2672-2678.

Aron, D. N. and Purinton, P. T. (1985a). Collateral ligaments of the tarsocrural joint - an anatomic and functional-study. *Veterinary Surgery* **14**, 173-177.

Aron, D. N. and Purinton, P. T. (1985b). Replacement of the collateral ligaments of the canine tarsocrural joint - a proposed technique. *Veterinary Surgery* **14**, 178-184.

Arwedsson, G. (1954). Arthrodesis in traumatic plantar subluxation of the metatarsal bones of the dog. *Journal of the American Veterinary Medical Association* **124**, 21.

Astion, D. J., Deland, J. T., Otis, J. C. and Kenneally, S. (1997). Motion of the hindfoot after simulated arthrodesis. *JBJS* **79**, 241-6.

Attarian, D. E., McCrackin, H. J., DeVito, D. P., McElhaney, J. H. and Garrett Jr, W. E. (1985). Biomechanical characteristics of human ankle ligaments. *Foot & ankle* **6**, 54-58.

Aulakh, K. S., Harper, T., Lanz, O., D'Amico, L., Butler, J., McLaughlin, R. and Werre, S. (2013). Effect of tibial insertion site for lateral suture stabilization on the kinematics of the cranial cruciate ligament deficient-stifle during early, middle and late stance. *Veterinary and Comparative Orthopaedics and Traumatology* **26**, 208-217.

Baker, R. (2007). The history of gait analysis before the advent of modern computers. *Gait & posture* **26**, 331-342.

Baltzopoulos, V. (1995). A videofluoroscopy method for optical distortion correction and measurement of knee-joint kinematics. *Clinical Biomechanics* **10**, 85-92.

Banks, S. A. and Hodge, W. A. (1996). Accurate measurement of three-dimensional knee replacement kinematics using single-plane fluoroscopy. *IEEE Transactions on Biomedical Engineering* **43**, 638-649.

Barnes, D. C., Knudsen, C. S., Gosling, M., McKee, M., Whitelock, R. G., Arthurs, G. I., Ness, M. G., Radke, H. and Langley-Hobbs, S. J. (2013). Complications of lateral plate fixation compared with tension band wiring and pin or lag screw fixation for calcaneoquartal arthrodesis. *Veterinary and Comparative Orthopaedics and Traumatology* **26**, 445-452.

Beever, L. J., Kulendra, E. R. and Meeson, R. L. (2016). Short and long-term outcome following surgical stabilization of tarsocrural instability in dogs. *Veterinary and Comparative Orthopaedics and Traumatology* **29**, 142-148.

Beggs, J. S. (1983). Kinematics: CRC Press.

Beimers, L., Tuijthof, G. J. M., Blankevoort, L., Jonges, R., Maas, M. and van Dijk, C. N. (2008). In-vivo range of motion of the subtalar joint using computed tomography. *Journal of Biomechanics* **41**, 1390-1397.

Bellenger, C., Johnson, K., Davis, P. and Ilkiw, J. (1981). Fixation of metacarpal and metatarsal fractures in greyhounds. *Australian veterinary journal* **57**, 205-211.

Benjamin, M., Toumi, H., Ralphs, J., Bydder, G., Best, T. and Milz, S. (2006). Where tendons and ligaments meet bone: attachment sites ('entheses') in relation to exercise and/or mechanical load. *J Anat* **208**, 471-490.

Bennell, K., Malcolm, S., Khan, K., Thomas, S., Reid, S., Brukner, P., Ebeling, P. and Wark, J. (1997). Bone mass and bone turnover in power athletes, endurance athletes, and controls: a 12-month longitudinal study. *Bone* **20**, 477-484.

Bennell, K. L., Malcolm, S. A., Thomas, S. A., Wark, J. D. and Brukner, P. D. (1996). The incidence and distribution of stress fractures in competitive track and field athletes: a twelve-month prospective study. *The American journal of sports medicine* **24**, 211-217.

Benoit, D. L., Ramsey, D. K., Lamontagne, M., Xu, L., Wretenberg, P. and Renström, P. (2006). Effect of skin movement artifact on knee kinematics during gait and cutting motions measured in vivo. *Gait & posture* **24**, 152-164.

Benson, J. A. and Boudrieau, R. J. (2002). Severe carpal and tarsal shearing injuries treated with an immediate arthrodesis in seven dogs. *Journal of the American Animal Hospital Association* **38**, 370-380.

Bergh, M. S., Piras, A., Samii, V. F., Weisbrode, S. E. and Johnson, K. A. (2012). Fractures in regions of adaptive modeling and remodeling of central tarsal bones in racing Greyhounds. *American Journal of Veterinary Research* **73**, 375-380.

Besancon, M. F., Conzemius, M. G., Evans, R. B. and Ritter, M. J. (2004). Distribution of vertical forces in the pads of Greyhounds and Labrador Retrievers during walking. *American Journal of Veterinary Research* **65**, 1497-1501.

Besl, P. J. and McKay, N. D. (1992). Method for registration of 3-D shapes. In *Robotics-DL tentative*, pp. 586-606: International Society for Optics and Photonics.

Biewener, A. A. and Blickhan, R. (1988). Kangaroo rat locomotion: design for elastic energy storage or acceleration? *Journal of Experimental Biology* **140**, 243-255.

Bitton, E., Joseph, R., Portman, L., Segev, G., Meiner, Y., Shipov, A. and Milgram, J. (2013). The effect of extension and loading of the carpus on radial rotation. *Veterinary Surgery* **42**, 909-917.

Blackwood, C. B., Yuen, T. J., Sangeorzan, B. J. and Ledoux, W. R. (2005). The midtarsal joint locking mechanism. *Foot Ankle Int* **26**, 1074.

Bottner, F., Su, E., Nestor, B., Azzis, B., Sculco, T. and Bostrom, M. (2005). Radiostereometric analysis: the hip. *HSS Journal* **1**, 94-99.

Boudrieau, R. J., Dee, J. F. and Dee, L. G. (1984a). Central Tarsal Bone Fracture in the Racing Greyhound - A Review of 114 Cases. *Journal of the American Veterinary Medical Association* **184**, 1486-1491.

Boudrieau, R. J., Dee, J. F. and Dee, L. G. (1984b). Treatment of Central Tarsal Bone Fractures in the Racing Greyhound. *Journal of the American Veterinary Medical Association* **184**, 1492-1500.

Brainerd, E. L., Baier, D. B., Gatesy, S. M., Hedrick, T. L., Metzger, K. A., Gilbert, S. L. and Crisco, J. J. (2010). X-ray reconstruction of moving morphology (XROMM): precision, accuracy and applications in comparative biomechanics research. *Journal of Experimental Zoology* **313**, 262-279.

Braune, W. and Fischer, O. (2012). The human gait: Springer Science & Business Media.

Burr, D. B., Martin, R. B., Schaffler, M. B. and Radin, E. L. (1985). Bone remodeling in response to in vivo fatigue microdamage. *Journal of Biomechanics* **18**, 189-200.

Caine, A., Agthe, P., Posch, B. and Herrtage, M. (2009). Sonography of the soft tissue structures of the canine tarsus. *Veterinary Radiology & Ultrasound* **50**, 304-308.

Campbell, J. R., Bennett, D. and Lee, R. (1976). Intertarsal and tarso-metatarsal subluxation in the dog. *Journal of Small Animal Practice* **17**, 427-442.

Cantatore, M. and Clements, D. (2015). Bilateral calcaneal stress fractures in two cats. *Journal of Small Animal Practice* **56**, 417-421.

Carlet, M. (1872). Essai expérimental sur la locomotion humaine. Etude de la marche. *Ann Sci Nat (Zool)* **16**, 1-92.

Carmichael, S. and Marshall, W. (2013). Tarsus and Metatarsus. In *Veterinary Surgery: Small Animal*, eds. K. M. Tobias and S. A. Johnston), pp. 1014-1028. St. Louis, Missouri: Elsevier Health Sciences.

Castile, R. M., Skelley, N. W., Babaei, B., Brophy, R. H. and Lake, S. P. (2016). Microstructural properties and mechanics vary between bundles of the human anterior cruciate ligament during stress-relaxation. *Journal of Biomechanics* **49**, 87-93.

Cavagna, G., Saibene, F. and Margaria, R. (1964). Mechanical work in running. *Journal of Applied Physiology* **19**, 249-256.

Cavagna, G. A., Heglund, N. C. and Taylor, C. R. (1977). Mechanical work in terrestrial locomotion: two basic mechanisms for minimizing energy expenditure. *American Journal of Physiology-Regulatory, Integrative and Comparative Physiology* **233**, R243-R261.

Chailleux, N., Lussier, B., De Guise, J., Chevalier, Y. and Hagemeister, N. (2007). In vitro 3-dimensional kinematic evaluation of 2 corrective operations for cranial cruciate ligament-deficient stifle. *Canadian journal of veterinary research* **71**, 175.

Chandrashekar, N., Mansouri, H., Slauterbeck, J. and Hashemi, J. (2006). Sex-based differences in the tensile properties of the human anterior cruciate ligament. *Journal of Biomechanics* **39**, 2943-2950.

Chow, E. P. and Balfour, R. J. (2012). Tarsometatarsal arthrodesis using tarsometatarsal intramedullary pin stabilization. *Veterinary Surgery* **41**, 733-737.

Cignoni, P., Callieri, M., Corsini, M., Dellepiane, M., Ganovelli, F. and Ranzuglia, G. (2008). Meshlab: an open-source mesh processing tool. In *Eurographics Italian Chapter Conference*, vol. 2008, pp. 129-136.

Cignoni, P., Ranzuglia, G., Callieri, M., Corsini, M., Ganovelli, F., Pietroni, N. and Tarini, M. (2011). MeshLab.

Clément, J., Hagemeister, N., Aissaoui, R. and de Guise, J. A. (2014). Comparison of quasi-static and dynamic squats: a three-dimensional kinematic, kinetic and electromyographic study of the lower limbs. *Gait & posture* **40**, 94-100.

Colborne, G. R., Good, L., Cozens, L. E. and Kirk, L. S. (2011). Symmetry of hind limb mechanics in orthopedically normal trotting Labrador Retrievers. *American Journal of Veterinary Research* **72**, 336.

Colborne, G. R., Hadley, N. R. and Wallace, A. M. (2013). A novel method for defining the Greyhound talocrural joint axis of rotation for hinged transarticular external skeletal fixation. *Veterinary and Comparative Orthopaedics and Traumatology* **26**, 298-303.

Colborne, G. R., Innes, J. F., Comerford, E. J., Owen, M. R. and Fuller, C. J. (2005). Distribution of power across the hind limb joints in Labrador Retrievers and Greyhounds. *American Journal of Veterinary Research* **66**, 1563-1571.

Colborne, G. R., Walker, A. M., Tattersall, A. J. and Fuller, C. J. (2006). Effect of trotting velocity on work patterns of the hind limbs of Greyhounds. *American Journal of Veterinary Research* **67**, 1293-1298.

Comerford, E. J., Smith, K. and Hayashi, K. (2011). Update on the aetiopathogenesis of canine cranial cruciate ligament disease. *Veterinary and Comparative Orthopaedics and Traumatology (VCOT)* **24**, 91-98.

Corbet, F. (2008). Child's Play. In *Develop 3D (X3DMedia):*, pp. 25–27. .

Crary, J. L., Hollis, J. M. and Manoli, A. (2003). The effect of plantar fascia release on strain in the spring and long plantar ligaments. *Foot Ankle Int* **24**, 245-250.

Crisco, J. and McGovern, R. (1997). Efficient calculation of mass moments of inertia for segmented homogenous three-dimensional objects. *Journal of Biomechanics* **31**, 97-101.

Crisco, J. J., McGovern, R. D. and Wolfe, S. W. (1999). Noninvasive technique for measuring in vivo three-dimensional carpal bone kinematics. *Journal of orthopaedic research* **17**, 96-100.

Cuesta-Vargas, A. I., Galán-Mercant, A. and Williams, J. M. (2010). The use of inertial sensors system for human motion analysis. *Physical Therapy Reviews* **15**, 462-473.

Dawson, T. J. and Taylor, C. R. (1973). Energetic cost of locomotion in kangaroos. *Nature* **246**, 313.

DeCamp, C., Soutas-Little, R., Hauptman, J., Olivier, B., Braden, T. and Walton, A. (1993). Kinematic gait analysis of the trot in healthy greyhounds. *American Journal of Veterinary Research* **54**, 627-634.

Denny, H. and Barr, A. (1991). Partial carpal and pancarpal arthrodesis in the dog: a review of 50 cases. *Journal of Small Animal Practice* **32**, 329-334.

Deruddere, K. J., Milne, M. E., Wilson, K. M. and Snelling, S. R. (2014). Magnetic Resonance Imaging, Computed Tomography, and Gross Anatomy of the Canine Tarsus. *Veterinary Surgery* **43**, 912-919.

Devas, M. (1967). Shin splints, or stress fractures of the metacarpal bone in horses, and shin soreness, or stress fractures of the tibia, in man. *Bone & Joint Journal* **49**, 310-313.

Devas, M. B. (1961). Compression stress fractures in man and the greyhound. *The Journal of bone and joint surgery. British volume* **43-B**, 540.

DeVries, N. A., Gassman, E. E., Kallemeyn, N. A., Shivanna, K. H., Magnotta, V. A. and Grosland, N. M. (2008). Validation of phalanx bone three-dimensional surface segmentation from computed tomography images using laser scanning. *Skeletal radiology* **37**, 35-42.

Diamond, D. W., Besso, J. and Boudrieau, R. J. (1999). Evaluation of joint stabilization for treatment of shearing injuries of the tarsus in 20 dogs. *Journal of the American Animal Hospital Association* **35**, 147-153.

Dieterich, H. (1974). Arthrodesis of the proximal intertarsal joint for repair of rupture of proximal plantar intertarsal ligaments. *Veterinary medicine, small animal clinician: VM, SAC* **69**, 995-1003.

Dimery, N. J. and Alexander, R. (1985). Elastic properties of the hind foot of the Donkey, Equus asinus. *Journal of Zoology* **207**, 9-20.

Dixon, S. J., Creaby, M. W. and Allsopp, A. J. (2006). Comparison of static and dynamic biomechanical measures in military recruits with and without a history of third metatarsal stress fracture. *Clinical Biomechanics* **21**, 412-419.

Dommelen, v. J. A. W. H., Minary Jolandan, M., Ivarsson, B. J., Millington, S. A., Raut, M., Kerrigan, J. R., Crandall, J. R. and Diduch. (2006). Nonlinear viscoelastic behavior of human knee ligaments subjected to complex loading histories. *Annals of Biomedical Engineering* **34**, 1008-1018.

Doornink, M. T., Nieves, M. A. and Evans, R. (2006). Evaluation of ilial screw loosening after triple pelvic osteotomy in dogs: 227 cases (1991–1999). *Journal of the American Veterinary Medical Association* **229**, 535-541.

Duck, T. R., Ferreira, L. M., King, G. J. and Johnson, J. A. (2004). Assessment of screw displacement axis accuracy and repeatability for joint kinematic description using an electromagnetic tracking device. *Journal of Biomechanics* **37**, 163-167.

Duerr, F. M., Pauls, A., Kawcak, C., Haussler, K. K., Bertocci, G., Moorman, V. and King, M. (2016). Evaluation of inertial measurement units as a novel method for kinematic gait evaluation in dogs. *Veterinary and Comparative Orthopaedics and Traumatology* **29**, 475-483.

Duval, J., Budsberg, S., Flo, G. and Sammarco, J. (1999). Breed, sex, and body weight as risk factors for rupture of the cranial cruciate ligament in young dogs. *Journal of the American Veterinary Medical Association* **215**, 811-814.

Dyce, J., Whitelock, R., Robinson, K., Forsythe, F. and Houlton, J. (1998). Arthrodesis of the tarsometatarsal joint using a laterally applied plate in 10 dogs. *Journal of Small Animal Practice* **39**, 19-22.

Egol, K. A., Kubiak, E. N., Fulkerson, E., Kummer, F. J. and Koval, K. J. (2004). Biomechanics of locked plates and screws. *Journal of orthopaedic trauma* **18**, 488-493.

Ellis, R., TOKSVIG-LARSEN, S., Marcacci, M., Caramella, D. and Fadda, M. (1996). Use of a biocompatible fiducial marker in evaluating the accuracy of computed tomography image registration. *Investigative Radiology* **31**, 658-667.

Evans, H. E., DeLahunta, A. and Miller, M. E. (2012). Miller's anatomy of the dog. Philadelphia, Pa;London;: Saunders.

Fassbind, M. J., Rohr, E. S., Hu, Y., Haynor, D. R., Siegler, S., Sangeorzan, B. J. and Ledoux, W. R. (2011). Evaluating foot kinematics using magnetic resonance imaging: from maximum plantar flexion, inversion, and internal rotation to maximum dorsiflexion, eversion, and external rotation. *Journal of biomechanical engineering* **133**, 104502.

Fat, D. L., Kennedy, J., Galvin, R., O'Brien, F., Mc Grath, F. and Mullett, H. (2012). The Hounsfield value for cortical bone geometry in the proximal humerus—an in vitro study. *Skeletal radiology* **41**, 557-568.

Feeney, L. C., Lin, C.-F., Marcellin-Little, D. J., Tate, A. R., Queen, R. M. and Yu, B. (2007). Validation of two-dimensional kinematic analysis of walk and sit-to-stand motions in dogs. *American Journal of Veterinary Research* **68**, 277-282.

Fettig, A. A., McCarthy, R. J. and Kowaleski, M. P. (2002). Intertarsal and tarsometatarsal arthrodesis using 2.0/2.7-mm or 2.7/3.5-mm hybrid dynamic compression plates. *Journal of the American Animal Hospital Association* **38**, 364-369.

Field, J. R., Törnkvist, H., Hearn, T. C., Sumner-Smith, G. and Woodside, T. D. (1999). The influence of screw omission on construction stiffness and bone surface strain in the application of bone plates to cadaveric bone. *Injury* **30**, 591-598.

Fischer, K. J., Manson, T., Pfaeffle, H., Tomaino, M. and Woo, S.-Y. (2001). A method for measuring joint kinematics designed for accurate registration of kinematic data to models constructed from CT data. *Journal of Biomechanics* **34**, 377-383.

Fischer, M. S. and Blickhan, R. (2006). The tri-segmented limbs of therian mammals: kinematics, dynamics, and self-stabilization—a review. *Journal of Experimental Zoology Part A: Comparative Experimental Biology* **305A**, 935-952.

Foumani, M., Blankevoort, L., Stekelenburg, C., Strackee, S., Carelsen, B., Jonges, R. and Streekstra, G. (2010). The effect of tendon loading on in-vitro carpal kinematics of the wrist joint. *Journal of Biomechanics* **43**, 1799-1805.

Foumani, M., Strackee, S., Jonges, R., Blankevoort, L., Zwinderman, A., Carelsen, B. and Streekstra, G. (2009). In-vivo three-dimensional carpal bone kinematics during flexion–extension and radio–ulnar deviation of the wrist: Dynamic motion versus step-wise static wrist positions. *Journal of Biomechanics* **42**, 2664-2671.

Fu, Y.-C., Torres, B. T. and Budsberg, S. C. (2010). Evaluation of a three-dimensional kinematic model for canine gait analysis. *American Journal of Veterinary Research* **71**, 1118-1122.

Funk, J., Hall, G., Crandall, J. and Pilkey, W. (2000). Linear and quasi-linear viscoelastic characterization of ankle ligaments. *Journal of biomechanical engineering* **122**, 15-22.

Galateanu, G., Apelt, D., Aizenberg, I., Saragusty, J. and Hildebrandt, T. B. (2013). Canine tarsal architecture as revealed by high-resolution computed tomography. *Veterinary Journal* **196**, 374-380.

Gannon, J. R. (1972). Stress fractures in the greyhound. *Australian veterinary journal* **48**, 244-250.

Gelaude, F., Vander Sloten, J. and Lauwers, B. (2008). Accuracy assessment of CT-based outer surface femur meshes. *Computer Aided Surgery* **13**, 188-199.

George, W. and Vashishth, D. (2005). Damage mechanisms and failure modes of cortical bone under components of physiological loading. *Journal of orthopaedic research* **23**, 1047-1053.

Gillette, R. L. and Angle, T. C. (2008). Recent developments in canine locomotor analysis: a review. *Vet J* **178**, 165-76.

Golub, G. and Kahan, W. (1965). Calculating the singular values and pseudo-inverse of a matrix. *Journal of the Society for Industrial and Applied Mathematics, Series B: Numerical Analysis* **2**, 205-224.

Gorse, M. J., Purinton, P., Penwick, R. C., Aron, D. N. and Roberts, R. E. (1990). Talocalcaneal Luxation An Anatomic and Clinical Study. *Veterinary Surgery* **19**, 429-434.

Goslow, G., Seeherman, H., Taylor, C., McCutchin, M. and Heglund, N. (1981). Electrical activity and relative length changes of dog limb muscles as a function of speed and gait. *Journal of Experimental Biology* **94**, 15-42.

Gregersen, C. S., Silverton, N. A. and Carrier, D. R. (1998). External work and potential for elastic storage at the limb joints of running dogs. *J Exp Biol* **201**, 3197-3210.

Grood, E. S. and Suntay, W. J. (1983). A joint coordinate system for the clinical description of three-dimensional motions: application to the knee. *Journal of biomechanical engineering* **105**, 136.

Gross, C. E. and Nunley, J. A. (2015). Navicular stress fractures. *Foot Ankle Int* **36**, 1117-1122.

Guerrero, T. G., Geyer, H., Hässig, M. and Montavon, P. M. (2007). Effect of conformation of the distal portion of the femur and proximal portion of the tibia on the pathogenesis of cranial cruciate ligament disease in dogs. *American Journal of Veterinary Research* **68**, 1332-1337.

Guilliard, M. (2007). Central tarsal bone fracture in the border collie. *Journal of Small Animal Practice* **48**, 414-417.

Guilliard, M. (2010). Third tarsal bone fractures in the greyhound. *Journal of Small Animal Practice* **51**, 635-641.

Guilliard, M. J. (2000). Fractures of the central tarsal bone in eight racing greyhounds. *Veterinary Record* **147**, 512-515.

Guilliard, M. J. (2005). Centrodistal joint lameness in dogs. *Journal of Small Animal Practice* **46**, 199-202.

guilliard, M. J. (2013). Conservative management of fractures of the third metatarsal bone in the racing greyhound. *Journal of Small Animal Practice* **54**, 507-511.

Hamel, A. J., Sharkey, N. A., Buczek, F. L. and Michelson, J. (2004). Relative motions of the tibia, talus, and calcaneus during the stance phase of gait: a cadaver study. *Gait & posture* **20**, 147-153.

Harris, A. P., Gil, J. A., Goodman, A. D., Nacca, C. R. and Borenstein, T. R. (2017). Acute plantar midtarsal dislocation with intercuneiform dislocation: Case study, diagnosis and management. *Journal of Orthopaedics* **14**, 26-29.

Hassan, E. A., Jenkyn, T. R. and Dunning, C. E. (2007). Direct comparison of kinematic data collected using an electromagnetic tracking system versus a digital optical system. *Journal of Biomechanics* **40**, 930-935.

Headrick, J. F., Zhang, S., Millard, R. P., Rohrbach, B. W., Weigel, J. P. and Millis, D. L. (2014a). Use of an inverse dynamics method to compare the three-dimensional motion of the pelvic limb among clinically normal dogs and dogs with cranial cruciate ligament–deficient stifle joints following tibial plateau leveling osteotomy or lateral fabellar–tibial suture stabilization. *American Journal of Veterinary Research* **75**, 554-564.

Headrick, J. F., Zhang, S., Millard, R. P., Rohrbach, B. W., Weigel, J. P. and Millis, D. L. (2014b). Use of an inverse dynamics method to describe the motion of the canine pelvic limb in three dimensions. *American Journal of Veterinary Research* **75**, 544-553.

Hoffmann, D. E., Kowaleski, M. P., Johnson, K. A., Evans, R. B. and Boudrieau, R. J. (2011). Ex Vivo Biomechanical Evaluation of the Canine Cranial Cruciate Ligament-Deficient Stifle with Varying Angles of Stifle Joint Flexion and Axial loads after Tibial Tuberosity Advancement. *Veterinary Surgery* **40**, 311-320.

Holler, P. J., Brazda, V., Dal-Bianco, B., Lewy, E., Mueller, M. C., Peham, C. and Bockstahler, B. A. (2010). Kinematic motion analysis of the joints of the forelimbs and hind limbs of dogs during walking exercise regimens. *American Journal of Veterinary Research* **71**, 734-740.

Holt, P. E. (1974). Ligamentous injuries to the canine hock. *The Journal of small animal practice* **15**, 457-474.

Hottinger, H. A., DeCamp, C., Olivier, N., Hauptman, J. and Soutas-Little, R. (1996). Noninvasive kinematic analysis of the walk in healthy large-breed dogs. *American Journal of Veterinary Research* **57**, 381-388.

Hudson, C. and Pozzi, A. (2012). Minimally invasive repair of central tarsal bone luxation in a dog. *Veterinary and Comparative Orthopaedics and Traumatology (VCOT)* **25**, 79-82.

Hudson, P. E., Corr, S. A. and Wilson, A. M. (2012). High speed galloping in the cheetah (Acinonyx jubatus) and the racing greyhound (Canis familiaris): spatio-temporal and kinetic characteristics. *J Exp Biol* **215**, 2425-34.

Hurter, K., Schawalder, P. and Schmökel, H. (2004). Talocalcaneocentral luxation combined with lateral instability of the talocrural joint in a dog and a cat. *VCOT Archive* **17**, 53.

Iaquinto, J. M., Tsai, R., Haynor, D. R., Fassbind, M. J., Sangeorzan, B. J. and Ledoux, W. R. (2014). Marker-based validation of a biplane fluoroscopy system for quantifying foot kinematics. *Medical Engineering and Physics* **36**, 391-396.

Inauen, R., Koch, D. and Bass, M. (2009a). Arthrodesis of the tarsometatarsal joints in a cat with a two hole advanced locking plate system. *Veterinary and Comparative Orthopaedics and Traumatology* **22**, 166.

Inauen, R., Koch, D., Bass, M. and Haessig, M. (2009b). Tibial tuberosity conformation as a risk factor for cranial cruciate ligament rupture in the dog. *Veterinary and Comparative Orthopaedics and Traumatology* **22**, 16-20.

Ito, K., Hosoda, K., Shimizu, M., Ikemoto, S., Kume, S., Nagura, T., Imanishi, N., Aiso, S., Jinzaki, M. and Ogihara, N. (2015). Direct assessment of 3D foot bone kinematics using biplanar X-ray fluoroscopy and an automatic model registration method. *Journal of Foot and Ankle Research* **8**, 21.

Ito, K., Hosoda, K., Shimizu, M., Ikemoto, S., Nagura, T., Seki, H., Kitashiro, M., Jinzaki, M., Imanishi, N. and Aiso, S. (2017). Three-dimensional measurement of the human cadaver foot bone kinematics under axial loading condition using biplane X-ray fluoroscopy. *Footwear Science* **9**, S148-S150.

Jaeger, G. H., Wosar, M. A., Marcellin-Little, D. J. and Lascelles, B. D. X. (2005). Use of hinged transarticular external fixation for adjunctive joint stabilization in dogs and cats: 14 cases (1999-2003). *Journal of the American Veterinary Medical Association* **227**, 586-591.

Johnson, A. L. and DeCamp, C. E. (1999). External skeletal fixation: linear fixators. *Veterinary Clinics: Small Animal Practice* **29**, 1135-1152.

Johnson, A. L., Houlton, J. E. and Vannini, R. (2005). AO principles of fracture management in the dog and cat: Georg Thieme Verlag.

Johnson, K. A., Muir, P., Nicoll, R. G. and Roush, J. K. (2000). Asymmetric adaptive modeling of central tarsal bones in racing greyhounds. *Bone* **27**, 257-263.

Johnson, K. A., Skinner, G. A. and Muir, P. (2001). Site-specific adaptive remodeling of Greyhound metacarpal cortical bone subjected to asymmetrical cyclic loading. *American Journal of Veterinary Research* **62**, 787-793.

Jones, S. C., Kim, S. E., Banks, S. A., Conrad, B. P., Abbasi, A. Z., Tremolada, G., Lewis, D. D. and Pozzi, A. (2014). Accuracy of noninvasive, single-plane fluoroscopic analysis for measurement of three-dimensional femorotibial joint poses in dogs. *American Journal of Veterinary Research* **75**, 477.

Kärrholm, J., Gill, R. H. and Valstar, E. R. (2006). The history and future of radiostereometric analysis. *Clinical orthopaedics and related research* **448**, 10-21.

Kedgley, A. E., Birmingham, T. and Jenkyn, T. R. (2009). Comparative accuracy of radiostereometric and optical tracking systems. *Journal of Biomechanics* **42**, 1350-1354.

Kelikian, A. S. and Sarrafian, S. K. (2011). Sarrafian's anatomy of the foot and ankle: descriptive, topographic, functional: Lippincott Williams & Wilkins.

Keller, S. A., Fürst, A. E., Kircher, P., Ringer, S. and Kuemmerle, J. M. (2015). Locking compression plate fixation of equine tarsal subluxations. *Veterinary Surgery* **44**, 949-956.

Ker, R., Bennet, M., Bibby, S., Kester, R. and Alexander, R. (1987). The spring in the arch of the human foot. *Nature* **325**, 147-149.

Kim, J., Rietdyk, S. and Breur, G. J. (2008). Comparison of two-dimensional and three-dimensional systems for kinematic analysis of the sagittal motion of canine hind limbs during walking. *American Journal of Veterinary Research* **69**, 1116-1122.

Kim, S.-Y., Torres, B. T., Sandberg, G. S. and Budsberg, S. C. (2017). Effect of Limb Position at the Time of Skin Marker Application on Sagittal Plane Kinematics of the Dog. *Veterinary and Comparative Orthopaedics and Traumatology* **30**, 438-443.

Kim, S. E., Jones, S. C., Lewis, D. D., Banks, S. A., Conrad, B. P., Tremolada, G., Abbasi, A. Z., Coggeshall, J. D. and Pozzi, A. (2015). In-vivo three-dimensional knee kinematics during daily activities in dogs. *Journal of orthopaedic research* **33**, 1603-1610.

Kim, S. E., Lewis, D. D. and Pozzi, A. (2012). Effect of tibial plateau leveling osteotomy on femorotibial subluxation: in vivo analysis during standing. *Veterinary Surgery* **41**, 465-470.

Kim, S. Y., Kim, J. Y., Hayashi, K. and Kapatkin, A. S. (2011). Skin movement during the kinematic analysis of the canine pelvic limb. *Veterinary and Comparative Orthopaedics and Traumatology* **24**, 326-332.

Kirby, K. A. (2000). Biomechanics of the normal and abnormal foot. *Journal of the American Podiatric Medical Association* **90**, 30-34.

Kneifel, W., Borak, D., Bockstahler, B. and Schnabl-Feichter, E. (2017). Use of a custom-made limb-press model to assess intra-and extracapsular techniques for treating cranial cruciate ligament rupture in cats. *Journal of Feline Medicine and Surgery*, epub ahead of print (https://doi.org/10.1177/1098612X17704562).

Korvick, D., Pijanowski, G. and Schaeffer, D. (1994). Three-dimensional kinematics of the intact and cranial cruciate ligament-deficient stifle of dogs. *Journal of Biomechanics* **27**, 77-87.

Kozanek, M., Rubash, H. E., Li, G. and de Asla, R. J. (2009). Effect of Post-traumatic Tibiotalar Osteoarthritis on Kinematics of the Ankle Joint Complex. *Foot Ankle Int* **30**, 734-740.

Kwan, M. K., Lin, T. H. C. and Woo, S. L. Y. (1993). On the viscoelastic properties of the anteromedial bundle of the anterior cruciate ligament. *Journal of Biomechanics* **26**, 447-452.

LaCroix, A. S., Duenwald-Kuehl, S. E., Brickson, S., Akins, T. L., Diffee, G., Aiken, J., Vanderby Jr, R. and Lakes, R. S. (2013). Effect of Age and Exercise on the Viscoelastic Properties of Rat Tail Tendon. *Annals of Biomedical Engineering* **41**, 1120-1128.

Lawson, D. D. (1960). Inter-tarsal Subluxation in the Dog. *Journal of Small Animal Practice* **1**, 179-181.

Leardini, A., Chiari, L., Della Croce, U. and Cappozzo, A. (2005). Human movement analysis using stereophotogrammetry: Part 3. Soft tissue artifact assessment and compensation. *Gait & posture* **21**, 212-225.

Leardini, A., O'Connor, J., Catani, F. and Giannini, S. (1999). Kinematics of the human ankle complex in passive flexion; a single degree of freedom system. *Journal of Biomechanics* **32**, 111-118.

Lee, M.-J., Kim, S., Lee, S.-A., Song, H.-T., Huh, Y.-M., Kim, D.-H., Han, S. H. and Suh, J.-S. (2007). Overcoming artifacts from metallic orthopedic implants at high-field-strength MR imaging and multi-detector CT. *Radiographics* **27**, 791-803.

Lee, P. H. (2010). Computed tomography for characterisation of wood samples in art conservation: European Congress of Radiology 2010.

Lewis, O. (1980). The joints of the evolving foot. Part II. The intrinsic joints. *J Anat* **130**, 833.

Loudon, J. K. and Reiman, M. P. (2012). Lower extremity kinematics in running athletes with and without a history of medial shin pain. *International journal of sports physical therapy* **7**, 356.

Lu, T.-W. and Chang, C.-F. (2012). Biomechanics of human movement and its clinical applications. *Kaohsiung Journal of Medical Sciences* **28**, S13-S25.

Lundgren, P., Nester, C., Liu, A., Arndt, A., Jones, R., Stacoff, A., Wolf, P. and Lundberg, A. (2008). Invasive in vivo measurement of rear-, mid-and forefoot motion during walking. *Gait & posture* **28**, 93-100.

Marai, G. E., Laidlaw, D. H. and Crisco, J. J. (2006). Super-resolution registration using tissue-classified distance fields. *Ieee Transactions on Medical Imaging* **25**, 177-187.

Matthews, L. S. and Ellis, D. (1968). Viscoelastic properties of cat tendon: effects of time after death and preservation by freezing. *Journal of Biomechanics* **1**, 65-71.

Mayagoitia, R. E., Nene, A. V. and Veltink, P. H. (2002). Accelerometer and rate gyroscope measurement of kinematics: an inexpensive alternative to optical motion analysis systems. *Journal of Biomechanics* **35**, 537-542.

McCartney, W. and Carmichael, S. (2000). Talar neck fractures in five cats. *Journal of Small Animal Practice* **41**, 204-206.

McCormick, J. D. and Watkins, J. (2014). Plate fixation for management of plantar instability of the distal tarsus/proximal metatarsus in 5 horses. *Veterinary Surgery* **43**, 425-429.

McLaughlin, R. M. (2001). Kinetic and kinematic gait analysis in dogs. *Veterinary clinics of North America: small animal practice* **31**, 193-201.

McLennan, M. (2007). Ankylosis of tarsometatarsal luxations using external fixation. *Journal of Small Animal Practice* **48**, 508-513.

Medved, V. (2000). Measurement of human locomotion: CRC press.

Milgrom, C., Giladi, M., Stein, M., Kashtan, H., Margulies, J., Chisin, R., Steinberg, R. and Aharonson, Z. (1985). Stress fractures in military recruits. A prospective study showing an unusually high incidence. *Bone & Joint Journal* **67**, 732-735.

Milner, C. E., Hamill, J. and Davis, I. S. (2010). Distinct hip and rearfoot kinematics in female runners with a history of tibial stress fracture. *journal of orthopaedic & sports physical therapy* **40**, 59-66.

Miranda, D. L., Schwartz, J. B., Loomis, A. C., Brainerd, E. L., Fleming, B. C. and Crisco, J. J. (2011). Static and dynamic error of a biplanar videoradiography system using marker-based and markerless tracking techniques. *Journal of biomechanical engineering* **133**, 121002.

Moon, D. K., Woo, S. L., Takakura, Y., Gabriel, M. T. and Abramowitch, S. D. (2006). The effects of refreezing on the viscoelastic and tensile properties of ligaments. *Journal of Biomechanics* **39**, 1153-1157.

Moore, D. C., Halilaj, E., Patel, T. K. and Crisco, J. J. (2015). Computed Tomographic Image-based Kinematic Analysis: An Overview. In *Handbook of Imaging in Biological Mechanics*, eds. C. P. Neu and G. M. Genin), pp. 115-126. New York: CRC Press.

Moore, E. J., Kim, S. E., Banks, S. A., Pozzi, A., Coggeshall, J. D. and Jones, S. C. (2016). Normal patellofemoral kinematic patterns during daily activities in dogs. *BMC veterinary research* **12**, 262.

Moro-oka, T. a., Hamai, S., Miura, H., Shimoto, T., Higaki, H., Fregly, B. J., Iwamoto, Y. and Banks, S. A. (2008). Dynamic activity dependence of in vivo normal knee kinematics. *Journal of orthopaedic research* **26**, 428-434.

Mu, S., Moro-Oka, T., Johal, P., Hamai, S., Freeman, M. and Banks, S. (2011). Comparison of static and dynamic knee kinematics during squatting. *Clinical Biomechanics* **26**, 106-108.

Muir, P. and Norris, J. L. (1999). Tarsometatarsal subluxation in dogs: partial arthrodesis by plate fixation. *Journal of the American Animal Hospital Association* **35**, 155-162.

Nester, C., Jones, R. K., Liu, A., Howard, D., Lundberg, A., Arndt, A., Lundgren, P., Stacoff, A. and Wolf, P. (2007). Foot kinematics during walking measured using bone and surface mounted markers. *Journal of Biomechanics* **40**, 3412-3423.

Nester, C., Liu, A., Ward, E., Howard, D., Cocheba, J. and Derrick, T. (2010). Error in the description of foot kinematics due to violation of rigid body assumptions. *Journal of Biomechanics* **43**, 666-672.

Nickoloff, E. L. and Alderson, P. O. (2001). Radiation exposures to patients from CT: reality, public perception, and policy. *American Journal of Roentgenology* **177**, 285-287.

Niemeyer, P. and Sudkamp, N. (2006). Principles and clinical application of the locking compression plate (LCP). *Acta Chir Orthop Traumatol Cech* **73**, 221-228.

Nigg, B. M. and Herzog, W. (2007). Biomechanics of the musculo-skeletal system: John Wiley & Sons.

Niinomi, M. (1998). Mechanical properties of biomedical titanium alloys. *Materials Science and Engineering: A* **243**, 231-236.

Niinomi, M. (2002). Recent metallic materials for biomedical applications. *Metallurgical and materials transactions A* **33**, 477.

Nunamaker, D., Butterweck, D. and Provost, M. (1990). Fatigue fractures in thoroughbred racehorses: relationships with age, peak bone strain, and training. *Journal of orthopaedic research* **8**, 604-611.

O'neill, H. (2012). Case Report: Simultaneous rupture of the fibularis tertius and subluxation of the proximal intertarsal joint of a horse. *Companion Animal* **17**, 4-6.

Okita, N., Meyers, S. A., Challis, J. H. and Sharkey, N. A. (2014). Midtarsal joint locking: New perspectives on an old paradigm. *Journal of orthopaedic research* **32**, 110-115.

Ost, P. C., Dee, J. F., Dee, L. G. and Hohn, R. B. (1987). Fractures of the calcaneus in racing greyhounds. *Veterinary Surgery* **16**, 53-59.

Panjabi, M. M. (1979). Centers and angles of rotation of body joints: a study of errors and optimization. *Journal of Biomechanics* **12**, 911-920.

Patel, V. V., Hall, K., Ries, M., Lotz, J., Ozhinsky, E., Lindsey, C., Lu, Y. and Majumdar, S. (2004). A three-dimensional MRI analysis of knee kinematics. *Journal of orthopaedic research* **22**, 283-292.

Pavlov, H., Torg, J. and Freiberger, R. (1983). Tarsal navicular stress fractures: radiographic evaluation. *Radiology* **148**, 641-645.

Pearce, M. S., Salotti, J. A., Little, M. P., McHugh, K., Lee, C., Kim, K. P., Howe, N. L., Ronckers, C. M., Rajaraman, P. and Craft, A. W. (2012). Radiation exposure from CT scans in childhood and subsequent risk of leukaemia and brain tumours: a retrospective cohort study. *The Lancet* **380**, 499-505.

Pelizzari, C. A., Chen, G. T., Spelbring, D. R., Weichselbaum, R. R. and Chen, C.-T. (1989). Accurate three-dimensional registration of CT, PET, and/or MR images of the brain. *Journal of computer assisted tomography* **13**, 20-26.

Perry, K. L., Adams, R. J., Woods, S. and Bruce, M. (2017). Calcaneal Fractures in Non-Racing Dogs and Cats: Complications, Outcome, and Associated Risk Factors. *Veterinary Surgery* **46**, 39-51.

Pfaeffle, J., Blankenhorn, B., Stabile, K., Imbriglia, J., Goitz, R. and Robertson, D. (2005). Development and validation of a computed tomography-based methodology to measure carpal kinematics. *Journal of biomechanical engineering* **127**, 541-548.

Poole, D. C. and Erickson, H. H. (2011). Highly athletic terrestrial mammals: horses and dogs. *Comprehensive Physiology*.

Pratt, F. H. (1935). The Ankle Lever and Its Classification. *Research Quarterly. American Physical Education Association* **6**, 276-279.

Premeaux, S. F. (2003). The Flying Horse: Eadweard Muybridge's Contribution to Motion Study. *Journal of Applied Management and Entrepreneurship* **8**, 36.

Prins, A., Kaptein, B., Banks, S., Stoel, B., Nelissen, R. and Valstar, E. (2014). Detecting condylar contact loss using single-plane fluoroscopy: A comparison with in vivo force data and in vitro bi-plane data. *Journal of Biomechanics* **47**, 1682-1688.

Provenzano, P., Lakes, R., Keenan, T. and vanderby Jr, R. (2001). Nonlinear Ligament Viscoelasticity. *Annals of Biomedical Engineering* **29**, 908-914.

Puthezhath, K., Veluthedath, R., Kumaran, C. M. and Patinharayil, G. (2009). Acute Isolated Dorsal Midtarsal (Chopart's) Dislocation: A Case Report. *The Journal of Foot and Ankle Surgery* **48**, 462-465.

Ragetly, C. A., Griffon, D. J., Mostafa, A. A., Thomas, J. E. and Hsiao-Wecksler, E. T. (2010). Inverse dynamics analysis of the pelvic limbs in Labrador Retrievers with and without cranial cruciate ligament disease. *Veterinary Surgery* **39**, 513-522.

Rainbow, M. J., Kamal, R. N., Leventhal, E., Akelman, E., Moore, D. C., Wolfe, S. W. and Crisco, J. J. (2013). In Vivo Kinematics of the Scaphoid, Lunate, Capitate, and Third Metacarpal in Extreme Wrist Flexion and Extension. *J Hand Surg* **38A**, 278-288.

Rathnayaka, K., Sahama, T., Schuetz, M. A. and Schmutz, B. (2011). Effects of CT image segmentation methods on the accuracy of long bone 3D reconstructions. *Medical engineering & physics* **33**, 226-233.

Reichert, E. E., Kunkel, K. A. R., Suber, J. T., Basinger, R. R. and Gerard, P. D. (2013). Radiographic localization and isometry of the origin and insertion of the canine cranial cruciate ligament. *Veterinary Surgery* **42**, 860-866.

Reif, U., Hulse, D. A. and Hauptman, J. G. (2002). Effect of tibial plateau leveling on stability of the canine cranial cruciate–deficient stifle joint: an in vitro study. *Veterinary Surgery* **31**, 147-154.

Renstrom, P., Ljungqvist, A., Arendt, E., Beynnon, B., Fukubayashi, T., Garrett, W., Georgoulis, T., Hewett, T. E., Johnson, R. and Krosshaug, T. (2008). Non-contact ACL injuries in female athletes: an International Olympic Committee current concepts statement. *British journal of sports medicine* **42**, 394-412.

Rey, J., Fischer, M. S. and Böttcher, P. (2014). Sagittal joint instability in the cranial cruciate ligament insufficient canine stifle. Caudal slippage of the femur and not cranial tibial subluxation. *Tierärztliche Praxis. Ausgabe K, Kleintiere/Heimtiere* **42**, 151.

Roberts, T. J. and Azizi, E. (2011). Flexible mechanisms: the diverse roles of biological springs in vertebrate movement. *Journal of Experimental Biology* **214**, 353-361.

Roch, S., Clements, D., Mitchell, R., Downes, C., Gemmill, T., Macias, C. and McKee, W. (2008). Complications following tarsal arthrodesis using bone plate fixation in dogs. *Journal of Small Animal Practice* **49**, 117-126.

Roe, S., Kue, J. and Gemma, J. (2008). Isometry of potential suture attachment sites for the cranial cruciate ligament deficient canine stifle. *Veterinary and Comparative Orthopaedics and Traumatology* **21**, 215-220.

Romani, W. A., Langenberg, P. and Belkoff, S. M. (2010). Sex, collagen expression, and anterior cruciate ligament strength in rats. *Journal of athletic training* **45**, 22-28.

Saevarsson, S. K., Romeo, C. I. and Anglin, C. (2013). Are static and dynamic kinematics comparable after total knee arthroplasty? *Journal of Biomechanics* **46**, 1169-1175.

Schmökel, H., Hartmeier, G., Kaser-Hotz, B. and Weber, U. T. (1994). Tarsal injuries in the cat: a retrospective study of 21 cases. *Journal of Small Animal Practice* **35**, 156-162.

Schwencke, M., Smolders, L. A., Bergknut, N., Gustas, P., Meij, B. P., Hazewinkel, H. A. W. and Sveriges, I. (2012). Soft tissue artifact in canine kinematic gait analysis. *Veterinary Surgery* **41**, 829-837.

Scrimgeour, A. B., Bruce, W. J., Bridges, J. P., Walsh, V. P. and Worth, A. J. (2012). Long-term outcomes after partial tarsal arthrodesis in working farm dogs in New Zealand. *N Z Vet J* **60**, 50-5.

Sennwald, G. R., Zdravkovic, V., Kern, H.-P. and Jacob, H. A. C. (1993). Kinematics of the wrist and its ligaments. *Journal of Hand Surgery* **18**, 805-814.

Shani, J. and Shahar, R. (2000). Repair of chronic complete traumatic rupture of the common calcaneal tendon in a dog, using a fascia lata graft. *VCOT Archive* **13**, 104-1008.

Shani, J., Yeshurun, Y. and Shahar, R. (2006). Arthrodesis of the tarsometatarsal joint, using type II ESF with acrylic connecting bars in four dogs. *Vet Comp Orthop Traumatol* **19**, 61-63.

Sharkey, N. A. and Hamel, A. J. (1998). A dynamic cadaver model of the stance phase of gait: performance characteristics and kinetic validation. *Clinical Biomechanics* **13**, 420-433.

Shefelbine, S. J., Ma, C. B., Lee, K. Y., Schrumpf, M. A., Patel, P., Safran, M. R., Slavinsky, J. P. and Majumdar, S. (2006). MRI analysis of in vivo meniscal and tibiofemoral kinematics in ACL-deficient and normal knees. *Journal of orthopaedic research* **24**, 1208-1217.

Shimamura, A. P. (2002). Muybridge in motion: Travels in art, psychology and neurology. *History of Photography* **26**, 341-350.

Shores, J. T., Demehri, S. and Chhabra, A. (2013). Kinematic "4 dimensional" CT imaging in the assessment of wrist biomechanics before and after surgical repair. *Eplasty* **13**.

Sidaway, B. K., McLaughlin, R. M., Elder, S. H., Boyle, C. R. and Silverman, E. B. (2004). Role of the tendons of the biceps brachii and infraspinatus muscles and the medial glenohumeral ligament in the maintenance of passive shoulder joint stability in dogs. *American Journal of Veterinary Research* **65**, 1216-1222.

Silver, F. H., Bradica, G. and Tria, A. (2002). Elastic energy storage in human articular cartilage: estimation of the elastic modulus for type II collagen and changes associated with osteoarthritis. *Matrix Biology* **21**, 129-137.

Simkin, A., Leichter, I., Giladi, M., Stein, M. and Milgrom, C. (1989). Combined effect of foot arch structure and an orthotic device on stress fractures. *Foot & ankle* **10**, 25-29.

Sjöström, L. and Håkanson, N. (1994). Traumatic injuries associated with the short lateral collateral ligaments of the talocrural joint of the dog. *Journal of Small Animal Practice* **35**, 163-168.

Skinner, O., Kim, S., Lewis, D. and Pozzi, A. (2013). In vivo femorotibial subluxation during weight-bearing and clinical outcome following tibial tuberosity advancement for cranial cruciate ligament insufficiency in dogs. *The Veterinary Journal* **196**, 86-91.

Smith, J. (1954). The elastic properties of the anterior cruciate ligament of the rabbit. *J Anat* **88**, 369.

Snel, J. G., Venema, H. W., Moojen, T. M., Ritt, M. J., Grimbergen, C. A. and den Heeten, G. J. (2000). Quantitative in vivo analysis of the kinematics of carpal bones from three-dimensional CT images using a deformable surface model and a three-dimensional matching technique. *Medical physics* **27**, 2037-2047.

Spoor, C. and Veldpaus, F. (1980). Rigid body motion calculated from spatial co-ordinates of markers. *Journal of Biomechanics* **13**, 391-393.

Staaden, R. (1984). The exercise physiology of the racing greyhound: Murdoch University.

Tan, C. J., Parr, W. C., Walsh, W. R., Makara, M. and Johnson, K. A. (2017). Influence of Scan Resolution, Thresholding, and Reconstruction Algorithm on Computed Tomography-Based Kinematic Measurements. *Journal of biomechanical engineering* **139**, 104503.

Tashman, S. and Anderst, W. (2003). In-vivo measurement of dynamic joint motion using high speed biplane radiography and CT: application to canine ACL deficiency. *Journal of biomechanical engineering* **125**, 238-245.

Tashman, S., Anderst, W., Kolowich, P., Havstad, S. and Arnoczky, S. (2004). Kinematics of the ACL-deficient canine knee during gait: serial changes over two years. *Journal of orthopaedic research* **22**, 931-941.

Taylor, J. R. (2005). Classical mechanics: University Science Books.

Taylor, W. R., Ehrig, R. M., Duda, G. N., Schell, H., Seebeck, P. and Heller, M. O. (2005). On the influence of soft tissue coverage in the determination of bone kinematics using skin markers. *Journal of orthopaedic research* **23**, 726-734.

Théoret, M.-C. and Moens, N. M. (2007). The use of veterinary cuttable plates for carpal and tarsal arthrodesis in small dogs and cats. *The Canadian Veterinary Journal* **48**, 165.

Thornton, G. M., Lemmex, D. B., Ono, Y., Beach, C. J., Reno, C. R., Hart, D. A. and Lo, I. K. Y. (2015). Aging affects mechanical properties and lubricin/PRG4 gene expression in normal ligaments. *Journal of Biomechanics* **48**, 3306-3311.

Törnkvist, H., Hearn, T. and Schatzker, J. (1996). The strength of plate fixation in relation to the number and spacing of bone screws. *Journal of orthopaedic trauma* **10**, 204-208.

Torres, B. T., Gilbert, P. J., Reynolds, L. R., Fu, Y. C., Navik, J. A., Sornborger, A. and Budsberg, S. C. (2015). The Effect of Examiner Variability on Multiple Canine Stifle Kinematic Gait Collections in a 3-Dimensional Model. *Veterinary Surgery* **44**, 581-587.

Torres, B. T., Punke, J. P., Fu, Y. C., Navik, J. A., Speas, A. L., Sornborger, A. and Budsberg, S. C. (2010). Comparison of canine stifle kinematic data collected with three different targeting models. *Veterinary Surgery* **39**, 504-512.

Torres, B. T., Whitlock, D., Reynolds, L. R., Fu, Y. C., Navik, J. A., Speas, A. L., Sornborger, A. and Budsberg, S. C. (2011). The effect of marker location variability on noninvasive canine stifle kinematics. *Veterinary Surgery* **40**, 715-719.

Udupa, J. K., Hirsch, B. E., Hillstrom, H. J., Bauer, G. R. and Kneeland, J. B. (1998). Analysis of in vivo 3-D internal kinematics of the joints of the foot [MRI analysis]. *IEEE Transactions on Biomedical Engineering* **45**, 1387-1396.

unknown, a. (1879). The Horse in Motion. *Once a week* **10**, 103-104.

Van den Broeck, J., Vereecke, E., Wirix-Speetjens, R. and Vander Sloten, J. (2014). Segmentation accuracy of long bones. *Medical engineering & physics* **36**, 949-953.

Vasseur, P., Pool, R., Arnoczky, S. and Lau, R. (1985). Correlative biomechanical and histologic study of the cranial cruciate ligament in dogs. *American Journal of Veterinary Research* **46**, 1842-1854.

Vedrine, B., Guillemot, A., Fontaine, D., Ragetly, G. and Etchepareborde, S. (2013). Comparative anatomy of the proximal tibia in healthy Labrador Retrievers and Yorkshire Terriers. *Veterinary and Comparative Orthopaedics and Traumatology* **26**, 266-270.

Vereecke, E. E. and Aerts, P. (2008). The mechanics of the gibbon foot and its potential for elastic energy storage during bipedalism. *Journal of Experimental Biology* **211**, 3661-3670.

Viidik, A., Sandqvist, L. and Mägi, M. (1965). Influence of postmortal storage on tensile strength characteristics and histology of rabbit ligaments. *Acta Orthopaedica Scandinavica* **36**, 3-38.

Voss, K., Keller, M. and Montavon, P. (2004). Internal splinting of dorsal intertarsal and tarsometatarsal instabilities in dogs and cats with the ComPact UniLock 2.0/2.4 TM System*. *Vet Comp Orthop Traumatol* **17**, 125.

Wagner, M. (2003). General principles for the clinical use of the LCP. *Injury* **34**, B31-42.

Walter, R. M. and Carrier, D. R. (2007). Ground forces applied by galloping dogs. *J Exp Biol* **210**, 208-16.

Walter, R. M. and Carrier, D. R. (2009). Rapid acceleration in dogs: ground forces and body posture dynamics. *Journal of Experimental Biology* **212**, 1930-1939.

Wang, M. C., Geng, X., Wang, S., Ma, M. X., Wang, M. X., Huang, M. J., Zhang, M. C., Chen, M. L., Yang, J. and Wang, K. (2016). In vivo kinematic study of the tarsal joints complex based on fluoroscopic 3D-2D registration technique. *Gait & posture* **49**, 54-60.

Warden, S. J., Burr, D. B. and Brukner, P. D. (2006). Stress fractures: pathophysiology, epidemiology, and risk factors. *Current osteoporosis reports* **4**, 103-109.

Warden, S. J., Hurst, J. A., Sanders, M. S., Turner, C. H., Burr, D. B. and Li, J. (2005). Bone adaptation to a mechanical loading program significantly increases skeletal fatigue resistance. *Journal of bone and mineral research* **20**, 809-816.

Warzee, C. C., Dejardin, L. M., Arnoczky, S. P. and Perry, R. L. (2001). Effect of tibial plateau leveling on cranial and caudal tibial thrusts in canine cranial cruciate–deficient stifles: An in vitro experimental study. *Veterinary Surgery* **30**, 278-286.

Wearing, S. C., Smeathers, J. E., Yates, B., Sullivan, P. M., Urry, S. R. and Dubois, P. (2005). Errors in measuring sagittal arch kinematics of the human foot with digital fluoroscopy. *Gait & posture* **21**, 326-332.

Weber, W. E. and Weber, E. (1992). Mechanics of the human walking apparatus. New York;Berlin;: Springer-Verlag.

Welch, J. A. (2003). The tarsus and Metatarsus. In *Textbook of small animal surgery*, (ed. D. H. Slatter). Philadelphia: Saunders.

Wendelburg, K., Dee, J., Kaderly, R., Dee, L. and Eaton-Wells, R. (1988). Stress fractures of the acetabulum in 26 racing Greyhounds. *Veterinary surgery : VS* **17**, 128-134.

Wentink, G. (1976). The action of the hind limb musculature of the dog in walking. *Cells Tissues Organs* **96**, 70-80.

Whitehair, J., Vasseur, P. and Willits, N. (1993). Epidemiology of cranial cruciate ligament rupture in dogs. *Journal of the American Veterinary Medical Association* **203**, 1016-1019.

Whittaker, E. C., Aubin, P. M. and Ledoux, W. R. (2011). Foot bone kinematics as measured in a cadaveric robotic gait simulator. *Gait & posture* **33**, 645-650.

Whittick, W. G. (1975). Canine orthopaedics. Philadelphia: Lea & Febiger.

Wilke, V. L., Conzemius, M. G., Besancon, M. F., Evans, R. B. and Ritter, M. (2002). Comparison of tibial plateau angle between clinically normal Greyhounds and Labrador Retrievers with and without rupture of the cranial cruciate ligament. *Journal of the American Veterinary Medical Association* **221**, 1426-1429.

Wilke, Y., Robinson, T. and Dueland, R. (2000). Intertarsal and tarsometatarsal arthrodesis using a plantar approach. *Vet Comp Orthop Traumatol* **13**, 28-33.

Wilken, J., Rao, S., Saltzman, C. and Yack, H. J. (2011). The effect of arch height on kinematic coupling during walking. *Clinical Biomechanics* **26**, 318-323.

Williams, S. B., Usherwood, J. R., Jespers, K., Channon, A. J. and Wilson, A. M. (2009). Exploring the mechanical basis for acceleration: pelvic limb locomotor function during accelerations in racing greyhounds (Canis familiaris). *J Exp Biol* **212**, 550-65.

Williams, S. B., Wilson, A. M., Rhodes, L., Andrews, J. and Payne, R. C. (2008). Functional anatomy and muscle moment arms of the pelvic limb of an elite sprinting athlete: the racing greyhound (Canis familiaris). *J Anat* **213**, 361-72.

Witsberger, T. H., Villamil, J. A., Schultz, L. G., Hahn, A. W. and Cook, J. L. (2008). Prevalence of and risk factors for hip dysplasia and cranial cruciate ligament deficiency in dogs. *Journal of the American Veterinary Medical Association* **232**, 1818-1824.

Wolf, P. (2006). Tarsal kinematics, vol. Doctor of sciences: Swiss Federal Institute of technology, Zurich.

Wolf, P., Luechinger, R., Boesiger, P., Stuessi, E. and Stacoff, A. (2007). A MR imaging procedure to measure tarsal bone rotations. *Journal of biomechanical engineering* **129**, 931-936.

Wolf, P., Stacoff, A., Liu, A., Nester, C., Arndt, A., Lundberg, A. and Stuessi, E. (2008). Functional units of the human foot. *Gait & posture* **28**, 434-441.

Wolfe, S. W., Neu, C. and Crisco, J. J. (2000). In vivo scaphoid, lunate, and capitate kinematics in flexion and in extension. *The Journal of hand surgery* **25**, 860.

Woltring, H., Huiskes, R., De Lange, A. and Veldpaus, F. (1985). Finite centroid and helical axis estimation from noisy landmark measurements in the study of human joint kinematics. *Journal of Biomechanics* **18**, 379-389.

Woo, S.-Y., Gomez, M. and Akeson, W. (1981). The time and history-dependent viscoelastic properties of the canine medial collateral ligament. *Journal of biomechanical engineering* **103**, 293-298.

Woo, S. L.-Y., Orlando, C. A., Camp, J. F. and Akeson, W. H. (1986). Effects of postmortem storage by freezing on ligament tensile behavior. *Journal of Biomechanics* **19**, 399-404.

Woodburn, J., Turner, D., Helliwell, P. and Barker, S. (1999). A preliminary study determining the feasibility of electromagnetic tracking for kinematics at the ankle joint complex. *Rheumatology* **38**, 1260-1268.

Worth, A., Danielsson, F., Bray, J., Burbidge, H. and Bruce, W. J. (2004). Ability to work and owner satisfaction following surgical repair of common calcanean tendon injuries in working dogs in New Zealand. *New Zealand Veterinary Journal* **52**, 109-116.

Wu, G., Siegler, S., Allard, P., Kirtley, C., Leardini, A., Rosenbaum, D., Whittle, M., D D'Lima, D., Cristofolini, L. and Witte, H. (2002). ISB recommendation on definitions of joint coordinate system of various joints for the reporting of human joint motion—part I: ankle, hip, and spine. *Journal of Biomechanics* **35**, 543-548.

Wu, G., Van der Helm, F. C., Veeger, H. D., Makhsous, M., Van Roy, P., Anglin, C., Nagels, J., Karduna, A. R., McQuade, K. and Wang, X. (2005). ISB recommendation on definitions of joint coordinate systems of various joints for the reporting of human joint motion—Part II: shoulder, elbow, wrist and hand. *Journal of Biomechanics* **38**, 981-992.

ACKNOWLEDGEMENTS

This thesis would not have been possible without the support of a large number of people.

Firstly, I would like to thank my supervisor, Professor Kenneth Johnson, who has always provided advice and support throughout my candidature, whilst allowing me time and space to develop and critique my own ideas.

I would also like to thank the staff at the University Veterinary Teaching Hospital for allowing me to work around your busy schedule. Particular thanks goes to Helen Laurendet, who patiently helped me acquire the CT images and Jack Neville-Towle for your assistance with the limb loading device and CT scanning.

Thanks to Professor Bill Walsh for opening up the wonderful facilities of the Surgical and Orthopaedic Research Laboratories, to me and for providing endless and valuable advice and encouragement. Thanks to Chris Christou, Nicky Bertollo, Nick Russell, Tian Wang and Matthew Pelletier for all providing technical support during my candidature. A special thanks to Will Parr for providing such wonderful guidance and always showing such enthusiasm towards every project.

I would also like to thank Paul Sheehy and Peter Williamson, who were part of my original supervision team, for your support and mentorship.

Thanks to Natasha, Andrew and my parents for allowing me to dedicate the required time to this thesis by helping take care of our family.

Thanks to Olivia and Alex, my beautiful children for being so patient and understanding and also for sharing your precious Lego!

And finally, the biggest thanks goes to Polina, my wife, for staying by my side throughout this epic adventure. I could not have done this without you.

APPENDIX A

resolution (high/low)	threshold (HU)	smoothing protocol	bone	volume (mm^3)	surface area (mm^2)	translational error (mm)			rotational error (degrees)		
						x	y	z	x	y	z
low	500	high	control fourth	4520.67	1591.62	0.01	0.03	0.04	0.01	0.04	0.07
low	500	optimal	control fourth	3985.04	1502.70	0.01	0.02	0.03	0.02	0.03	0.13
low	500	smoothed	control fourth	3862.15	1415.97	0.04	0.05	0.05	0.04	0.09	0.01
low	900	high	control fourth	4004.36	1486.31	0.04	0.03	0.05	0.03	0.07	0.04
low	900	optimal	control fourth	3523.81	1401.54	0.00	0.02	0.05	0.01	0.04	0.03
low	900	smoothed	control fourth	3417.80	1317.77	0.01	0.02	0.04	0.02	0.11	0.04
low	1300	high	control fourth	3598.29	1407.59	0.10	0.07	0.02	0.01	0.07	0.00
low	1300	optimal	control fourth	3145.38	1348.65	0.02	0.02	0.02	0.08	0.09	0.05
low	1300	smoothed	control fourth	3043.25	1238.88	0.02	0.04	0.05	0.20	0.12	0.04
high	500	high	control fourth	3956.41	1515.06	0.01	0.02	0.02	0.03	0.01	0.01
high	500	optimal	control fourth	3714.31	1476.02	0.01	0.02	0.03	0.01	0.04	0.02
high	500	smoothed	control fourth	3676.80	1430.09	0.01	0.03	0.03	0.00	0.01	0.04
high	900	high	control fourth	3699.81	1460.33	0.01	0.00	0.04	0.01	0.01	0.03
high	900	optimal	control fourth	3468.66	1421.59	0.01	0.04	0.04	0.04	0.05	0.01
high	900	smoothed	control fourth	3432.14	1375.42	0.01	0.04	0.03	0.01	0.01	0.00
high	1300	high	control fourth	3508.56	1422.46	0.00	0.01	0.04	0.03	0.00	0.01
high	1300	optimal	control fourth	3285.54	1391.78	0.01	0.01	0.07	0.05	0.02	0.07
high	1300	smoothed	control fourth	3253.37	1337.30	0.00	0.03	0.03	0.06	0.04	0.01
low	500	high	CTB trans	2696.57	1124.20	0.02	0.04	0.12	0.23	0.04	0.31
low	500	optimal	CTB trans	2324.72	1048.72	0.05	0.04	0.12	0.30	0.01	0.29
low	500	smoothed	CTB trans	2225.80	978.64	0.04	0.13	0.13	0.27	0.13	0.07
low	900	high	CTB trans	2387.36	1046.60	0.03	0.03	0.11	0.29	0.09	0.14
low	900	optimal	CTB trans	2046.10	972.38	0.01	0.05	0.14	0.19	0.12	0.19
low	900	smoothed	CTB trans	1962.11	908.87	0.03	0.09	0.16	0.39	0.13	0.09
low	1300	high	CTB trans	2104.89	980.39	0.04	0.02	0.11	0.26	0.11	0.01
low	1300	optimal	CTB trans	1796.48	917.96	0.03	0.05	0.10	0.36	0.09	0.14
low	1300	smoothed	CTB trans	1718.94	849.60	0.00	0.12	0.13	0.44	0.23	0.09
high	500	high	CTB trans	2357.09	1066.13	0.01	0.01	0.13	0.28	0.03	0.15
high	500	optimal	CTB trans	2186.40	1030.12	0.02	0.08	0.12	0.28	0.00	0.10
high	500	smoothed	CTB trans	2158.68	998.35	0.03	0.11	0.13	0.44	0.10	0.15
high	900	high	CTB trans	2187.48	1022.04	0.01	0.05	0.14	0.29	0.04	0.10

high	900	optimal	CTB trans	2025.22	986.84	0.03	0.12	0.12	0.31	0.05	0.05
high	900	smoothed	CTB trans	2002.26	956.32	0.02	0.11	0.12	0.28	0.05	0.00
high	1300	high	CTB trans	2040.22	985.25	0.03	0.08	0.14	0.39	0.02	0.10
high	1300	optimal	CTB trans	1885.47	951.96	0.03	0.07	0.16	0.29	0.04	0.09
high	1300	smoothed	CTB trans	1862.88	918.93	0.27	0.10	0.13	0.28	0.03	0.10
low	500	high	CTB triple	2758.12	1133.92	0.16	0.01	0.04	0.15	0.12	0.22
low	500	optimal	CTB triple	2384.90	1056.25	0.19	0.01	0.07	0.06	0.02	0.17
low	500	smoothed	CTB triple	2284.28	987.55	0.22	0.04	0.03	0.06	0.02	0.17
low	900	high	CTB triple	2442.13	1056.49	0.19	0.02	0.03	0.45	0.14	0.19
low	900	optimal	CTB triple	2091.72	979.62	0.16	0.01	0.07	0.16	0.11	0.17
low	900	smoothed	CTB triple	2007.79	917.30	0.19	0.02	0.07	0.10	0.33	0.30
low	1300	high	CTB triple	2167.18	992.03	0.16	0.00	0.03	0.31	0.13	0.16
low	1300	optimal	CTB triple	1842.74	925.26	0.15	0.03	0.05	0.11	0.09	0.09
low	1300	smoothed	CTB triple	1758.97	859.35	0.16	0.01	0.09	0.21	0.34	0.10
high	500	high	CTB triple	2394.03	1070.30	0.20	0.02	0.09	0.11	0.07	0.28
high	500	optimal	CTB triple	2223.17	1034.21	0.20	0.02	0.06	0.15	0.35	0.43
high	500	smoothed	CTB triple	2195.01	1002.96	0.21	0.03	0.06	0.12	0.31	0.15
high	900	high	CTB triple	2226.00	1028.77	0.20	0.03	0.10	0.09	0.18	0.30
high	900	optimal	CTB triple	2063.20	993.55	0.22	0.04	0.08	0.08	0.18	0.38
high	900	smoothed	CTB triple	2039.35	962.40	0.21	0.04	0.06	0.15	0.05	0.35
high	1300	high	CTB triple	2090.60	995.10	0.21	0.03	0.07	0.17	0.14	0.35
high	1300	optimal	CTB triple	1932.98	962.52	0.21	0.03	0.10	0.11	0.04	0.40
high	1300	smoothed	CTB triple	1913.39	929.96	0.21	0.03	0.07	0.18	0.17	0.37
low	500	high	First rot	688.64	463.30				0.13	0.37	0.04
low	500	optimal	First rot	535.28	409.75				0.23	0.98	0.10
low	500	smoothed	First rot	490.03	373.57				0.94	0.98	0.48
low	900	high	First rot	513.98	396.69				0.70	0.59	0.93
low	900	optimal	First rot	386.77	350.48				0.45	0.58	0.13
low	900	smoothed	First rot	345.25	311.02				1.23	1.16	0.67
low	1300	high	first rot	356.16	367.64				0.02	0.29	0.59
low	1300	optimal	first rot	241.00	341.68				1.20	-0.14	1.27
low	1300	smoothed	first rot	210.22	283.46				1.07	-0.06	0.75
high	500	high	First rot	539.29	423.69				0.80	-0.08	0.30
high	500	optimal	first rot	470.17	397.03				0.69	-0.01	0.99
high	500	smoothed	first rot	454.90	378.47				0.61	-0.10	1.10
high	900	high	first rot	465.69	389.33				0.74	-0.31	0.65
high	900	optimal	first rot	402.65	363.92				0.83	-0.04	0.90
high	900	smoothed	first rot	389.47	346.45				0.90	-0.05	1.04

high	1300	high	first rot	413.42	369.50				1.02	-0.29	1.32
high	1300	optimal	first rot	353.76	349.55				0.64	-0.35	1.19
high	1300	smoothed	first rot	341.09	325.61				0.65	-0.16	0.72
low	500	high	First triple	640.11	447.31	0.00	0.12	0.18	0.28	0.11	0.36
low	500	optimal	First triple	497.44	398.07	0.03	0.15	0.14	0.34	0.06	0.04
low	500	smoothed	First triple	443.10	356.58	0.06	0.03	0.24	0.07	0.33	0.23
low	900	high	First triple	503.60	389.23	0.09	0.14	0.21	0.46	0.63	0.32
low	900	optimal	First triple	382.93	347.72	0.08	0.12	0.14	0.52	0.12	0.32
low	900	smoothed	First triple	339.25	309.75	0.08	0.07	0.19	0.52	0.13	0.02
low	1300	high	First triple	409.87	355.78	0.07	0.20	0.11	2.21	0.46	0.20
low	1300	optimal	First triple	305.12	331.73	0.13	0.23	0.09	1.64	0.19	0.23
low	1300	smoothed	First triple	264.40	280.03	0.07	0.09	0.11	0.84	0.83	0.11
high	500	high	First triple	540.68	421.21	0.05	0.11	0.20	0.39	0.00	0.07
high	500	optimal	First triple	470.98	396.13	0.04	0.07	0.23	0.32	0.01	0.09
high	500	smoothed	First triple	455.45	379.36	0.01	0.06	0.27	0.18	0.06	0.14
high	900	high	First triple	465.07	386.55	0.03	0.10	0.18	0.08	0.02	0.03
high	900	optimal	First triple	402.05	363.01	0.06	0.05	0.22	0.27	0.26	0.08
high	900	smoothed	First triple	388.05	345.55	0.01	0.05	0.23	0.16	0.26	0.05
high	1300	high	First triple	410.41	364.28	0.05	0.06	0.21	0.87	0.07	0.28
high	1300	optimal	First triple	352.78	346.69	0.05	0.06	0.18	0.79	0.15	0.26
high	1300	smoothed	First triple	338.93	322.86	0.05	0.06	0.22	0.42	0.20	0.18
low	500	high	Fourth triple	4426.13	1583.16	0.04	0.22	0.02	0.03	0.06	0.32
low	500	optimal	Fourth triple	3890.87	1495.07	0.05	0.24	0.02	0.08	0.11	0.33
low	500	smoothed	Fourth triple	3773.69	1404.44	0.05	0.14	0.01	0.11	0.14	0.22
low	900	high	Fourth triple	3915.92	1481.10	0.00	0.20	0.01	0.01	0.09	0.55
low	900	optimal	Fourth triple	3424.19	1394.84	0.04	0.20	0.03	0.02	0.06	0.33
low	900	smoothed	Fourth triple	3322.32	1310.58	0.01	0.19	0.01	0.21	0.11	0.39
low	1300	high	Fourth triple	2818.08	1850.05	0.08	0.19	0.03	0.03	0.28	0.39
low	1300	optimal	Fourth triple	2198.21	1866.20	0.06	0.25	0.03	0.27	0.27	0.50
low	1300	smoothed	Fourth triple	2150.76	1702.81	0.03	0.17	0.01	0.16	0.09	0.23
high	500	high	Fourth triple	3881.06	1516.98	0.04	0.22	0.01	0.12	0.12	0.35
high	500	optimal	Fourth triple	3635.07	1474.75	0.00	0.18	0.00	0.10	0.18	0.20
high	500	smoothed	Fourth triple	3598.36	1431.67	0.00	0.16	0.00	0.10	0.16	0.23
high	900	high	Fourth triple	3622.47	1455.14	0.02	0.19	0.03	0.07	0.14	0.25
high	900	optimal	Fourth triple	3391.15	1411.84	0.01	0.14	0.00	0.09	0.19	0.25

high	900	smoothed	Fourth triple	3357.86	1370.10	0.00	0.14	0.00	0.31	0.02	0.30
high	1300	high	Fourth triple	3041.48	1932.17	0.02	0.16	0.00	0.21	0.05	0.28
high	1300	optimal	Fourth triple	2692.73	2067.13	0.01	0.17	0.03	0.21	0.04	0.24
high	1300	smoothed	Fourth triple	2686.96	1880.15	0.01	0.16	0.00	0.27	0.08	0.25
low	500	high	second rot	480.74	338.40				2.44	1.23	2.22
low	500	optimal	second rot	384.31	299.34				0.51	1.08	0.65
low	500	smoothed	second rot	342.08	263.44				0.17	1.36	0.48
low	900	high	second rot	380.94	293.56				1.06	0.53	0.03
low	900	optimal	second rot	299.78	256.32				0.04	0.74	0.94
low	900	smoothed	second rot	262.96	225.99				0.78	0.62	0.39
low	1300	high	second rot	311.14	263.06				0.68	0.35	0.19
low	1300	optimal	second rot	233.54	237.86				0.37	0.66	1.52
low	1300	smoothed	second rot	201.48	201.82				0.00	0.13	0.54
high	500	high	second rot	380.71	310.72				0.70	1.35	1.05
high	500	optimal	second rot	335.68	291.66				0.00	1.17	0.83
high	500	smoothed	second rot	324.00	274.23				0.29	1.05	0.66
high	900	high	second rot	338.00	282.72				0.05	1.48	1.00
high	900	optimal	second rot	298.20	263.62				0.48	0.79	1.20
high	900	smoothed	second rot	286.12	250.00				0.45	0.49	1.30
high	1300	high	second rot	295.41	260.80				0.18	0.61	0.90
high	1300	optimal	second rot	258.86	242.67				0.42	1.20	1.14
high	1300	smoothed	second rot	248.36	228.49				0.15	1.07	1.11
low	500	high	Talus trans	7874.30	2632.91	0.09	0.05	0.01	0.03	0.01	0.14
low	500	optimal	Talus trans	6921.16	2500.93	0.10	0.04	0.02	0.07	0.05	0.16
low	500	smoothed	Talus trans	6741.68	2376.42	0.09	0.06	0.07	0.11	0.02	0.19
low	900	high	Talus trans	7075.39	2500.12	0.10	0.06	0.08	0.06	0.05	0.10
low	900	optimal	Talus trans	6185.49	2379.31	0.09	0.04	0.02	0.08	0.07	0.06
low	900	smoothed	Talus trans	6007.96	2251.82	0.09	0.02	0.03	0.08	0.03	0.14
low	1300	high	Talus trans	6400.74	2402.55	0.08	0.05	0.04	0.16	0.16	0.01
low	1300	optimal	Talus trans	5558.79	2300.80	0.07	0.01	0.02	0.02	0.11	0.06
low	1300	smoothed	Talus trans	5387.67	2148.58	0.07	0.06	0.01	0.09	0.07	0.18
high	500	high	Talus trans	6913.69	2553.55	0.09	0.01	0.00	0.03	0.02	0.11
high	500	optimal	Talus trans	6479.69	2493.40	0.08	0.04	0.03	0.03	0.01	0.16
high	500	smoothed	Talus trans	6422.24	2432.18	0.08	0.04	0.04	0.04	0.04	0.14

high	900	high	Talus trans	6483.74	2481.52	0.08	0.02	0.01	0.04	0.00	0.10
high	900	optimal	Talus trans	6064.35	2429.03	0.08	0.06	0.04	0.02	0.04	0.20
high	900	smoothed	Talus trans	6011.83	2362.02	0.08	0.06	0.03	0.06	0.04	0.15
high	1300	high	Talus trans	6147.83	2438.99	0.09	0.04	0.04	0.03	0.03	0.13
high	1300	optimal	Talus trans	5736.32	2406.34	0.09	0.04	0.01	0.00	0.02	0.15
high	1300	smoothed	Talus trans	5687.92	2321.71	0.09	0.05	0.03	0.03	0.03	0.19
low	500	high	third rot	1962.77	934.29				0.19	0.12	0.16
low	500	optimal	third rot	1612.98	912.30				1.16	0.09	0.06
low	500	smoothed	third rot	1508.62	828.04				0.52	0.02	0.14
low	900	high	third rot	1588.94	795.37				0.88	0.28	0.12
low	900	optimal	third rot	1328.49	729.78				1.21	0.01	0.08
low	900	smoothed	third rot	1237.34	671.73				1.12	0.07	0.27
low	1300	high	third rot	1224.95	845.11				0.03	0.09	0.24
low	1300	optimal	third rot	925.03	817.04				1.25	0.09	0.03
low	1300	smoothed	third rot	857.36	724.08				1.17	0.19	0.08
high	500	high	third rot	1539.23	809.80				1.17	0.01	0.36
high	500	optimal	third rot	1407.02	775.14				1.17	0.20	0.05
high	500	smoothed	third rot	1379.81	746.49				1.20	0.05	0.04
high	900	high	third rot	1418.27	768.74				1.25	0.02	0.23
high	900	optimal	third rot	1293.93	736.52				1.27	0.07	0.01
high	900	smoothed	third rot	1268.66	708.07				1.29	0.01	0.01
high	1300	high	third rot	1307.02	753.01				1.12	0.00	0.18
high	1300	optimal	third rot	1178.60	741.86				1.24	0.13	0.07
high	1300	smoothed	third rot	1155.65	703.73				1.22	0.43	0.08
low	500	high	Third trans	1754.72	852.00	0.02	0.07	0.06	0.06	0.00	0.10
low	500	optimal	Third trans	1474.46	779.88	0.03	0.08	0.08	0.24	0.07	0.21
low	500	smoothed	Third trans	1387.37	721.87	0.06	0.05	0.01	0.23	0.04	0.05
low	900	high	Third trans	1521.68	783.16	0.07	0.08	0.03	0.02	0.49	0.33
low	900	optimal	Third trans	1265.11	711.58	0.01	0.07	0.09	0.31	0.02	0.11
low	900	smoothed	Third trans	1194.06	659.79	0.03	0.01	0.10	0.03	0.18	0.22
low	1300	high	Third trans	1303.36	776.71	0.01	0.06	0.07	0.56	0.30	0.35
low	1300	optimal	Third trans	1019.28	797.55	0.02	0.03	0.05	0.39	0.26	0.03
low	1300	smoothed	Third trans	976.71	716.03	0.05	0.02	0.05	0.25	0.29	0.13
high	500	high	Third trans	1509.03	803.88	0.01	0.02	0.07	0.12	0.04	0.01

high	500	optimal	Third trans	1374.87	767.66	0.02	0.01	0.06	0.17	0.17	0.01
high	500	smoothed	Third trans	1352.30	739.55	0.02	0.03	0.01	0.08	0.22	0.24
high	900	high	Third trans	1377.09	762.41	0.00	0.02	0.06	0.01	0.07	0.13
high	900	optimal	Third trans	1252.45	727.24	0.02	0.01	0.05	0.18	0.20	0.03
high	900	smoothed	Third trans	1230.41	701.72	0.01	0.01	0.04	0.05	0.04	0.06
high	1300	high	Third trans	1216.09	835.14	0.02	0.01	0.07	0.19	0.02	0.10
high	1300	optimal	Third trans	1068.23	850.58	0.02	0.01	0.09	0.19	0.05	0.06
high	1300	smoothed	Third trans	1053.48	796.34	0.02	0.01	0.05	0.25	0.06	0.08

APPENDIX B:

A Givens rotation is a rotation in the plane acting on two elements of a given vector. It can be represented in matrix form as

where the *cos{\theta}* and *sin{\theta}* appear at the intersection of the *i*th and *j*th rows and columns. When acting on a vector *x*, *G(i,j,\theta) x* performs a rotation of the *(i,j)* elements of *x*. Givens rotations are typically used to introduce zeros in vectors, such as during the QR decomposition of a matrix. In this case, it is typically desired to find *c* and *s* such that

with *r = \sqrt{a^2 + b^2}*.

Function: *void* **gsl_linalg_givens** *(const double a, const double b, double * c, double * s)*

> This function computes *c = \cos{\theta}* and *s = \sin{\theta}* so that the Givens matrix *G(\theta)* acting on the vector *(a,b)* produces *(r, 0)*, with *r = \sqrt{a^2 + b^2}*.

Function: *void* **gsl_linalg_givens_gv** *(gsl_vector * v, const size_t i, const size_t j, const double c, const double s)*

> This function applies the Givens rotation defined by *c = \cos{\theta}* and *s = \sin{\theta}* to the *i* and *j* elements of *v*. On output, *(v(i),v(j)) \leftarrow G(\theta) (v(i),v(j))*.
>
> (*ref: GNU Scientific Library – reference Manual: Givens Rotations: https://www.gnu.org/software/gsl/manual/html_node/Givens-Rotations.html*)

APPENDIX C:

vectors for helical axis of individual bones loaded to force

specimens name	point x	point y	point z	vector X	vector Y	vector Z
1L calcaneus	-41.52	2.72	-5.79	-0.79	0.60	-0.12
1R calcaneus	-40.29	6.11	-5.91	-0.79	0.61	-0.06
2L calcaneus	-52.06	0.34	-1.20	-0.62	0.62	-0.47
2R calcaneus	-76.55	-8.48	20.69	-0.66	0.54	-0.52
3L calcaneus	-46.82	3.94	-1.32	-0.60	0.78	-0.19
3R calcaneus	-49.53	3.30	0.08	-0.70	0.67	-0.23
4L calcaneus	-42.95	2.11	-3.31	-0.77	0.59	-0.24
4R calcaneus	-43.83	3.61	-4.31	-0.79	0.55	-0.27
5L calcaneus	-50.11	1.62	1.78	-0.79	0.56	-0.24
5R calcaneus	-54.30	-24.54	25.58	-0.99	0.12	-0.13
1L CTB	-23.20	-10.60	-4.09	-0.50	0.83	-0.24
1R CTB	-20.65	-7.63	-6.86	-0.48	0.87	-0.07
2L CTB	-31.46	-10.41	-1.07	-0.29	0.87	-0.39
2R CTB	-36.24	-12.68	9.55	-0.55	0.69	-0.46
3L CTB	-28.23	-14.77	-0.28	-0.54	0.84	-0.07
3R CTB	-30.29	-13.55	2.98	-0.58	0.81	-0.10
4L CTB	-24.51	-13.19	1.61	-0.40	0.89	-0.21
4R CTB	-26.50	-10.80	1.04	-0.37	0.91	-0.19
5L CTB	-21.44	-11.90	2.45	-0.73	0.68	-0.04
5R CTB	-25.67	-16.10	4.88	-0.85	0.50	-0.16
1L fourth	-26.10	-4.15	-5.72	-0.55	0.79	-0.26
1R fourth	-22.20	-1.25	-7.47	-0.58	0.79	-0.19
2L fourth	-30.66	-3.36	-2.27	-0.45	0.77	-0.44
2R fourth	-33.32	-0.08	1.19	-0.47	0.71	-0.53
3L fourth	-31.94	-5.14	-2.13	-0.41	0.88	-0.23
3R fourth	-31.82	-4.98	-0.61	-0.55	0.80	-0.24
4L fourth	-25.87	-2.92	-1.76	-0.36	0.90	-0.26
4R fourth	-26.42	0.43	-3.78	-0.30	0.92	-0.24
5L fourth	-23.64	-5.95	1.12	-0.71	0.66	-0.26
5R fourth	-27.49	-3.39	-0.77	-0.62	0.65	-0.43
1L MTIII	-7.84	1.80	-14.18	0.11	0.97	-0.22
1R MTIII	-5.70	0.17	-11.34	0.02	1.00	-0.08
2L MTIII	-7.79	9.18	-13.35	0.28	0.92	-0.29
2R MTIII	-4.57	11.75	-12.12	0.26	0.95	-0.19
3L MTIII	-13.95	-2.89	-6.68	0.06	0.99	-0.08
3R MTIII	-15.31	-5.48	-5.92	-0.05	0.98	-0.17
4L MTIII	-9.67	1.98	-6.23	0.10	0.97	-0.23
4R MTIII	-11.11	0.65	-5.98	0.04	0.99	-0.14
5L MTIII	-9.66	-7.66	-0.94	-0.12	0.97	-0.21
5R MTIII	-4.43	8.12	-9.85	0.28	0.94	-0.20
1L MTII	-9.32	-3.99	-13.82	0.12	0.97	-0.22

1R MTII	-8.62	-5.14	-11.68	0.04	0.99	-0.15
2L MTII	-12.67	-3.21	-10.16	0.14	0.92	-0.35
2R MTII	-9.10	0.67	-9.61	0.16	0.93	-0.32
3L MTII	-16.28	-8.95	-6.32	0.06	0.99	-0.15
3R MTII	-17.85	-11.02	-4.99	-0.05	0.97	-0.23
4L MTII	-12.99	-3.23	-6.50	0.12	0.94	-0.31
4R MTII	-12.07	-6.16	-4.84	0.02	0.98	-0.20
5L MTII	-13.05	-12.11	-0.66	-0.09	0.96	-0.28
5R MTII	-8.93	-0.68	-9.03	0.22	0.94	-0.24
1L MTIV	-7.42	-2.17	-12.05	-0.16	0.92	-0.36
1R MTIV	-4.02	-2.32	-11.00	-0.22	0.95	-0.20
2L MTIV	-9.65	2.50	-9.66	-0.04	0.93	-0.37
2R MTIV	-5.10	1.59	-6.63	-0.16	0.95	-0.27
3L MTIV	-10.55	-12.02	-4.46	-0.29	0.94	-0.15
3R MTIV	-7.92	-11.73	-3.96	-0.38	0.89	-0.25
4L MTIV	-8.87	1.11	-5.45	-0.08	0.96	-0.28
4R MTIV	-9.89	4.06	-6.56	-0.06	0.99	-0.16
5L MTIV	4.80	-15.35	2.01	-0.53	0.81	-0.24
5R MTIV	-1.25	-5.95	-3.03	-0.30	0.89	-0.34
1L MTV	-10.37	5.35	-15.73	-0.13	0.93	-0.36
1R MTV	-5.75	3.55	-13.42	-0.22	0.96	-0.16
2L MTV	-9.69	11.98	-13.97	0.02	0.94	-0.33
2R MTV	-6.55	13.81	-12.66	-0.01	0.97	-0.24
3L MTV	-11.84	-7.96	-5.89	-0.33	0.93	-0.15
3R MTV	-10.27	-6.61	-5.90	-0.39	0.88	-0.25
4L MTV	-11.45	6.06	-7.26	-0.10	0.96	-0.27
4R MTV	-12.63	11.32	-8.76	-0.03	0.99	-0.15
5L MTV	-0.12	-8.75	-0.72	-0.50	0.83	-0.24
5R MTV	-5.16	0.13	-6.39	-0.29	0.91	-0.31
1L second	-16.17	-11.49	-7.70	-0.25	0.91	-0.34
1R second	-14.83	-7.17	-9.28	-0.13	0.98	-0.16
2L second	-19.53	-13.27	-2.95	-0.24	0.89	-0.39
2R second	-18.23	-6.21	-4.50	0.01	0.80	-0.60
3L second	-23.38	-16.22	-3.54	-0.22	0.98	0.01
3R second	-26.36	-21.61	5.81	-0.65	0.74	-0.18
4L second	-16.84	-13.37	-1.46	-0.14	0.98	-0.17
4R second	-19.08	-9.00	-3.70	-0.02	0.92	-0.40
5L second	-20.46	-18.77	5.92	-0.60	0.75	-0.27
5R second	-22.07	-14.46	1.52	-0.32	0.92	-0.24
1L third	-21.25	-7.81	-7.37	-0.27	0.93	-0.24
1R third	-19.10	-5.21	-8.49	-0.30	0.93	-0.21
2L third	-26.02	-5.20	-5.95	-0.04	0.92	-0.39
2R third	-25.07	-0.03	-7.05	0.04	0.93	-0.37
3L third	-26.63	-12.35	-2.55	-0.27	0.95	-0.15
3R third	-26.70	-11.10	-0.78	-0.39	0.90	-0.19

4L third	-22.85	-8.63	-1.77	-0.14	0.95	-0.27
4R third	-24.20	-7.07	-2.24	-0.20	0.95	-0.23
5L third	-22.18	-15.03	6.08	-0.60	0.78	-0.15
5R third	-25.68	-11.19	1.11	-0.38	0.87	-0.32
1L tibia	-36.19	-3.74	-4.35	0.05	-0.99	0.16
1R tibia	-35.02	-4.67	-4.07	-0.03	-0.99	0.16
2L tibia	-41.11	-0.71	-2.73	0.13	-0.99	0.09
2R tibia	-37.59	-0.29	-0.21	0.12	-0.99	0.12
3L tibia	-41.25	-4.62	-0.16	-0.06	-1.00	0.02
3R tibia	-41.86	-2.05	0.34	-0.03	-1.00	0.08
4L tibia	-37.89	-4.66	0.38	0.06	-0.99	0.12
4R tibia	-38.87	0.12	-1.56	0.08	-1.00	0.05
5L tibia	-41.04	2.80	1.45	0.00	-1.00	0.04
5R tibia	-44.41	0.23	0.78	0.03	-1.00	0.09

vectors for helical axis of individual bones loaded to displacement

specimen	point x	point y	point z	vector X	vector Y	vector Z
1L calcaneus	-41.58	2.92	-6.48	-0.78	0.61	-0.15
1R calcaneus	-40.65	7.88	-7.89	-0.75	0.61	-0.25
2L calcaneus	-48.82	-3.34	-3.18	-0.83	0.47	-0.30
2R calcaneus	-49.17	-10.73	6.00	-0.94	0.12	-0.32
3L calcaneus	-46.83	3.80	-0.25	-0.60	0.79	-0.16
3R calcaneus	-49.10	2.87	1.19	-0.75	0.64	-0.16
4L calcaneus	-42.10	2.80	-3.29	-0.74	0.62	-0.25
4R calcaneus	-43.06	3.99	-4.48	-0.78	0.57	-0.25
5L calcaneus	-48.99	3.13	0.39	-0.80	0.52	-0.29
5R calcaneus	-48.26	-13.86	8.36	-0.97	-0.10	-0.20
1L CTB	-24.74	-8.91	-5.56	-0.33	0.91	-0.26
1R CTB	-23.60	-4.90	-5.01	-0.34	0.89	-0.29
2L CTB	-29.44	-11.44	-2.30	-0.36	0.86	-0.36
2R CTB	-32.52	-6.76	0.30	-0.28	0.81	-0.52
3L CTB	-29.20	-13.39	-0.63	-0.42	0.90	-0.08
3R CTB	-30.51	-11.51	1.48	-0.49	0.86	-0.17
4L CTB	-24.68	-11.87	0.43	-0.31	0.92	-0.22
4R CTB	-25.74	-9.36	-0.95	-0.31	0.91	-0.25
5L CTB	-24.54	-10.54	3.17	-0.58	0.78	-0.23
5R CTB	-31.14	-11.34	2.71	-0.46	0.84	-0.28
1L fourth	-27.39	-0.45	-7.39	-0.40	0.86	-0.31
1R fourth	-25.94	3.30	-6.82	-0.41	0.85	-0.33
2L fourth	-31.26	-4.52	-3.53	-0.46	0.80	-0.39
2R fourth	-37.87	0.78	-0.61	-0.37	0.74	-0.56
3L fourth	-32.14	-3.68	-2.53	-0.34	0.92	-0.20
3R fourth	-32.99	-3.57	-0.62	-0.50	0.82	-0.28
4L fourth	-27.17	-2.33	-1.87	-0.32	0.91	-0.26
4R fourth	-26.86	0.60	-3.84	-0.30	0.93	-0.23
5L fourth	-26.77	-2.51	1.05	-0.54	0.79	-0.29
5R fourth	-30.73	0.32	-2.50	-0.38	0.83	-0.41
1L MTIII	-7.35	2.73	-13.51	0.12	0.97	-0.21
1R MTIII	-3.17	8.80	-13.36	0.18	0.97	-0.13
2L MTIII	-9.69	5.34	-11.54	0.19	0.95	-0.26
2R MTIII	-4.59	11.70	-12.34	0.25	0.94	-0.23
3L MTIII	-13.65	-1.42	-6.58	0.08	0.99	-0.06
3R MTIII	-14.32	-1.15	-7.20	0.03	0.99	-0.15
4L MTIII	-8.85	2.65	-5.30	0.09	0.98	-0.18
4R MTIII	-9.49	3.02	-5.82	0.06	0.99	-0.13
5L MTIII	-9.12	0.34	-3.21	0.03	0.99	-0.17
5R MTIII	-1.29	9.89	-9.02	0.32	0.94	-0.13
1L MTII	-8.96	-4.79	-12.63	0.09	0.98	-0.20
1R MTII	-6.63	1.86	-12.74	0.17	0.97	-0.16

2L MTII	-12.20	-2.37	-10.24	0.15	0.95	-0.28
2R MTII	-5.57	8.13	-13.22	0.32	0.91	-0.27
3L MTII	-15.87	-8.19	-6.36	0.08	0.99	-0.10
3R MTII	-16.49	-10.46	-5.61	-0.04	0.98	-0.20
4L MTII	-10.68	-3.02	-5.19	0.12	0.98	-0.18
4R MTII	-9.69	-0.46	-6.41	0.12	0.99	-0.10
5L MTII	-11.26	-1.98	-4.23	0.13	0.98	-0.16
5R MTII	-2.78	6.06	-9.68	0.40	0.91	-0.08
1L MTIV	-6.62	-1.33	-11.80	-0.15	0.93	-0.35
1R MTIV	-4.37	3.66	-11.80	-0.10	0.95	-0.29
2L MTIV	-9.67	-1.65	-8.07	-0.13	0.92	-0.37
2R MTIV	-5.87	4.28	-8.52	-0.10	0.94	-0.33
3L MTIV	-12.19	-9.03	-4.61	-0.23	0.96	-0.15
3R MTIV	-8.62	-9.76	-4.28	-0.34	0.90	-0.27
4L MTIV	-8.93	-1.28	-3.67	-0.13	0.95	-0.27
4R MTIV	-9.88	3.55	-5.91	-0.08	0.98	-0.19
5L MTIV	-0.52	-10.35	0.68	-0.40	0.88	-0.26
5R MTIV	-3.90	-1.07	-5.07	-0.17	0.94	-0.31
1L MTV	-9.31	4.52	-14.56	-0.15	0.93	-0.35
1R MTV	-6.70	9.25	-14.07	-0.11	0.95	-0.28
2L MTV	-11.38	6.57	-11.64	-0.10	0.93	-0.35
2R MTV	-7.69	15.79	-14.22	0.03	0.95	-0.31
3L MTV	-14.59	-2.90	-6.48	-0.23	0.96	-0.16
3R MTV	-12.63	-3.15	-6.88	-0.32	0.91	-0.27
4L MTV	-11.44	3.37	-5.30	-0.16	0.95	-0.28
4R MTV	-12.66	9.78	-7.93	-0.07	0.98	-0.20
5L MTV	-2.95	-4.57	-1.59	-0.41	0.87	-0.27
5R MTV	-4.98	1.89	-6.66	-0.25	0.92	-0.31
1L second	-22.46	-11.24	-6.36	-0.20	0.90	-0.38
1R second	-14.95	-7.27	-7.59	-0.17	0.98	-0.09
2L second	-21.63	-12.02	-4.71	-0.11	0.96	-0.25
2R second	-11.09	-13.20	4.19	-0.63	0.77	0.04
3L second	-20.15	-18.44	-2.37	-0.26	0.85	0.45
3R second	-49.62	-14.79	5.67	-0.27	0.78	-0.56
4L second	-22.66	-13.43	-1.00	-0.14	0.95	-0.29
4R second	-23.23	-11.71	-1.84	-0.17	0.93	-0.33
5L second	-21.18	-15.99	4.81	-0.40	0.92	-0.02
5R second	-29.42	-11.09	-0.51	-0.07	0.92	-0.38
1L third	-22.49	-5.65	-8.69	-0.16	0.94	-0.30
1R third	-20.53	-1.57	-8.66	-0.14	0.94	-0.30
2L third	-26.82	-7.53	-5.74	-0.15	0.90	-0.40
2R third	-28.28	-0.62	-6.82	0.00	0.86	-0.51
3L third	-27.23	-11.65	-2.03	-0.23	0.96	-0.13
3R third	-28.72	-9.62	-1.27	-0.31	0.93	-0.22
4L third	-23.10	-9.23	-1.44	-0.18	0.94	-0.29

4R third	-24.49	-6.52	-2.93	-0.18	0.95	-0.25
5L third	-25.31	-9.50	2.80	-0.34	0.91	-0.24
5R third	-27.73	-6.51	-2.78	-0.09	0.95	-0.29
1L tibia	-36.05	-3.42	-4.21	0.05	-0.99	0.15
1R tibia	-34.77	-2.55	-4.70	0.00	-0.99	0.14
2L tibia	-40.61	-1.88	-2.16	0.11	-0.99	0.09
2R tibia	-37.73	-1.34	-0.17	0.12	-0.98	0.13
3L tibia	-41.22	-4.34	-0.18	-0.06	-1.00	0.01
3R tibia	-41.74	-0.69	0.45	-0.02	-1.00	0.07
4L tibia	-38.09	-5.06	0.28	0.06	-0.99	0.12
4R tibia	-38.74	-1.10	-1.17	0.09	-0.99	0.07
5L tibia	-41.37	3.90	1.29	0.01	-1.00	0.04
5R tibia	-44.77	0.44	0.55	0.03	-1.00	0.08

APPENDIX D

Terminology regarding LEGO bricks

Below: A LEGO brick with 8 studs (rounded cylindrical protrusions)

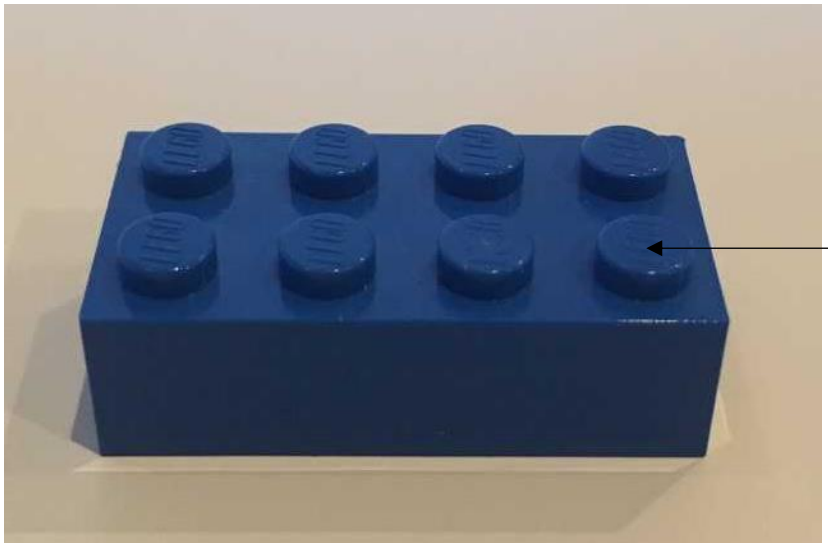

In contrast to a LEGO brick (below left), the LEGO plate (below right) has one third the height of a brick

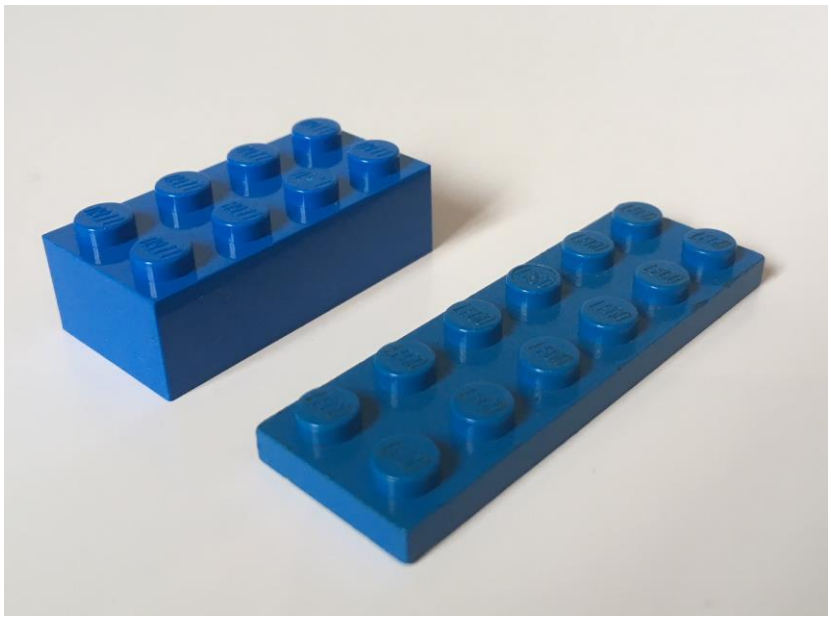

Motion of LEGO bricks.

A blue 8 stud LEGO brick has been placed on a green LEGO board below.

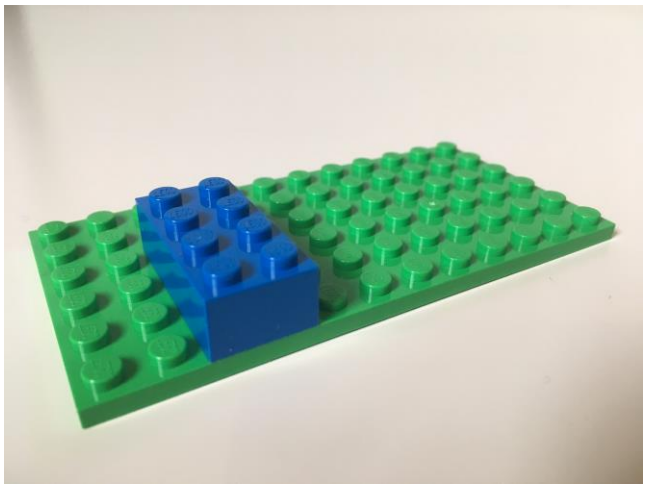

This brick can now be moved in three directions along the 3 cardinal axes.

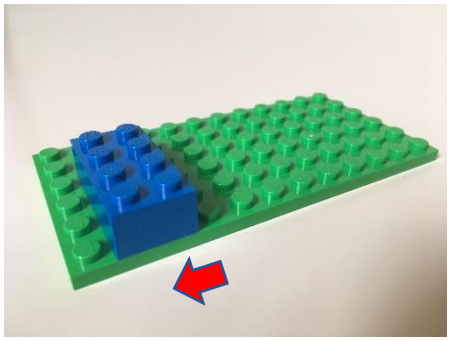

Moved “sideways” by one stud

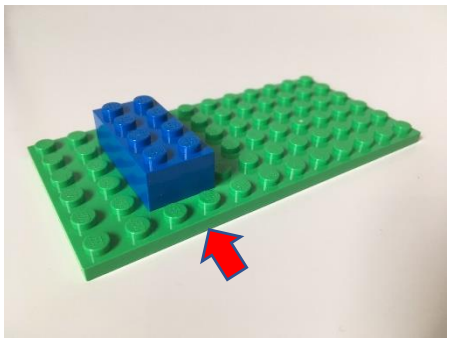

Moved “backwards” by one stud

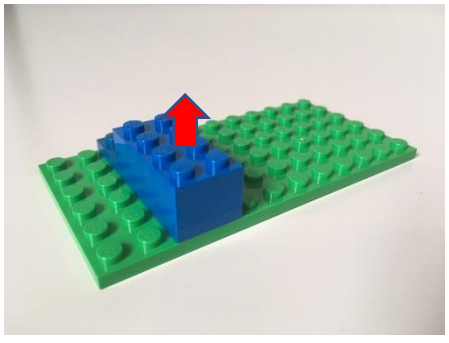

Moved “up” by the thickness of one plate